Flow induced crystallisation of polyethylene in presence of nanoparticles

by

Nilesh Patil

Doctoral Thesis
Submitted in partial fulfillment of the requirements
for the award of Doctor of Philosophy

Department of Materials
Loughborough University
Loughborough LE11 3TU, Leicestershire
England, United Kingdom (U.K.)

The work submitted is original research conducted by candidate and the proper credit has been given while referring to the work of others

Research Student Office, Academic Registry
Loughborough University Leicestershire LE11 3TU UK
Switchboard: +44 (0) 1509 263171 Fax: +44 (0) 1509 223938

CERTIFICATE OF ORIGINALITY

This is to certify that I am responsible for the work submitted in this thesis, that the original work is my own except as specified in acknowledgements or in footnotes, and that neither the thesis nor the original work contained therein has been submitted to this or any other institution for a higher degree.

…….. **(Signed)**

…….. **(Date)**

To my parents,

Contents

List of Figures

List of Tables

Summary

Polymeric systems become increasingly complicated and multifunctional if they involve a larger level of structural complexity. In the last couple of decades the level of interest has gradually shifted from the μm-scale to the nm-scale region, for instance, systems having at least one structural size below 100*nm*, e.g. nanocomposites. The physical properties of polymers such as crystallisation, tensile modulus, impact strength and viscosity are strongly influenced by the presence of additives in the polymer matrix. Semicrystalline polymers comprise nearly two-thirds of all synthetic polymers. These are processed to form films, fibers, and moulded articles using operations such as extrusion, moulding, fiber spinning, film blowing etc. During these processes, the polymer melt is subjected to complex and intense flow fields (shear or elongational) after which the polymer crystallises. The morphology of the semicrystalline polymer in the final product and subsequently its properties and quality, depend on the manner in which the polymer crystallises from the flowing melt. The subject is continuously driven by the quest to understand the molecular mechanism of flow induced crystallisation; nevertheless, the flow induced crystallisation in presence of nanofillers has received little attention.

The thesis deals with the crystallisation studies of polymer molecules during shear in presence of nanofillers (viz. single walled carbon nanotube (SWCNT) and zirconia particle) having different aspect ratio. For this purpose, the polyethylene (PE) consisting of desired molar mass and molar mass distribution within the processing range is utilised. The morphology of semicrystalline polymer is revealed using time resolved X-ray scattering (SAXS/WAXS) techniques. The rheological aspects of polymer melt in presence of nanoparticles are manifested.

In chapter 2, the effect of SWCNTs on the crystallisation kinetics of polymers has been studied with and without application of shear rate. The shear rate effect on the formation of shish-kebab structures in the polymer containing SWCNTs is investigated. The effect of shear rates on the stretching of long chains of PE is verified using the approach involving the use of Deborah number. The study reveals the significance of SWCNTs on crystallisation of PE. In chapter 3, the influence of zirconia nanoparticles on crystal orientation of polymers is studied. Enhanced crystallisation kinetics is observed due to presence of zirconia nanoparticles. Overall

crystal orientation is improved as a result of zirconia nanoparticles in the polymer matrix.

In chapter 4 of the thesis, the role of broad molecular weight distribution of PE in formation of oriented (shish-kebab) structures is demonstrated. The presence of nanoparticles of different aspect ratios and binding efficiency with polymer on the formation of highly oriented structures in the early stage crystallisation is verified. The study reveals the significant role of SWCNTs in shish-kebab structure formation as compared to zirconia nanoparticles. Further, the insight on the selective adsorption of polymer chains to the nanoparticles is provided. In chapter 5 of the thesis, the molecular interaction between polymer and nanoparticles under shear above the equilibrium point *(T = 141.2°C)* is investigated. The study reveals the major role of SWCNTs with high aspect ratio, in the stability of flow induced precursor (FIP) and formation of extended chain crystals, as a result of strong interaction with PE molecules. On contrary, the poor interaction of Zirconia particles having low aspect ratio, with PE molecules prohibits molecular chain extension.

Keywords: Flow induced crystallisation, polyethylene, nanoparticles, shish-kebab structures, crystallisation kinetics

Acknowledgements

I am very grateful to my supervisor, Prof. Sanjay Rastogi for accepting me in his research group to perform this work. His support, crucial inputs, excellent scientific guidance, continuous motivation, innovative thinking, precious discussions and suggestions throughout this period made this work possible. I have learned a great deal of research activity for which I owe large debt of gratitude to him. I thank Dr. Bala Vaidyanathan for being second supervisor and providing me much needed encouragement during the whole period of PhD. I thank Professor Marianne Gilbert for her support and guidance throughout my PhD. Her positive critical comments at crucial stage of my work have been of great help for improving my thesis.

My sincere thanks to Dr. Luigi Balzano *(TU/e, Eindhoven)* for his keen interest in my work and for providing the encouragement throughout this work. I have thoroughly benefited from the discussions during the beamtimes at ESRF and visits to Loughborough. I appreciate him for his inputs during synchrotron data analysis. I would also like to thank Dr. Giuseppe Portale *(BM26B, ESRF)* for assisting me during experiments in beamline and his fruitful discussions, comments even in the cafeteria. I also appreciate the assistance from Dr. Aleksei Bytchkov *(ID11, ESRF)* during the experiments in the ID11 beamline. It was very productive working with him.

I gratefully acknowledge, Department of Materials, Loughborough University (UK) for giving me the opportunity to study the PhD and providing me the departmental studentship funding during the 3 years. I also appreciate European Synchrotron Radiation Facility *(ESRF, Grenoble, France)* and Netherlands Organization of Scientific Research *(NWO, Den Haag, The Netherlands)* for granting the beamtimes needed for making this research successful.

I would like to thank;

- Dr. Wim Bras *(BM26B, ESRF)*, Dr. Theyencheri Narayanan *(ID02, ESRF)* and Dr. Gavin Vaughan *(ID11, ESRF)* for support during the beamtimes for experimental work.
- Dr. Peter Boesecke *(ID02, ESRF)* for fruitful discussions and for perfect setup on the ID02 beamline – the best setup I have ever seen in ESRF in past 3 years of PhD.

- Dr. Guido Heunen *(UCL, Louvain-la-Neuve)* for providing the precise instructions on calibration of CSS 450 shear cell during the beamtime in ID11.
- Prof. Alejandro J. Müller *(Universidad Simón Bolívar, Venezuela)* for his kind assistance and guidelines to fit the data using Avrami analysis for crystallisation kinetics of polymer.
- Dr. Ann Terry *(ISIS, Rutherford Appleton Laboratory, Oxfordshire)*, Dr. Nilesh Kukalyekar *(DSM Research, Geleen)*, Dr. Jules Harings *(Teijin Aramid B.V., Arnhem)* and Dr. Saied Talebi *(DSM Research, Geleen)* for providing tips during their visits to Loughborough.
- Dr. Bing Wang *(Avantium Technologies B.V., Amsterdam)* for his support, guidance and motivation during initial period of my PhD.
- Mr. Frederik Geomoets *(Dow Benelux B.V., Hoek)* for supplying the polyethylene required for the research work and assisting me in getting GPC analysis.

I would also like to appreciate all the people from my research group, both at Eindhoven and Loughborough for providing wonderful working atmosphere within the group, i.e.

- Maurizio, Maria, Sai, Han for the good time.
- Carmine for the fantastic time during all beamtimes at ESRF and essential discussions on the subject of polymer crystallisation.
- Anurag for introducing me to the polymer rheology and assisting me for experiments.
- Dr. Sara Ronca for helping me during SEM experiments, Dr. Yohan Champouret for useful discussions. Giuseppe Forte for helping me in the lab.

I appreciate rest of the staff from the Department of Materials, for their assistance during 3 years of my PhD research. Finally, I express my deepest gratitude to my family for their boundless moral support and inspirations during my studies.

Chapter 1

General Introduction

Preface

Polymers represent an important class of materials due to their several tunable properties that is realised in their applications ranging from a commodity plastic to highly demanding applications. Basically, polymer materials exhibit important structural features from subnanometer range up to several microns. Flexibility in applications arises directly from versatility in physical properties, which manifests molecular synthesis and design, relationships between molecular architectures and material response, and efficient processing strategies. The material properties in the solid state (final) and the dynamic response in the liquid state used in both molecular characterisation and processing governs the polymer design and optimisation of performance. However, it is often the case that polymeric materials do not achieve an equilibrium state; similarly, the processing of polymers usually involves strong undefined flow conditions, temperature gradients that take the system far from equilibrium. This makes it rather difficult to predict the ultimate structure, at the nanoscopic, mesoscopic, and even macroscopic levels.

Polymer science has achieved certain level of development in the last 60 years. For instance, from the recognition of macromolecules by ***Hermann Staudinger (1953 Nobel Prize in Chemistry)*** *to the work on organometallic catalysts for synthesis of polyolefin by* ***Karl Zeigler*** *and* ***Giulio Natta (1963 Nobel Prize in Chemistry)****, theoretical and experimental work in the physical chemistry of macromolecules by* ***Paul J. Flory (1974 Nobel Prize in Chemistry)****, the knowledge and concepts of molecular rheology; based on the fundamental work of* ***Pierre-Gilles de Gennes (1991 Nobel Prize in Physics)*** *and very recently on polymer catalysis by* ***Robert Grubbs, Richard Schrock and Yves Chauvin (2005 Nobel Prize in Chemistry)****.*

In this thesis, effort is made to understand relatively less understood structure formation processes under defined flow conditions in the presence or absence of nanoparticles. (1) Nanoparticle interaction with macromolecules in the melt state; (2) Chain dynamics of polymer melt in the presence of nanoparticles, which influences viscoelastic response and mechanical properties; (3) Processing, which establishes the performance of materials.

1.1 Brief history and development of polyethylene

The development of polyethylene (PE) is extremely important commercially, industrially and scientifically. It was produced serendipitously several times before the utility of synthetic polymers was appreciated. It was not until the 1930s that chemists from Imperial Chemical Industries (ICI), trying to produce an entirely different product, inadvertently created polyethylene and recognized its potential. In 1933, the investigations on the high pressure reaction of ethylene with benzaldehyde by Eric Fawcett and Reginald Gibbon produced a subgram quantity of a white waxy solid lining the reaction vessel. The solid was identified as a polymer of ethylene. However, it was not before 1935, that Michael Perrin established a set of conditions that could be used to polymerise ethylene more consistently. The polyethylene made by Perrin was a ductile material with a melting temperature of about 115°C. This material was what we know today as low density polyethylene (LDPE). [1] However, the fundamental limitations to the applications of polyethylene were realised during World War II due to its flexibility, low tensile strength and low softening temperature. All these limitations had the same origin; the high degree of short chain branching that hindered the formation of crystallites in terms of size and perfection.

The potential for polymerising ethylene was recognised based on the early investigations from the research group of Karl Ziegler *(Max Planck Institute in West Germany)* during 1950s, on various transition metals with respect to their ability to form more effective, catalysts. Subsequently as a result, a new form of polyethylene was obtained by low pressure, low temperature polymerisation process [2], with its negligible branching, displayed many properties that were superior to those of the previously available highly branched resins. The physical properties such were stiffness and strength also increased. With its higher degree of crystallinity along with higher density; it was named high density polyethylene (HDPE).

The significance of Ziegler's discovery was recognised and as a result Karl Ziegler [3] and Giulio Natta [4-5] received the 1963 Nobel Prize in Chemistry for organometallic catalysts capable of producing linear high density polyethylene (HDPE) and polypropylene (PP), respectively. With the breakthrough in the development of catalyst technology, copolymers of ethylene with small amounts of α-olefins were

produced. Using such polymerisation the incorporation of short chains or branches on the ethylene backbone became possible resulting in the development of linear low density polyethylene (LLDPE). Subsequently, the potential to investigate the morphology of semicrystalline polymer in stirred solutions [6-8], sheared melts [9], drawn melts [10] and undercooled melts [11] were realised. These studies lead to the advances in achieving the high performance of materials.

Ultra high molecular weight polyethylene (UHMWPE) produced by Ziegler process has a high melt viscosity which results from a high molecular weight (HMW) and enhanced degree of chain entanglements. Hence, UHMWPE is relatively difficult to process. The advantages of using UHMWPE arise because of high impact properties, high abrasion resistance, low creep and excellent resistance to stress cracking of material. In late 1970s, Smith and Lemstra [12-14] at DSM Research at Geleen, the Netherlands, developed a process to produce ultra high strength PE filaments based on solution spinning and hot drawing of UHMWPE from semi-dilute solution. The process proved to be very crucial in terms of achieving a high modulus of 150 GPa and tensile strength to break in the vicinity of 4 GPa in synthetic man made fibers.

Lately, in the 1980s, single-site catalysts emerged in the polymer field with the discovery of metallocene catalysts by Sinn and Kaminsky [15], based on transition metals (Zr, Ti, Hf). These highly active catalysts exhibit advantages over the conventional multi-site Zeigler-Natta and chromium catalysts. Single-site catalysts have exceptional ability to polymerise olefin monomers, producing extremely uniform polymers and copolymers. This lead to the production of superior polyethylenes with narrow molecular weight distribution for better control over chain structures.

1.2 Morphology and crystallisation of polyethylene

Polyethylene is the most widely used model semicrystalline polymer for morphological investigations due to its simple chemical structure. In 1939, Bunn [16] verified the crystal structure of PE. At ambient temperature and atmospheric pressure polyethylene chains pack in the thermodynamically stable orthorhombic lattice shown in figure 1.1.

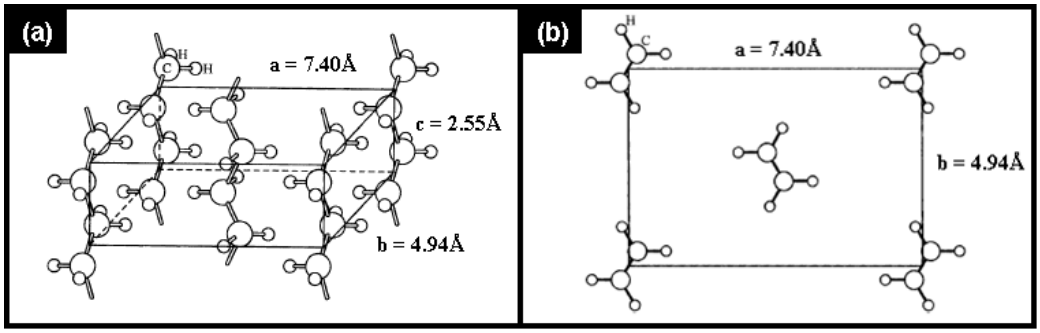

Figure 1.1: The orthorhombic crystal symmetry [17] of PE. Each cell consists of two C_2H_4 – groups. (a) The orthogonal view and (b) view along the chain axis.

Subsequently, the dimensions at ambient temperature and atmospheric pressure of orthorhombic unit cell of linear PE was reported [18] as; a = 7.40 Å, b = 4.94 Å and c (chain axis) = 2.55 Å. Polymorphism in polymers is a common phenomenon. In polyethylene it is realised during mechanical deformation or under constrained conditions. For an example, the thermodynamically less stable monoclinic structures are present in mechanically stressed polymer materials such as stretched and oriented films. Bassett et al. [19] reported the presence of a hexagonal phase in linear PE at elevated pressures (p) and temperatures (T). These findings were further supported by Hikosaka et al. [20] where the equilibrium triple point Q_o (at 250°C and 5.3 kbar) in the p-T phase diagram is defined as the intersection of the orthorhombic to liquid, orthorhombic to hexagonal and hexagonal to liquid transition lines. Consequently, Rastogi et al. [21] provided evidence for the presence of a hexagonal phase during polymer crystallisation. According to these authors, depending on the explored region of the phase diagram, below the equilibrium triple point, a growing crystal initially in the hexagonal phase goes through thermodynamically stable and metastable states before transformation to the orthorhombic phase. The newly transformed crystals, from hexagonal to orthorhombic crystal packing, act as nucleation centres for many new crystals starting in the hexagonal phase. The life time for the crystal in the thermodynamically metastable hexagonal phase decreases with increasing supercooling. This study was crucial since single crystals can be grown directly in the melt and some insight into the nucleation and growth of spherulites at ambient pressure could be provided. Hence, it became possible to recognise that the crystallisation of linear PE proceeds through a metastable phase, even in the

thermodynamically stable orthorhombic region of the *p-T* phase diagram. This topic has been further pursued by Strobl and co-workers. [138]

The crystallisation of PE from solution or melt leads to the formation of lamellae through the process of organised chain folding [22-23] (figure 1.2a). Keller [7], Fischer [24] and Till [25] through their independent investigations revealed that linear polyethylene crystallises into thin platelet crystals, the so called lamellae, from dilute solutions. These lamellae could grow several microns in lateral dimensions however they were very thin (~10 nm) along the chain axis with polymer molecules, repeatedly being folded back and forth. Fischer [24] and Kobayashi [26] independently showed that crystals in melt grown spherulites of PE were lamellar rather than fibrillar, thus confirming that chain folded crystals play a major role in the morphology of semi-crystalline polymer.

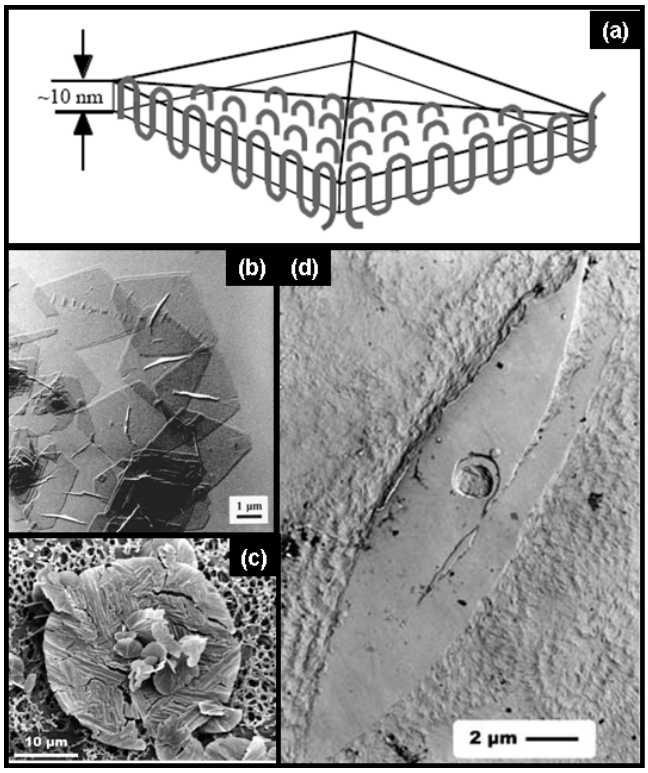

Figure 1.2: Single crystals of linear PE (a) schematic of regular chain folding in single crystals (b) electron micrograph of solution grown single crystals of linear PE; [27] (c) electron micrograph of PE crystallised at 0.3 GPa as uniform circular disc; twinned texture at ambient temperature and pressure with lines inclined at 60° is observed in the sample cooled to room temperature; [28] (d) electron micrograph of PE crystallized at 130 °C, grown from melt at atmospheric pressure. [29]

The crystal shape of PE changes with time and the defined supercooling. [30] The process is often cited as surface roughening. [31] On isothermal annealing, chains within the crystals tend to reorganise and overall crystallinity increases. The process of isothermal crystal thickening occurs in PE crystals during growth from both melt [32-33] and solution. [34-35] Crystals of ultra long alkanes, show crystal thickening from an initial chain folded crystal to thermodynamically stable, extended chain. Crystal thickening has been followed using DSC, FTIR, time resolved X-ray scattering and transmission electron microscopy. [35] In general, the thickness of crystal lamellae depends on the crystallisation conditions, i.e. the crystallisation temperature and annealing or quenching treatments. [36] Geometrically, the well-formed crystals are formed when PE is crystallised under a low degree of supercooling [37-38], whereas short, thin curved crystals grow under a high degree of supercooling. [38-39] The percentage thickness-to-width ratio of solution grown or melt-grown crystals has been reported to be in the range from 0.1% to 10%.[40-41] The lamella thickness and thickness distribution has been the subject of many investigations and is determined by several experimental techniques, such as Transmission Electron Microscopy (TEM) [42-44], Differential Scanning Calorimetry (DSC) [44], Small-Angle X-ray Scattering (SAXS) [44-45] and Atomic Force Microscopy (AFM). [44-46] Recently, morphological implications on lamellar thickening have been explored in the regularly stacked UHMWPEs. The authors showed that compared to the melt crystallised samples in the regularly stacked crystals, thickening proceeds via lamellar doubling. [47] These observations on quantum increase in crystal thickness above the alpha relaxation temperature were further supported by AFM studies performed on the overlayed single crystals of linear polyethylenes. [48]

To bridge polymer crystallisation from solution and melt, it is also proposed that polymer crystallisation from the melt proceeds from single lamella. The single crystals rapidly branch to form more complicated morphologies, filling space in three dimensions to form a spherulite. The crystallographic chain-axis is oriented in the tangential plane of the spherulite and the *b*-axis is oriented along the spherulite radius. [49] Depending on the molar mass and crystallisation temperature, linear PE forms different kinds of superstructures as shown in figure 1.3. Under a high degree of supercooling, and with a

molar mass between ~15,000-120,000 g/mol, banded spherulites are reported. [50-51] With low degree of supercooling and narrow molar mass of ~65,000 g/mol, non-banded spherulites are reported. [51] Whereas a low degree of supercooling and a molar mass ranging between ~18,000-115,000 g/mol leads to an irregular non-spherical sheaf-like structures. [50] In very high molar mass PE, random lamellar structures without any clear superstructure are observed. [52]

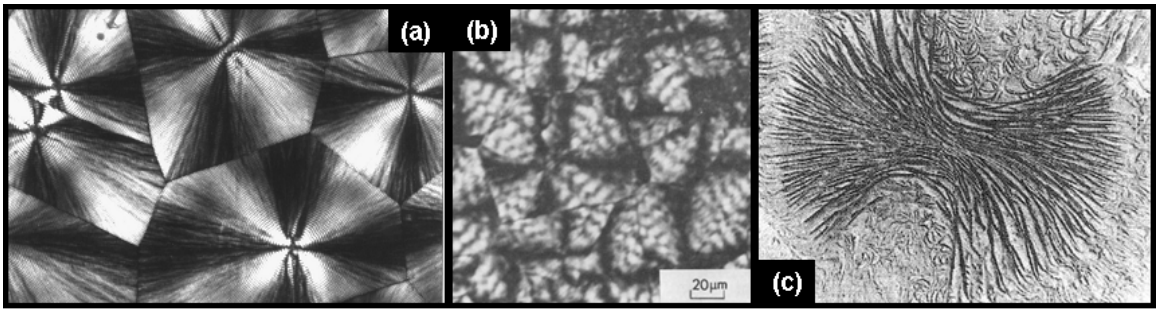

Figure 1.3: The spherulite structures in linear polyethylenes, (a) banded spherulite structures; [53] (b) non-banded spherulite structures; [51] (c) sheaf-like structures. [54]

Crystallisation of PE from the melt mainly leads to a two-component structure having the layer of crystalline and amorphous regions. Another component of a transitional (interfacial) region between the crystallites and the liquid-like amorphous region has been identified using NMR [55] and Raman [56] spectroscopy techniques, which are sensitive to probe chain mobility and the conformational statistics of the molecules. According to Strobl and Hagedorn [56], the interfacial region is a disordered phase of an anisotropic nature where chains show all-trans sequences but have lost their lateral order. Mandelkern et al. [57], later suggested that the percentage fraction of interfacial component increases with increasing degree of chain branching. Mutter et al. [58] stated that the interfacial component of PE is refined further into two different components: an interfacial crystal core and an interfacial liquid-like component. The interfacial crystal core is associated with all-trans sequences of the chain molecules outside the orthorhombic crystalline lattice, whereas the interfacial liquid-like component is associated with the conformational states of the amorphous phase, which differ from the completely disordered state of the liquid-like amorphous component.

1.3 Flow induced crystallisation (FIC) in polyolefins

Flow enhances the crystallisation dynamics and results in a specific semicrystalline morphology. The application of flow permits the extension of polymer chains; moreover, thermodynamically it increases the opportunity of crystal formation by increasing the melting point, while kinetically the extended chain is closer to a crystal state than a random chain. Hence, flow leads to local ordering of the polymer chains; as a result, decrease of the entropy barrier for nucleation, which contributes to the increase in crystallisation rate of the polymer chains. [59] The formation of extended chain crystals during flow is an outcome of the high end tail of the molecular weight distribution. [60-61] These high end tail molecules, having higher relaxation time are stretched leaving the rest unchanged; a stronger elongational rate influences the chain dynamics of a broader part of the molecular weight distribution. The elongational rate, therefore, determines the amount of extended chain crystals arising during flow. These extended chain crystals serve as nuclei for lamellar crystallisation of the non oriented low molar mass polymer, which contribute to lamellar over-growth perpendicular to the central core at later stages of crystallisation. [61]

The chain dynamics in polymer melts has been recognised as the critical parameter in the resultant morphology after flow. Since the relaxation time is proportional to the molecular weight, long chains would possess much longer relaxation times than short chains. As a result, after the cessation of flow, long polymer chains may not have sufficient time to relax back to the coiled state and would remain in the stretched state, whereas the stretched short chains can quickly relax back to the coiled state without preferred orientation. Hence, the Weisenberg number (Wi) which is product of relaxation time and characteristic deformation rate for a flow process is greater than one for flow fields in processing operations. If $Wi > 1$, polymer coil conformations are significantly restricted compared to the equilibrium random coil state thus lowering the energy barrier for polymer crystallisation. Thus the overall crystallisation is enhanced. At low shear rates, due to local ordering, the nucleation density gets enhanced and large numbers of spherulites are formed, while at higher shear rates, due to stretching of chains, highly anisotropic oriented crystallites resulting in “shish-kebab” structures [62-64] are formed. Moreover, if the number of shish-kebabs is sufficiently high (i.e. their distance is

sufficiently small), they can join and form complex zip fastener structures. [60] Shish-kebab morphology in polymers was first reported by Pennings et al. [8] who during fractionation process of high molar mass PE came across such unique structural formation. The schematic representation of shish-kebab morphology is depicted in figure 1.4.

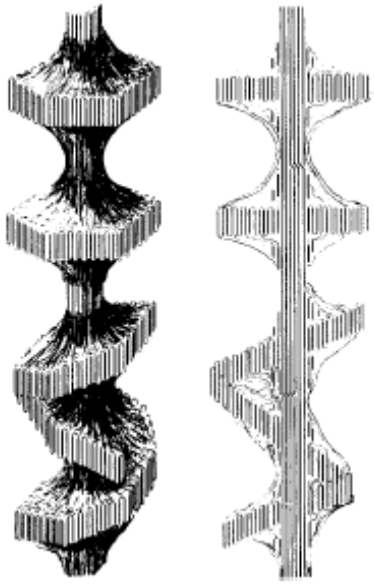

Figure 1.4: Shish-Kebab structure showing the central core consisting of extended chains that provides suitable nucleating sites for the growth of lamellae perpendicular to central core. These lamellae consist of folded chains aligned in the direction parallel to the central core. [65]

Seki et al. [66] indicated the formation of shish-kebab morphology due to HMW chains exceeding the critical overlap concentration. This finding suggests that the formation of a shish structure is a result of a cooperative effect between the HMW chains. However, the number density of shish structure appears to saturate with increasing shearing time and the mass fraction of HMW chains.

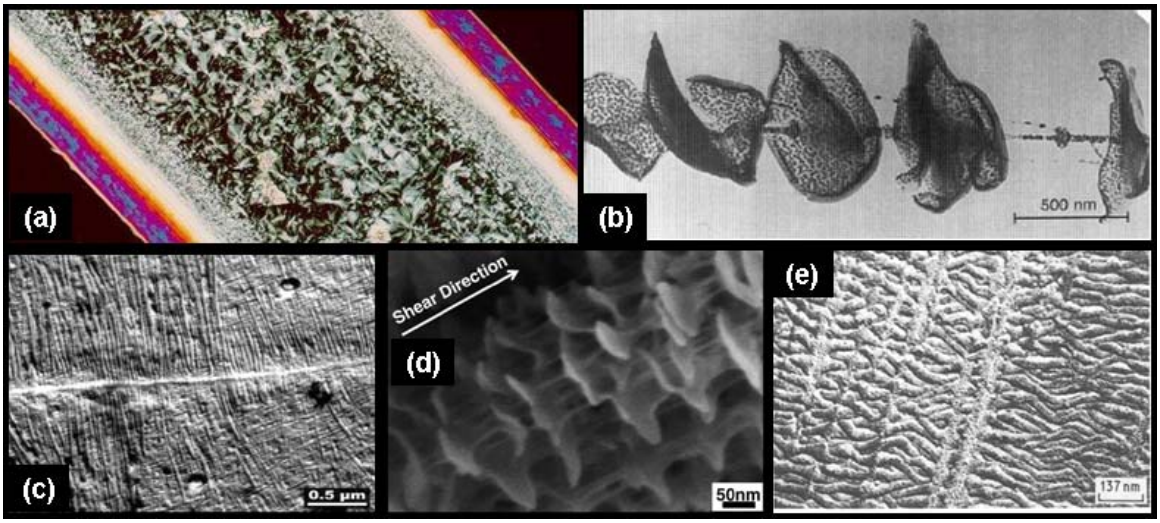

Figure 1.5: (a) optical micrograph of cross section of an injection molded sample consisting spherulitic structure in the inner portion and extended chains (shish) in the edges; [67] (b) electron micrograph of 'shish-kebab' structure grown from a stirred solution of ultra high molecular weight polyethylene (UHMWPE) in xylene; [62] (c) Shish-kebab structures in polypropylene at 140 °C; [63] (d) SEM micrograph of shish-kebab structures having multiple shishes in toluene-extracted UHMWPE; [64] (e) TEM image of PE shish-kebabs forming zip fastener structures. [60]

The crystallisation behaviour and subsequent morphological development are directly dictated by the initially formed precursor structures (e.g. shish-kebab structures, where shish represents extended chain crystal and kebab represents folded-chain crystal) induced by flow. [68-76]

1.3.1 Factors influencing formation of oriented structures

Several physical paramaters have been demonstrated to explain the formation of oriented structures in FIC. For instance, the resultant anisotropic shish-kebab structure arises when the flow is applied above a critical shear rate, whereas isotropic spherulitic nucleation occurs when the applied shear is below the critical shear rate. [66, 73, 77-83] For instance, Langouche [84], confirmed the characteristic upturn in the flow birefringence pattern at high shear rates using a shear cell and optical setup. Kumaraswamy et al. [85] recently studied the control of short-term shearing using in-situ optical (birefringence) and wide-angle X-ray diffraction (WAXD) and ex-situ microscopy techniques on isotactic polypropylene (iPP). They suggested the formation of highly oriented crystallites ultimately leading to the shish-kebab morphology. Lamellae

tend to grow in the perpendicular direction of the shish. The lamellae growth is hindered with the growth process on the neighbouring shish, that may lead to the interlocking of kebabs. [60]

Bove and Nobile [86], reported strong enhancement in crystallisation kinetics of polymers; when step shear flow was applied at the crystallisation temperature. The overall crystallisation rate increases with the increasing applied shear rate at a constant strain of 60 %. At higher shear flow temperatures, slower kinetics occured until the effect of the applied shear flow was lost. Many investigations suggest that the application of a flow field at temperatures above the nominal melting temperature (T_m) can still enhance the crystallisation rate. [66, 77, 79, 87-88] The enhanced crystallisation rate decreases with increasing residence time in the melt after flow. i.e. the flow induced precursors formed in the melt vanishes with temperature, which is evaluated using an Arrhenius activation law. [89-94]

A crucial function governing the overall chain dynamics in melt under shear is the relaxation behavior of the oriented chain segments. For the applied shear rate Keller et al. [68, 95] suggested the role of critical molecular weight M^* in the orientation of chain segments. Thus in the sheared polymer melt, while the chains longer than M^* will retain chain orientation after deformation, the short chains would relax to the random coil state as their relaxation times are short. Lagasse and Maxwell [96], reported that the enhancement in crystallisation kinetics for a polymer is more pronounced for high molecular weight samples during shear flow. Janeschitz-Kriegl and Eder [70] showed that the crystallisation of polymer was highly dependent on the concentration of long chains under shearing at a low degree of supercooling. According to Kornfield et al. [97], both crystallisation kinetics and orientation increased with increasing amount of long chains. They argued that the role of long chains in the shear-induced crystallisation is cooperative rather than a single chain event. Vleeshouwers and Meijer [98] further confirmed that in sheared polymer melt, crystallisation behaviour is highly sensitive to molecular weight (M_w) and molecular weight distribution (MWD). In all studies under defined conditions, temperature played an important role as crystallisation rates are an exponential function of the under cooling.

Similar to the others, Yang et al. [77] and Somani et al. [99] also noticed that the degree of chain orientation is proportional to the fraction of high molar mass content. They attributed the enhanced nucleation after flow to coil-stretch transition of high molecular weight chains during the applied flow. The results are in accordance with Monte Carlo simulation experiments from Wang et al. [100] to study the athermal relaxation of bulk extended chains and the isothermal crystallisation in an intermediately relaxed melt. These studies are in agreement with in situ SAXS/WAXD studies performed by Agarwal et al. [101] on the role of long chain branched iPP in enhanced crystal orientation and improved crystallisation kinetics and further exhibiting improved melt strength, mechanical properties such as flexural modulus and tensile yield strength etc. Van Meerveld et al. [102], verified the formation of oriented (shish-kebab) structure with the rotational isomerisation of the high molecular weight tail of molecular weight distribution, namely a critical stretching of the chain, rather than simply enhanced orientation. Acierno et al. [103] related the development of oriented crystals on shearing and molecular weight dependence of the shear induced enhancement in the crystallisation kinetics to Weissenberg number *(Wi)*. In their studies, they reported that flow is not effective in enhancing crystallisation kinetics for $Wi < 1$ and does not strongly disturb the polymer chain conformation from its isotropic equilibrium state. Acierno et al further stated that spherulitic to rod like transition for the crystals only happens for much higher shear rates.

Nucleating agents also play a synergetic role in enhancing shear induced crystallisation of polymers by acting as point nuclei to form oriented crystals. [67, 104] Jain [105] showed that the flow-induced crystallisation of polypropylene/silica nanocomposites is faster compared to pure polymer. The increase in orientation was attributed to the locally increased stress due to the presence of particles. Conversely some studies [96] indicated that the presence of carbon black additive or a hetergeneous nucleating agent in propylene polymer does not play a significant role in shear induced crystallisation. Instead, they attributed the elastic chain extension due to entanglement couplings between molecules as the hydrodynamic origin of shear induced crystallisation. Spruiell et al. [106] claimed that addition of nucleating agent in copolymers leads to decrease in stress-level and polymer orientation at molecular length scale. Huo et al.

[107], with the aid of WAXD suggested that a high content of β-nucleating agent in iPP leads to the formation of β-form cystals. However, they commented on the shear dependence of β-form crystallinity where they observed increases in crystallinity with increase in shear rate upto a certain point and its decrease with further increases in shear rate.

1.4 Processing of polymers

Flow fields are often realised during processing of polymers, thus have an influence in the resultant morphology. Here we recall some of the salient features of polymer processing and link them to flow induced crystallisation. Processing refers to the conversion of polymers in to finished plastic parts and objects. During processing, polymers are heated and under finite deformations, macromolecules stretch, disentangle, and orient to form a final product after crystallisation. Depending on the processing operations and temperatures, the ultimate properties of the final product can be influenced. The processing operations [108] usually involve the use of extrusion, injection molding, film blowing, fiber spinning, blow molding, thermoforming, compression molding etc.

However, the processing behaviour of polymeric melts is highly dependent on several molecular features. For instance: The size of the molecule or its molar mass is one of the key functions. The relatively low molecular weight polymers ($M_w < M_c$, where M_w is molecular weight of polymer and M_c is critical molecular weight which signifies the onset of molecular entanglements) has simple proportionality between zero-shear viscosity and molecular weight. However, polymers with higher molecular weight ($M_w > M_c$) has rather strong dependence i.e. ($\eta_0 = M_w^{3.4}$). The difference is because of the ability of long chains to form entanglements that restrict flow during processing. The motion of chains within an entangled polymer melt is described by the reptation model. [109-110] In the reptation model, a polymer chain in the molten state (polymer melt) is considered to be surrounded by its neighbours, providing a virtual tube thus confining the pathway of the polymer chain to its own contour length. The chain dynamics in an equilibrium melt, arising from Brownian motion, is consequently a snake-like motion

(reptation) of the polymer chain. The constraint chain dynamics give rise to a characteristic time for a chain to diffuse one tube length, that scales (and thereby the zero-shear viscosity (η_0)) with $M_w^{3.0}$. The experimentally observed discrepancy, $\eta_0 \sim M_w^{3.4}$ from the 3.0 dependence is attributed to "contour-length fluctuations" i.e. fluctuation-driven stretching and contractions of the chain along the tube. [111]

These basic restrictions cause increase in melt viscosity thus making high molecular weight polymers rather intractable via conventional processing routes. However, final properties such are toughness, strength and wear increase with molecular weight. Such superior properties are essential to meet requirements for highly demanding applications.

1.5 Importance of Nanoscale fillers

The primary reasons for adding fillers to polymers are to improve their mechanical performance and speed up processing rates. For example, the addition of high-modulus fillers increases the modulus and the strength of a polymer. On contrary to fillers with micrometer size, well-dispersed nanofillers can improve the modulus and strength and maintain or even improve ductility because their small size does not create large stress concentrations. The surface area/volume ratio (A/V) plays important role in understanding the structure-property relationship in nanocomposites. The reduction of particle size from micrometer to nanometer changes the ratio by three orders of magnitude. This leads to increase in interfacial area for nanofillers and hence the properties of composites are dominated by the properties of interface. The increase in interfacial area makes the dispersion of fillers more difficult due to the greater tendency to agglomerate as a result of large contact surfaces. The potential effect of nanofillers is on the modulus, failure stress/strain, toughness, glass transition and wear behaviour of polymers. The nanoscale fillers constrain the mobility of the polymer chains as well as their relaxation spectra, which can change the glass transition temperature and modulus of matrix. Nanofillers can also change the degree or type of crystallinity in a polymer which changes the modulus.

Unlike isolated SWCNT, multi-walled carbon nanotube (MWCNT) has a low modulus and low crystalline quality. Hence, MWCNTs are not suitable for application involving high-performance polymer fibers. Bower et al. [112] showed that MWCNT buckle under a compressive strain of about 4.7 % and that this buckling is reversible under very large strains, probably due to the ability of the nanotubes to slide within each other. Many studies showed the effect of nucleating agents like 1,3:2,4-bis(3,4-dimethylbenzylidine)sorbitol (DMDBS) on crystallisation behaviour of isotatic polypropylene (iPP). [113-114] DMDBS is a chiral molecule that can self-assemble into fibrillar structures due to hydrogen bonding. Hydrogen bonding proceeds in one direction and drive the molecules to pile up. This leads to unidirectional growth of fibrillar crystals. DMDBS fibrils have diameter of ~10 nm and length up to several microns. They can also form bundles with diameter up to 100 nm. Crystallisation in DMDBS in iPP matrix corresponds to a liquid-solid phase separation. However, it was found that in order to have significant effect on crystallisation under shear, DMDBS must undergo dissolution in polymer matrix at high temperatures to form homogenous solution. [113]

1.6 Applications and properties - Zirconia versus SWCNTs

Zirconia is classified as zero dimensional (nanosphere). Zirconia has been widely used for their excellent mechanical and wear resistant properties. [115-116] The superior properties, hardness, strength and toughness together with chemical stability can be beneficial in adhesive and abrasive wear conditions. However, due to sensitivity of zirconia to aqueous environment at 200 °C which enhances the transformation process, the reduction in tetragonal zirconia with temperature can be perceived. The zirconia performs well in sliding wear because of smearing of surface which gives very smooth finish. Zirconia blades have been commonly used in paper industry due to their corrosion resistance. Zirconia wire drawing dies and hot extrusion dies have been found to posses the superior compared to conventional dies particulary in finishing runs where good dimensional tolerance and a high surface quality are required. Seals in valves, chemical and slurry pumps are also being made of zirconia ceramics. One of potential application of zirconia is in the automotive industry, particularly in engine parts. The low thermal conductivity of zirconia is useful for components such as piston crowns, head face plates

and piston liners. It results in reduction of heat loss from combustion chamber, wear and increased engine efficiency and life. Zirconia is also used as a biological implant material to replace worn joints due to its excellent bio-compatibility.

The three polymorphs of zirconia (ZrO_2) have been well understood, the monoclinic, tetragonal and cubic phases, also the existence of high pressure orthorhombic have been reported. [117] The monoclinic phase is stable upto 1170 °C where it transforms to the tetragonal phase which is then stable upto 2370 °C and further cubic phase exist upto the melting point of 2680 °C. Garvie et al. [118] recognised the use of zirconia for improving strength and toughness by tetragonal to monoclinic phase transformation of metastable tetragonal particles due to presence of stress field ahead of crack. If ZrO_2 is finely divided or constraining pressure is exerted on it by the matrix, the zirconia particle can be retained into metastable tetragonal form. In principle, the tetragonal to monoclinic transformation generally occurs on cooling ZrO_2 from above 1200 °C to room temperature.

The mechanism of toughening is commonly known as stress induced transformation of metastable tetragonal particles to the monoclinic form. If a crack is extended under stress, the large tensile stresses are generated around the crack near crack tip. These stresses release the matrix constraint on the tetragonal zirconia particles and could lead to net tensile stress on the particles which under the new condition will get transformed to monoclinic symmetry. Thus the martensitic reaction is caused due to development of volume expansion and shear strain in the particle and resultant compressive strain gets developed in the matrix. As this occurs in the region surrounding the crack, extra work is required in order to move the crack through the ceramic hence resulting in the increase in toughness and strength. Figure 1.6 shows the stress-induced transformation toughening of zirconia particles under elastic stress field.

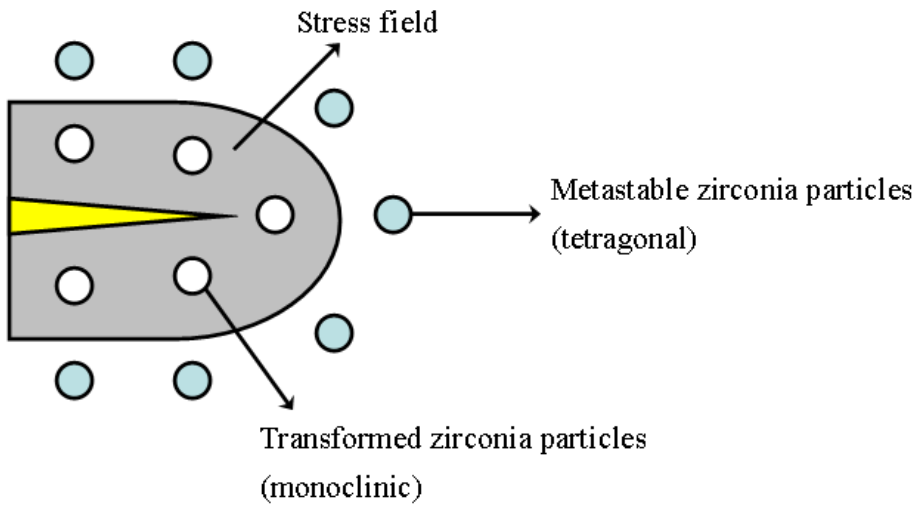

Figure 1.6: Stress induced transformation toughening of zirconia particles under elastic stress field.

Thus there exists a critical particle size range for zirconia. It depends on the composition of zirconia and matrix constraint. Below this critical particle size transformation of tetragonal particles by stress do not occur. Above critical particle size, the transformation is spontaneous. Hence, transformation takes place within a particular size range. These concepts in ceramics could be realised in a polymer composite, when a hard particle such as zirconia is embedded in the viscoelastic polymer matrix. For example, the polymer Ultra High Molecular Weight Polyethylene (average molar mass greater than a million g/mol) oriented in the uniaxial direction, having high modulus and high strength, is used in hard ballistic applications such as body armours and helmets. The polymer properties change from elastic to viscous with decreasing velocity of the projectile after impact, a concept that has been expalined by Deborah number later in this thesis. The strong elastic properties of the polymer, at the very initial stages of the projectile on impact, help in its fragmentation. The presence of zirconia that tends to phase transform on impact in the polymer matrix could be advantageous to absorb stress. Such composites could provide a possibility of much needed weight reduction in body armour.

SWCNT represent the ideal, most perfect, ordered carbon fiber, the structure of which is classified as one-dimensional (cylindrical or tube). SWCNTs are a distinctive

class of molecules that exhibit unique mechanical and electrical properties. Since the discovery of SWCNTs, numerous applications have arose in a wide variety of scientific disciplines such as electronics (wires, transistors, switches, interconnects, memory storage devices), opto-electronics (light-emitting diodes, lasers), sensors, field emission devices (displays, scanning and electron probes/microscopes), batteries/fuel cells, fibers, reinforced composites, medicine/biology (fluorescent markers for cancer treatment, biological labels, drug delivery carriers), catalysis and gas storage. [119]

The modulus of nanotubes may be significantly higher than that of any graphite fiber, and therefore, they have the potential to yield higher composite moduli at the same filler volume fraction than a graphite fiber composite. The mechanical resistance of SWCNT is due to one of the strongest bonds in nature. Because of their flexibility, SWCNT can be bent repeatedly up to 90° without breaking or damaging them. The exceptional mechanical properties, tensile strength, low density, and high aspect ratio of SWCNTs find two different applications: the strengthening of fibers in high-performance composite materials, replacing standard C fibers, Kevlar, and glass fibers; and as probes for scanning tunneling microscopes (STM) and atomic force microscopy (AFM). Fibers and yarns are among the most promising forms for using nanotubes on a macroscopic scale, mainly because, in analogy to high-performance polymer fibers, they allow nanotubes to be aligned and then woven into textile structures or used as cables. [120]

SWCNT are assembled as ropes or bundles. The modulus of SWCNT can be realised only when individual SWCNTs are isolated from the bundles and/or the bundles are small enough that matrix is in contact with each one. To maximise their interaction in a polymer matrix, they need to be chemically modified and separated from the bundles. One way to increase the chemical activity is to use an SWCNT with a smaller radius of curvature. A second method is to add functional groups to the ends of SWCNT. Carboxylic groups have been linked to SWCNT ends, and then the SWCNTs have been tethered to nanoparticles via thiol linkages. SWCNTs have been placed in solvent through the addition of octadecylamine groups on the ends and a small amount of dichlorocarbenes on the sidewalls. The first successful method for adding functional groups to the sidewalls involved fluorination at elevated temperatures. The tubes could then be solvated in alcohols and reacted with other species, particularly strong

nucleophiles such as alkylithium reagents. A simpler route based on a process used on other carbon species was developed, in which an aryl diazonium salt was reduced electrochemically, resulting in a free radical that can attach to the carbon surface of small diameter tubes. [121]

The most exciting development in terms of composites, however, is the dissolution of full-length SWCNTs that have been separated from the bundles. The separation of SWCNTs from the bundles can be achieved by dispersion in appropriate solvents with or without the aid of a surfactant and/or by choosing an appropriate synthesis method. A polymer chain can then be attached to a bonding site by sonication, plasma activation, chemical etching of the tube ends, or chemical adsorption. Some evidence suggests that polymers can be patterned by the nanotube surface, providing a method for templating polymer structures near the surface. [120]

In this thesis, to explore the influence of aspect ratio on the orientation of polyethylene chains under defined flow conditions, chain orientation in the presence of spherical zirconia particles is compared with anisotropic SWCNTs. Though the interfacial energies between the chosen nanoparticles are different, the ease in homogenous dispersion of zirconia over carbon black has been of immense advantage. Experimental observations on the two nanoparticles are summarised in chapter 5 of this thesis.

1.7 Outstanding issues

The modern availability of sensitive experimental techniques using synchrotron beams for investigation of the mechanism of polymer crystallisation has stimulated current interest and unveiled various issues while at the same time leaving some unsolved issues open to answer. In flow induced crystallisation, the morphology of semicrystalline polymer in the final product and therefore its properties strongly depends on the polymer crystallisation from flowing melt. However, the past models in flow fields and simulation experiments consider Avrami equations [122-124] as a function of deformation history obtained by invoking the rates of nucleation and growth or consider Flory's model [59] obtained by relating the decrease in entropy of the melt during deformation to the

increase in apparent undercooling or changing rate of crystal growth in Hoffman's kinetic model. [125] Hence, these models do not provide adequate understanding at molecular length scale between flow and crystallisation. [126] They do not explain the enhancement of crystallisation rates due to flow induced orientation of chains.

Keller and Kolnaar [68] in their rheological studies attributed the enhanced nucleation to the coil-stretch transition of high molecular weight chains in the melt. In response to their theories, Hsiao et al. [64] using SAXS/WAXD techniques related the formation of a shish-kebab crystalline structure with the coil-stretch transition of high molecular weight chains which act as oriented nuclei. Both models differ from the model proposed by Janeschitz-Kriegl [127] which suggests that athermal nuclei are formed only in a certain characteristic temperature range where less ordered structures are expected. However, no direct evidence for coil-stretch transition in flow field experiments for linear polymers exists. Lieberwith et al. [128] have shown that shish formation in melt experiences extensional flow which tends to grow adjacent to the quiescent regions that did not experience the flow. They attributed this phenomenon to the mechanism in which polymer chains are reeled into the growing tip of shish since it propagates in quiescent regions. However, these finding are in disagreement with the recent investigations by Kumaraswamy et al. [129] who found that shish growth ceases after cessation of shear flow.

The presence of nanoparticles usually improves the elastic modulus and optical properties along with ease in processability, in terms of decrease in viscosity. It is currently believed that local and chain dynamics are greatly affected by the polymer-surface interactions. Polymer nanocomposites include three phases; *viz.* matix, matrix-filler interface and reinforcing filler. It is understood that the partial reduction of average molecular weight results from interaction with fillers. However, any change in atomic structure or configuration of polyolefins requires systematic study. Further, nanoparticle-matrix interface governs structural characterization due to its role of interaction zone in deformation and fracture at microscopic level. Sufficient understanding of the interaction zone is a prerequisite. Recently, Zhang et al. [130] and Jain et al. [131] found that viscosity of polymer decreases in the presence of nanoparticles. They have attributed this effect to the molar mass and molar mass distribution of the polymer matrix. However,

this is yet to be resolved since there is no solid evidence for its occurrence and it is a subject of detailed investigation.

1.8 The objectives of thesis

Polyethylene being a commodity polymer is of considerable industrial interest. The degree of crystal morphology and crystallinity both affect the mechanical properties of polyethylene materials. The mechanical properties of of semi-crystalline polymers improve with increasing the amount of long polymer chains that function as 'tie-molecules' between crystals. A preferred molecular orientation in a produc enhances the properties in the orientation direction, while properties in perpendicular direction are reduced. An extreme application is fiber spinning process of HPPE (High Perfomance Polyethylene Fibers) where all molecules are aligned along the fiber. In this context, shish-kebab structures are of prime importance because it is structural origin of ultra-high strength and ultra-high modulus fiber. The rationale of the study is to understand the influence of high molar mass component in the polyethylene during flow and thorough monitoring of structure development under shear. The end product properties are influenced considerably by the crystallisation process. To achieve the desired properties, fundamental study of crystallisation behavior and the condition at which the highly oriented structures can be obtained is a prerequisite. Hence, a given polymer system can be exploited by a combination of suitable molar mass, molar mass distribution and nanoparticles under appropriate thermal and shear conditions. The goal of study is to enhance the shish-kebab structure formation in presence of nanoparticles. The study may extend the use of nanoparticles in polyethylene to achieve high-modulus fibers. The research involves the use of polyethylene having broad molar mass distribution and two types of nanoparticles (*viz.* single walled carbon nanotube (SWCNT) and zirconia) which are physically dispersed in the PE matrix.

The specific objectives are,

a) To investigate the influence of molar mass and molar mass distribution on the formation of oriented structures.

b) To study the influence of chain-particle interactions of nanoparticles with polymer chains in the melt state under defined flow conditions with the help of time resolved X-ray scattering techniques.

c) To understand the chain dynamics for determination of the viscoelastic response of the polymer in the presence of nanoparticles with the aid of rheology.

d) To understand the crystallisation kinetics of polyethylene in the presence of nanoparticles in quiescent conditions with the help of rheometry and DSC.

Chapter 2

Influence of shear in the crystallisation of polyethylene in the presence of SWCNTs

The aim of this chapter is to demonstrate that even in quiescent conditions and relatively low shear rates, the presence of single-walled carbon nanotube (SWCNT) accelerates the crystallisation kinetics of polyethylene (PE). The influence of SWCNTs on the crystallisation kinetics in the quiescent condition is followed with the help of rheological and DSC studies. The flow effects on the stretch of long chains of PE are probed using time-resolved X-ray scattering (SAXS) and are verified using the Deborah number. The SAXS data indicate that strong shearing conditions (shear rate greater than 50/s for 1s) are required to form shish-kebab structure in the neat polymer. However, the shish-kebab structure formation is enhanced on the addition of SWCNTs at low shear (50/s for 1s). The development of oriented structures in SWCNTs/PE composites and their absence in the neat polymer under low shear rate indicates that the SWCNTs play a significant role in the formation of shish-kebab along with the applied shear rate. Overall, the results illustrate the influence of SWCNTs on the chain relaxation of polymer.

2.1 Introduction

Carbon nanotubes [132] (CNTs) offer excellent mechanical [133], electrical [134-135] and thermal [136] properties to polymer materials [137-139] due to their high aspect ratios (~1000). CNTs have potential to suppress the nucleation barrier for polymer crystallisation. [140] Several studies have conclusively demonstrated the influence of SWCNTs on the resultant morphology of the polymer. [141-145] Recent studies based on rheometry showed that CNTs act nucleating agents for polyethylene chains and enhance the crystallisation kinetics. The adsorbed chains on CNTs influence the mechanical properties and molten state of the polymer. [146] Trujillo et al. [147-148] supported a single site catalyst on CNTs and investigated the nucleating effect of CNTs on the thus polymerised polyethylene. They showed the development of bottle brush morphology around CNTs. Shish-kebab structures [8] induced by SWCNTs for the nanocomposites based on polyethylene have been widely reported. [130, 149-150]

It is generally believed that flow plays important role in extension of polymer chains to form the highly anisotropic oriented structures. [68, 70] The final morphology of polymer and the physical properties [151] depend on the way in which the polymer crystallises from the sheared melt. The simulation studies [152] revealed the existence of two distinctive morphologies in a polymer having broad molar mass distribution; while the chain segments in the long chains get extended to crystallise into shish, the short chains lead to chain folding to form kebabs on crystallisation. Hsiao and coworkers [64, 77, 153-156] have used small angle and wide angle X-ray scattering techniques (SAXS/WAXS) to investigate the role of the high molar mass tail on the formation of anisotropic structures under shear in polymer melts. They observed the formation of fibrillar shish structures due to the scattering in the equator after the application of shear and further development of kebabs from the shish as indicative of scattering in the meridian. However, the molecular contribution of short and medium chains in the shish formation was also found to be significant. [157]

Using rheology, the polymer chain dynamics, onset and development of crystalline structures under shear have been commonly investigated in the past few decades. [86, 96, 98] The enhancement of crystallisation kinetics for polymer melts is observed only above the critical shear rate and is a result of high molecular weight

component. [96, 158] Van Meerveld et al. [102], have reported that with the increase in deformation rate, polymer chains initially in the equilibrium conformation are stretched to an extent that Gaussian statistics are no longer applicable to chain conformation. They stated that the resultant rotational isomerisation of the high molar mass tail in the non-Gaussian state plays a major role in the formation of shish structures above the critical stretching of the polymer chain.

However, the effect of nanoparticles on shish-kebab morphology is unresolved. The flow induced studies in nanotube filled polymer materials suggest that the nanometric cross-section of nanotubes (i.e. critical size of SWCNTs with L/D = 500, having L = 500 nm and D = 1 nm) facilitates the deformation under flow. [159] According to Jerschow and Janeschitz-Kriegl [67] the nucleating agents act as point nuclei for the growth of oriented precursors under flow to form oriented crystals. These studies are in accordance with the findings from Somwangthanaroj et al. [160], who used organically modified nanoclay and reported a significant increase in the crystallisation kinetics under flow. According to them, the nanoclay modifies the local stress levels and the orientation of iPP and further enhances crystallisation. However, studies from Garcia-Gutierrez et al, suggest the minor effects of shear on crystallisation kinetics and the orientation level in crystallised poly (butylene terephthalate)/SWCNT nanocomposites. Nevertheless, the effect of SWCNTs to counterbalance nuclei relaxation by providing surfaces has been proposed. [161]

The purpose of this chapter is to study the role of single walled carbon nanotubes (SWCNTs) on crystallisation kinetics of linear polyethylene. The novelty of using SWCNTs coated PE in this study is to show that even small concentrations of SWCNTs under low shear are capable of accelerating rate of crystallisation and able to suppress the nucleation barrier for polymer crystallisation. The significance of shear rates on chain orientation and Deborah numbers in the early stages of polymer crystallisation is reported. Furthermore, to investigate the effect of SWCNTs and shear rates on the formation of oriented structures at low temperature, the structure formation after application of low shear rate in the melt is probed in SWCNTs/PE composites.

2.2 Experimental Section

2.2.1 Materials

The linear PE used in the present study was specifically synthesised and supplied by Dow Benelux B.V., The Netherlands in the powder form obtained through the slurry process, polymerised using a Zeigler-Natta catalyst. The polymer consists of very broad molar mass distribution. The molecular weight information of PE, obtained using gel permeation chromatography (GPC) was supplied by Dow Benelux B.V. The detailed information regarding the molar mass and molar mass distribution determined through GPC and thermal characterisation through differential scanning calorimetry (DSC) is reported in the Table 2.1,

Table 2.1: GPC and DSC characterisation of polyethylene

GPC data				DSC data				
M_w (g/mol)	M_n (g/mol)	M_z (g/mol)	PDI	T_m (°C)	T_c (°C)	$T_{m\text{-}on}$ (°C)*	$T_{c\text{-}on}$ (°C)*	X_c (%)
246,000	10,100	1,184,000	24.2	129.5	119.3	120.1	120.4	66.0

* $T_{m\text{-}on}$ and $T_{c\text{-}on}$ are the onset temperatures for the melting and crystallisation

The single walled carbon nanotubes (SWCNTs) of high purity grade with less than 15% ash content having high aspect ratio (L/D>>1) were obtained from Unidym Inc., USA. The SWCNTs were obtained by high pressure CO conversion (HiPCO) method. This method consists of metal catalyst which nucleates SWCNT at high temperature and pressure. SWCNTs obtained by this process have excellent structural integrity. SWNCTs are achiral (arm-chair) type which is supposed to play key role in polymer deformation under tension due to reversible diatomic interchange. This results in structure having two pentagons and two heptagons in pair, commonly known as "Stone Wales transformation". [162] The SWCNT diameter ranges between ~0.8-1.2 nm and length ranges between ~100-1000 nm.

2.2.2 Determination of molecular weight and molecular weight distribution

The molecular weight (M_w) and molecular weight distribution (MWD) were determined using rheometry. The oscillatory shear mode was applied to PE sample within the frequency spectrum of 100 to 0.01 rad/s at 160 °C. Log-normal method which mainly makes use of crossover modulus was utilised to determine the molecular weight of PE. The determination of molar mass and molar mass distribution using crossover modulus based methods, explained in detail elsewhere, and could be applied in this study. [163] However, Wu et al [164] and Nobile and Cocchini [165] proposed a better approach that involves the use of terminal crosspoint of G′and G'' ($G_x = G' = G''$ at angular frequency, $\omega = \omega_x$). The method proposed by Wu et al relates the ratio between the crossover modulus and plateau modulus to polydispersity using equation 2.1

$$\log\left\{\frac{G_N^o}{G_x}\right\} = 0.38 + \left\{\frac{2.63\log\left(M_w/M_n\right)}{1+2.45\log\left(M_w/M_n\right)}\right\} \tag{2.1}$$

Where, G_x is the crossover modulus, M_w/M_n should not exceed the magnitude of 3. Whereas Nobile and Cocchini considered M_z/M_w ratio to modify the equation 2.1, to get the accuracy as demonstrated in the form of the equation 2.2

$$\log\left\{\frac{G_x}{G_N^o}\right\} = \left\{\frac{-0.524 + 0.341\log\left(M_w/M_n\right) - 1.843\log\left(M_z/M_w\right)}{1 - 0.559\log\left(M_w/M_z\right) + 0.841\log\left(M_z/M_w\right)}\right\} \tag{2.2}$$

However, it is to be noted that the equations above cannot provide the exact values due to consideration of some approximations. The molecular weight and molecular weight distribution, determined using the plate-plate rheometer, is represented in figure 2.1. The log-normal method is used for the determination of MWD in the present study. The detailed results are listed in the inset of the figure 2.1

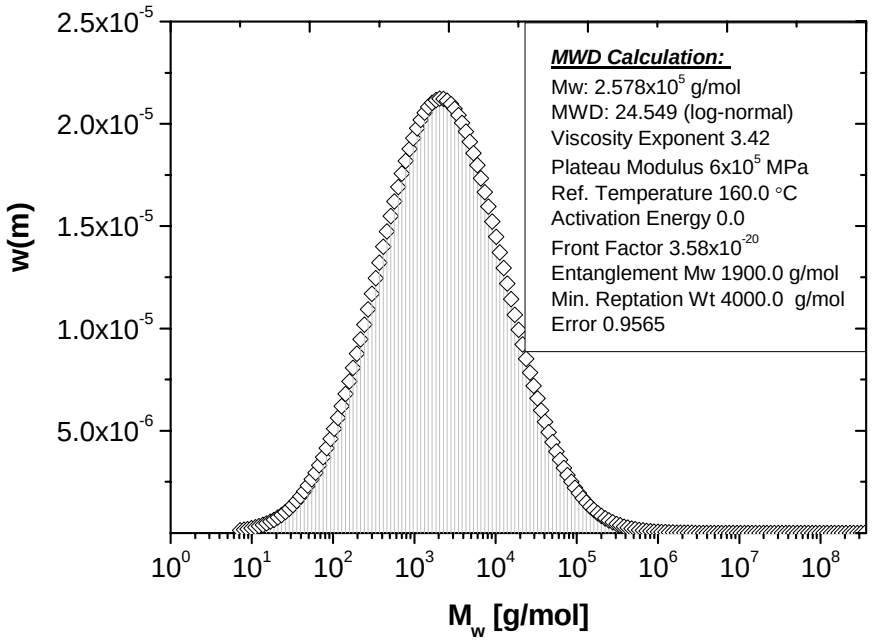

Figure 2.1: The representation of log-normal distribution of molar mass and molar mass distribution obtained using rheometry.

2.2.3 Dispersion of SWCNTs in water and preparation of SWCNT/ PE composites

An aqueous suspension of SWCNTs was prepared using surfactant as reported in literature. [130, 166] 20 ml of de-ionised water containing 0.04 g (0.2 wt %) SWCNT's and 0.2 g (1 wt %) of sodium dodecyl sulfate (SDS) surfactant was sonicated for 45 min. at room temperature (20 °C) and then centrifuged at 3000 rpm for 20 min. More than 95 % of suspended SWCNTs were sprayed uniformly on the polyethylene powder. The powders were mixed thoroughly to ensure the uniform adsorption of SWCNTs on PE powders. The PE adsorbed on SWCNTs was dried for 12.0 hours at 60 °C in vacuum oven. The flat disk-like polymer films were prepared by compression molding at 160 °C for 5 min. The thickness of 400 μm and diameter of 30 mm was utilised for the X-ray measurement, while, the polymer disks of 1 mm thickness and 12 mm diameter were used for rheological measurements. All the samples were mixed with Irganox 1010 to avoid the possible degradation while measuring.

2.2.4 Scanning electron microscopy (SEM)

The scanning electron microscopy (SEM) images of PE and SWCNTs/PE composites were obtained using a field emission gun scanning electron microscopy instrument (FEGSEM, LEO 1530VP). The voltage of 5.00 kV was used to observe the polymer morphology. The dried PE powder coated with and without SWCNTs was placed on specimen holder using double-sided carbon conductive tape. Samples were gold coated to enhance the contrast on the PE surfaces.

2.2.5 Rheometry

Isothermal crystallisation experiments were performed using rheology. Advanced Rheometric Expansion System (ARES) with parallel plate geometry, the diameter of 8mm under nitrogen atmosphere was used in small amplitude oscillatory shear mode, for the experiments. The compression molded, SWCNT coated PE samples placed between two parallel plates were left in a quiescent condition at 160 °C for 10 min. to remove any crystalline history. The samples were cooled from 160 °C to isothermal crystallisation temperature of 125 °C at 5 °C/min, before starting dynamic time sweep to follow the time evolution of storage modulus, G'. The constant strain $\gamma = 0.5\ \%$ and frequency $\omega = 10$ rad/s was used for the measurements.

2.2.6 Differential scanning calorimetry (DSC)

Thermal measurements were performed using differential scanning calorimetry (DSC) on TA Instruments Q2000, calibrated with indium under ultra-high purity nitrogen atmosphere having a purge rate of 50 ml min^{-1}. Samples of 1.0 to 1.5 mg mass were weighed on a Mettler-Toledo XS3DU precision balance and placed in the Tzero aluminum pans. The crystalline thermal history was erased by heating the samples at 160 °C for 5 min. The controlled rate of 10 °C/min was employed during measurements to determine the melting temperature (T_m), heat of fusion (ΔH_f), crystallisation temperature (T_c) and crystallinity (X_c). The degree of crystallinity was determined by normalising the observed heat of fusion of the sample to that of heat of fusion of 100 % PE crystal (~293 J/g) [167]. For isothermal crystallisation kinetic experiments, the

samples were heated to 160 °C and left in the melt for 5 min, to erase previous crystalline thermal history. The samples were quenched to the selected isothermal crystallisation temperature at the controlled cooling rate of 50 °C/min. The samples were kept at isothermal temperature (123 °C and 124 °C) for 60 min.

2.2.7 Time resolved small angle X-Ray scattering (SAXS)

Flow induced crystallisation (FIC) experiments are performed at DUBBLE/BM26B, European Synchrotron Radiation Facility (ESRF), Grenoble, France using time-resolved small angle X-ray scattering (SAXS), with a beam energy of 10 keV. The beamline consists of a two dimensional (2D) gas filled detector having a resolution of 512×512 pixels and $260\ \mu m \times 260\ \mu m$ pixel size. The flow induced crystallisation experiments were carried out using a Linkam shear cell CSS 450 aligned on the beamline. The sample in the form of a flat disk-like was mounted between the two parallel plates of the shear cell. The quartz windows of the shear cell were modified by kapton windows to get the required scattering. The calibration of the shear cell was done with a precision having tolerance limit of 30 μm for proper contact of plates with polymer disks for desired application of shear. The wavelength of 1.24 Å and the sample to detector distance of 6.06 m was maintained in all experiments. A vacuum chamber in the BM26B beamline between the sample and detector was used for reduction of scattering and absorption from air as shown in figure 2.1. The 2D-SAXS patterns were acquired with an acquisition time of 10 s and dead time of 0.5 s to transfer the data followed by intensity correction of the primary beam and required absorption between the adjacent images. The length scale of the scattering vector (q) was 0.001-0.5 nm^{-1}. The scattering vector was $q = 4\pi \sin\theta / \lambda$, where, 2θ is the scattering angle. The 2D-SAXS patterns were integrated to obtain the integrated intensity as a function of scattering vector (q). The integrated intensity as function of time is defined as, $I_{SAXS}(t) = \int_{q_{min}}^{q_{max}} I(q,t)dq$, where q_{max} and q_{min} being the maximum and minimum of q values. The obtained intensity data is subtracted with intensity prior to the application of shear. The 400 μm thickness of the flat polymer disk was reduced to 200 μm in the shear cell, before application of shear to the polymer melt. The steady shear was applied on the

flat polymer disks mounted between the two parallel plates of the shear cell to follow the structure development in sheared polymer melts.

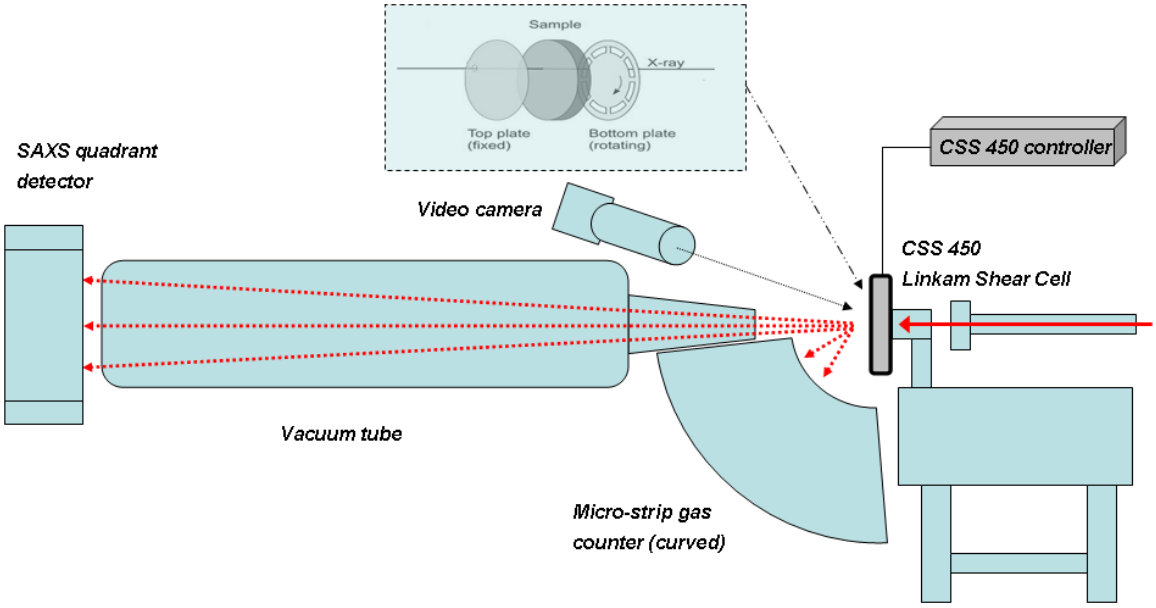

Figure 2.2: SAXS setup in DUBBLE/BM26 beamline used for the experiments. The sample to detector distance was 6.06 m. The whole setup is online connected to controllers in the hutch of BM26B.

The two different schemes used to understand the flow effects were, *Scheme-1:* Steady shear ($\gamma^{\bullet}$ = 100 s^{-1} and $\gamma^{\bullet}$ = 50 s^{-1} for the time duration, t_s = 1 s) at 136 °C followed by immediate cooling (10 °C/min) to room temperature. *Scheme-2:* Steady shear ($\gamma^{\bullet}$ = 50 s^{-1} and 100 s^{-1} for 1s) at isothermal crystallisation temperature of 136 °C, In this case, (a) the sample was heated to 160 °C from room temperature at a rate of 30 °C/min (b) the sample was kept at 160 °C in the melt for 5 min. to remove the melt history (c) the sample was cooled at the rate of 10 °C/min to isothermal crystallisation temperature of 136 °C The shear rate ($\gamma^{\bullet}$ = 50 s^{-1} for the time duration, t_s = 1 s) was applied at 136 °C. (d) holding isothermal for 600 s at 136 °C during experiment to follow the structure development under shear. (e) the sample was cooled to room temperature at a rate of 10 °C/min to monitor the crystallisation process with decreasing temperature.

The schematic representation of flow and thermal history applied during the shear experiment is shown in figure 2.3

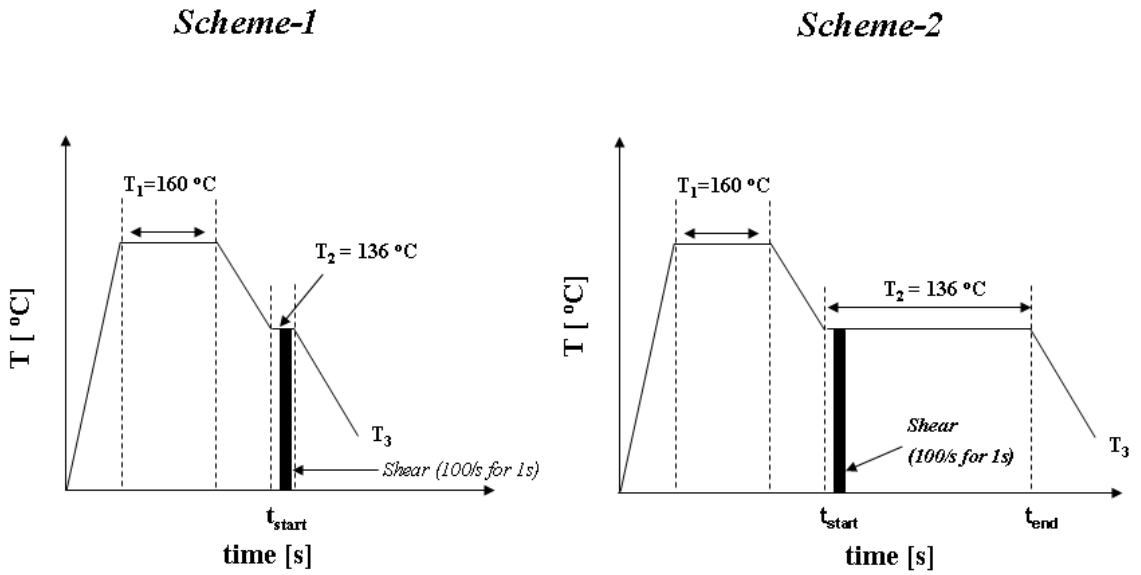

Figure 2.3: The schematic representation of flow and thermal application during shear experiments.

2.3 Results and Discussions

2.3.1 Morphology of SWCNT/PE composites

Figure 2.4 show the surface morphology of nascent PE and SWCNTs/PE composites. It is noticeable in the figure 2.4a that the PE powder has irregular surface. The average particle size of PE (~100 μm) having high surface energy, with irregular surface makes it suitable for SWCNTs to adsorb on the surface after spraying. The adsorbed small bundles of SWCNTs are clearly visible (~300 nm) in figure 2.4d.

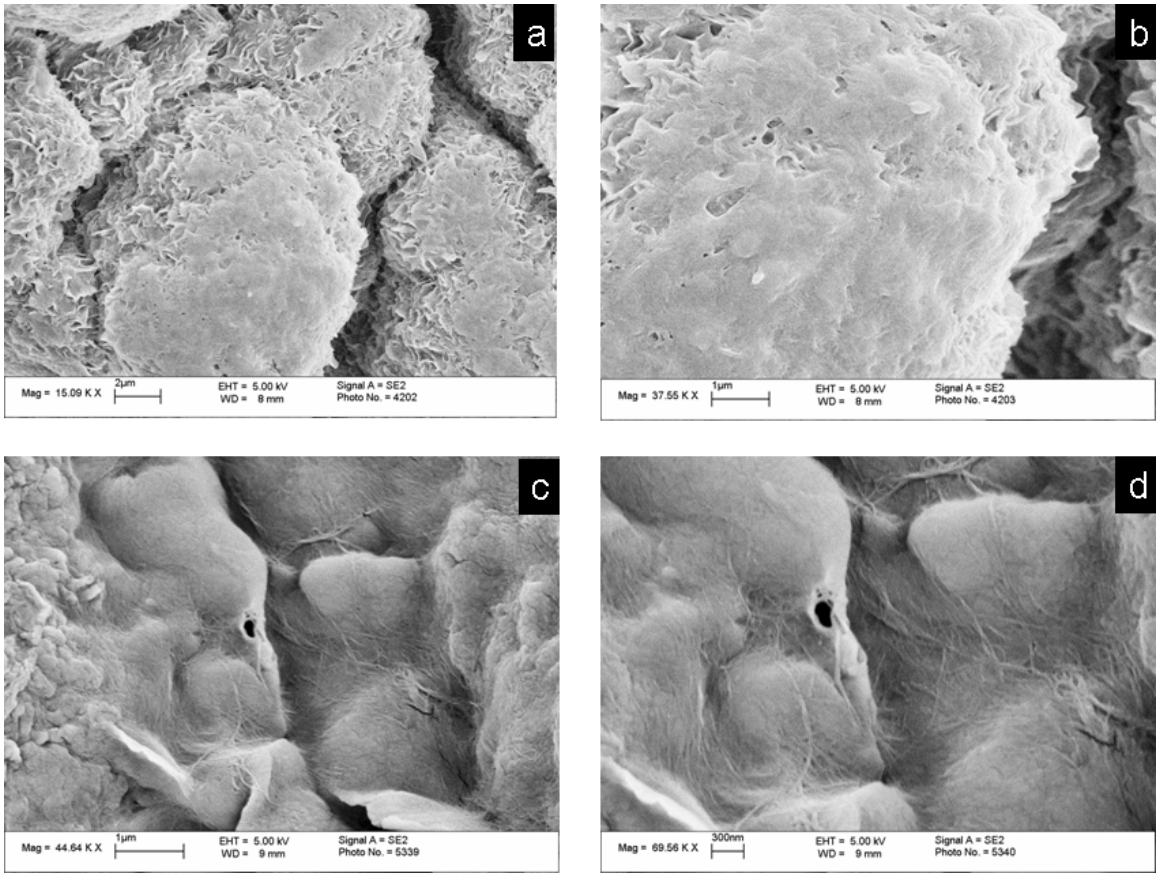

Figure 2.4: SEM images of the surface morphology of nascent PE powder - (a) at 2 µm (b) at 1 µm. Surface morphology of 0.6 wt% SWCNT coated PE powder -(c) at 1 µm (d) at 300 nm. The SWCNTs are adsorbed on PE surface by spraying uniformly dispersed aqueous suspension of SWCNTs.

2.3.2 Isothermal crystallisation of PE in presence of SWCNTs

The influence of SWCNTs during isothermal crystallisation of PE at 125 °C was investigated to understand the enhancement of crystallisation kinetics. Figure 2.5 shows the evolution of storage modulus, G', as a function of time. The onset of crystallisation occurs earlier with the increase in SWCNT content in PE. The quantitative information of time required for the early onset of storage modulus build up is shown in Table 2.2. The onset of crystallisation occurs almost 3 times earlier with 0.1 wt% SWCNT content in PE. The result suggests that the polymer chains are crystallised on the surface of SWCNTs and hence, the SWCNT surface acts as a nucleation site for crystallisation of PE.

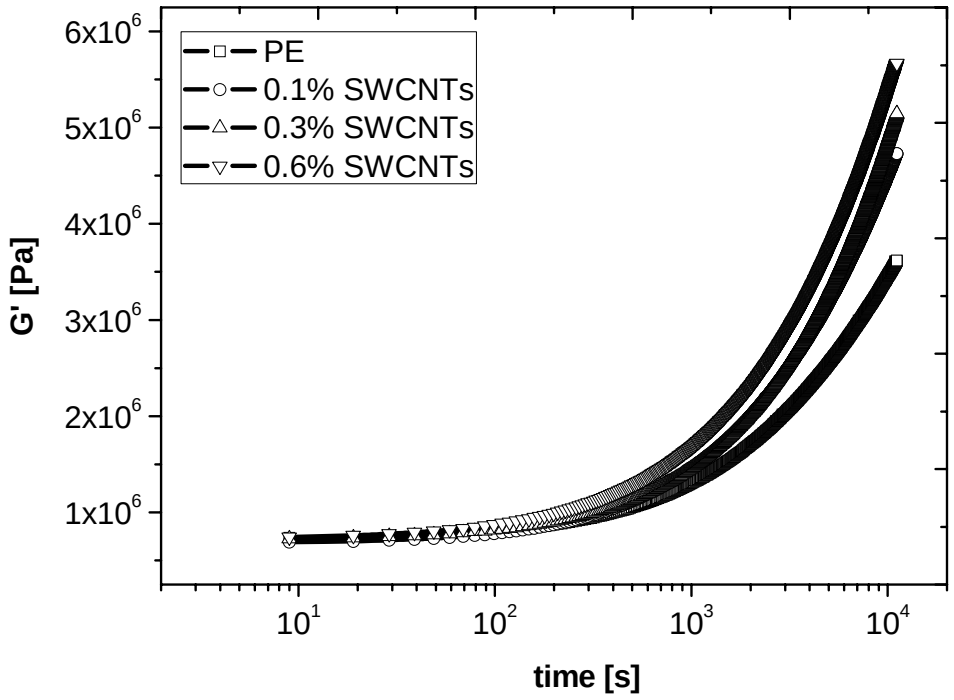

Figure 2.5: Isothermal crystallisation of PE in the presence of SWCNTs at 125 °C. The evolution of storage modulus, G', as a function of time at constant strain and frequency.

Table 2.2: Quantitative data of onset crystallisation time of PE in SWCNTs/PE composite obtained from figure 2.5

SWCNT content (wt %)	Onset of crystallisation (s)
0.0	**800**
0.1	**300**
0.3	**200**
0.6	**90**

Standard DSC results are shown in Table 2.1 for PE. The isothermal crystallisation experiments were performed using DSC at 123 °C and 124 °C to study the nucleation effect of SWCNTs on PE as shown in figure 2.6. The crystallisation peak shifts to a lower time with the increase in SWCNTs content in PE. The results were fitted [168] with Avrami equation [122-124] to describe the nucleation and growth process in SWCNT/PE

composites. Avrami equation [109-111] is used for characterising the dimensionality through Avrami exponent that can be written as,

$$\varphi_c(t) = 1 - \exp(-Kt^n) \tag{2.3}$$

Where, φ_c is relative crystalline volume fraction at crystallisation time t, K is overall crystallisation rate constant which defines the nucleation and growth, and n is Avrami exponent. The Avrami exponent relates the dimensionality and growth of crystals to the nucleation with respect to time. The value of n appropriate to systems with invariant nucleation and growth rates is dependent on the geometry of the growth. For a thermal heterogeneous nucleation n = 3 and a sphere-like crystal growth geometry is expected; for the same type of nucleation and n = 2 corresponds to a disk-like growth, and n = 1 corresponds to linear crystal growth. The sporadic homogenous nucleation and spherulitical growth is expected when n = 4. In literature it is considered that the line-like structures corresponds to 1D crystal growth, while circular lamellar-like structure corresponds to 3D crystal growth. The circular structures obtained in 2D crystal growth are due to thermal hetergenous nucleation where nuclei are being exhausted resulting decrease in nucleation rate and hence n decreases from 3 to 2 as observed in this study. [30] The values of exponent n for various types of nucleation and growth acts is summarised from the literature [169] as shown in Table-2.3

Table-2.3: The values of avrami exponent (n) for various type of nucleation and growth.

Growth habit	Homogenous nucleation				Heterogeneous nucleation
	Linear growth		Diffusion controlled growth		Linear growth
	Steady state	$t = 0$	Steady state	$t = 0$	
Sheaf-like	6	5	7/2	5/2	$5 \leq n \leq 6$
3D	4	3	5/2	3/2	$3 \leq n \leq 4$
2D	3	2	2	1	$2 \leq n \leq 3$
1D	2	1	3/2	1/2	$1 \leq n \leq 2$

It is believed that the rate at which crystallisation occurs is very important parameter for crystallisation kinetics. A measure of the rate at which crystallisation occurs at a fixed temperature is often referred as crystallisation half-time. Crystallisation half-time can be defined as time taken by sample to undergo half of the crystallisation when left at a given temperature indefinitely. [17]

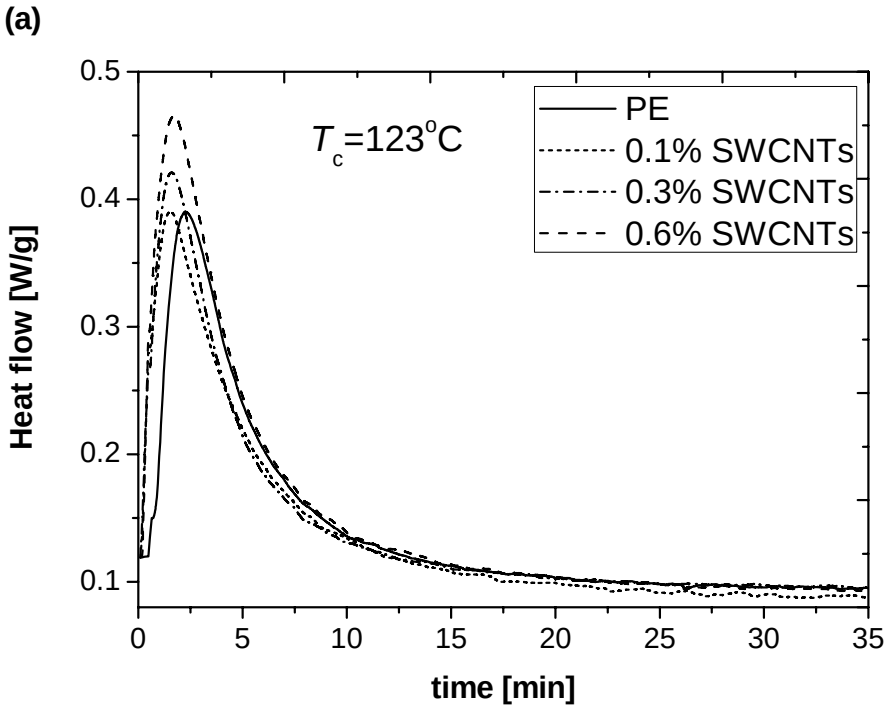

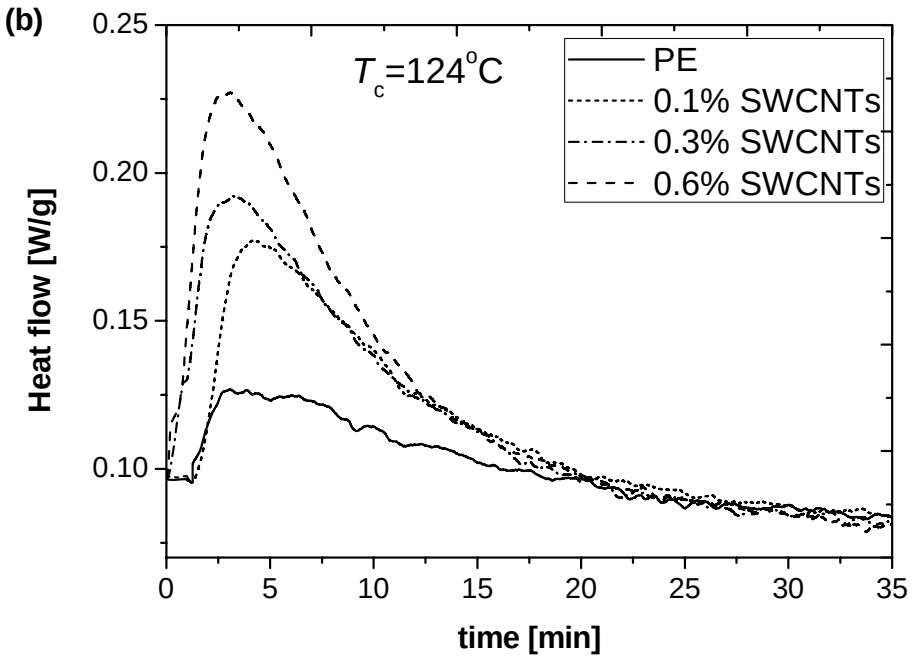

Figure 2.6: Isothermal crystallisation probed using DSC for the polyethylene in presence of different concentration of SWCNTs (a) at 123 °C (b) at 124 °C.

Figures 2.7a and 2.7b show the Avrami plots obtained after fitting the data to the Avrami equation for isothermal crystallisation temperature 123 °C and 124 °C. At both the isothermal temperatures (123 °C and 124 °C), the overall rate constant (as shown in Table 2.4) increases with the SWCNT concentration, hence, suggesting faster crystallisation due to presence of SWCNTs in PE. The Avrami exponents (*n*) for all samples are in the range ~2.0 to 2.4 which can be attributed to 2D-structures with instantaneous nucleation. As the density of nuclei is higher, the distance between two adjacent nuclei is not large enough to allow the 2D structures of lamellar stacks; as a result, it becomes difficult to form perfect spherulites. Moreover, the Avrami exponent decreases with the increase in SWCNT concentration as found in literature. [149] The decrease in Avrami exponent with increase in SWCNT content can be attributed to change in crystal growth and microstructure. However, considering the low concentration of SWCNTs, the disk-like growth of microstructures can not be neglected. Thus, increasing the SWCNT loading can significantly alter the morphology. It is anticipated that the microstructure of the PE crystallite changes to the disk shape due to nucleation

on the anisotropic SWCNT bundles, where SWCNTs provide good epitaxy matching to the PE chain.

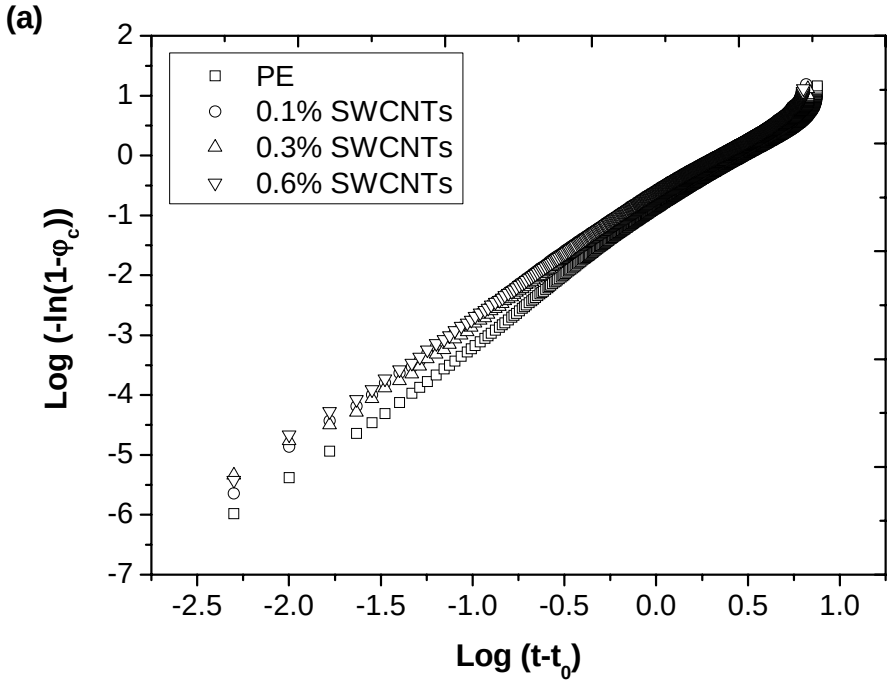

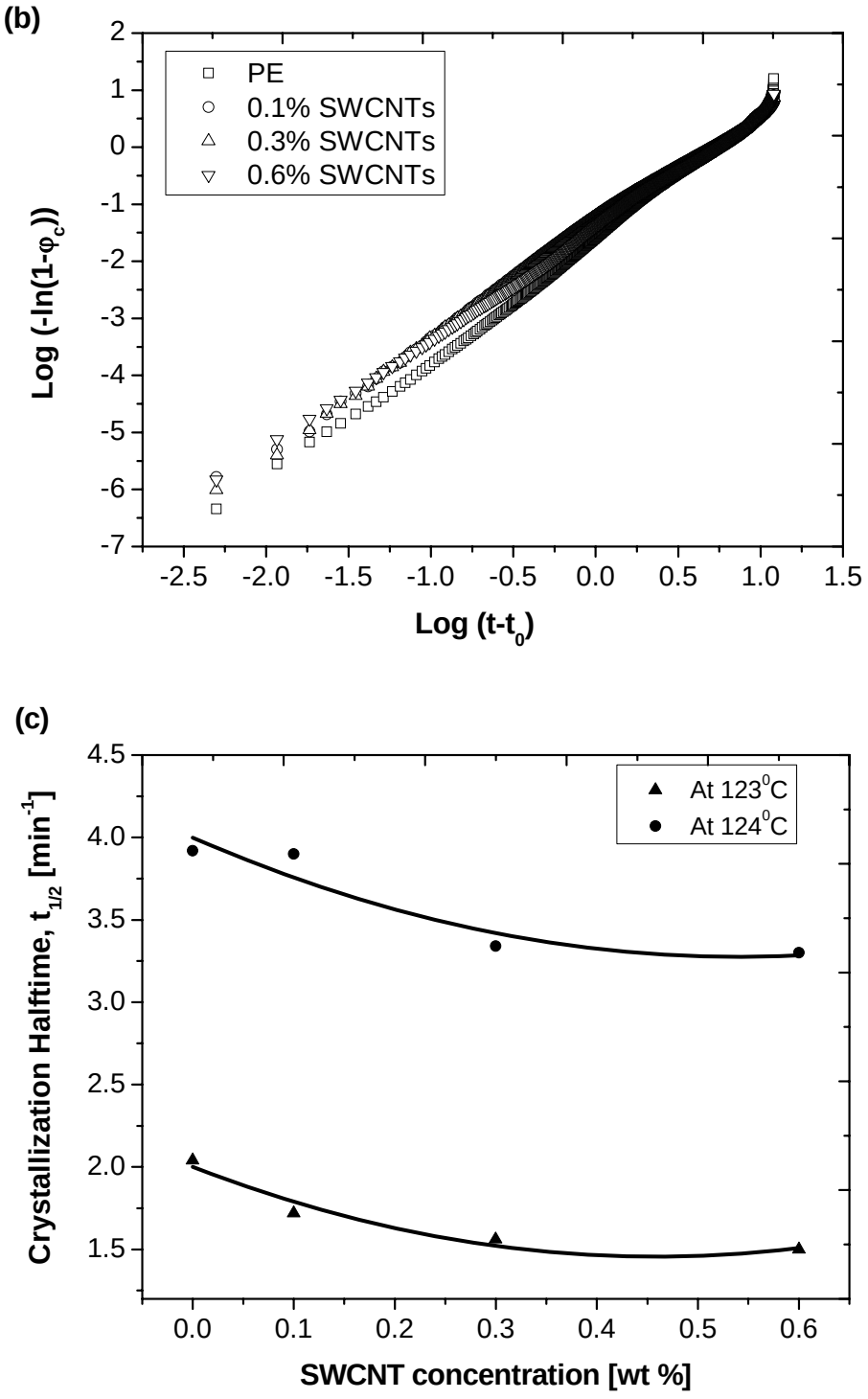

Figure 2.7: The Avrami plots obtained from the isothermal crystallisation of SWCNT/PE composites. (a) 123 °C, (b) 124 °C and (c) half time crystallisation as function of SWCNT content in PE for different crystallisation temperatures.

Figure 2.7c shows the crystallisation half time as a function of SWCNT content in PE. The halftime crystallisation decreases with increase in the SWCNT content in PE at the two crystallisation temperatures (123 °C and 124 °C). The results are consistent with the isothermal crystallisation experiments from the rheometry, where the onset of crystallisation time decreases by almost 3 times in the presence of 0.1 wt% of SWCNTs, suggesting the enhancement of crystallisation kinetics of PE due to the presence of SWCNTs.

Table 2.4: Values of Avrami exponent (n), half crystallisation time ($t_{1/2}$) and overall rate constant of crystallisation (K) from Avrami analysis during the isothermal crystallisation (123 °C and 124 °C) of PE and SWCNT/PE composites

SWCNT content (wt %)	T_c (°C)	n	K (min^{-n})	$t_{1/2}$ (min^{-1})
0.0	**123**	**2.27**	**0.138**	**2.04**
0.1	**123**	**2.19**	**0.213**	**1.72**
0.3	**123**	**2.16**	**0.265**	**1.56**
0.6	**123**	**2.14**	**0.280**	**1.50**

SWCNT content (wt %)	T_c (°C)	n	K (min^{-n})	$t_{1/2}$ (min^{-1})
0.0	**124**	**2.38**	**0.026**	**3.92**
0.1	**124**	**2.08**	**0.040**	**3.90**
0.3	**124**	**2.06**	**0.057**	**3.34**
0.6	**124**	**2.04**	**0.060**	**3.30**

2.3.3 Crystallisation on cooling in SWCNT/PE composites after application of shear

The experiments are performed following the scheme-1 described in section 2.2.7. After the application of shear ($\gamma^{\bullet} = 100\ s^{-1}$, $\gamma^{\bullet} = 50\ s^{-1}$ for $t_s = 1$ s) at 136 °C the SAXS data collected while cooling are depicted in figure 2.7. A comparison of the 2D-SAXS patterns acquired before the application of shear in each experiment shows an increase in diffused scattering with the increase in SWCNT content in the PE. On cooling after the application of shear ($\gamma^{\bullet} = 100\ s^{-1}$ for $t_s = 1$ s), the streak-like scattering due to the

presence of shish is observed at 134 °C, figure 2.8a. . The pattern collected at 134 °C showed weak scattering in the equator for neat PE. However, the presence of small or less shishes in the sample incapable of being detected by SAXS at 134 °C cannot be ignored. The SAXS pattern collected at 131 °C shows the emergence of scattering along the equator and the meridian indicating the presence of shish-kebab morphology. The streak-like scattering detected at 134 °C is predominant in the samples containing different amount of SWCNTs. The streak-like scattering along the equator increases with the increasing amount of SWCNTs. Around 131 °C the equatorial scattering increases and broadens, which is evident for 0.6 wt% SWCNT concentration. This suggests the occurrence of large anisotropic electron density fluctuations due to alignment of nanotubes in the flow direction. At 131 °C, the meridional scattering due to formation of kebabs increases. For the same applied shear and crystallisation conditions the intensity along the meridian increases with the increasing SWCNT concentration in PE. Hence, on cooling, with the crystallisation of shish that further enables the growth of kebabs the overall shish-kebab morphology is frozen. The patterns collected at 60 °C show the shish-kebab structures, where the intensity along the meridian increases with the increasing SWCNT concentration, so does the anisotropy. These results confirm the presence of enhanced shish-kebab structures in SWCNT/PE composites.

It is interesting to note that the small streak-like scattering in figure 2.8b, is detected in the equator at 134 °C even in samples sheared with $\gamma^{\bullet} = 50\ s^{-1}$ for $t_s = 1$ s at 136 °C. On cooling, at 130 °C after the applied shear, the development of anisotropic scattering in the meridian suggests the kebab formation. The anisotropic meridional scattering increases with the SWCNT concentration. The increase in meridional intensity with the increasing concentration of SWCNTs, for the same applied shear conditions, suggests an increased amount of shish formation with increasing SWCNT concentration, even if the presence of shish could not be detected along the equator. The SAXS patterns acquired at 60 °C, show the combination of isotropic (spherulites) and anisotropic scattering (shish-kebab). However, a substantial amount of isotropic scattering at 60 °C in neat PE could be explained due to (1) the fever chains that could be extended due to the applied low shear, (2) the presence of few shish-kebab structures, and thus (3) the presence of spherulites in between the few shish-kebab structures. Although, the

isotropic scattering increases with the increase in SWCNT concentration in PE, it is to be noted that shish-kebab structure formation is also enhanced. In the case of SWCNT/PE composites, considering the length of individual nanotubes and their high characteristic ratio compared to the flexible PE chains, the low shear would be capable of aligning the bundles of SWCNTs in the flow direction. However, under low shear, only a few SWCNTs are likely to align along the flow direction, providing perfect epitaxial growth of low molar mass chains and thus enhanced shish-kebab structures. Thus the isotropic scattering in SWCNT/PE composites under low shear may be attributed to (1) SWCNT bundles which are not perfectly aligned in the flow direction and are spread in the PE matrix leading to random growth of spherulites. (2) The presence of spherulites between the few aligned SWCNTs. Since the loading of SWCNTs in polymer matrix is low (upto 0.6 wt%), the dilute SWCNTs system may be considered in this study. It is believed that higher loading of SWCNTs may lead to formation interconnected or entangled network. Such a network may increase complex viscosity of polymer matrix making it difficult for polymer chains and SWCNTs to align in flow direction to form shish. In otherwords, in entangled network system, shear may not have any effect to form anisotropic structures, ultimately resulting in spherulite formation. Comparing the final structures in the obtained patterns acquired at 60 °C from figure 2.8a and figure 2.8b, it is clear that the shish-kebab structures are enhanced with SWCNT concentration and can be arrested by immediate cooling after the application of shear. Hence, the frozen initial structures obtained on cooling eventually lead to a large amount of shish-kebab structures.

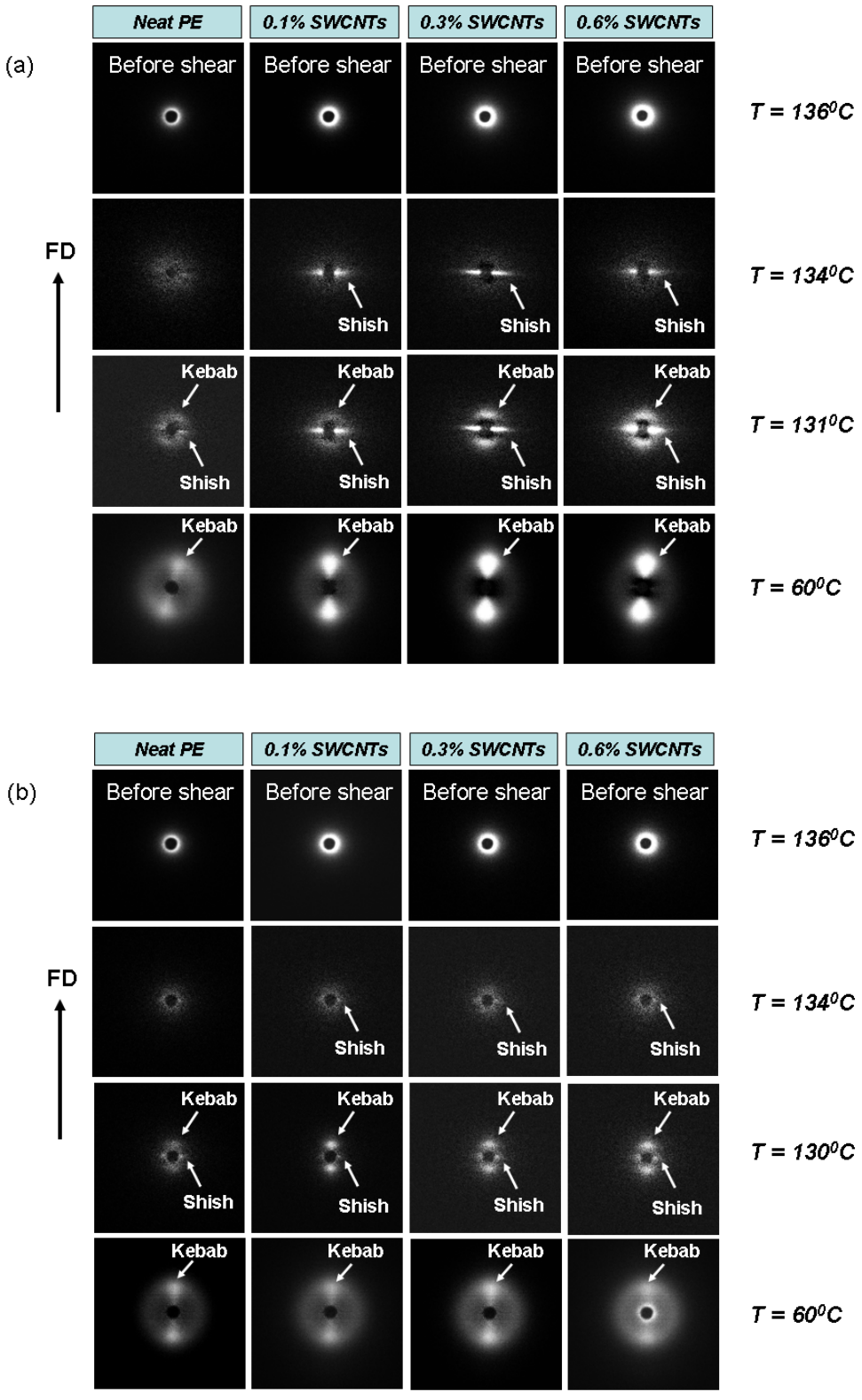

Figure 2.8: 2D-SAXS patterns of SWCNT/PE composites collected at selected temperatures while cooling after the application of two different shear rates at the same temperature and time (a) 100 s^{-1} for 1 s at 136 °C (b) 50 s^{-1} for 1 s at 136 °C

Figure 2.9 shows the integrated intensity along the meridian for samples sheared with two different shear rates applied for the same time (1 s); i.e. 100 s^{-1} and 50 s^{-1}. The intensity is monitored while the samples are cooled to room temperature after the application of shear. From the patterns acquired in figure 2.8 and intensity build up shown in figure 2.9, it is apparent that on cooling the samples to room temperature with increasing concentration of SWCNTs the onset of increase in intensity occurs at higher temperatures. Secondly, the intensity increases faster with increasing SWCNT concentration. The onset of increase in intensity and the subsequent build up of intensity also increases with the increasing shear rate as is shown conclusively in figures 2.9a and 2.9b for 100 s^{-1} and 50 s^{-1} respectively.

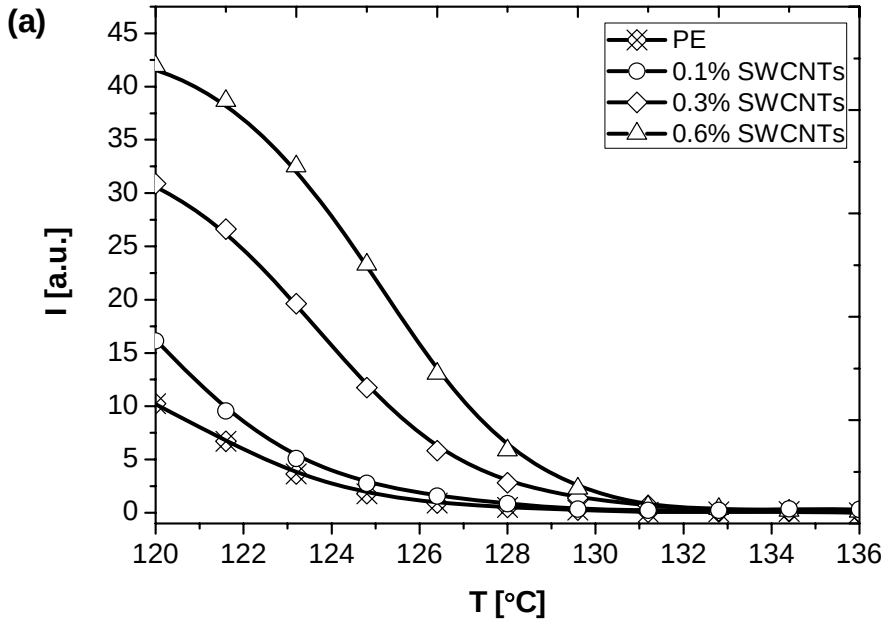

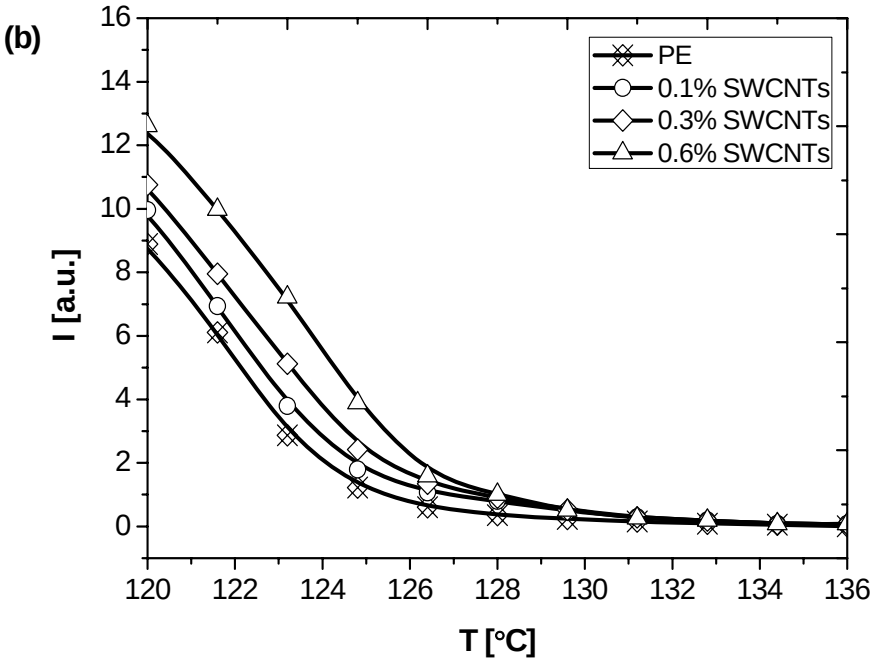

Figure 2.9: The meridional integrated intensity as a function of temperature monitored while cooling the samples to room temperature after the application of shear (a) 100 s^{-1} for 1 s (b) 50 s^{-1} for 1 s.

2.3.4 Effect of shear rates on stretch of long chains in polyethylene (PE) melt at isothermal condition

Figure 2.10a, shows the selected 2D-SAXS patterns of PE collected at an isothermal temperature (as explained in the scheme-2 of the section 2.2.7) of 136 °C for 600 s after the application of strong shear rate ($\gamma^{\bullet}$ = 100 s^{-1}, t_s = 1 s). The image acquired before the application of shear in all the cases at t = 0 s showed the diffuse scattering. After the application of steady shear rate of 100 s^{-1} for 1 s, the broad scattering in the equator arises at t = 50 s and tends to develop as a function of time. The scattering in the meridian appears at 100*s* and grows as a function of time. The scattering in the equator is attributed to the presence of shish (extended chain segments) and emergence of scattering in the meridian is attributed to the presence of kebab (folded chains). The growth of shish-kebab structures as a function of time suggests the enhancement of crystallisation. The alignment of chains along the flow direction influences the electron density fluctuation in the direction normal to the flow direction that results in scattering along the

equator. The broad equatorial scattering which transforms into streak-like scattering, with the appearance of the kebabs (intensity along the meridian) as a function of time, indicates the presence of anisotropic structure at the initial stages of crystallisation under isothermal conditions after the application of shear. Thus the shish provides the nucleation sites for the growth oriented lamellae in radially perpendicular direction to the stretched chains.

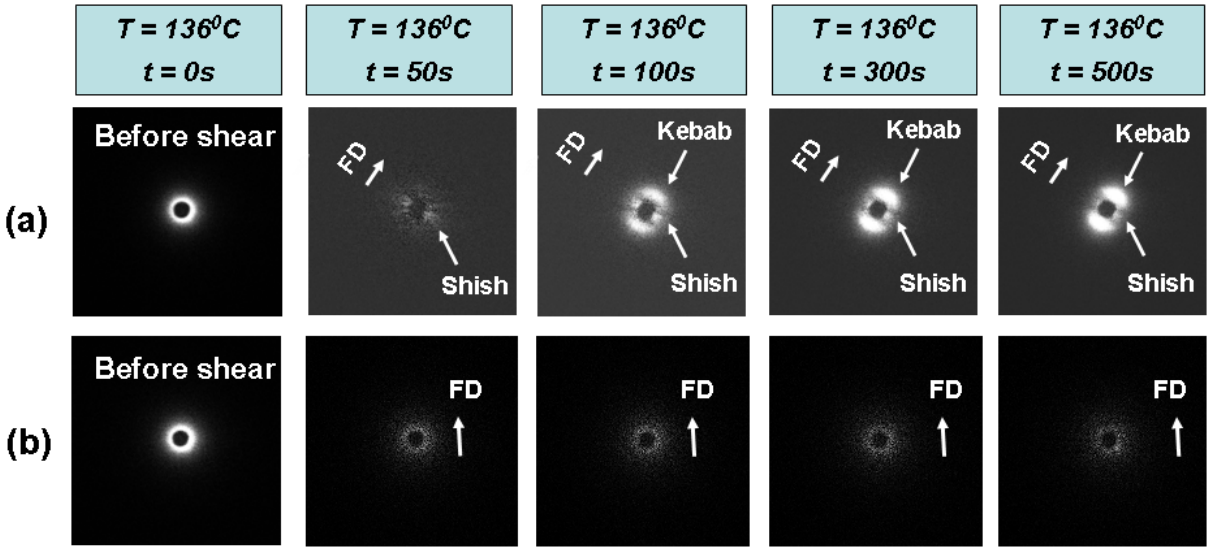

Figure 2.10: The two dimensional SAXS patterns of PE at selected times as a function of time at isothermal temperature of 136 °C for 600 s. (a) SAXS patterns acquired after the application of strong shear of 100 s^{-1} for 1 s. (b) SAXS patterns after the application of shear rate of 50 s^{-1} for 1 s.

Figure 2.10b shows the patterns collected after the application of shear ($\dot{\gamma}$ = 50 s^{-1}, t_s = 1 s). The selected 2D-SAXS patterns collected after the application of shear reveals the weak scattering across beamstop. Considering the no appearance of the streaks along the equator and intensity along the meridian, it could be stated that the shear rate of 50 s^{-1} for 1 s is not efficient in stretching the chains at the isothermal temperature of 136 °C. Differences in the arising 2D patterns with the applied shear rates can be explained by the Deborah number approach. The concept of the Deborah number was introduced by Reiner [170], to describe a measure of departure from fluidity. Basically, the Deborah number is a dimensionless measure of the fastness of change in rheological

conditions in terms of both deformation and stress of a material element within a deforming body. In the literature [171], a satisfactory definition of the Deborah number has been given for suddenly accelerated flows. The Deborah number can be defined [172] as a measure of the ratio between characteristic time of observation, t_{obs}, and the timescale of inherent processes in a material, t_{inh}.

$$De = \left(\frac{t_{obs}}{t_{inh}} \right) \tag{2.4}$$

In general, t_{inh} characterises the rate of the inherent rearrangement of the materials structure. Since the level of structure organisation, its rupture and restoration can vary, variations in the values of characteristic times for the same material may be expected. In case of steady flows, for instance, the flows whose kinematic description does not contain time explicitly – the time elapsed from startup of flow is essentially infinite; yet , the Deborah number for such flows is not necessarily zero, unless some very restrictive conditions are imposed. Noll [173] discussed the concept of constant stretch history flows. These flows consists the principal stretches of deformation carrying the configuration at time '*t'* into the configuration at time $t - \tau$ independent of '*t'*. Oldroyd [174] introduced the general concept of flow with perpetual rheological history. This concept includes the history of deformation of a material element, history of stress and the history of temperature for non-isothermal flows. The Deborah number has been used in shear flow to study the formation of oriented structures in FIC. [89, 102, 175] For this purpose, the time-temperature superposition is applied to determine the variation of two time scales τ_{rep} and τ_s with *T*, where – reptation time τ_{rep} corresponds to the relaxation time of molecular orientation and chain retraction time τ_s corresponds to the relaxation time of molecular stretch. The potential of flow in inducing the orientation and stretch can be quantified using two Deborah numbers reported in equations 2.5 and 2.6

$$De_{rep} = \tau_{rep} \dot{\gamma} \tag{2.5}$$

$$De_s = \tau_s \dot{\gamma} \tag{2.6}$$

The formation of oriented (shish-kebab) structure occurs with the magnitude of $De_s \approx 1-10$. Thus, it is likely that strong chain stretching governs the formation of shish-kebab structures. The displacement of chains in a polymer melt occurs as a result of reptative motion that determines the viscoelastic properties. The Deborah number of reptation and stretch for the HMW chains of neat polyethylene at two different shear rates is calculated based on MWD information as reported in literature [102, 110, 176-177] using equations 2.5 and 2.6,

The approach makes use of equilibrium time (τ_e) at given temperature conditions and the number of entanglements per chain (*Z*) based on HMW chains. Hence, stretching time (τ_s) is not affected by MWD if Z_{HMW} and τ_e are known. [102] To determine the Deborah number of reptation (De_{rep}^{HMW}) and stretch (De_s^{HMW}) at 136 °C, the time-temperature superposition (TTS) principle is applied with the aid of rheology. To determine the relaxation times associated with chain reptation (τ_{rep}^{HMW}) and chain stretch (τ_s^{HMW}), the entanglement equilibration time, $\tau_e = 7\times10^{-9} s$ at 190 °C and the entanglement molecular weight, M_e = 828 g/mol is assumed. [178]

The relaxation times of reptation (τ_{rep}^{HMW}) and stretch (τ_s^{HMW}), for HMW *(M_z* ~ 1.18 x 10^6 g/mol*)* chain, were calculated using following equations,

$$\tau_{rep}^{HMW} = 3\tau_e Z^3 \left(1 - \frac{1.51}{\sqrt{Z}}\right)^2 \tag{2.7}$$

$$\tau_s^{HMW} = \tau_e Z^2 \tag{2.8}$$

Where, τ_e is entanglement equilibration time of segments between entanglements and entanglement per unit chain (*Z*) is defined by the ratio M_z/M_e. *Z* can be estimated as 1430.

The values of relaxation times related to chain reptation (τ_{rep}^{HMW}) and chain stretch (τ_{s}^{HMW}) were found to be 56.651 s and 0.0143 s repectively. The average molecular weight between topological constraints (M_e) of PE at 190 °C can be defined [109-110] as,

$$M_e = 4\rho RT / 5G_N^o \tag{2.9}$$

where, G_N^o is plateau modulus. The calculation of characteristic relaxation times requires the information of τ_e for PE. In general, τ_e can be estimated from the monomeric friction coefficient ($\zeta_\circ$) and some physical constants. The equation can be expressed [179-180] as,

$$\tau_e = \frac{\zeta_\circ \left(\left\langle R^2 \right\rangle / M \right) M_e^2}{3\pi^2 k_B T \, m_o} \tag{2.10}$$

Where, $\left\langle R^2 \right\rangle / M$ is the monodisperse chain end to end distance molecular weight ratio for ideal equilibrium random coil, M_e is the average molecular weight between topological constraints, T is the absolute temperature, $m_\circ$ is the molecular weight of monomeric unit and k_B is the Boltzmann constant.

The Arrhenius type of temperature dependence with activation energy E_a = 29.057 kJ/mol is found for the horizontal shift factor (a_T) at T = 136 °C. The vertical shift factor (b_T) does not show strong temperature dependence. The shift factors for different temperatures are determined experimentally on the application of TTS principle to storage modulus (G') curves obtained in the frequency spectrum of 0.01 to 100 rad/s. The Arrhenius activation energy for TTS principle can be expressed [94] as,

$$a_T(T) = \exp\left[\frac{E_a}{R} \left(\frac{1}{T} - \frac{1}{T_\circ} \right) \right] \tag{2.11}$$

Where, E_a is Arrhenius activation energy, $a_T(T)$ is shift factor at absolute temperature, R is gas constant (8.314 J/mol. K^{-1}), T = 409 K is absolute temperature and $T_\circ$ = 463 K is reference temperature. The obtained shift factor (i.e. a_T = 2.70) at 136°C is considered while using equations 2.5 and 2.3 to calculate the *De* for HMW chains at 136 °C. The calculated relaxation times and Deborah numbers for the applied shear rate are reported in Table-2.5.

Table 2.5: The Deborah number of reptation and stretch of HMW chains for different shear rates at 136 °C.

Shear rate (s^{-1})	**Shear time (s)**	De_{rep}^{HMW}	De_{s}^{HMW}
100	1	1.5×10^{4}	3.8
50	1	7.5×10^{3}	1.9

The horizontal (a_T) and vertical (b_T) shift factors for different temperatures obtained from rheological experiments are shown in Table-2.6. Thus from the Table-2.6, τ_e at 136 °C is 1.89 x 10^{-8} s.

Table-2.6: Rheological parameters for PE at different temperatures.

Temperature (°C)	a_T	b_T
136	2.70	0.90
142	2.43	0.91
145	2.35	0.92
160	1.86	0.95
180	1.30	0.98
190	1	1

The Deborah number of stretch for HMW chain at 136 °C after the application of shear rate of 50 s^{-1} for 1 s is 1.9. Since the stretch Deborah number is not significantly more than 1, only few high molecular weight chains can be stretched to form a weak shish that would not suppress the nucleation barrier for the kebab formation. Such a weak

shish formation is not detectable within the applied SAXS setup. This explains the absence of intensity along the equator and meridian in figure 2.10b

Whereas, for the applied shear rate of 100 s^{-1} for 1 s, Deborah number of stretch for the high molar mass significantly exceeds the value of 1.0. Thus the high molar mass chains are stretched to an extent that the strong shish formation occurs, which is consistent with the appearance of intensity along the equator. With the appearance of shish, nucleation barrier for the formation of kebabs is suppressed and the crystallisation proceeds. The formation of shish-kebabs is seen in figure 2.10a

Figures 2.11a and 2.11b show the integrated intensities corresponding to equator and meridian as a function of time after the application of two different shear rates. The shear of 100 s^{-1} and 50 s^{-1} are applied at 136 °C for 1 s. The intensity in the meridian dominates in the later stages of the isothermal crystallisation temperature in both cases, though the difference is very small in the case of 50 s^{-1} for 1 s of the applied shear. From the SAXS patterns and rheological approach, it is quite clear that for the shear rate of 100 s^{-1} for 1 s, shear is effective for the formation of shish-kebab structure. Lack of drop in intensity along the equator with time suggests that the long chains are stretched and remain extended due to high relaxation times. The resultant shish morphology is frozen with the appearance of kebabs. This further strengthens the shish formation with time providing the nucleation for the growth of kebabs. Hence, the meridional intensity in the later stages dominates due to the formation of kebab-like structures. However, for the shear rate of 50 s^{-1} for 1 s, the higher intensity along the meridian (from figure 2.11b) relative to the equator in the later stages of isothermal crystallisation suggests the existence of some anisotropy, which may arise due to the formation of some oriented structures that are not fully detectable. The anisotropy suggests that some long chains do get stretched even at a lower Deborah number of stretch and are capable of forming very weak shish. However, the data along the equator and meridian is widely scattered making it difficult to draw any robust conclusions.

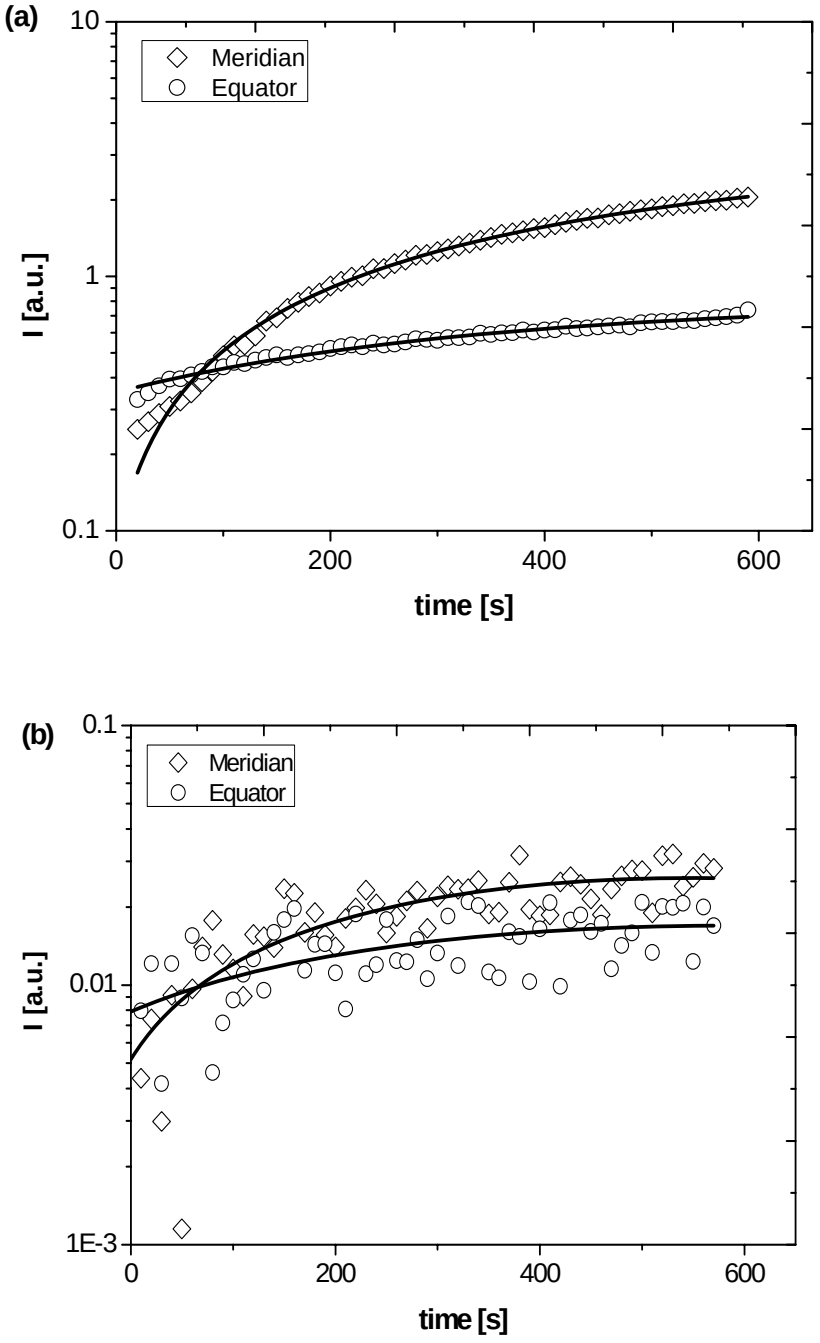

Figure 2.11: The evolution of integrated intensity along the equator and the meridian as a function of time after the application of shear at isothermal temperature 136 °C. (a) After application of the shear, 100 s^{-1} for 1 s, at 136 °C. (b) After the application of shear, 50 s^{-1} for 1 s, at 136 °C.

Figures 2.12a and 2.12b, show the ordering of lamellae as the neat polymer crystallises on decreasing temperature after the application of two different shear rates (100 s^{-1} and 50 s^{-1} for 1 s) at an isothermal temperature, 136 °C and residence time of the sheared melt at 136 °C for 600 s prior to cooling. In the neat PE sample sheared with 100 s^{-1} for 1 s, with decreasing temperature broad distinctive lobes emerge along the meridian. The increase in intensity suggests an overall increase in electron density fluctuation due to re-organisation of chain segments with crystallisation on cooling. With the application of high shear rate, as more long chains are likely to be stretched, a well defined oriented structure emerges in the crystallisation process whereas, the application of low shear rate results in less chain stretching, ultimately resulting in the complete relaxation of stretched chains (if any) to give isotropic scattering. The isotropic scattering that emerges at 122.7 °C as shown in figure 2.12b, may be attributed to the presence of spherulites. Thus this sample is expected to have less oriented lamellae at low temperatures.

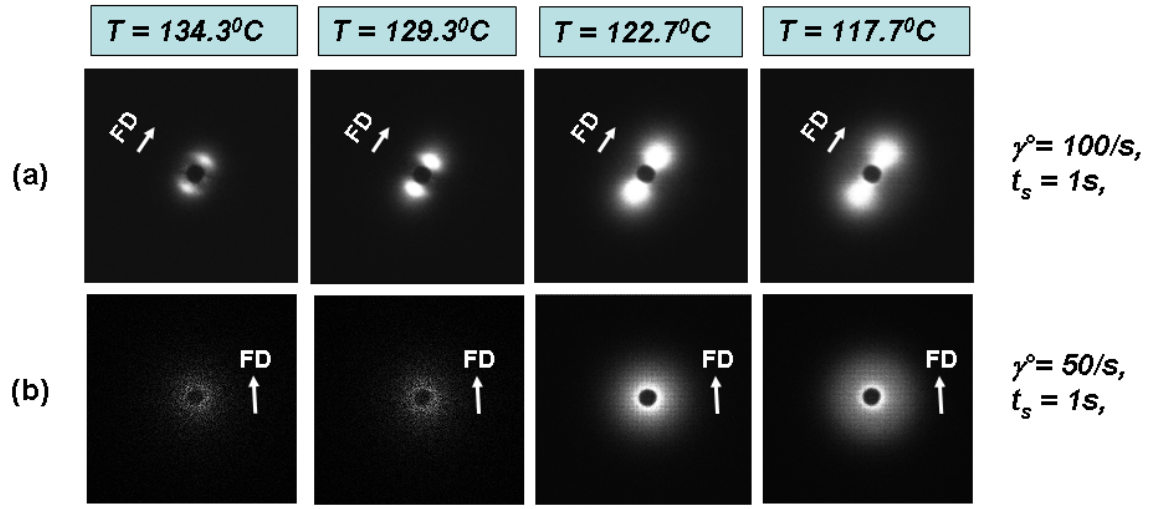

Figure 2.12: The acquired 2D-SAXS patterns in neat polymer at different temperatures while cooling to room temperature at different shear rates.

2.3.5 Structure development of SWCNT/PE composites at isothermal crystallisation under low shear rate

From the results above it is apparent that strong shear promotes chain extension in the early stages that results into the formation of shish-kebab structures. To make distinction in the origin of the shish structures in the presence of SWCNTs, on purpose we performed experiments at low shear rates. To recall, the application of shear in the neat polymer (50 s^{-1} for 1 s) at isothermal temperature of 136 °C, as shown in the figure 2.9b gives isotropic scattering. When the same low shear rate conditions are applied to polymer/nanotube composites, the isotropic scattering (absence of streak-like scattering) increases with increasing amount of SWCNTs in PE, Figure 2.13a. Although, the scattering appears to be isotropic in the patterns, the intensity in the vicinity of the beamstop increases with the increasing amount of nanotubes at 136°C after the application of shear at the same temperature. Thus the structures arising due to the presence of SWCNTs in the sheared samples cannot be excluded. It is worthwhile to note that the detection of structures at the very initial stages is limited by the resolution of the SAXS detector. However, the overall intensity increases with time. The increase in intensity becomes apparent in the patterns collected at t = 300 s and t = 500 s for the 0.6 wt% SWCNT/PE composites. The presence of anisotropy in these sheared samples become apparent in the azimuthal plots shown in figure 2.13b. The anisotropy suggests that SWCNTs are aligned in the flow direction to form shish. The increasing amount of SWCNTs influences the relaxation time of the polymer chains. Hence, the presence of SWCNTs influences the oriented structure formation in the samples sheared with a shearing rate of 50 s^{-1} for 1 s.

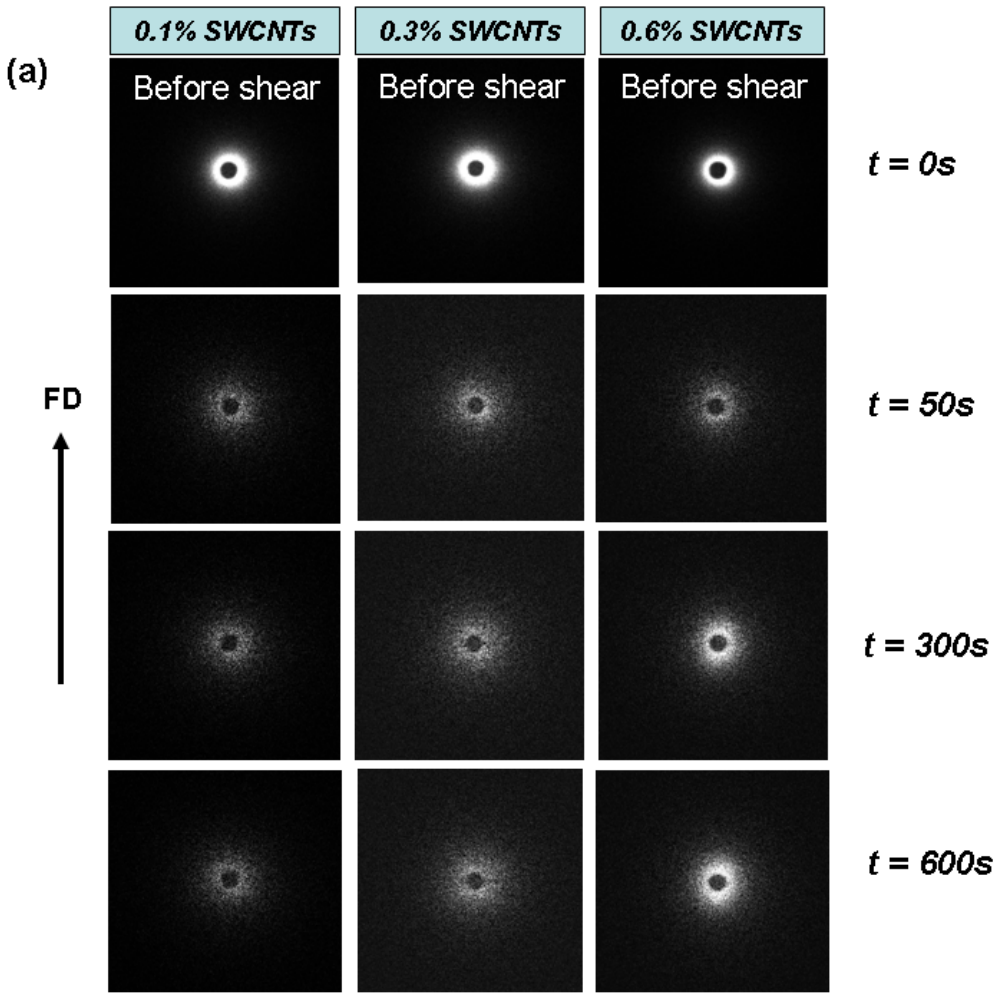
(a)
0.1% SWCNTs
0.3% SWCNTs
0.6% SWCNTs
Before shear
Before shear
Before shear
t = 0s
FD
t = 50s
t = 300s
t = 600s

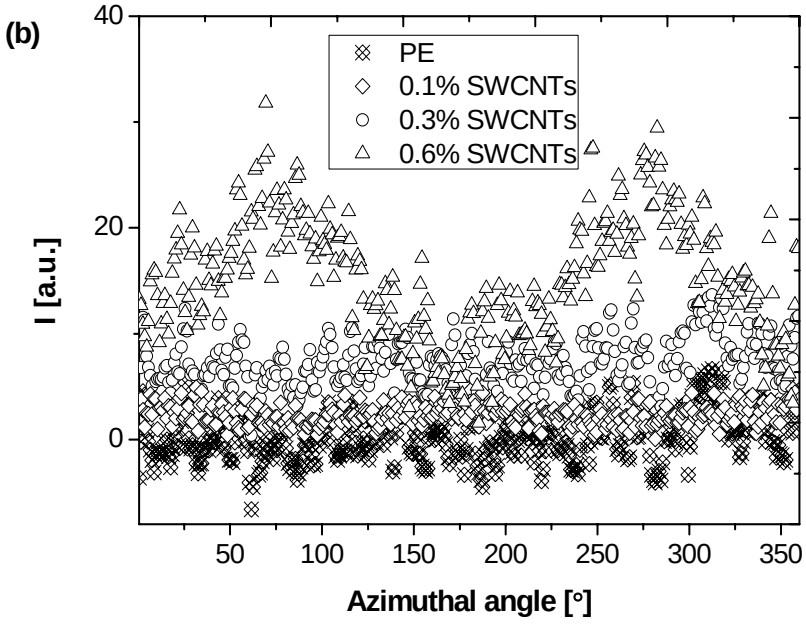

Figure 2.13: (a) 2D-SAXS patterns collected at different times after the application of shear at the isothermal temperature of 136 °C for polyethylene having different concentration of SWCNTs (b) Azimuthal plots for the 2D-SAXS patterns acquired after 600 s of isothermal condition at 136 °C.

Figure 2.14 shows integrated intensity corresponding to the equatorial region of the SAXS patterns for SWCNT/PE composites, collected during the isothermal temperature of 136 °C after the application of shear (50 s^{-1} for 1 s). The intensity along the equator increases with the increase in SWCNTs content in PE. The intensity remains stable for 600 s under isothermal conditions after the application of shear. This suggests that the presence of SWCNTs leads to stable shish formation. However, for 0.3 wt% and 0.6 wt% SWCNTs in PE, an increase in intensity in the later stages (>300 s) under isothermal conditions is noticed suggesting the crystallisation and growth of oriented structures even at low shear rate $\gamma^{\bullet} = 50\ s^{-1}$ for $t_s = 1$ s.

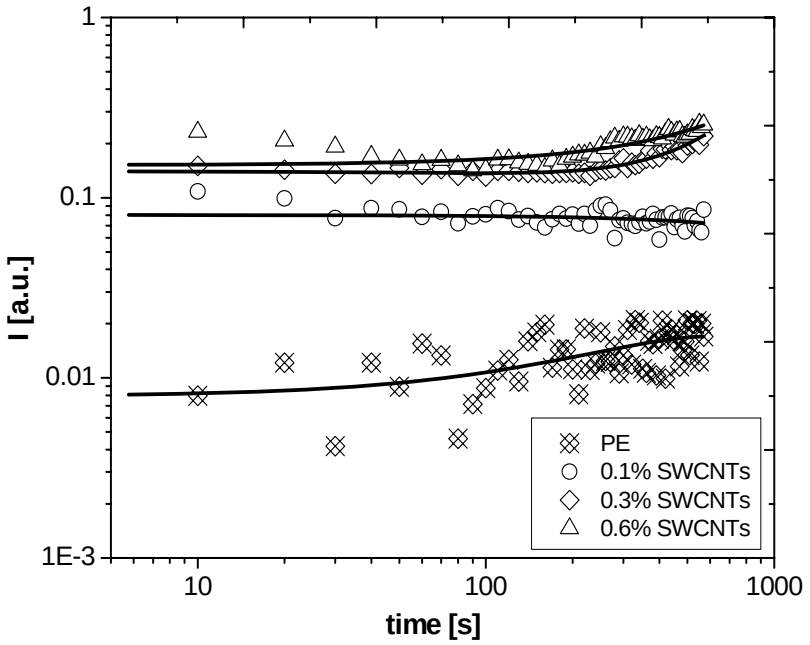

Figure 2.14: The integrated intensity corresponding to equator (streaks) as a function of time for the PE having different amount of SWCNTs. The shown intensity is probed for 600 s at 136 °C after the application of shear ($\dot{\gamma} = 50\ s^{-1}$, $t_s = 1$ s).

Figure 2.15, shows increase in the intensity at the meridian at the isothermal temperature 136 °C after the application of shear ($\dot{\gamma} = 50\ s^{-1}$ for $t_s = 1$ s). The meridional intensity increases with the SWCNT content in PE. This suggests enhanced crystallisation in SWCNT/PE composites. This increase in intensity may be attributed to slow crystallisation as a result of low shear rates. The effect of SWCNTs on the nucleation of polyethylene chains even at low shear rates can be understood well from the present study. In otherwords, the result conclusively demonstrates that SWCNT bundles acts as nucleation sites when PE crystallises indicating that initial PE crystallites are in contact with nanotubes irrespective of shear rates.

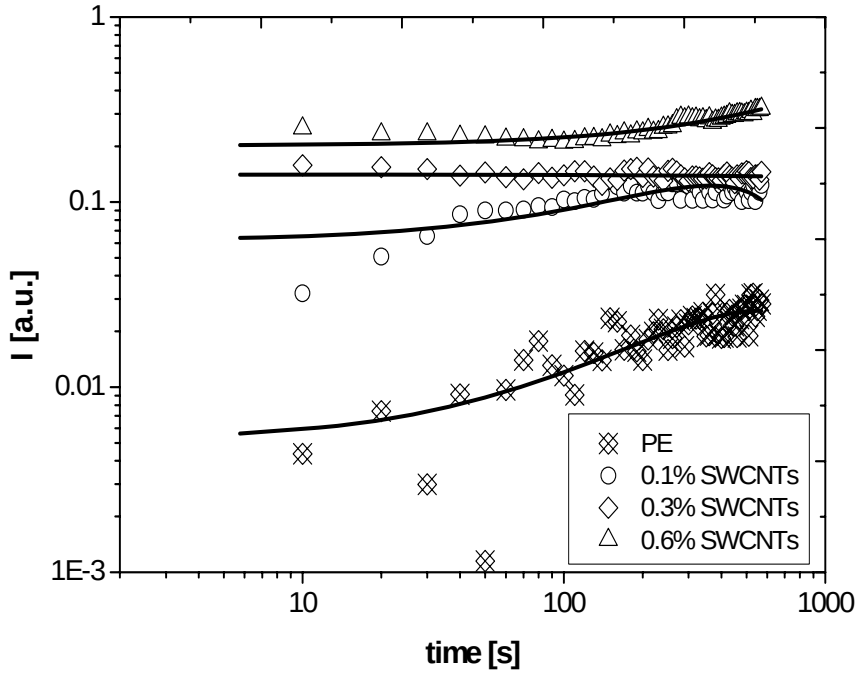

Figure 2.15: The meridional integrated intensity at 136 °C for SWCNT/PE composites as function of time. The intensity corresponds for 600 s of isothermal temperature for sheared (50 s^{-1} for 1 s) samples.

Figure 2.16 shows the 2D-SAXS patterns of sheared (50 s^{-1} for 1 s) SWCNT/PE composites collected at 60 °C while cooling to room temperature. It is evident that the scattering is completely isotropic for the neat PE leading to spherulite formation. The mixed morphology consisting of shish-kebab (anisotropy) and spherulite (isotropy) is detected for SWCNT/PE samples at 60 °C. With the increase in SWCNTs in PE, the anisotropy increases, as observed from the increase in the meridional scattering. Hence, the presence of SWCNTs increases the shish-kebab formation.

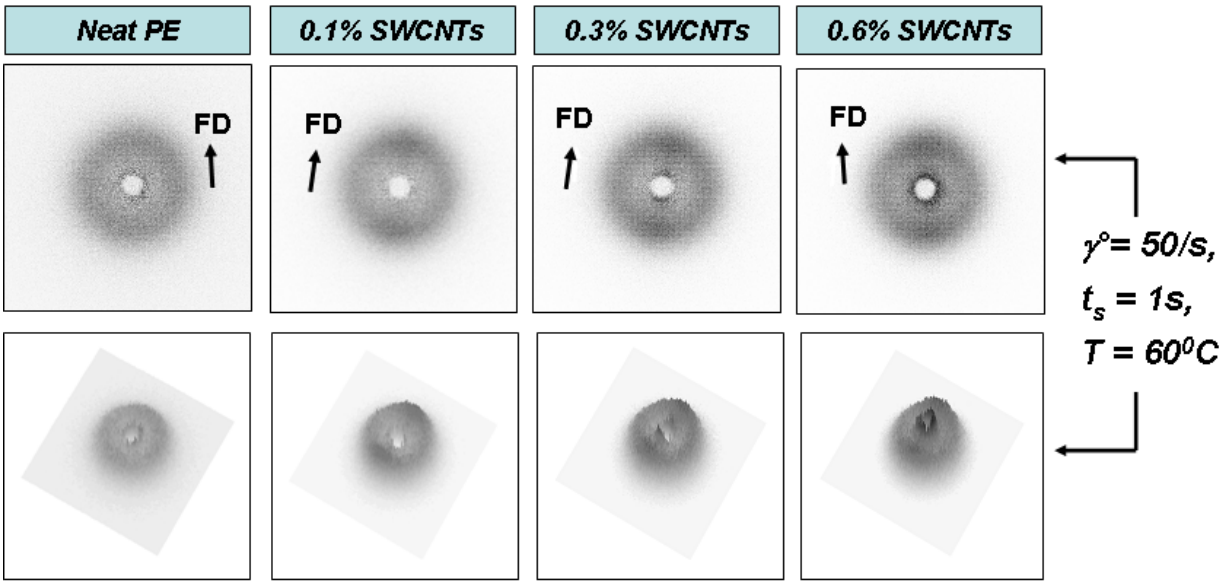

Figure 2.16: 2D-SAXS patterns of different SWCNT/PE samples acquired at 60 °C after the application of shear ($\gamma^{\bullet}$ = 50 s^{-1} for 1 s) at 136 °C. The sheared samples are annealed at 136 °C for 600 s prior to cooling at a rate of 10 °C/min (following scheme-2 in the experimental section).

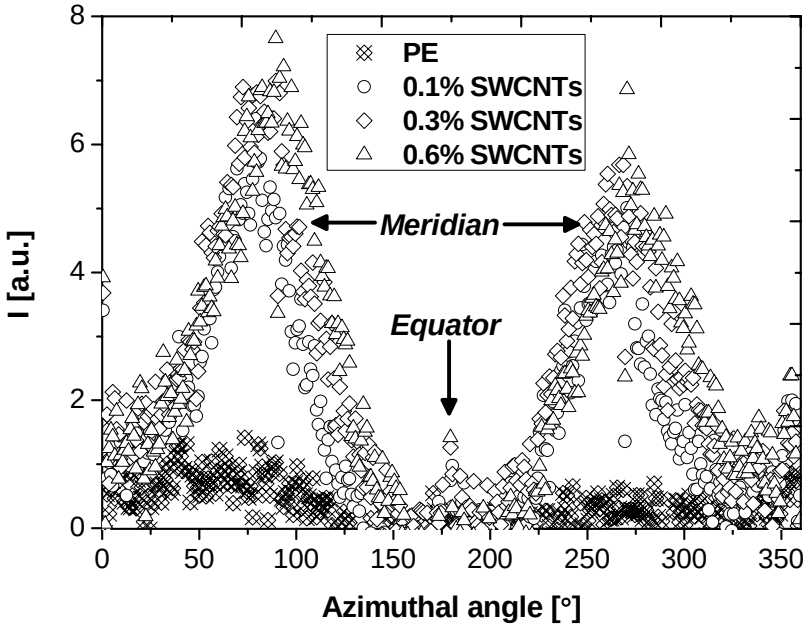

Figure 2.17: Azimuthal distribution of intensity for the pattern acquired at 60 °C for the sheared SWCNT/PE samples following the scheme-2 in the experimental section.

Figure 2.17 depicts the azimuthal distribution of intensity for neat PE and SWCNT/PE composites at 60 °C. This confirms the isotropic pattern for neat PE with the absence of meridional maxima. However, the presence of SWCNTs in PE leads to maxima in the meridian confirming the presence of shish-kebab structures at 60°C. It is interesting to note that the intensity increases along the equator with increase of SWCNTs in PE and may be attributed to oriented SWCNTs, which acts as shish in the suppression of the nucleation barrier. The Herman's orientation [181-183] function (f_h) is determined using equations 2.12 and 2.13 to calculate information about PE orientation in the presence of SWCNTs after the application of different shear rates at isothermal temperature 136 °C.

$$f_h = \left\{ \frac{\left(3[\cos^2 \phi] - 1\right)}{2} \right\} \tag{2.12}$$

Where ϕ is the angle between equator and meridian, the mean square cosine ($\cos^2 \phi$) of the azimuthal angle can be defined as,

$$\cos^2 \phi = \frac{\int_0^{\pi/2} I(\theta).\cos^2 \theta.\sin \theta d\theta}{\int_0^{\pi/2} I(\theta).\sin \theta d\theta} \tag{2.13}$$

Where, $I(\theta)$ is the diffracted intensity from the planes normal to the *c*-axis. When f_h = 1, 0 and -0.5, the scattering is parallel, random and perpendicular to the *c*-axis. The detailed analysis of orientation function in our case is reported elsewhere. [184] The 2D-SAXS patterns are analyzed by taking different regions in specific ways as shown in the figure 2.18. The patterns are integrated azimuthally in an anticlockwise direction from $\theta = 0°$ at equator to get full intensity profile within the regions. The values for integration used in the calculation of Herman's orientation function are taken from the intensity corresponding to azimuthal angle ($\theta = 0°$) to azimuthal angle ($\theta = 90°$).

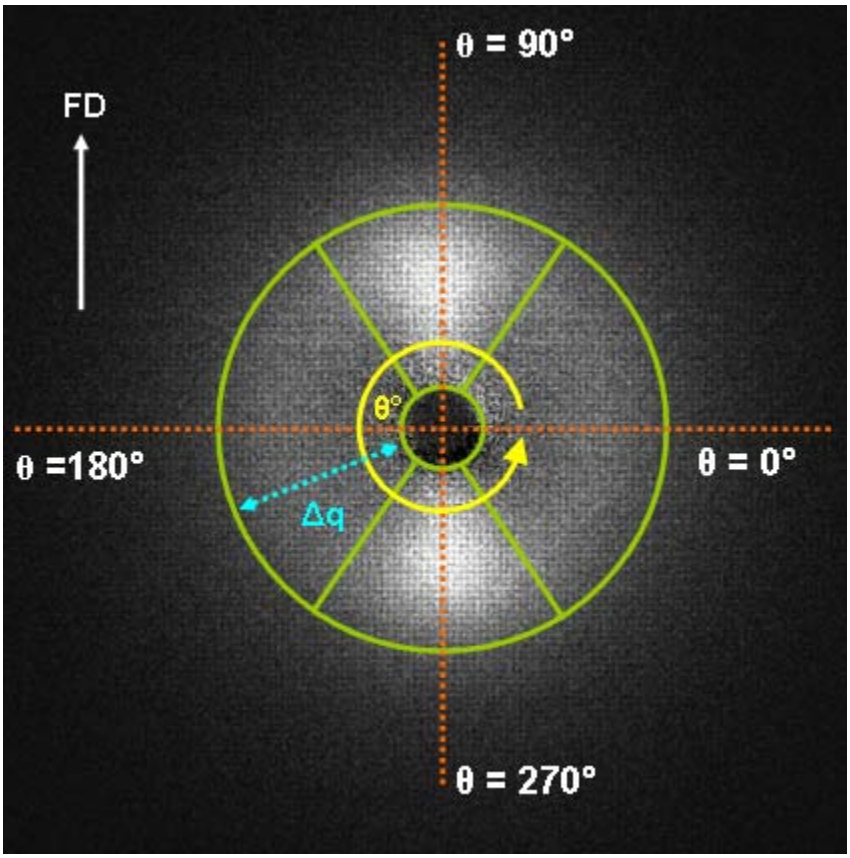

Figure 2.18: The SAXS data analysis performed for estimation of Herman's orientation function (f_h) using two dimensional patterns. (a) Shows the regions considered for calculation as defined in four quadrants for complete azimuthal integration (θ = 0° to 360°) for obtaining the azimuthal distribution of integrated intensity, where θ = 0° and 90° represents equator and meridian respectively. The integrated intensity corresponding to θ = 90° to 180° is considered to obtain orientation function. The SAXS pattern shown here is taken at the 60 °C

The Herman's orientation function for SWCNT/PE composites at isothermal temperature after the application of shear is shown in figure 2.19. After the application of shear (50 s^{-1} for 1 s) at an isothermal temperature of 136 °C, the orientation function for the sheared neat PE sample is close to 0 due to isotropic scattering. In the presence of SWCNTs in PE, the orientation function is dominated by chain extension in the early stages due to the presence of shish and by loosely packed lamellae in the later stages due to the presence of kebabs. [184] However, the overall values of orientation functions are close to 0, nevertheless, the changes are apparent with the increase in SWCNT content in PE due to

scattered intensities in the equatorial and the meridional regions. The increase in the scattering in the meridian at the later stages (>250 s) for sheared 0.6 wt% SWCNT/PE sample (refer figures 2.13 and 2.19) and corresponding changes in the orientation function suggest that the presence of SWCNTs enhances the crystallisation of PE with the growth of kebabs as short chains relax on the surface of SWCNTs. SWCNT nucleate PE crystal growth and accelerate the crystallisation rate. SWCNT bundles template PE crystallisation such that lamellae grow perpendicular from the SWCNT surface with PE chains (*c*-axis) parallel to the SWCNTs axis. Hence, SWCNTs surface provide higher density of nucleation site for the radial growth of straight lamellae without twisting. [146, 149] Although, the orientation functions are close to zero but higher than 0 in the early stages, the presence of oriented SWCNTs structures cannot be neglected after application of low shearing condition – as the SWCNTs are more rigid compared to the flexible polyethylene chains. Hence, it can be anticipated that SWCNTs have important role in suppression of the nucleation barrier, irrespective of the low shear conditions, that favors the growth of kebabs in the later stages of crystallisation process. The results also indicate that SWCNTs surfaces could themselves act as nucleation sites for the growth of kebabs even at low shear rates.

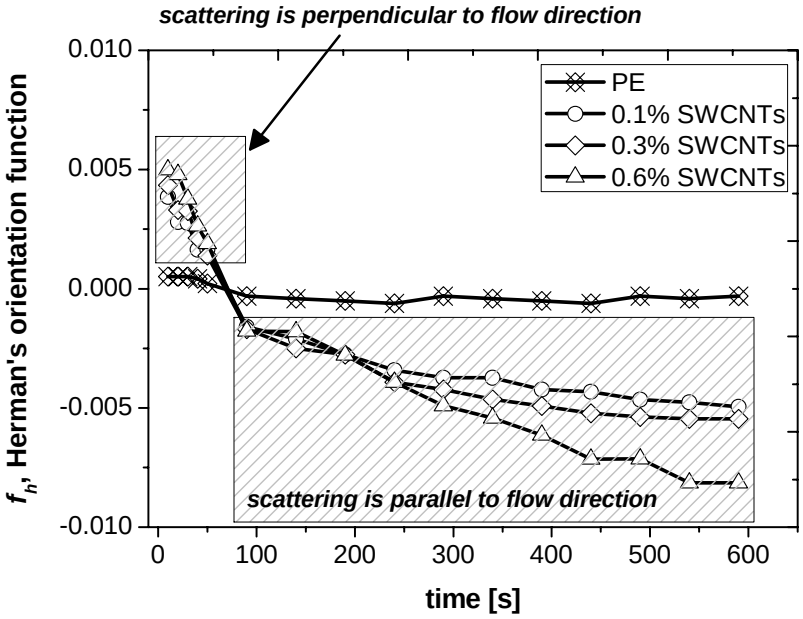

Figure 2.19: Herman's orientation function (f_h) for the sheared samples at isothermal temperature 136 °C after the application of different shear ($\dot{\gamma} = 50\ s^{-1}$ for $t_s = 1$ s)

2.4 Conclusions

The crystallisation behavior of SWCNTs coated PE was investigated using different experimental techniques. The isothermal crystallisation was probed by rheometry and DSC confirmed the role of SWCNTs as nucleating agents for polyethylene chains suppressesing the nucleation barrier and accelerating the rate of crystallisation with change in the overall morphology from spherical to disc shape of the crystallites. The onset of crystallisation and the overall crystal growth rate is enhanced due to the presence of SWCNTs in PE. Flow induced crystallisation studies were performed to study the structure development in SWCNT/PE composites. The presence of SWCNTs under shearing conditions accelerated crystallisation kinetics and promoted the development of anisotropic structures, similar to shish-kebab. The enhanced oriented structure formation in SWCNT/PE composites as compared to neat polymer, even after the application of low shear at isothermal condition has implications on chain relaxation in the polymer melt.

Chapter 3

Structure development in sheared polyethylene: the influence of zirconia nanoparticles on crystal orientation

In this chapter structure development in high density polyethylene having a broad molecular weight distribution (MWD) in the presence of zirconia nanoparticles under the strong shear (100 s^{-1} for 1 s) is investigated. Experimental techniques used for the studies are time resolved small angle X-ray scattering (SAXS) and wide angle X-ray diffraction (WAXD). The SAXS patterns show evolution of scattering along the equator immediately after the cessation of shear. Subsequent increase in intensity along the meridian is observed on cooling. The intensity along the equator is attributed to shish formation, whereas the intensity along the meridian to kebab formation. The growth of kebab formation is monitored at isothermal crystallisation temperature, T_c = 125°C, for polyethylene in the presence of different concentrations of zirconia nanoparticles. Shift in the onset of crystallisation to higher temperatures is observed with increase in zirconia content in the polyethylene. With the increase in zirconia content, crystallinity increases. The increase in crystallinity with time and zirconia concentration is determined from WAXD. Along with the increase in crystallinity the intensity along the meridian increases, as determined by SAXS. The increase in fraction of oriented crystals is determined by the ratio of intensity scattered from oriented crystallites to the total scattered intensity. From WAXD data the Herman's orientation function is determined to study the enhancement of orientation along the flow direction. Scherrer's equation is used to measure the apparent lateral dimensions of kebabs in the hkl direction. The long period in all cases is found to decrease slightly in the early stages of crystallisation, before the plateau value is reached.

3.1 Introduction

The presence of flow during processing deforms macromolecular chains producing very specific organisations. Such specific organisations pertaining to the formation of highly oriented structures have been widely reported in semicrystalline polymers, where the polymer at least at the initial stages crystallises under shear or elongation flow. [89, 97, 185-188] Specifically, a fundamental mechanism governing the role of molar mass and molar mass distribution in the formation of such highly oriented structures under flow is of interest in polymer science. The well established view maintains that long and extended chains dominate the central innermost portion of 'shish-kebab' structures. [189] Moreover, 'shish' (extended chains) provides nucleating sites for the growth of 'kebab' (folded chains).

The effect of processing conditions on polymer crystallisation has been studied for a long time. The rate of crystallisation highly depends on the influence of flow because of chain alignment or segmental orientation of molecular chains. This chain orientation leads to change in crystallisation kinetics by suitably providing nucleation sites causing oriented lamellae to grow radially perpendicular to the chain axis. However, the understanding at molecular length dimensions has been limited. The monitoring of shear induced structures effectively by using small and wide angle X-ray techniques (SAXS/WAXD) has made it possible to probe long range ordering of lamellar stacking by SAXS and crystal structure development by WAXD. Thus advances in time resolved SAXS and WAXD through synchrotron radiation sources with shearing devices has enabled the crystallisation of semi-crystalline polymers to be monitored. The influence of the high molar mass component of polyethylene (PE) in the development of chain orientation is the stimulus to the studies performed in this chapter. This chapter addresses the influence of spherical zirconia nanoparticles on the formation of structures under strong steady shear protocol and further highlights the increase in orientation induced due to the presence of zirconia particles.

The influence of different shear rates and time on the crystallisation kinetics of iPP has been reported. [98] These findings suggest that, at higher shear rates, low shear times are more efficient for maximum orientation. Studies performed using different molecular weight and molecular weight distribution lead to the conclusion that chain

orientation is strongly influenced by increasing molar mass. Recently, SAXS/WAXD studies confirmed that a high molar mass tail also plays a significant role in enhancing the formation of highly oriented structures. [68, 78, 89, 154, 190] This formation relates to the concept of coil-stretch transition, where the gauche conformations in the random coil chains transform into trans-conformations. The development of shish-kebab morphology under elongational flow in dilute solutions was extensively investigated by Keller et al. [61-62, 191-192] According to them, $\varepsilon_c = [M^*]^\beta$ for the flow induced crystallisation under elongation in dilute solution, where ε_c is critical rate of elongation, β is equal to 1.5 (factor for polyethylene) and M^* is the critical orientation molecular weight that defines coil- stretch transition. [68, 95] After deformation, the polymer chains having molecular weight more than critical orientation molecular weight (long chains) retain extension while short chains relax back to their original coil conformation. Over the decades, it has become clear that the formation of shish-kebab morphology is a local event that depends on the chain dynamics and thermodynamics applicable in the polymer melt. [67, 193-196] The concept of shish-kebab morphology is realised in the dilute solutions as well as in polymer melts.

The shish-kebab structure morphology has been subject of extensive investigations using X-rays. [99, 154, 186, 190] The effect of altering the concentration of long chains in polyethylene blends has been studied. The presence of oriented nuclei under shear in melt occurs due to the distribution of relaxation time. [83, 197] It is also known that precursors are formed even at temperatures above equilibrium melting point, where the time scale for the growth of nucleus decreases with the increase in temperature. It is further noticed that Flory's statements [59] have limitations since orientation of polymer chains, occurring due to flow, eliminates the free energy barrier to form a nucleus. According to Coppola et al. [198] the temperature governs the thermodynamic driving force which is then enhanced due to the orientation and stretching of high molar mass chain depending on particular flow regimes. Seki et al. [66] demonstrated that oriented nuclei are formed due to high molecular weight chains exceeding the overlap concentration. Somani et al. [99] proposed the nucleation and growth in orientation induced crystallisation of polymers during flow. According to them, orientation causes alignment of chain segments of polymer molecules and results in the formation of

primary nuclei in the flow direction. Further it is shown that the polymer molecules above the critical orientation molecular weight (M^*) could be oriented at a given shear rate ($\gamma^{\bullet}$). Ogino et al. [199] showed that the anisotropy increases above certain critical concentration of HMW chains. This critical concentration of HMW chains in polymer is 0.5-0.6 %. According to them the critical concentration of HMW chains must be more than overlap concentration (i.e. 0.178 g/cm^3) to form shish-kebab structures. Thus anisotropy increases with the increase in high molecular weight while decreases with the increase in low molecular weight.

The studies on bimodal molecular weight distribution (MWD) also revealed the overgrowth of FIPs by twisted kebabs resembling lamellae within spherulites. The twist is likely to arise from tilting of the chains when the concentration of shish-kebabs is low. [175] The phenomenon of lamellar twisting was investigated by Hoffman and Lauritzen. [200] They attributed the cause to the different congestions of fold surfaces resulting in surface stresses. This phenomenon has been widely studied in polyethylene [201-204] and holds a significant importance during the initial stages of kebab development. In this chapter, the fundamental mechanism responsible for morphological development in PE under flow in defined shear conditions is elucidated. Further, the influence of nanozirconia on morphological development has been demonstrated.

3.2 Experimental Section

3.2.1 Materials

High density polyethylene (HDPE) having broad molecular weight distribution was selected. The corresponding molecular weight information obtained using GPC is summarised in Table 2.1 of Chapter 2. The HDPE sample in powder form was kindly supplied by Dow Chemicals B.V., Terneuzen, Netherlands. The polymer was polymerised using Ziegler- Natta catalyst in a slurry process. The zirconia nanoparticles (particle size of 20 nm) from Mel Chemical Ltd, UK were obtained in aqueous suspension form consisting 25.5 wt% of solid content.

3.2.2 Preparation of zirconia/PE composites

The solid content of the zirconia suspension was reduced to 0.25 wt% by adding a suitable amount of de-ionised water. The obtained concentration is sonicated for 45 min and then centrifuged at 3000 rpm for 20 min. More than 95 % of zirconia nanoparticles were suspended in the aqueous solution while the rest were deposits. The suspended aqueous solution with zirconia nanoparticles of 0.25 % was sprayed onto the surface of HDPE. The substrate with the thin layer of HDPE is shaken in order to ensure that zirconia nanoparticles are uniformly coated on HDPE powder. The HDPE powder adsorbed with zirconia nanoparticles was dried for 12 hours at 60 °C in a vacuum oven. The polymer films of about 0.4 mm thickness with and without zirconia nanoparticles were prepared by compression molding at 160 °C for 5 min. For X-ray measurements, samples in the form of disks having diameter of 30 mm were obtained from the melt compressed films.

3.2.3 X-Ray characterisation (SAXS/WAXD)

The structure formation was probed by SAXS and WAXD. SAXS was used to probe lamellae and their stacking; while WAXD is sensitive to atomic order within the lamellae (Bragg peaks). The excess of scattering in 2D-SAXS patterns were due to spherical zirconia particles with diameter (20 nm) much greater than those of SWCNTs (1 nm). SAXS patterns did not show the formation anisotropic structures and hence it was necessary to determine if there exist any ordered lamellae (kebabs) in 2D-SAXS patterns. Hence, WAXD technique was used to understand the reasons of less anisotropy. For instance: Kebab twisting may lead to decrease in anisotropy and orientation in polymer matrix which can be determined preferably by WAXD as compared to SAXS. Two dimensional (2D) SAXS and WAXD measurements were carried out separately at BM26B/DUBBLE and ID11 synchrotron beamlines in the European Synchrotron Radiation Facility (ESRF), Grenoble, France respectively. The wavelengths of synchrotron radiation are 1.24 Å for SAXS and 0.49 Å for WAXD. The shear cell is clamped perpendicular to the incident X–ray beam. Time resolved 2D-SAXS patterns were recorded on a two dimensional gas filled detector (512×512 pixels and $260\ \mu m \times 260\ \mu m$ pixel size) with sample to detector distance of 5.26 m. The vacuum

chamber was placed between the sample and detector to reduce the scattering and absorption from air. The acquisition time of 7 s was used to acquire images with a dead time of 3 s for data transfer between the adjacent images which was followed by correction for intensity of the primary beam, absorption and sample thickness. After subtraction, the images were integrated to determine the scattered intensity (I) as a function of the modulus of the scattering vector: $q = 4\pi \sin(\theta / \lambda)$ where, 2θ is scattering angle. The integrated intensity as function of time is defined as, $I_{\mathrm{SAXS}}(t) = \int_{q_{\min}}^{q_{\max}} I(q,t)dq$, where $q_{\max}$ and $q_{\min}$ being the maximum and minimum of q values. The obtained intensity data is subtracted with intensity prior to the application of shear. WAXD patterns are collected with a two dimensional Frelon detector having a resolution of 512 × 512 pixels (with pixel size of 50 μm × 50 μm) and a sample to detector distance of 33.1 cm. The WAXD patterns were recorded with acquisition time of 30*s* and dead time of 5 s for transferring of data. The images were integrated to obtain the intensity distribution (I) as a function of scattering angle 2θ by correcting for the spatial distortions and scattering of empty sample holder. Quantitative analysis was performed on the corrected X-ray patterns.

The shear flow experiments for both SAXS/WAXD were performed using a Linkam shear cell (CSS-450) modified with kapton windows. The samples were annealed at 160 °C for 5 min to erase memory effects. The samples were cooled from 160 °C to 136 °C at a controlled rate of 10 °C/min. The pulse of shear ($\gamma^{\bullet} = 100\ \mathrm{s}^{-1}, t_s = 1\ \mathrm{s}$) was applied at 136°C followed by cooling to 125 °C at a controlled rate of 5 °C/min. The structure development was followed isothermally at 125 °C for 600 s. Finally, the sheared samples were cooled to 60 °C at the controlled rate of 10 °C/min. A schematic of flow and thermal protocol is shown in the figure 3.1.

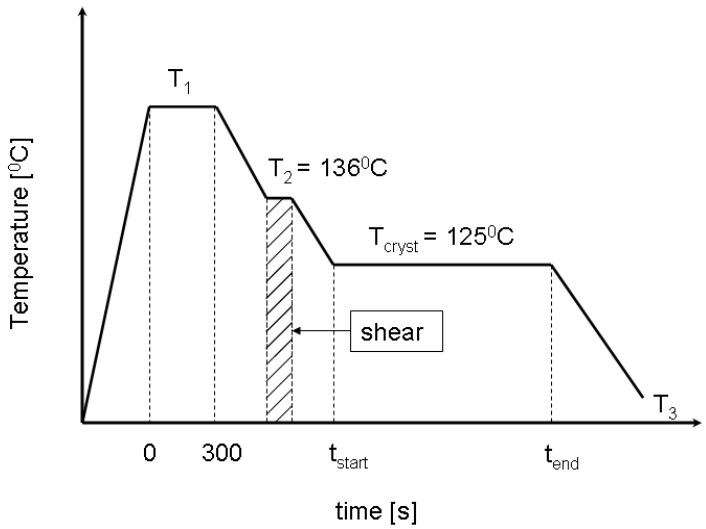

Figure 3.1: The schematic of flow and thermal protocol used in the experiments.

3.3 Results and discussions

3.3.1 Crystallisation on cooling in PE and Zirconia/PE composites after application of shear

Figure 3.2 shows the growth of intensity as a function of time for PE while cooling from 136 °C to T_c = 125 °C. The intensity at the equator, in the form of a streak, appears immediately upon the cessation of shear at 136 °C representing the formation of shish. The equatorial streak in SAXS can be also correlated to precursor formation that tend to disappear if the flow is applied at relatively higher temperatures [89]. The segmental interaction increases due to aggregation of oriented chains from different molecules that are less distant to each other. This process leads to the formation of bundled chain segments. The bundles of chain segments grow over the period of time as a result of accumulation of new chain segments and become stable i.e. in other words may form highly ordered crystalline structures. The stable chain segments are considered to possess a high degree of orientation. In our case, where the sample is set to cool just after the applied shear, the stretched chains are likely to crystallise. The occurrence of multiple shish formations can be assumed since a single shish may be too weak or dilute to be detected by SAXS. With decrease in temperature, intensity along the meridian increases

more than along the equator (it can be noticed at 50*s* after application of shear. The temperature at this point is 131.8 °C). This indicates the formation of kebabs perpendicular to shish, due to rapid relaxation of short chains that tend to adopt the random coil state (lamella).

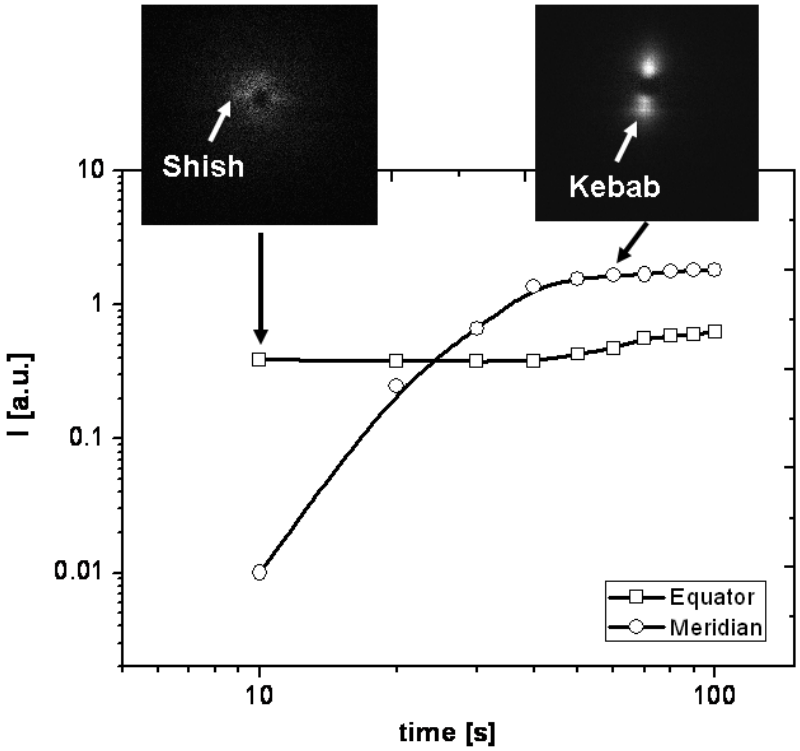

Figure 3.2: The early development of intensity in meridian and equator for neat PE; under cooling to T = 125 °C, after the application of shear ($\gamma^{\bullet}$ = 100 s^{-1}, t_s = 1 s) at 136 °C.

Figure 3.3a, shows development of SAXS intensity under isothermal conditions, at T_c=125 °C. The increase in intensity arises from the growth of kebabs that tend to grow steadily under isothermal conditions. The hump in the intensity profile at higher *q* values refers to the oriented crystals i.e. kebabs. The hump increases consistently for 600 s at the isothermal condition suggesting the steady growth of lamella. Figure 3.3b, shows the WAXD intensity evolution corresponding to 110 and 200 reflections as a function of 2θ at isothermal *T* = 125 °C. The growth of oriented structures can be noticed by the increase in the intensity corresponding to 110 and 200 reflections.

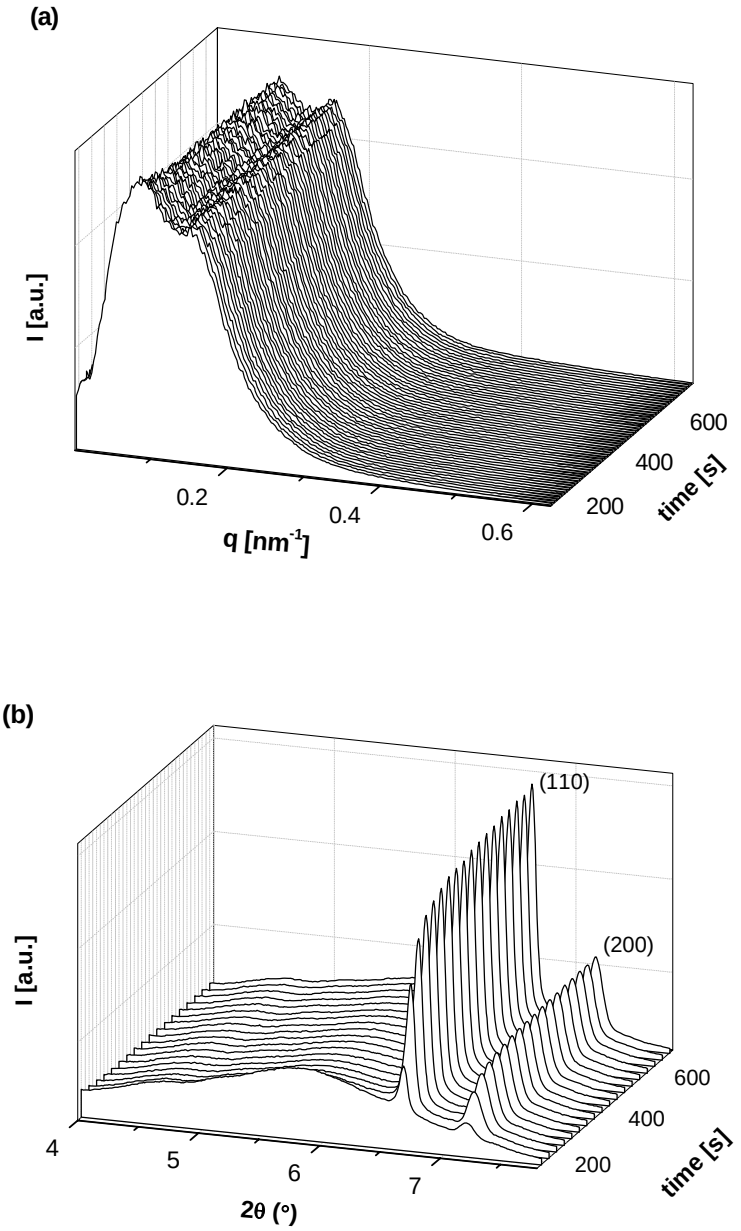

Figure 3.3: (a) The SAXS intensity evolution associated with meridian during isothermal crystallisation T = 125 °C as a function of scattering vector (q) and time. (b) The WAXD intensity evolution corresponding to 110 and 200 reflections as function of 2θ at isothermal T = 125 °C.

Figure 3.4 shows increase in intensity as a function of time on cooling from 136 °C to 125 °C. The earlier onset of crystallisation in polyethylene containing zirconia is noticed. The intensity corresponding to the meridian rises early as a function of time for

zirconia/PE composites. The results are in agreement with crystallisation studies using rheometry [184] addressed in the chapter 4. Hence, on shearing, the presence of zirconia nanofillers enhances the nucleation process causing the growth of kebabs earlier compared to neat polyethylene.

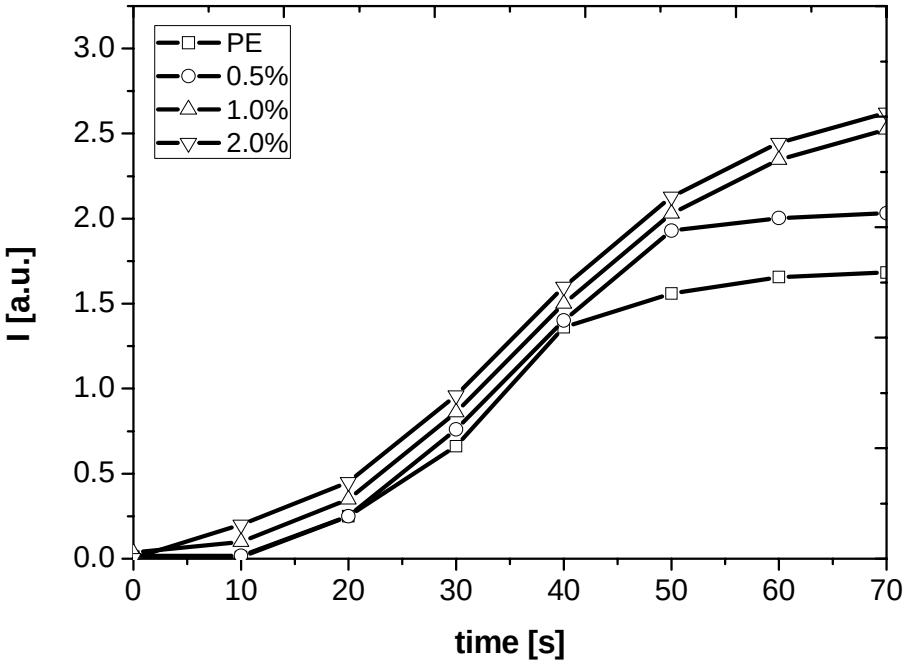

Figure 3.4: The rise of intensity as a function of time under cooling from 136 °C to 125 °C for PE in presence of zirconia nanofillers. The samples are sheared (100 s^{-1} for 1 s) at 136 °C before cooling to 125 °C.

Figure 3.5a, shows 2D SAXS patterns acquired after the selected time on cooling PE with and without zirconia. The patterns acquired on cooling after 10 s (T = 135 °C) of the applied shear at 136 °C show streak-like scattering. The intensity of streak-like scattering increases with increasing concentration of zirconia. This suggests that the presence of zirconia influences the relaxation behaviour of polymer chains and thus the amount of shish in PE. The patterns acquired after 50 s (T = 132 °C) on cooling shows the development of kebabs. The intensity corresponding to the meridian at this point is more for PE containing zirconia compared to neat PE (refer figure 3.4). Hence, the dominant shish formation in the presence of zirconia leads to the formation of kebabs. Figure 3.5b, shows 2D-WAXD patterns collected after 70 s (T = 130 °C). The 110

reflection is observed in all patterns, though the intensity of 110 arcs in neat PE is much lower compared to the ones observed in the presence of zirconia. The difference in intensity in the sample with or without zirconia can be also attributed to higher onset of crystallisation temperature in the presence of zirconia. However, taking both SAXS and WAXD images into consideration, the increase in intensity of the 110 diffraction peak with increasing concentration of zirconia, at the same crystallisation conditions, also suggests the presence of a greater volume of oriented structures – i.e. shish.

Considering the higher acquisition time (35 s) for the WAXD image compared to the SAXS (10 s) intensity arising in the WAXD pattern before 35 s after the applied shear could not be detected. Thus the developing WAXD pattern with the formation of shish is not detectable. Figure 3.5b shows a sequence of WAXD images where the intensities of 110 and 200 reflections increase after shear on cooling in the presence of 0.5 wt% of zirconia. In the initial stages, the two reflections appear perpendicular to the flow direction. However, with the increasing time i.e. decreasing temperature, the intensity of 200 reflection perpendicular to the flow direction (meridian) increases, whereas the intensity of the 200 reflection that appeared just after the flow along the equator does not change. It is to be realised that with the change in the position of 200 reflection, the position of 110 reflection stays the same. Such a shift in the position of 200 reflection can be accounted for by twisting of crystals (kebabs) between different shish. [205-206]

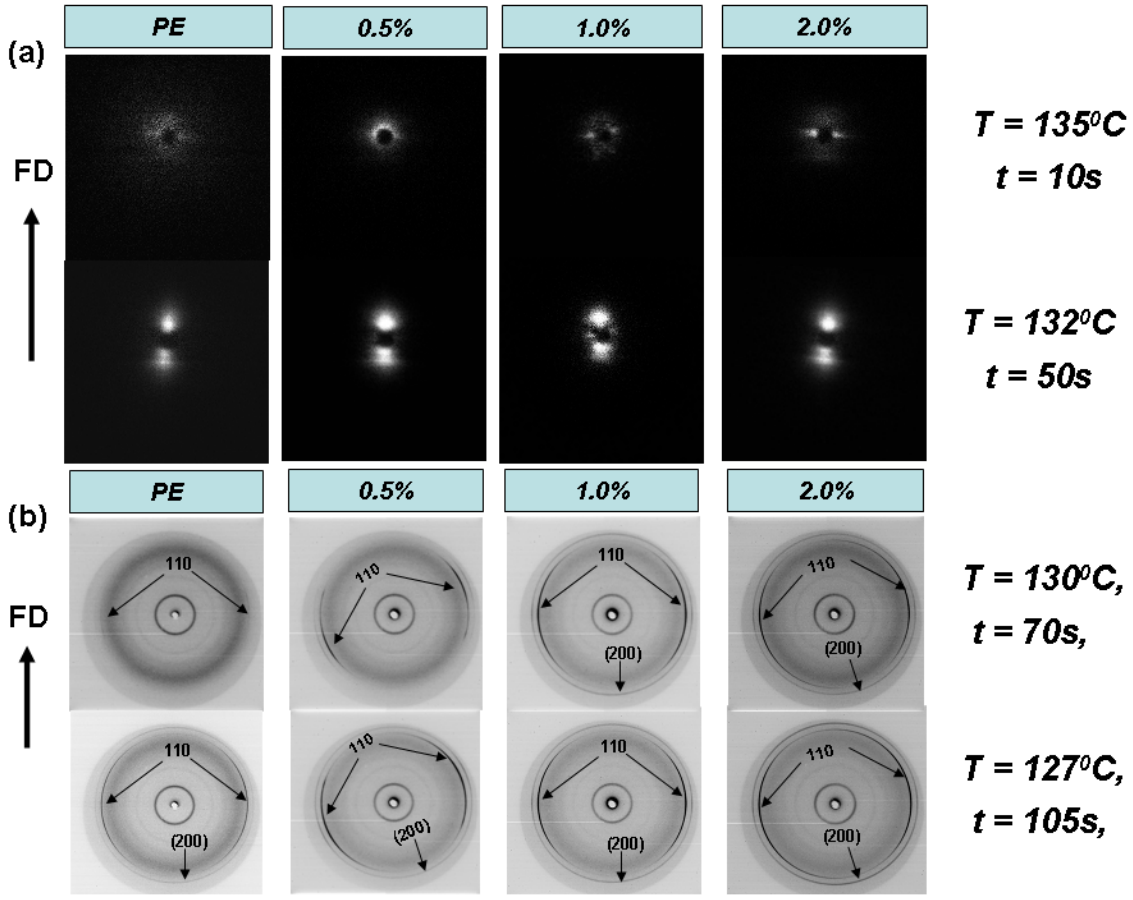

Figure 3.5: (a) 2D SAXS patterns after 10 s (T = 135 °C) and 50 s (T = 132 °C) are recorded for PE in presence of zirconia nanoparticles under cooling. (b) 2D WAXD patterns acquired after 70 s (T = 130 °C) and 105 s (T = 127 °C) on cooling.

3.3.2 Structure development at isothermal temperature

The SAXS and WAXD measurements were performed to study crystal growth at 125 °C. The shear rate of 100 s^{-1} for 1 s was applied at 136 °C followed by immediate cooling to isothermal temperature, 125 °C. 2D SAXS and WAXD patterns for neat PE and PE having different concentration of zirconia nanoparticles at the isothermal crystallisation temperature, 125 °C were collected. Figure 3.6 represents a composite of XRD patterns collected at 125°C after application of shear.

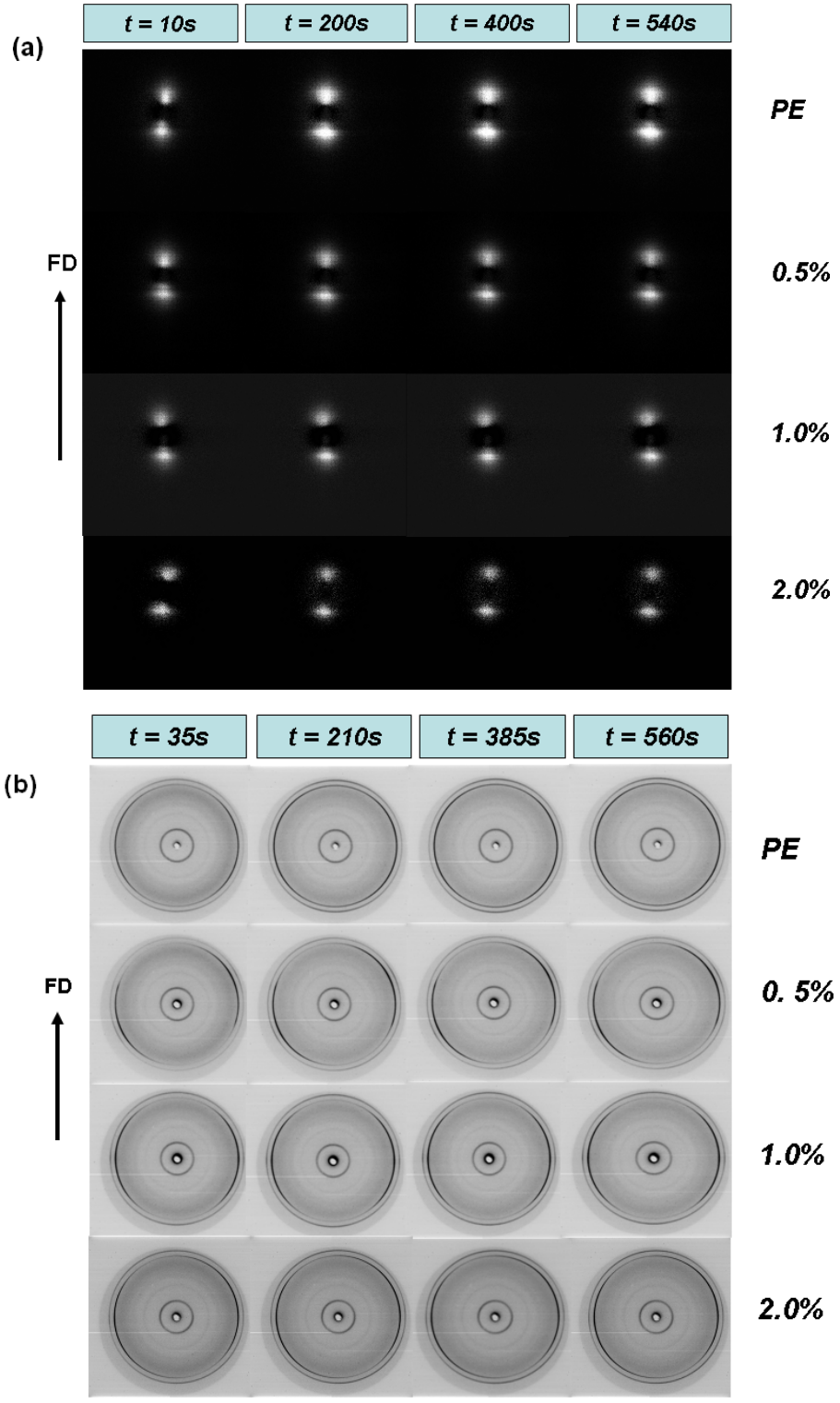

Figure 3.6: (a) 2D SAXS and (b) 2D WAXD patterns at selected times; acquired at 125 °C for PE having different concentration of zirconia.

The meridional scattering, shown in figure 3.6a, is obtained in the SAXS patterns at isothermal temperature T = 125 °C. Increase in intensity along the meridian is due to the development of lamellae structure – kebab formation which grows perpendicular to central core consisting of extended chain crystalline segments through the process of chain diffusion and adsorption. It is to be noticed that in the case of neat PE; pronounced scattering on the meridian after 10 s at isothermal temperature, 125 °C, increases with time before it reaches a plateau. The increase in intensity suggests significant growth of kebabs. The scattering remains stable from 200 s to 600 s during isothermal crystallisation after shear. In the presence of zirconia, unlike neat PE the obtained scattering in the meridian remains constant for the complete 600 s of the isothermal crystallisation. Selected 2D WAXD patterns were collected during isothermal crystallisation at 125 °C as shown in figure 3.6b. In neat PE, the initial diffraction patterns at the early stages of isothermal crystallisation 125 °C exhibit two highly oriented 110 and 200 arcs along the equator and the meridian respectively. This suggests that both *a*-axis and *b*-axis are perpendicular to the flow direction. In zirconia/PE composites, the 110 arcs along the equator and 200 arcs along the meridian become more sharp and intense with time. The sharp reflections indicate the formation of highly oriented PE crystals having better crystallinity. Thus, the WAXD results at 125 °C, strengthen the viewpoint of twisting of kebabs, reported in section 3.3.1 of this chapter.

Figure 3.7 shows the integrated meridional SAXS intensities for the zirconia/PE composites after the application of shear. The shaded region indicates the isothermal crystallisation region (T = 125 °C). The samples are cooled to the isothermal crystallisation temperature immediately after the cessation of shear at the controlled rate of 5 °C/min. The intensities for all the samples remain constant suggesting ordering of lamellar structures.

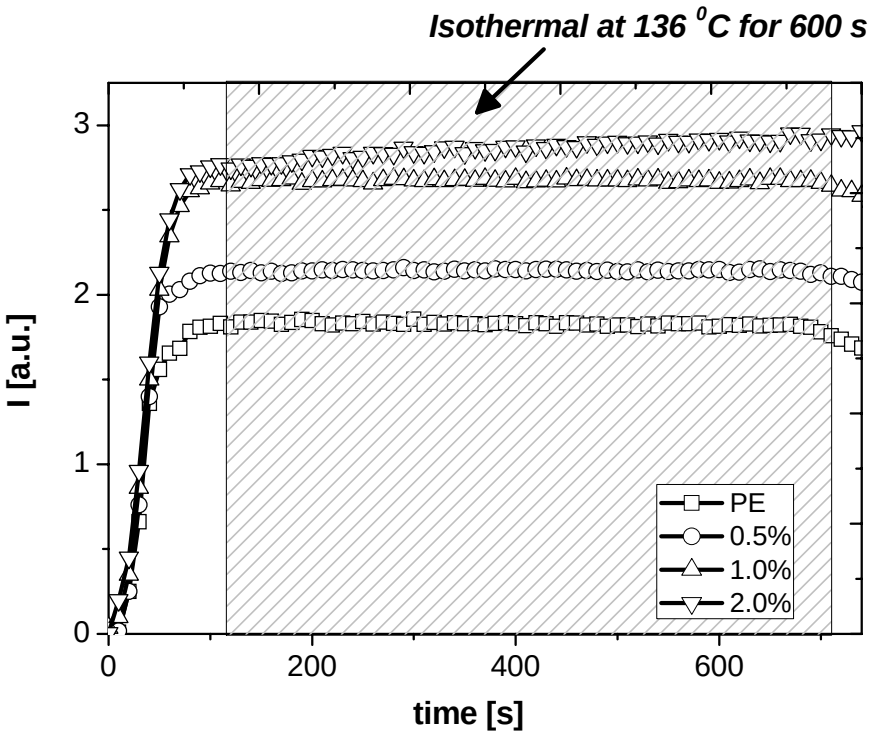

Figure 3.7: The integrated intensity of meridian from SAXS analysis; as a function of time obtained after cessation of shear ($\gamma^{\bullet} = 100\ s^{-1}$, $t_s = 1$ s at 136 °C). The isothermal crystallisation (T = 125 °C) is indicated by shaded region where the intensity remains almost constant for 600 s before cooling to room temperature. The unshaded region from 0 s to 120 s corresponds to control cooling from 136 °C to 125 °C.

3.3.3 Crystallisation at low temperature

Figure 3.8 shows the 2D SAXS and WAXD patterns acquired at 60 °C for PE and zirconia/PE composites. The 2D SAXS patterns from figure 3.8a, suggest the presence of oriented lamellae indicative of meridional scattering. The meridional scattering increases with the zirconia concentration in PE attributed to shish-kebab structures. The 2D WAXD patterns in figure 3.8b acquired at 60 °C show well oriented structures with the increase in zirconia content in PE. The 110 and 200 arcs become sharp with the increase in zirconia concentration, which becomes apparent on azimuthal integration of the intensity. It is also interesting to mention that unlike in the case of neat PE, the 2D WAXD patterns for zirconia/PE composites show weak 200 arcs along the equator together with the intense arcs along the meridian. Figures 3.9a and 3.9b show the azimuthal distribution of intensity obtained from the patterns acquired at 60 °C for the

110 and 200 reflections in all samples. From the full width half maximum of the110 reflection, it is apparent that the broad peak sharpens with the increase in the amount of zirconia. The peak intensity increases with the increasing amount of zirconia. This indicates that in the presence of zirconia crystals are more oriented along the flow direction.

The 200 reflection is present along the equator as well as meridian in all samples, with or without zirconia. However, the intensity of the 200 reflection in the meridian/equator changes with the concentration of the zirconia particles. For an example, with the increasing concentration of zirconia, the 200 reflection along the meridian increases.

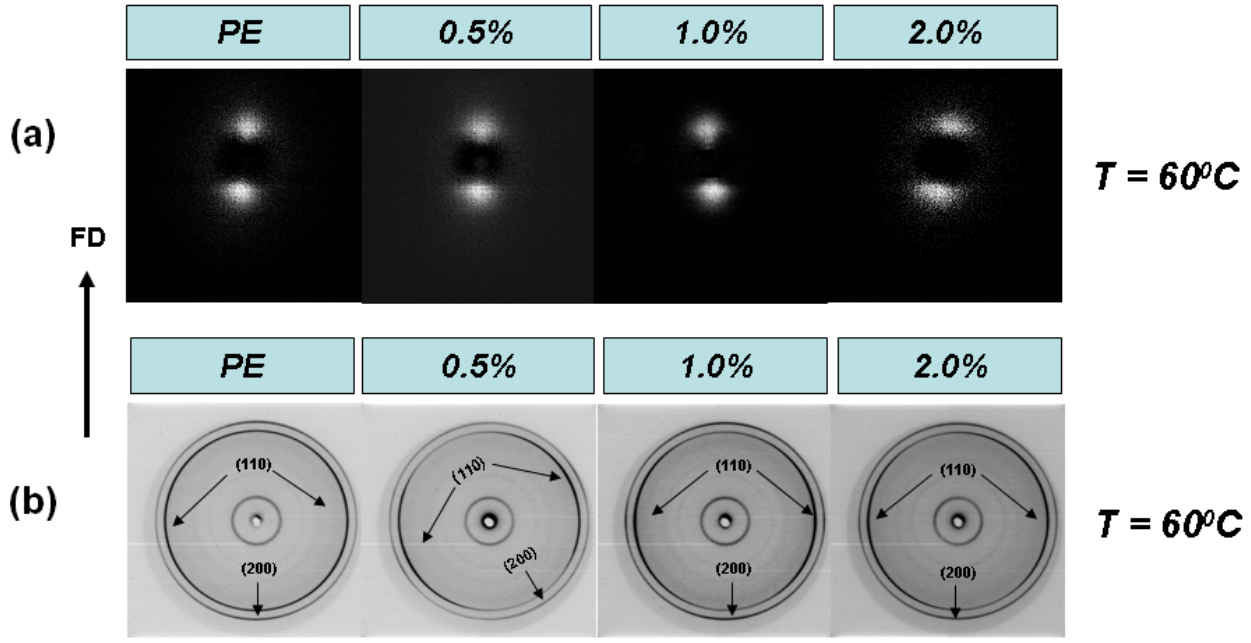

Figure 3.8: 2D X-ray patterns acquired at 60 °C for PE and Zirconia/PE composites; (a) from SAXS; (b) from WAXD.

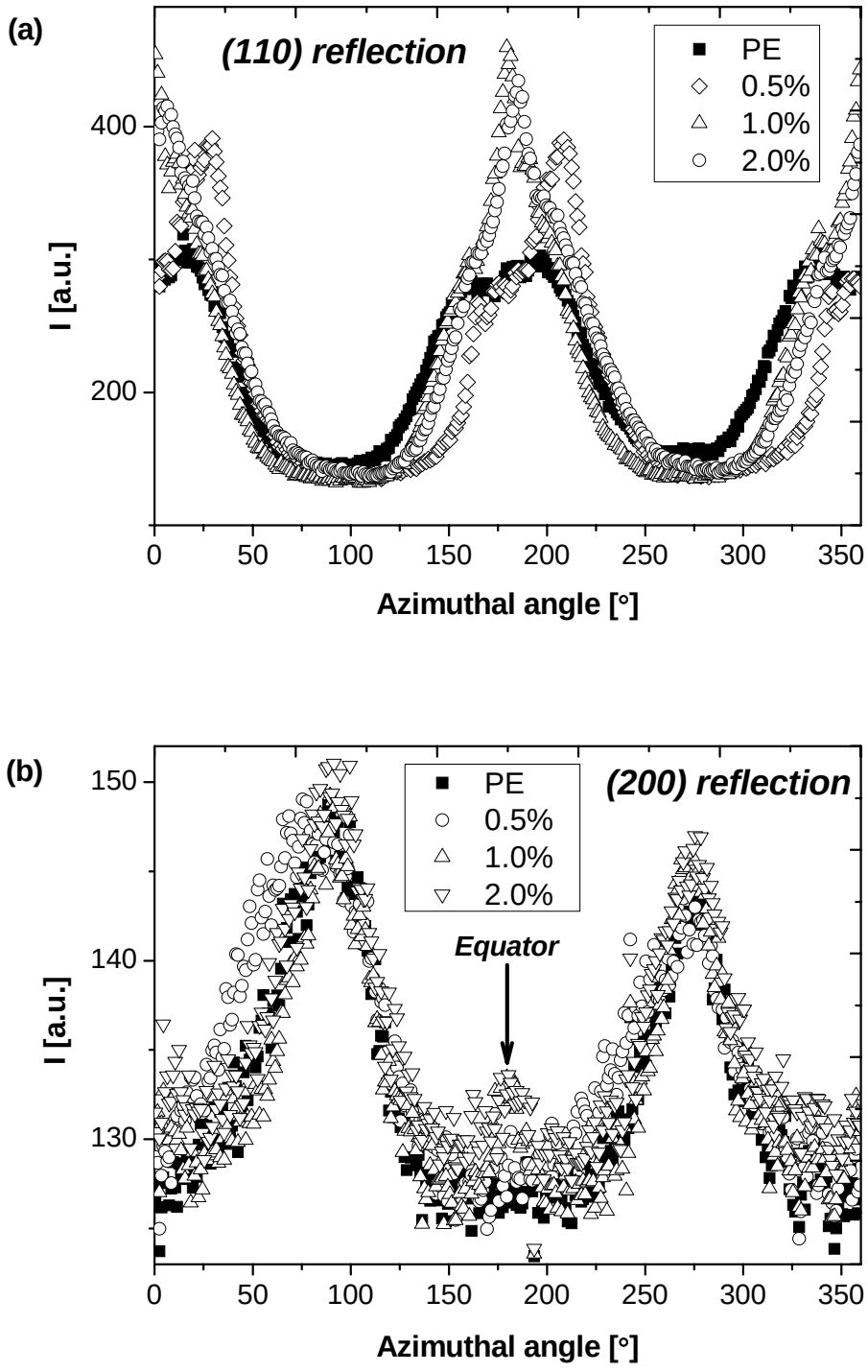

Figure 3.9: The evolution of azimuthal distribution of scattered intensity for; (a) 110 reflection; (b) 200 reflections at T = 60 °C for PE in presence of different concentration of zirconia nanoparticles.

3.3.4 Crystal orientation in broad MWD PE in the presence of zirconia nanoparticles

WAXD data was analysed quantitatively to provide information on the crystallinity in the semi-crystalline polymer. The overall intensity (X_T) obtained from WAXD data is proportional to the amount of crystalline phase. The WAXD crystallinity index is calculated after deconvolution of intensity scattered by the amorphous (X_A) and the crystalline phase (X_C) using procedures explained in other studies. [207] Further, the one-dimensional profiles of crystallinity are calculated.

$$X_T = \frac{X_C}{X_C + X_A} \times 100 \tag{3.1}$$

The value of X_C in this formula can be basically calculated from the intensity of crystalline peaks integrated between the two limits.

$$X_C = \int_{\theta_1}^{\theta_2} I_C(\theta) d\theta \tag{3.2}$$

Whereas, on integrating total scattered intensity between the same limits gives $X_C + X_A$ and can be represented as:

$$X_C + X_A = \int_{\theta_1}^{\theta_2} I_{C+A}(\theta) d\theta \tag{3.3}$$

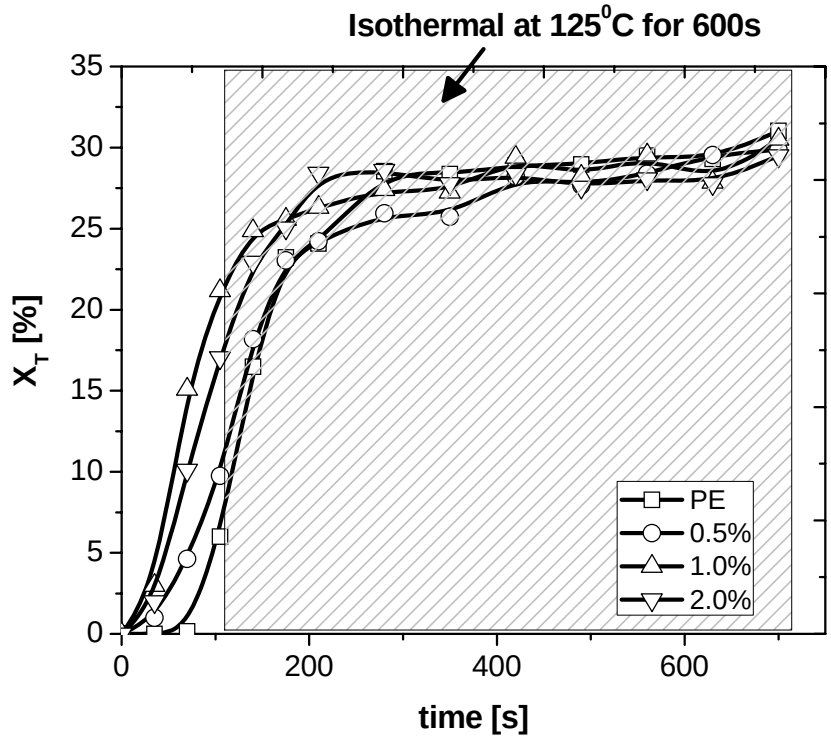

Figure 3.10: The overall crystallinity developments in sheared PE melt in the presence of nanoparticles. The shaded region corresponds to isothermal crystallisation.

Figure 3.10 shows increase in crystallinity as a function of time immediately after cessation of the shear ($\gamma^{\bullet} = 100\ s^{-1}$ for 1 s). The steady growth in the crystallinity is observed at the isothermal crystallisation temperature, T_c = 125 °C for 600 s. The polyethylene samples having different concentrations of zirconia nanoparticles (0.5 wt% to 2.0 wt%) gain higher crystallinity in the early stages compared to the neat PE. While on cooling from the sheared temperature to the isothermal crystallisation temperature, the earlier onset of crystallisation for polyethylene in the presence of zirconia is observed. This finding is in agreement with the SAXS analysis shown in the figure 3.4, where the earlier increase in intensity corresponding to meridian in the samples containing zirconia nanofillers is also observed.

The degree of orientation of crystals is determined using Herman's orientation function. [181]

$$f_h = 0.5 \times \left[3\left(\cos^2 \beta_c\right) - 1 \right] \tag{3.4}$$

Where, β is the azimuthal angle. The f_h value is 1.0, when *c*-axis of the crystallized particles is parallel to the flow direction; f_h value is -0.5, when when *c*-axis of the crystallized particles is perpendicular to the flow direction and in the case of randomly oriented sample f_h value is 0. Wilchinsky's method [208] can be used to calculate $\cos^2 \beta_c$ from 110 and 200 reflections by using formula,

$$\cos^2 \beta_c = 1 - 0.565(\cos^2 \beta_{200}) - 1.435(\cos^2 \beta_{110}) \tag{3.5}$$

Hence for the set of 200 or 110 reflection, the average orientation expressed in terms of $(\cos^2 \beta_{200})$ or $(\cos^2 \beta_{110})$ can be mathematically calculated using formula,

$$\cos^2 \beta_{hkl} = \frac{\int_0^{\pi/2} I(\beta) \cos^2 \beta \sin \beta d\beta}{\int_0^{\pi/2} I(\beta) \sin \beta d\beta} \tag{3.6}$$

Where, *hkl* is the set of 200 or 110 planes. Figure 3.11 shows the orientation function calculated from WAXD profiles. The polyethylene containing zirconia nanofillers shows higher orientation compared to the neat polyethylene.

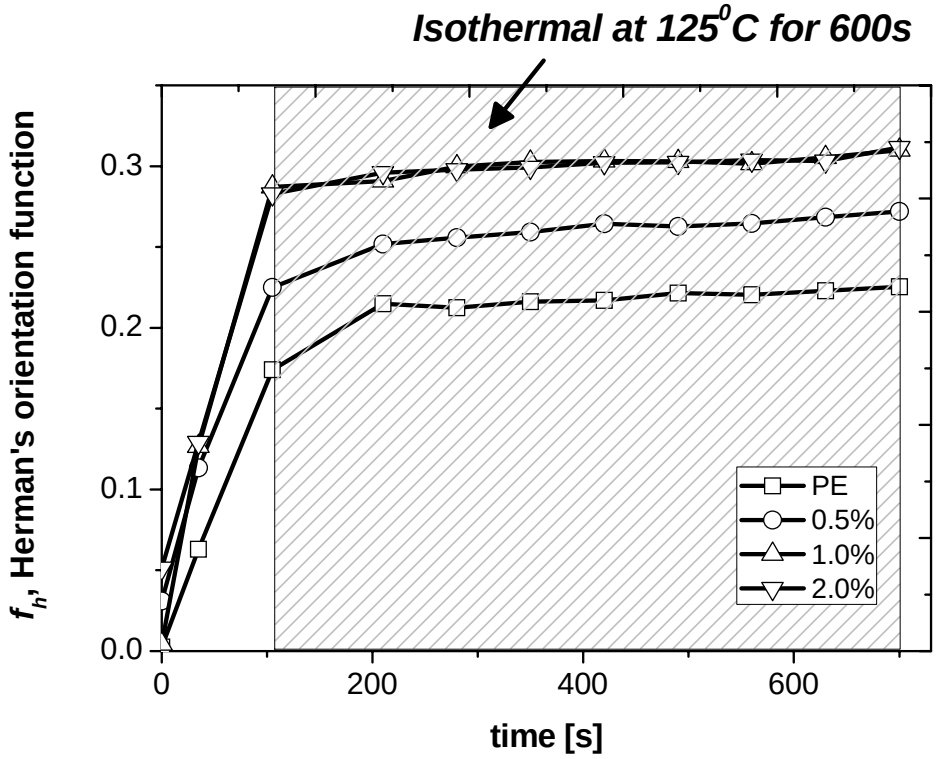

Figure 3.11: Herman's orientation function calculated after the application of shear ($\gamma^{\bullet} = 100\ s^{-1}$, $t_s = 1$ s at 136 °C) for PE melt in presence of different concentration of zirconia nanoparticles.

2D-SAXS images are analysed to determine the orientation fraction of polyethylene in the presence of zirconia. Figure 3.12 shows the oriented fraction as a function of time obtained from SAXS analysis.

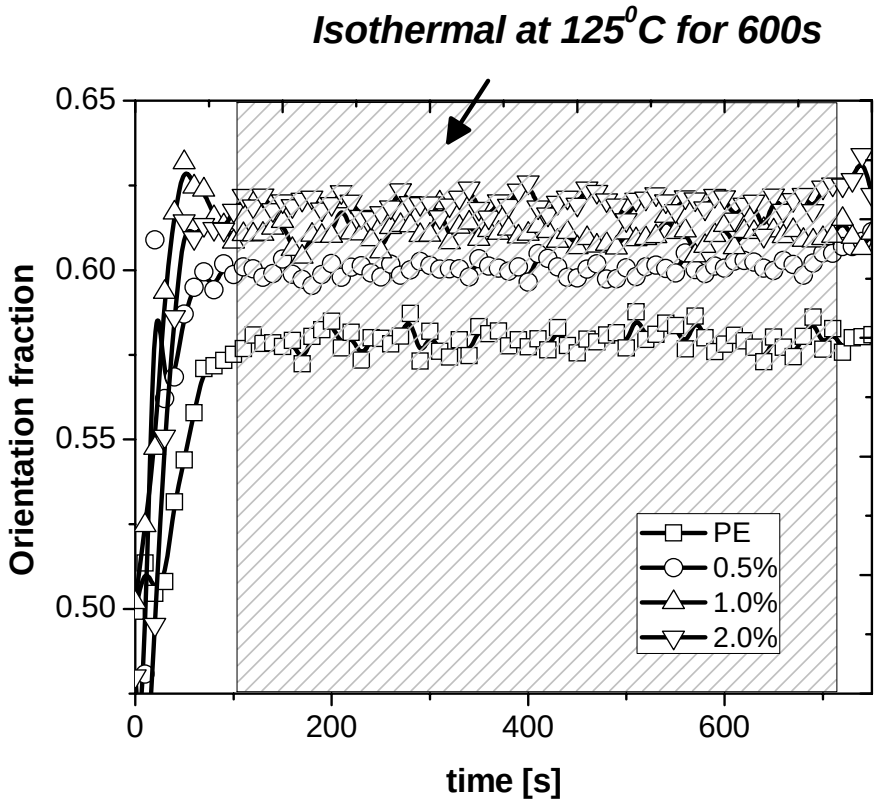

Figure 3.12: The orientation fraction obtained from integrated intensities of different regions extracted from 2D SAXS after the application of shear ($\gamma^{\bullet} = 100\ s^{-1}$, $t_s = 1$ s at 136 °C)

The intensity scattered from oriented crystallites is considered to be the sum of intensity obtained on the equator and the meridian [175].

$$I_O = I_E + I_M \tag{3.7}$$

Where, I_E and I_M are the scattered intensities corresponding to the regions of the equator and meridian. Thus the fraction of the oriented crystals of lamellae (ψ) from SAXS can be obtained on addition of the scattered intensities in the different azimuthal regions:

$$\psi = \frac{I_O}{I_T} \tag{3.8}$$

Where, I_T is total scattered intensity. The value of orientation fraction increases immediately after cessation of the shear and remains almost constant during isothermal crystallisation (T_c = 125 °C). The orientation fraction increases with increase in concentration of zirconia in polyethylene which is in agreement with the degree of orientation obtained from WAXD. The increase in the orientation under shear at higher concentrations is due to locally increased shear stresses produced as a result of zirconia nanoparticles and small inter-particle distances. The lower distance between adjacent particles at higher concentrations leads to interaction within themselves. Hence an increase in viscosity may be expected to lead high orientation in PE containing zirconia nanoparticles.

3.3.5 Distribution of crystallite size and long period in the adjacent kebab formation

The crystallite size was calculated from diffraction peaks of WAXD using Scherrer's equation. [209-211] Scherrer's equation assumes that the line broadening of reflections results from the finite crystallite size.

$$L_{hkl} = \frac{0.9\lambda}{\beta_{hkl} \cos\theta_{hkl}} \tag{3.9}$$

Where, L_{hkl} is the crystallite size in the direction perpendicular to the diffraction plane (hkl), 0.9 is crystalline shape function and β_{hkl} the peak width at half maximum intensity (in radians).

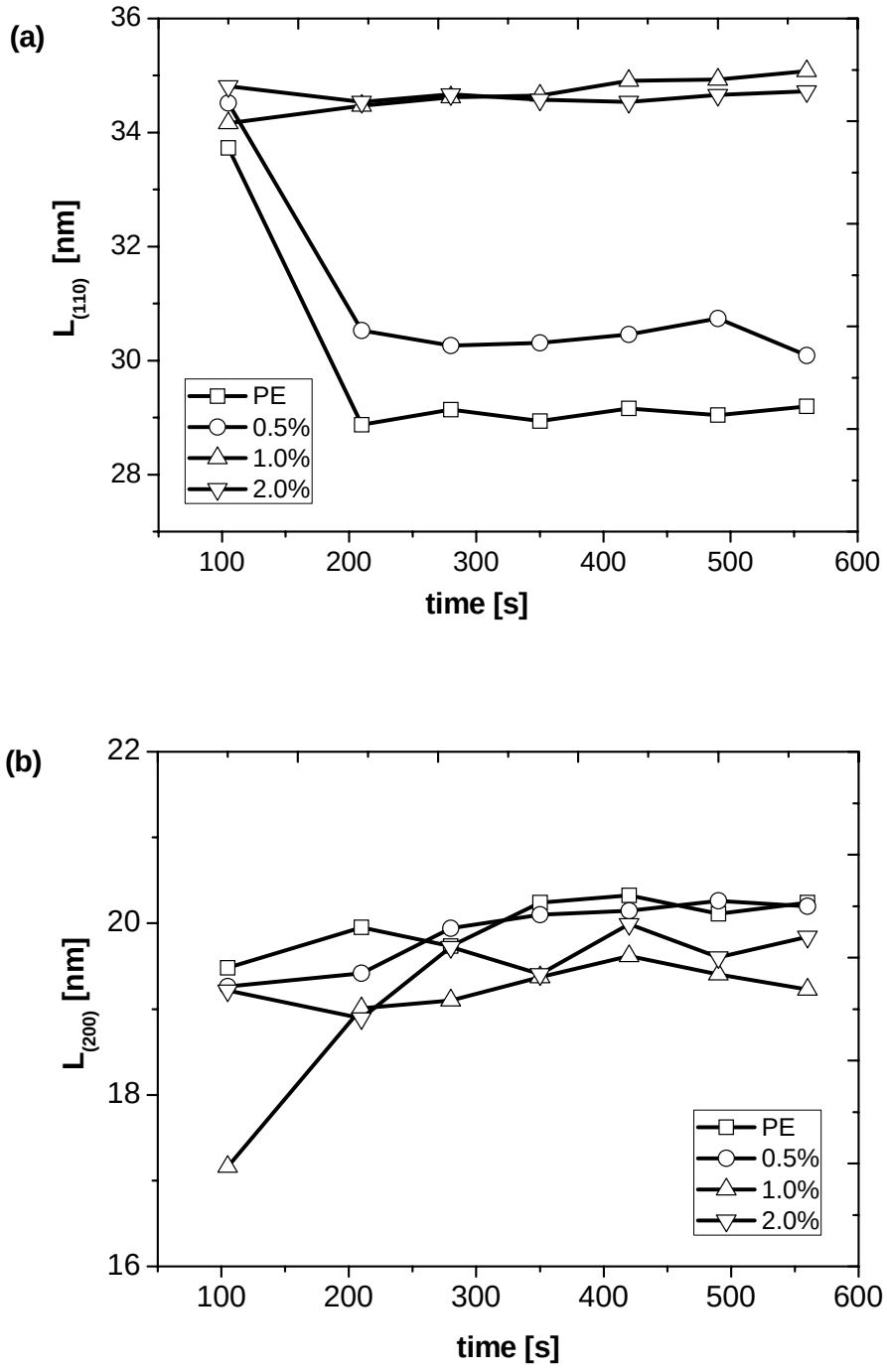

Figure 3.13: Distribution of dimensions of crystallites at isothermal crystallisation temperature (T= 125 °C) for zirconia/PE composites; (a) shows dimensions of crystallite in 110 direction. (b) shows dimensions of crystallites in 200 direction.

Figure 3.13, shows the apparent lateral dimensions L_{hkl} of kebabs in the hkl direction estimated using Scherrer's equation. The crystallite sizes for neat PE vary between 28 nm to 30 nm for the equatorial 110 reflections. In the presence of nanofillers, the crystallites size increases with increasing amount of zirconia content. The dimension of 110 crystallites vary between 34 nm to 35 nm. However in all cases, the dimension of meridional 200 crystallites fluctuates between 17 nm to 21 nm. The long period is calculated as,

$$L_p = 2\pi / q_{Max} \tag{3.10}$$

Where 'q_{Max}' corresponds to the maximum in the scattered intensity. Changes in the long period with time at the isothermal crystallisation condition after the cessation of the shear in polyethylenes with or without zirconia are summarised in figure 3.14.

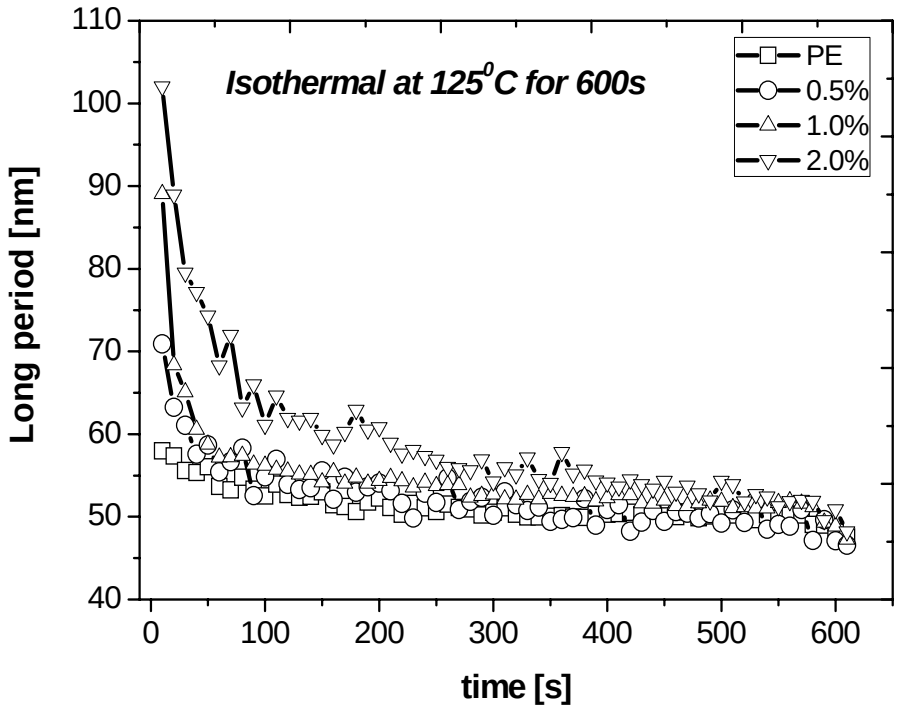

Figure 3.14: Long period obtained at isothermal crystallisation temperature (T=125 °C).

The long period decreases in the initial stages and reaches plateau after 200 s. The decrease in long period corresponds with the overall increase in the crystallinity. [68] (see figure 3.10) The electron density fluctuation of system is proportional to the invariant (Q). For instance, the invariant becomes zero for a homogenous system that does not have any concentration fluctuation. The invariant can be calculated using equation 3.11,

$$Q = \int_0^\infty I(q) \cdot q^2 ds \tag{3.11}$$

In case of an isotropic polymer sample, the electron densities arising from crystalline (ρ_c) and amorphous phases (ρ_a) can be obtained using equation 3.12,

$$Q = \varphi \cdot (1-\varphi) \cdot (\rho_c - \rho_a)^2 \tag{3.12}$$

The long period in the early stages in the presence of zirconia may arise due to high average electron density fluctuation between the zirconia particles (electron density of zirconia particle is 2.95 mole electron per cm^3) and the polymer melt/crystals (average electron density of PE is 0.5366 mole electron per cm^3). During isothermal crystallisation, with the increasing volume of polymer crystals the overall electron density of the crystals increases. Once the overall crystal density exceeds, the presence of zirconia particles, the measured lamellar thickness corresponds to the average distance between the crystalline and amorphous regions; prior to this the measured long period in the presence of zirconia is not the long period between the crystalline and the amorphous regions. As apparent from the figure 3.14 the time required for the true measurement of the long period between the average crystalline and the amorphous regions increases with the increasing content of the zirconia particles. From here it could be stated with certainty that within the experimental limitation, ultimately no difference in the average long period is observed after 300 s. Differences in the long period with increasing concentration of nanoparticles are simply a result of homogeneous distribution of spherical particles i.e. high electron density motifs.

3.4 Conclusions

Time resolved X-ray scattering (SAXS/WAXD) studies provide close monitoring of structure development under shear in polymers. The results in this chapter show the significant role of zirconia nanoparticles in formation of oriented structures after cessation of shear. The onset of crystallisation is found to shift to higher temperatures with the increase of zirconia content in polyethylene. The structure development under shear at an isothermal crystallisation temperature of 125 °C shows steady growth of lamella. The higher crystal thickness in zirconia/PE composites indicates that the overall crystallisation kinetics can be enhanced by addition of zirconia nanoparticles. The crystal orientation obtained from WAXD matches with SAXS data where the orientation is enhanced in polyethylene with increase in zirconia concentration. The study indicates the role of zirconia in increasing local shear stresses produced as a result of zirconia nanoparticles and small inter-particle distances. The analysis provides insight into the slight increase in viscosity as demonstrated in chapter 4 using rheology; in presence of zirconia, due to a smaller distance between adjacent zirconia nanoparticles, constructive interactions occur on a molecular scale.

Chapter 4

Influence of nanoparticles on the rheological behaviour and initial stages of crystal growth in linear polyethylene

In this chapter the role of broad molecular weight distribution (MWD) polyethylene (PE), in the presence of nanoparticles of different aspect ratios and binding efficiency with the polymer is demonstrated on the formation of shish-kebab structures under specified shear protocol using time-resolved small angle X-ray scattering (SAXS). The results show the scattered intensity in the form of streaks at the equator while maxima on the meridian confirm the presence of oriented structure in the polymer. SAXS facilitated the probing of steady growth of obtained shish-kebab structures at an isothermal crystallisation temperature, 136 °C. The study reveals the influence of nanoparticles (single walled carbon nanotube (SWCNT) and zirconia) on chain orientation. The presence of nanoparticles promotes a high degree of orientation, where shish is formed along the flow direction and kebab perpendicular to it. A higher degree of chain orientation is observed in the presence of SWCNT's compared to zirconia nanoparticles. SWCNTs present at low concentration (<0.6 wt %) are aligned in the flow direction leading to a increase in shish length as estimated from Ruland's streak analysis. The stable shishes in the early stages of crystallisation suppress the nucleation barrier for further crystallisation. Compared to the polymer without nanoparticles the shish length increases in the presence of zirconia, however the increase in shish length is much more pronounced in the presence of SWCNTs compared to zirconia nanoparticles. Nanoparticles increase the orientation fraction as deduced from the integrated intensity of equator and meridian in the patterns. Absence of the plateau in the low frequency region of the polymer-SWCNT composites suggests the absence of network formation. Nevertheless, comparing the storage modulus at two different temperatures (142 °C and 160 °C), suggests a strong temperature dependence and difference in adsorption energy of the two nanoparticles.

4.1 Introduction

The resultant morphology of a viscoelastic melt is strongly dependent on the molecular characteristics and the applied processing conditions. Morphology thus obtained influences the mechanical properties of the polymer, thus it has been always a quest to develop knowhow on the structure-property relationship. Because of their simplicity and commercial viability linear polyethylenes and polypropylenes are the semicrystalline polymers that have been investigated for sometime. One of the frequently used characterisation tools to follow structure development is time resolved X-ray scattering, where the intensity in the low angle region arises due to electron density fluctuation with the organisation of chains in the region of 1 to 100 nm. When the polymer melt is subjected to flow highly anisotropic structures, similar to shish-kebab are formed. To have insight in to the development of shish-kebab structures a series of studies have been performed. In all these studies the quest has been to understand the initial stages of shish formation. The structure formation is an outstanding issue still active due to less information available in the early stages of crystallisation as a result of different parameters such as effect of average molecular weight (M_w) and molecular weight distribution (MWD), melt memory, shear rate and temperature. What follows is a brief overview of some of the salient findings reported in the literature.

Shish-kebab morphology in polymers was first observed during fractionation process of high molar mass PE. [8, 212-213] Binsbergen [9] studied crystallisation in isotactic polypropylene (iPP) from melt. Using cross polarized optical microscopy under flow conditions, he observed birefringence arising due to chain orientation while cooling after application of shear at 180 °C. Keller et al. [68] proposed a hypothesis on the chain orientation above the critical molar mass M^*. In sheared polymer melts with a particular polydispersity at a given temperature, the chains longer than M^* can remain in an extended state and oriented after deformation while short chains relax back to form a random coil state as their relaxation times are short. Rheological studies [198, 214-215] have indicated the effect of shear rate and quenching on crystallisation under shear flow. According to Janeschitz-Kriegl and coworkers [79, 216-217] the oriented nuclei which are formed at high shear rates at temperatures close to the equilibrium melting point are practically stable at temperatures at which spherulites melt. Nevertheless, the application

of shear rates at temperatures below the melting point of the spherulites leads to the stable precursors due to longer relaxation times as compared to deformation time. As a result, the long lasting deformation under low stresses leads to the same precursors as that of short term deformation under high stresses. Schultz et al. [155] studied the mechanism of early stages of structural development under flow in polymer melt spinning using in-situ simultaneous X-ray scattering (SAXS/WAXS). They reported the presence of shish-kebab structures in the polyethylene melt and further verified such structures by SAXS without any detection by wide angle X-ray scattering (WAXS). Samon et al. [218] further reported that the onset of crystallisation is a result of chain orientation and does not depend on chain chemistry or specific undercooling.

Muthukumar and coworkers [152] with the help of molecular dynamics simulation studies showed that the emergence of shish-kebabs is related to the discontinuous coil-stretch transition of isolated chains. They demonstrated the presence of stretched and coiled conformations at a given flow rate. The stretched chains crystallise into shish, the coiled chains form single chain lamellae and then adsorb on to the shish constituting kebabs. Hsiao et al. [64] made use of a polyethylene (PE) blend containing 2 wt% of ultrahigh molecular weight polyethylene (UHMWPE) and 98 wt% of low molecular weight PE copolymer matrix to investigate FIC. The scanning electron micrographs of a solvent extracted sheared PE revealed the presence of shish-kebab structures with multiple shish. They stated that the disentanglements of UHMWPE in the blend, if any, were extremely low and further considered the hypothesis that the "entangled thread" upon stretching will show straight sections with short thread lengths aligned parallel to each other and remaining parts of thread will stay entangled or form globular sections. The multiple shish originates from the stretched chain sections and kebabs originate from coiled chain section following the diffusion controlled crystallisation process. The concentration of HMW chains in PE must be more than overlap concentration to form shish-kebab structure. The optimum concentration of HMW chains is 0.2 wt %. to form shish-kebab structure. Yang et al. [153] reported a higher degree of crystal orientation due to the role of long chains in the enhancement of shear induced precursor formation in bimodal PE blend. Zuo et al. [190] reported the melting and re-formation of shish-kebab precursor structure in sheared polyethylene

bimodal blend. The results indicated that shish-kebab re-formation is directly related to the relaxation behavior of stretched chain segments confined in a topologically deformed entanglement network.

Ogino et al. [199] studied the effect of ultra high molecular weight (UHMW) component in the formation of shish-kebab structures. They followed the crystallisation of PE blends of low molecular weight (LMW) and ultra high molecular weight (UHMW) components using time- resolved depolarized scattering (DPLS) techniques. Their studies showed the evident streaks in the equator of two dimensional patterns suggesting the role of the UHMW component. They argued that the critical concentration is two to three times larger than the overlap concentration of the chain (C^*_{Rg}), indicating the role of entanglements of UHMW PE chains in the formation of oriented structures. Keum et al. [219] demonstrated the nucleation and growth behavior of twisted kebabs from shear induced scaffold in entangled PE melts. According to them, low shear rates generate a lower shish density which enhances kebab twisting. Matsuba et al. [220] studied the role of UHMW PE on shish-kebab formation. Their investigations revealed a significant effect of crystallisation rate and the relaxation rate of the UHMW component on shish-kebab formation process. Kimata et al. [157] adopted small- angle neutron scattering to show that long chains are not overrepresented in the shish relative to their concentration in the material as a whole. They concluded that the molecular deformation of short and medium chains in the shish, being greater than that of long chains, enhanced fluctuations in the local molar mass distribution due to shear or a difference in the concentration of short and medium chains in the shish relative to the bulk.

Balzano et al. [89, 175] used a specially synthesised linear high density polyethylene with bimodal molar mass distribution. They demonstrated the presence of extended chains arising due to the high molar mass component in polymer melt while shearing above but close to the equilibrium melting temperature (T_m = 141.2 °C). They found a match between the dissolution time scale of the extended chains and the time scale for the reptation of HMW chains suggesting the role of HMW in the formation of flow induced precursors (FIPs). Studies also indicated that streak-like FIPs crystallised with an orthorhombic lattice producing only crystalline shishes. Kumaraswamy et al. [83, 197] showed that oriented crystals are formed as a result of value exceeding a critical

shear rate and shearing time. They claimed the presence of oriented nuclei under shear in the melt due to the distribution of relaxation time. Balzano et al. [221] recently studied precursor formation in the early stages of the flow induced crystallisation of iPP from the melt during and immediately after the application of strong shear. They reported the nucleation of crystalline structures during shear further affecting the development in structure and morphology. Recently, Haggenmueller et al. [149] showed the formation of shish-kebab structures as result of fiber spinning in SWCNT/PE composites. They demonstrated a higher chain orientation for the PE in presence of SWCNTs and stated that SWCNTs nucleate PE crystal growth, accelerating the crystallisation rate.

However, how the shish structure is influenced in the presence of nanofillers is not well investigated and is emphasised in this chapter. In general, the role of broad molecular weight distribution on the crystallisation process of PE is investigated and discussed, using a time resolved X-ray scattering technique to monitor the formation of shish-kebabs from early stages of crystallisation. The role of nanoparticles such as SWCNTs and zirconia, in the formation of highly anisotropic structures is further demonstrated. For polyethylene, while SWCNTs provide a good epitaxial matching and high aspect ratio, the presence of spherical zirconia particles provide very high surface to volume ratio with an aspect ratio of nearly one. This aims to provide an insight in to the structure development under shear in the formation of shish-kebab structures.

4.2 Experimental section

4.2.1 Materials and sample preparations

In this work, a linear PE with broad molecular weight distribution was utilised. The detailed thermal, MWD analysis and supplier's information is provided in chapter 2. SWCNTs are obtained from Unidym Inc., USA. The aqueous suspension of nano-sized yttria stabilized zirconia particles was obtained from MEL Chemicals, U.K. The suspensions of different nanoparticles were uniformly sprayed on to the PE powder (having average particle size of 100 μm) in the similar way as reported in chapter 2 and 3, as well as in the literature. [130, 222] The specific dimensions of individual SWCNT and spherical zirconia nanoparticle are reported in chapters 2 and 3.

4.2.2 Time resolved small angle X-ray scattering (SAXS)

The two dimensional (2D) time-resolved SAXS measurements were performed in DUBBLE/BM26B beamline at European Synchrotron Radiation Facility (ESRF), Grenoble, France. A two dimensional gas filled detector having resolution of 512×512 pixels and $260\ \mu m \times 260\ \mu m$ pixel size was employed to detect time-resolved small angle X-ray scattering (SAXS) patterns for shear experiments. The sample to detector distance for SAXS measurements was 6.057 m. The beamline consists of a vacuum chamber in between the sample and detector to reduce the scattering and absorption from air. The wavelength of synchrotron radiation used in SAXS experiments was 1.24 Å. An acquisition time of 10 s was used to acquire images with a dead time of 0.5 s for data transferring, following the correction of intensity of the primary beam, sample thickness and absorption needed between the adjacent images. The images were integrated to determine the scattered intensity (I) as a function of scattering vector (q). The range of length of scattering vector q in the SAXS measurements was 0.001 – 0.5 nm^{-1}, where q is given by $q = 4\pi \sin\theta/\lambda$, with, 2θ being the scattering angle. The integrated intensity as function of time is defined as, $I_{SAXS}(t) = \int_{q_{min}}^{q_{max}} I(q,t)dq$, where q_{max} and q_{min} being the maximum and minimum of q values. The obtained intensity data is subtracted with intensity prior to the application of shear.

In these experiments, samples in the form of flat disks of 400 μm thickness were obtained from compression molding. All the samples were mixed with Irganox 1010 to avoid the possible degradation. The flat disk-like samples were mounted between two plates of a Linkam shear cell CSS 450. The quartz windows of the shear cell were replaced by kapton windows to get the desired scattering. The shear cell was calibrated to a tolerance range of 30 μm to have maximum contact of plates with sample while shearing. The 400 μm sample was compressed in the shear cell upto 200 μm in the melt to ensure the correct application of shear on the sample during the experiment. The temperature and applied shear protocol (refer figure 4.1) for the shear cell was as follows.

1. Heat the sample from room temperature to 160 °C at a rate of 30 °C/min
2. Hold the sample at 160 °C in the melt for 5 min. to remove the melt history

3. Cool the sample at the rate of 10 °C/min to an isothermal crystallisation temperature of 136 °C and soon thereafter apply the shear (100 s^{-1} for 1 s).
4. Keep isothermal for 10 min at 136 °C during the experiment to follow the structure development under shear
5. Cool the sample to room temperature at the rate of 10 °C/min to monitor the crystallisation process while cooling

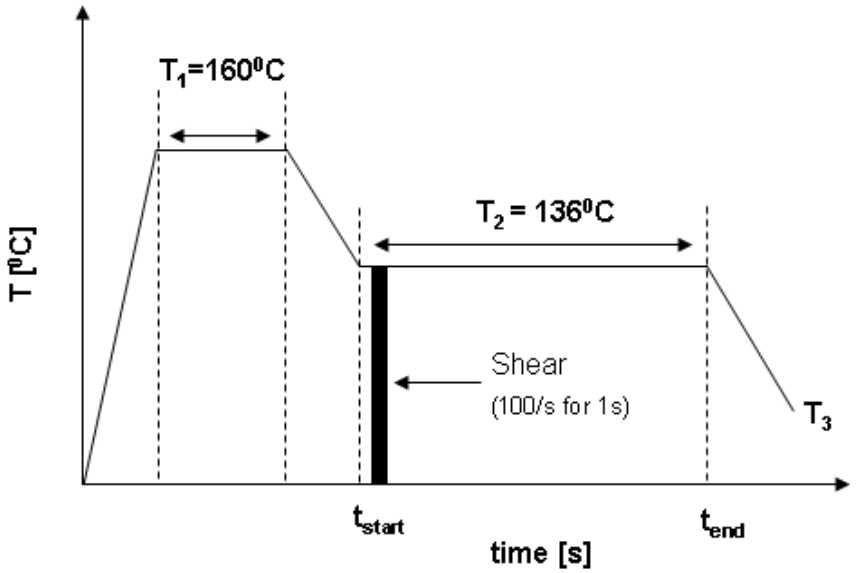

Figure 4.1: The schematic of the thermal and flow history applied in the present study. Shear rate of 100 s^{-1} for 1s is applied in isothermal crystallisation temperature of 136 °C to study the growth of structures. Here, T_1 represents the temperature in the melt i.e. 160 °C for 5 min. to remove the melt history. T_2 represents the isothermal crystallisation temperature of 136 °C and T_3 is 60 °C

Samples are subjected to steady shear at an isothermal crystallisation temperature of 136 °C to follow the structure development for 10 min. The shear rate of 100 s^{-1} for 1 s i.e. strain of 100 % was implemented. Steady 2D-SAXS patterns were continuously obtained for the whole profile of thermal and flow history.

4.2.3 Rheometry

Dynamic rheological properties were investigated using an ARES Rheometer. An oscillatory shear mode using parallel plate geometry with a diameter of 25 mm at 142 °C and 160 °C under the nitrogen atmosphere was adopted for the measurements. A frequency sweep ranging between 0.01 and 100 rad/s at low strain rate of 2.0 % was applied. The samples were placed between the preheated plates and allowed to equilibrate for approximately 5 min. prior to each run. The compression molded samples inside the rheometer were cooled from 142 °C to follow the evolution of storage modulus G' with the constant strain of 2.0 % and frequency of 10 rad/s. A slow cooling rate of 0.1 °C/min is used in all the cases for precise monitoring of the onset of crystallisation.

4.3 Results and Discussions

4.3.1 Role of broad molecular weight distribution in formation of shear induced structures

2D-SAXS patterns of polyethylene having a broad molecular weight distribution for selected times after the application of steady shear (100 s^{-1} for 1 s) at 136 °C are presented in figure 4.2. After shear the sample was left at the isothermal temperature of 136 °C for ten minutes. The steady shear in the polymer melt resulted in the formation of broad weak equatorial scattering which with time strengthened into streak-like scattering. From figure 4.2, it is evident that at the initial stages the broad weak scattering along the equator is constant for some time (refer to the pattern taken after 50 s). After 100 s of the applied shear development of scattering along the meridian occurs. In general, the appearance of streak-like scattering in the equator is attributed to the presence of a shish-like structure as explained in chapter 2. Considering variations in the intensity along the equator at the initial stages such a structure can be metastable, where the chains are oriented along the flow direction. At the later stage the appearance of maxima in meridian is related to the formation of kebab-like structure due to lamellar stacking resulting in outward growth of chains perpendicular to the central core. The results indicate that the applied strong shearing condition resulted in the formation of shish-

kebab morphology and enhanced crystallisation process in the broad molecular weight distribution polymer. The growth of shish-kebabs structures is enhanced at this flow protocol, an observation in agreement with the earlier reported findings [221]. Similarly the studies also suggest the role of critical shear rate below which the streak-like scattering in the equator do not occur. If this happens it is beyond the detection limit of the applied experimental conditions and presence of shish could be realised in the appearance of the intensity along the meridian during formation of the kebabs.

The SAXS intensity and the flow induced oriented crystals tend to increase as a function of time. The time resolved 2D-SAXS patterns give the real-time structure development in a sheared polymer melt: (1) After application of shear the increase in the streak like scattering with time along the equator suggest growth of shish. (2) The increase in intensity along the meridian with time at isothermal temperature, suggests the growth of kebabs after 100 s. These findings are in accordance with literature data [99] where at least in the initial stages of shear application the high molar mass component present in the polymer melt facilitates the shish formation. The chain orientation changes the crystallisation kinetics by providing the nucleation sites from which the oriented lamellae grow radially perpendicular to the chain axis.

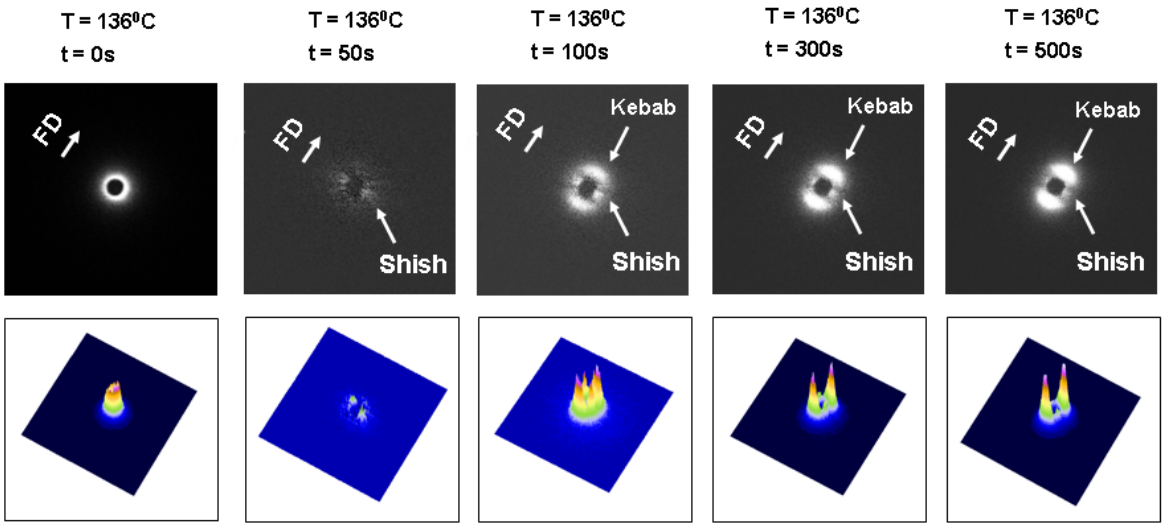

Figure 4.2: 2D-SAXS patterns of sheared broad MWD PE at isothermal crystallisation temperature of 136 °C for 600 s after application of shear rate of 100 s^{-1} for 1 s. The growth of kebab starts at 100 s and can be noticed in the image. The patterns show the steady growth of shishes and kebabs at isothermal crystallisation temperature.

The 2D-SAXS patterns, shown in figure 4.3, are taken at selected temperatures while cooling the polymer melt to room temperature after following the structure development process at the isothermal temperature, 136 °C. With decrease in temperature, the scattering in the meridian broadens and intensity increases. The kebab grows and meridional scattering separates out and gets transformed in to distinctive lobes at low temperatures. From the SAXS patterns it can be noticed that such a process of nucleation and transformation of meridional scattering into the formation of lobes starts at 126.9 °C. The persistence of anisotropic intensity on cooling suggests the near absence of spherulites in the shish-kebab dominated morphology. The increase in intensity suggests a volume increase in the electron density fluctuation due to re-organisation process of chain segments that occurs on cooling.

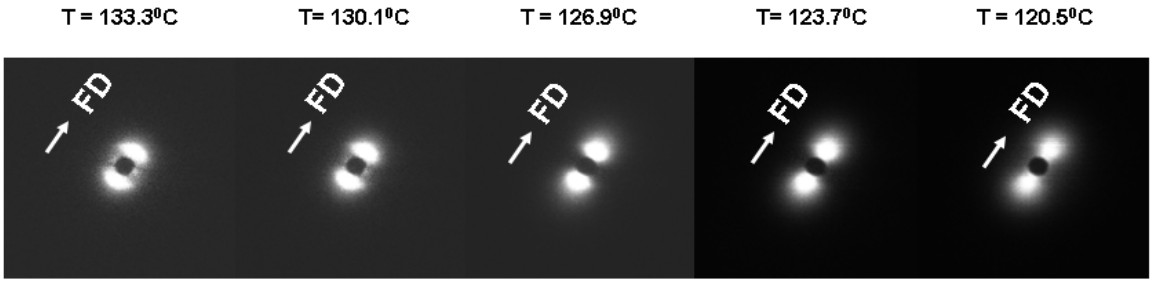

Figure 4.3: Selected 2D-SAXS patterns at different temperatures while cooling the polymer melt to room temperature after isothermal crystallisation at 136 °C for 600 s to follow the structure development.

The intensity build up during the crystallisation process at 136°C after the application of shear is shown in the figure 4.4. It is evident that after 100 s the intensity corresponding to the meridian dominates suggesting the development of kebabs in the obtained patterns. The equatorial intensity dominates in the early stages indicating the formation of shishes (extended chains) due to chain alignment or segmental orientation of molecular chains in a preferred direction. The intensities tend to grow as a function of time, consequently, accelerating the rate of crystallisation.

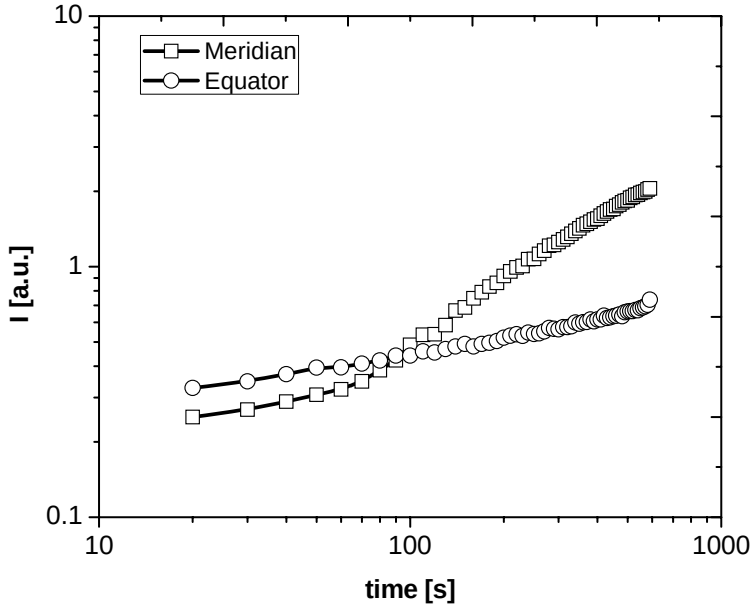

Figure 4.4: SAXS intensity built up as a function of time in the meridian and equator at isothermal crystallisation (136 °C) after application of shear (100 s^{-1} for 1 s) obtained from SAXS. The intensity in the initial stages is more in the equator as compared to meridian.

Observations in figure 4.4 are further supplemented by the evolution of scattered intensity as shown in figure 4.5 at isothermal temperature. The presence of a shoulder at higher *q*-values after 100 s suggests the growth of meridional maxima in the 2D SAXS pattern. This shoulder is attributed to the formation of kebab-like structures that result due to the growth of lamellar stacks perpendicular to the direction of the central core in the shish-kebab morphology. The overall intensity tends to grow as a function of time developing the oriented structures. The strong meridional maxima occurring in the patterns suggest a high volume fraction of kebab like structures. The results are in agreement with the similar studies performed in chapters 2 and 3 on neat PE. All the studies prove the role of HMW component of broad molecular weight distribution in formation of oriented structures.

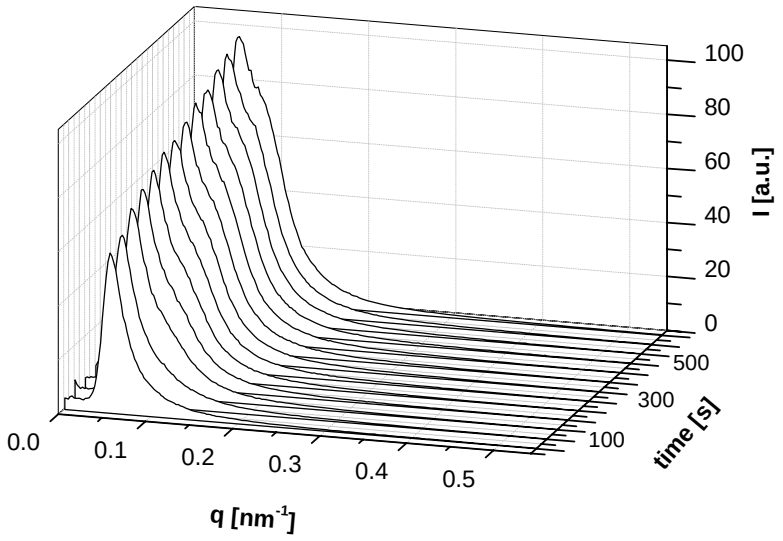

Figure 4.5: Evolution of total intensity scattered after the application of shear at isothermal condition of 136 °C.

4.3.2 Crystallisation in polymer melts of PE having broad molecular weight distribution (MWD) in the presence of nanoparticles

From literature [89] and the studies addressed in this chapter, it is evident that broad molecular weight distribution plays important role in the formation of shish-kebab structures, we further investigated the effect of nanoparticles on development of this morphology. The results indicate the acceleration of crystallisation kinetics after addition of nanoparticles in polymer melt. The crystallisation temperature shifts to higher temperatures in presence of nanoparticles. It is obvious from the SAXS patterns that more X-rays scattering takes place around the beam center in presence of single walled carbon nanotubes (SWCNTs) due to their high aspect ratios. The spherical shape of zirconia nanoparticles limits this excess of scattering to a certain extent as the particle size of such zirconia nanoparticles used in our studies is 20 nm. However, in either case, the extent of formation of oriented structure increased with increase in the concentration of nanoparticles. The 2D-SAXS patterns of polymer in presence of different concentration

of single walled carbon nanotubes and zirconia nanoparticles taken at selected times are presented in figure 4.6 and figure 4.7 respectively. The presence of nanoparticles enhances the alignment of chain segments under applied shearing conditions. The growth of formation of kebabs occurs early in polymers containing nanoparticles as compared to a pure polymer melt suggesting the early onset of crystallisation.

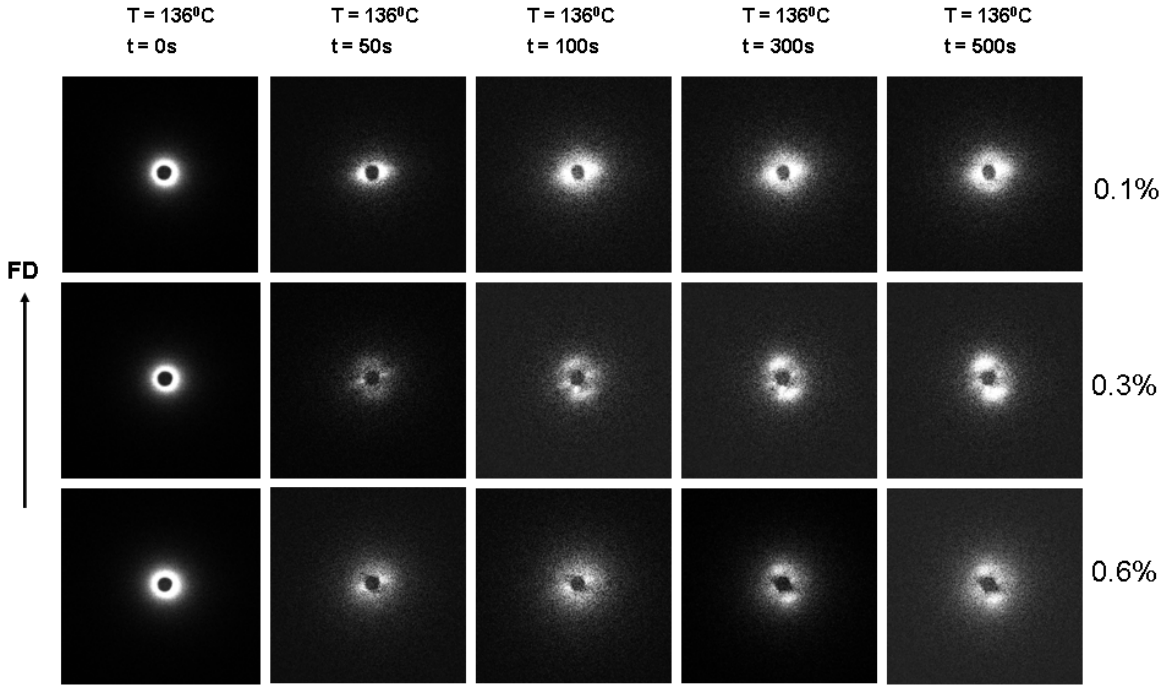

Figure 4.6: 2D-SAXS patterns of broad MWD PE in presence of SWCNTs at 136 °C at selected times after application of shear.

From figure 4.7 it is apparent that scattering in the vicinity of the beamstop in the presence of nanoparticles imposes difficulty in probing the weak scattering arising at the initial stages of shish formation. However, with time the evolution of intensity gives desired information about structure development under preferred shearing conditions. Smeared isotropically distributed intensity just before the shear (at t = 0 s), which increases with the concentration of nanoparticles, suggests the dispersion of nanoparticles in polymer matrix. After the application of step shear, now the subtracted intensity from t = 0 s, shows continuous increase in the intensity along the equatorial and meridional direction. The increase in intensity suggests the evolution of shish-kebab morphology in the presence of nanoparticles.

The increasing concentration of nanoparticles enhances the formation of shishes in the structure thus ultimately leading to formation of oriented kebabs. In all cases, streak-like scattering occurs in the equator resulting in the formation of multiple shishes in the polymer melt. Such scattering at the equator is soon followed by the meridional maxima leading to the formation of shish-kebab structures.

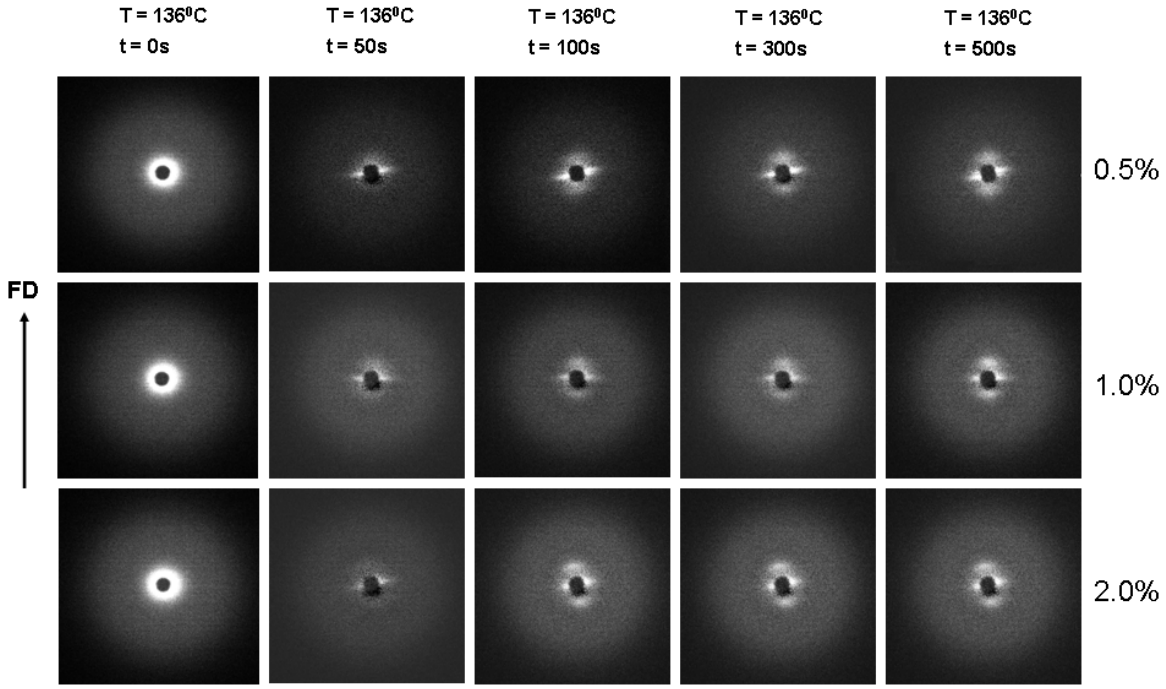

Figure 4.7: 2D-SAXS patterns of broad MWD PE in presence of zirconia nanoparticles at 136 °C after application of shear. The images are taken after selected times during isothermal crystallisation.

The figure 4.8 represents the equatorial intensity developments occurring after the application of shear (100 s^{-1} for 1 s, at isothermal crystallisation of 136 °C) to polymer melts containing different concentration of nanoparticles: SWCNT and zirconia. The presence of nanoparticles leads to increase in the intensities as compared to pure polymer melt. Equatorial intensity in the pure polymer grows as a function of time. In the presence of SWCNTs near constant intensities corresponding to the polymer melt represent the stability of these flow induced precursors. In the case of polymer melts having different

concentration of zirconia nanoparticles, integrated intensity corresponding to the equatorial region increases as a function of time indicating the possible growth of crystalline shishes as a function of time.

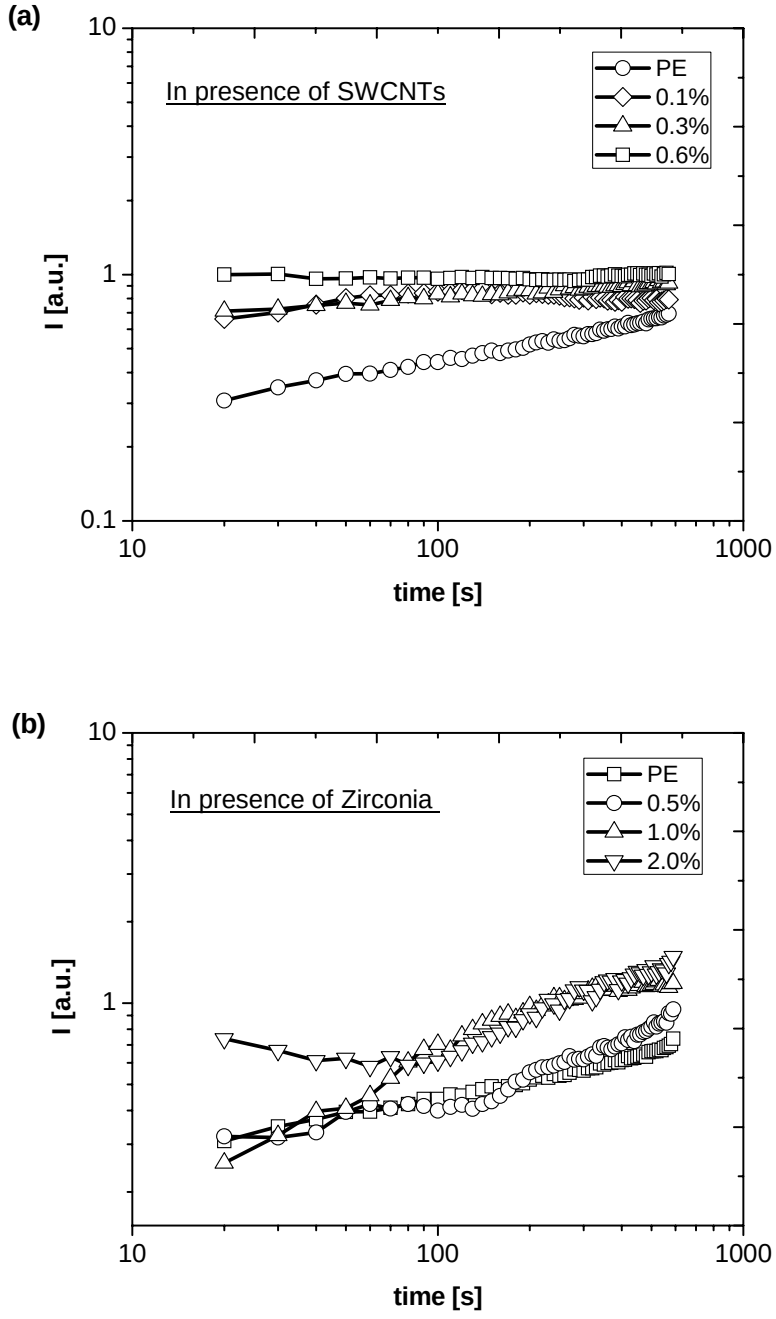

Figure 4.8: The intensity development in the equator for polymer melts at isothermal crystallisation after application of shear (a) at different SWCNT concentration (b) at different zirconia concentration. It is clear that increase in the concentration of nanoparticles leads to increase in intensity in equator suggesting the growth of shishes.

The figure 4.9 shows the 2D-SAXS patterns collected at 60 °C for different concentration of nanoparticles. All patterns show the partially oriented morphology which is basically a mixture of oriented and isotropic distribution of lamellae. This indicates the existence of shish-kebabs and spherulitic structures.

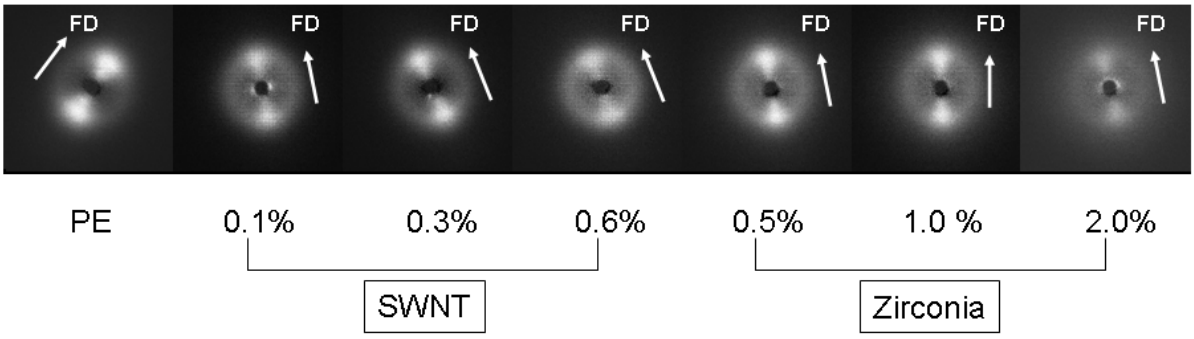

Figure 4.9: SAXS patterns of polymer melt in presence of different concentration of nanoparticles taken at 60 °C.

It is worthwhile to note that the increase in the scattering in the meridian occurs as a result of nucleation and growth of unoriented crystals and possible re-organisation of chains segments or oriented crystals within the lamellae causing the increase in electron density.

4.3.3 Determination of crystal orientation; along the equatorial and meridonial direction

Herman's orientation function [182] was used in our studies to determine the orientation for PE with different concentrations of nanoparticles. Detailed analysis of our SAXS data gave orientation of crystalline lamella as demonstrated elsewhere. [161] The equations used to calculate the Herman's orientation function are defined in detailed in chapter 2. Analysing the pattern in this way gives the values of Herman's orientation function *(f_h)*, i.e. $f_h = 1$, when scattered intensity is concentrated only perpendicular to the flow direction in 2D-SAXS patterns, $f_h = -0.5$, when scattered intensity is parallel to flow

direction in 2D-SAXS patterns and $f_h = 0$, when scattered intensity is diffused (isotropic in nature) and spread across the pattern.

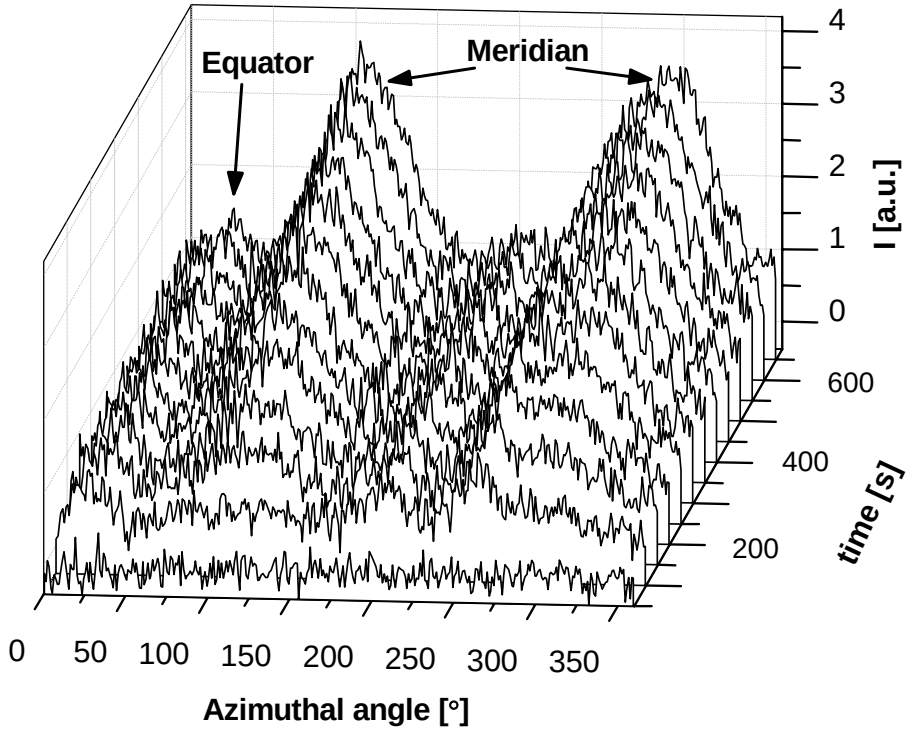

Figure 4.10: The illustrated azimuthal distribution of neat PE as a function of intensity obtained from the SAXS data analysis at different times for isothermal crystallisation temperature of 136 °C. The distinctive peaks corresponding to equator and meridian can be noticed in the intensity distribution.

The figure 4.11 shows the comparison of Herman's orientation functions obtained for the polymer melts in the presence of different concentrations of nanoparticles by the regressive analysis of SAXS data. Within 50 s, after the applied step shear, it is apparent that intensity along the equator exists, giving a positive value to the Herman's orientation function. When compared with the different nanoparticles, it is evident that the orientation function in the presence of nanotubes is higher than in the presence of zirconia. With the increasing concentration of nanoparticles the equatorial orientation arising due to shish formation increases, suggesting that the presence of nanoparticles favours the shish formation. Shish formation further promotes the kebab morphology leading to the evolution of intensity along the meridian. As anticipated, a greater amount

of shish provides more nuclei for crystallisation thus the higher orientation along the meridian. This becomes apparent in figure 4.11 after approximately 100 s of the applied shear.

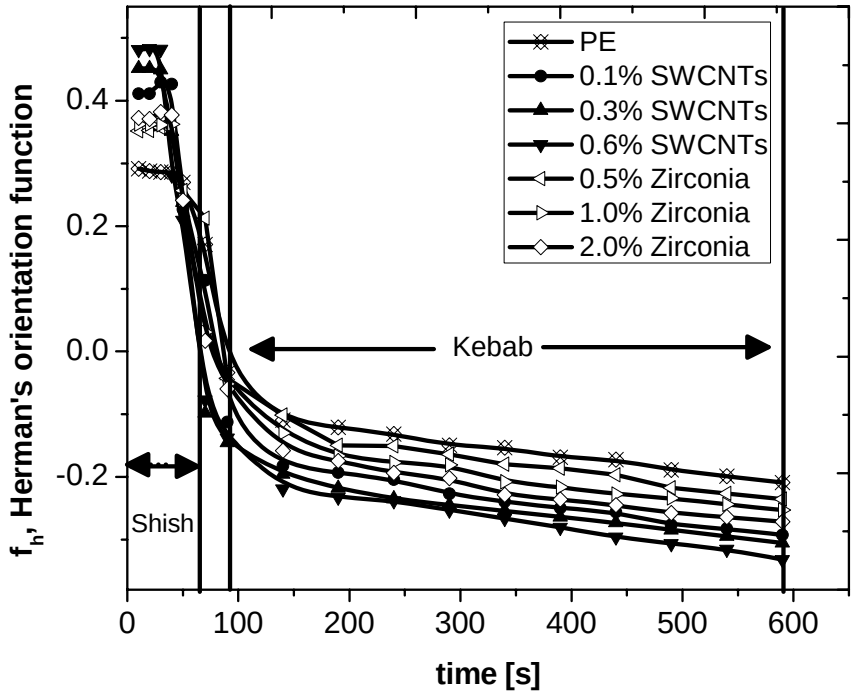

Figure 4.11: Herman's orientation function (f_h) for the polymer melt in the presence of nanoparticles. The orientation is dominated parallel to flow direction (shishes) in the initial stages obtained from equatorial scattering while the orientation is dominated by growing of polymer crystals (kebabs) as a function of time perpendicular to flow as a result of meridional scattering.

It is evident from the experiments and figures 4.2, 4.6, 4.7 and 4.11, that there is rapid increase of intensity in the meridian (kebabs) as a function of time because accelerated crystallisation kinetics dominates the orientation functions. In general, flow increases the orientation functions, the f_h increases with the increase of nanoparticles in either of the cases (SWCNT and zirconia). The early fall of orientation functions in the presence of nanoparticles suggest the possible role of nanoparticles in shifting the crystallisation process to a higher temperature (as consistent with the rheological studies performed in later part of this chapter). The SWCNTs orient more polymer crystals

parallel to the flow direction in the early stages as compared to zirconia which we attribute to alignment of nanotubes parallel to the flow direction.

The influence of nanoparticles in the development of oriented structures is further strengthened by the quantitative analysis performed below. From the 2D-SAXS patterns (refer figures 4.2, 4.6 and 4.7), it is obvious that the intensity along the equator and meridian increase with time. For this reason, both the intensities obtained in the equator and meridian are considered for calculation of the total orientation fraction from experimental techniques as also acquired from literature. [175] Only half of the 2D-SAXS patterns corresponding to two quadrants (i.e. from $\theta = 0°$ to 180°) is considered to yield the intensity value related to different regions. Thus intensity scattered due to oriented crystallites is considered to be the sum of intensity obtained in the equator and meridian.

$$I_O = I_E + I_M, \tag{4.1}$$

Where, I_E and I_M represents the intensities related to corresponding regions and can be considered as the intensity of oriented crystallites obtained by summation. Thus, the amount of oriented crystals (ψ) in the SAXS patterns is

$$\psi = \frac{I_O}{I_T} \tag{4.2}$$

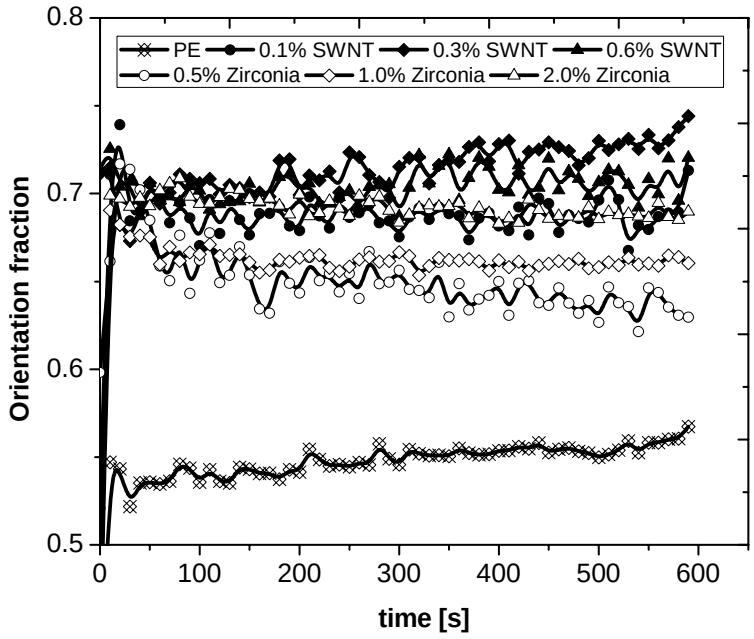

Figure 4.12: The orientation fraction (ψ) estimated through the intensities obtained in the equator and meridian direction.

Like figure 4.11, figure 4.12 shows that with increasing amount of nanoparticles the overall orientation increases. For the amount of nanoparticles used, compared to the zirconia, SWCNTs seem to be more effective in the development of oriented structures. What follows is the quantitative analysis on the length of shish structures that could be observed in the presence of nanoparticles.

4.3.4 Analysis for estimation of length of shishes using Ruland's streak method

The length of shishes present in the obtained shish-kebab structures was estimated using Ruland's streak method. [223-226] The integral width of angular distribution of the scattered intensity B_{obs} was used to estimate the true width of the orientation distribution B_{ϕ} (misorientation) and the average length (L) of the shishes aligned in the direction of the c-axis. The azimuthally distributed scans of intensities at different q values were analysed using the Lorentz function to yield the average width of the angular distribution.

The width of the equatorial streaks in reciprocal space can be related to obtain the length of shish (L). The relationship between the L and B_ϕ can be approximated as,

$$q^2 B_{obs}^2 = \frac{1}{L^2} + q^2 B_\phi^2 \qquad (4.3)$$

The relationship gives linear plot between $q^2 B_{obs}^2$ and q^2. The shish length (L) and degree of misorientation (B_ϕ) are determined through the linear least square fitting applied to our data. In the relation, $q = 4\pi \sin\theta/\lambda$ (2θ is the scattering angle whereas; q is the scattering vector, λ is wavelength). The length of shish (L) is determined from the intercept of the linear plot while B_ϕ represents the misorientation parameter. The interpretation of 'L' for shish is considered to be orderly aligned in the direction of c-axis.

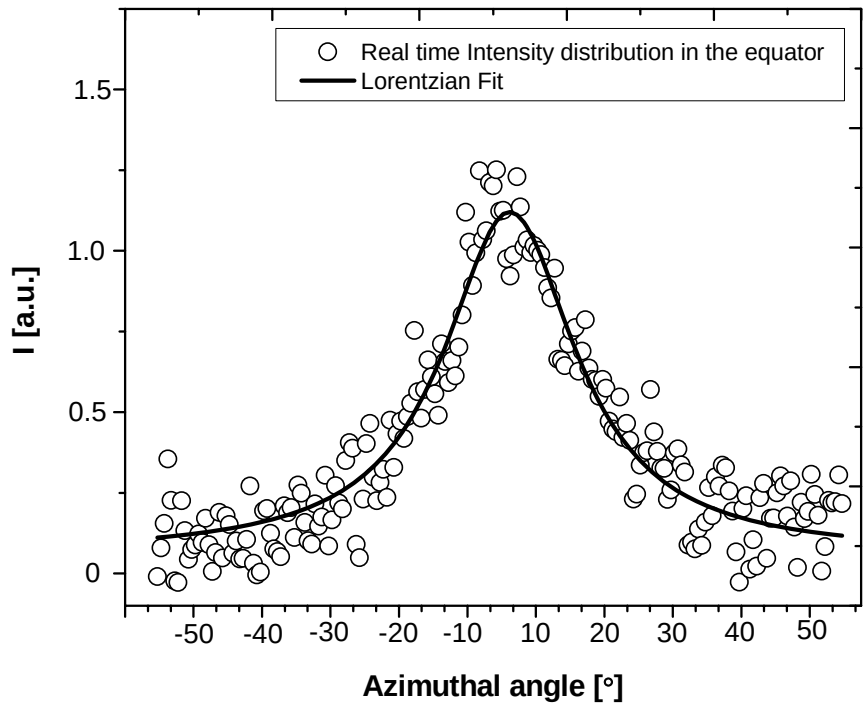

Figure 4.13: Typical distribution of azimuthal scattered intensity at equator in presence of streaks obtained for neat PE. The intensity usually fluctuates due to metastable nature of these FIPs in the intial stages of crystallisation. In order to analyze, the data points are fitted with Lorentzian function to get proper values of integral width of angular distribution (B_{obs})

The figure 4.13 shows the typical azimuthal distribution fitted with the Lorentzian function to estimate the integral width of angular distribution (B_{obs}) required for obtaining the length of shish (L). The obtained integral width of angular distribution (B_{obs}) was plotted as a function of scattering vector (q) based on the equation (4.5). The average values of shish length obtained are plotted as a function of different concentration of nanoparticles (figure 4.14).

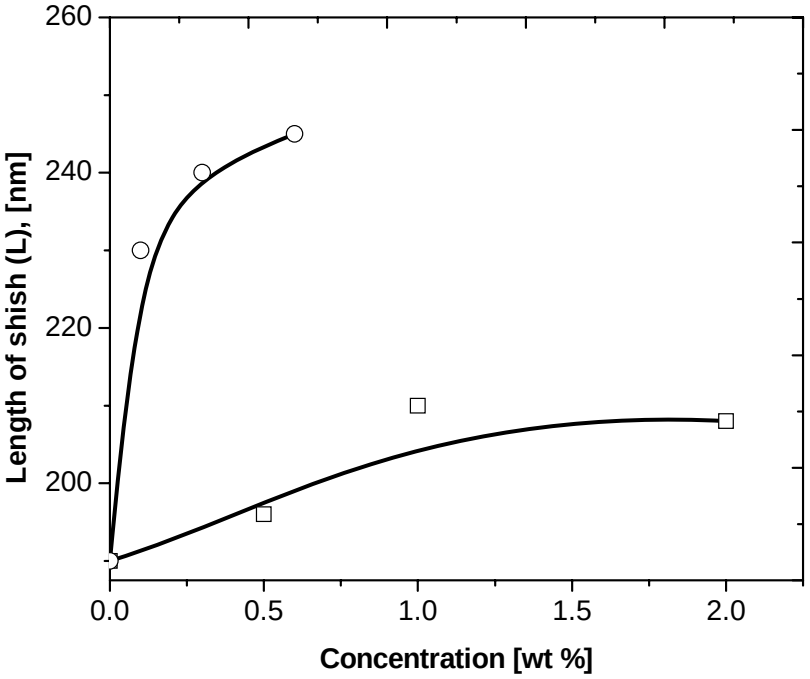

Figure 4.14: Average length of shish as a function of different concentration of nanoparticles. (○-represents the shish length in presence of SWCNTs, □-represents the shish length in presence of zirconia)

The average values of shish length are found range from 190-250 nm. The presence of SWCNTs favors shish formation as is evident through the rapid increase in shish length at low concentration as compared to that of zirconia nanoparticles. In presence of both nanoparticle types, the average length of shish grows with increasing concentration. The increase in the shish length further supports the observations in figure 4.11 where it is observed that the growth of kebabs occurs earlier in the presence of nanotubes than in zirconia, and is concentration dependent. The kebabs grow rapidly in

the perpendicular direction to the shish. In contrast to some studies [227] (where, the shrinking of shish length as a function of time at isothermal crystallisation conditions is observed), the present study showed the steady growth of shish within the range of 20-30 nm at constant temperature as a function of time. Other interesting features are the values of misorientation obtained from the Ruland's streak method. The degree of misorientation (B_ϕ) decreases with the increase in nanoparticle concentration (shown in table 4.1). The average value of misorientation of shishes is lower in presence of nanoparticles indicating the better orientation in the obtained shish-kebab structures. These results are in agreement with the conclusions drawn from figure 4.11.

Table 4.1: The degree of misorientation (B_ϕ) for PE in presence of nanoparticles

Samples	**PE**	**SWCNT Concentration (%)**			**Zirconia Concentration (%)**		
		0.1	***0.3***	***0.6***	***0.5***	***1.0***	***2.0***
Misorientation , B_ϕ (°)	33	20	19.5	17	26	22	23

4.3.5 Rheological properties of PE melt in presence of nanoparticles

Before analysing rheological properties, some of the salient findings reported in earlier experiments performed on polyethylenes in the presence of nanotubes, where polyethylenes having molar mass greater than a million g/mol, show network formation. In rheological studies such a network formation is realised at low frequencies, where the modulus of the polymer-SWCNT network is much lower than the network arising due to the entanglement formation. One of the other findings reported in such studies is the decrease in viscosity at a specific concentration of nanotubes (0.2 wt%). One of the explanations provided for the decrease in viscosity is the selective adsorption of high molar mass component in the polydisperse polyethylene. [130, 222] Because of the van der Waals interaction, PE chains tend to be adsorbed on the SWCNTs (also suggested by the crystallization studies, see figure 4.19). In the applied experimental time, the probability of the high molar mass to remain adsorbed on the SWCNTs will be higher than the low molar mass chains. The adsorbed polymer, especially of high molar mass, can be considered as an immobilised part of the SWCNT at least for times larger than the

experimental time. Thus, the polymer forming the remaining matrix will effectively have a lower average molecular weight than the pure polymer (dashed chains in the illustration of figure 4.15). This would cause faster relaxation of chains thus a decrease in the storage modulus (or viscosity) as found in figure 4.18

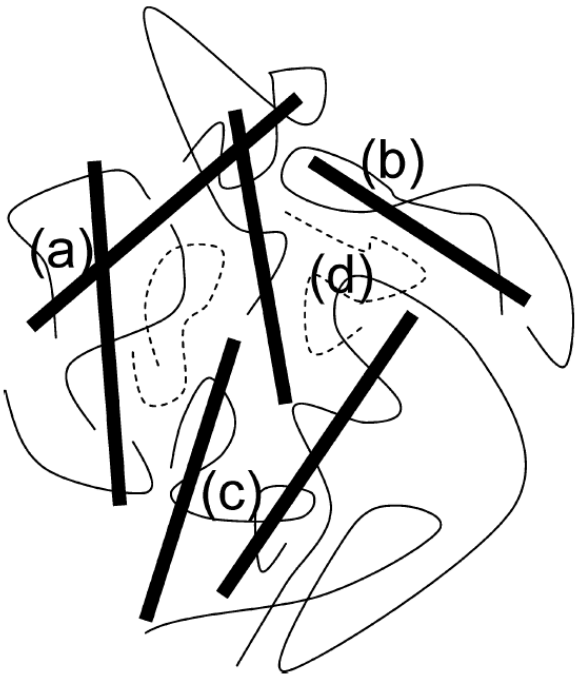

Figure 4.15: Illustration of SWCNT-polymer interactions. The figure shows presence of different networks: (a) SWCNT-SWCNT network formation; (b) SWCNT-polymer interaction (adsorption); (c) SWCNT-polymer-SWCNT bridging; (d) polymer-polymer network through temporary entanglements. [130, 228]

Figure 4.16, shows the change in the storage modulus G' at two different temperatures (T = 142 °C and 160 °C) for different concentrations of SWCNTs in PE. Considering the low molar mass of PE used in this thesis, unlike UHMW-PE, in the presence of nanotubes no plateau at the low frequency region is observed. However, with the increasing amount of nanotubes, parallel shift in the modulus as a function of frequency become apparent. Similar to the earlier reported findings the presence of nanotubes in the polymer matrix also shows nonlinear increase in viscosity with increasing amount of nanotubes. The nonlinear increase in viscosity, complemented by the parallel shift in the modulus at different frequencies, show temperature dependence. That is with the increase in temperature from 142 °C to 160 °C the effect of drop in viscosity is suppressed. A cause for such a drop in viscosity is attributed to selective

adsorption of high molar mass chains on to the dispersed nanoparticles. Considering the similar molecular arrangement of nanotubes and polyethylene chains, compared to the zirconia and polyethylene as shown in figure 4.17, a lower barrier for the selective adsorption between the nanotubes and polyethylene could be anticipated. Such a possibility becomes apparent on comparing the changes occurring in the viscosity with increasing concentration of zirconia nanoparticles in polymer matrix, where with the increasing concentration of zirconia a regular increase in the modulus occurs and no drop in viscosity is observed [130-131, 146, 222, 229-230] as shown in figure 4.18.

To have more insight on the influence of selective adsorption, crystallisation behaviour on cooling from the polyethylene melt in the presence of nanoparticles has been followed by rheological studies. From figure 4.19 it is apparent that the onset of crystallisation shifts to higher values with increasing amount of nanotubes from 0.1 wt% to 0.6 wt%, whereas, the shift in the onset of crystallisation in the presence of zirconia is observed above 0.5 wt% of dispersed particles in the polymer matrix. The change in slope in the modulus build up with crystallisation further strengthens the pronounced effect of nanoparticles. Below 122 °C, due to possibility of slippage data are not reliable.

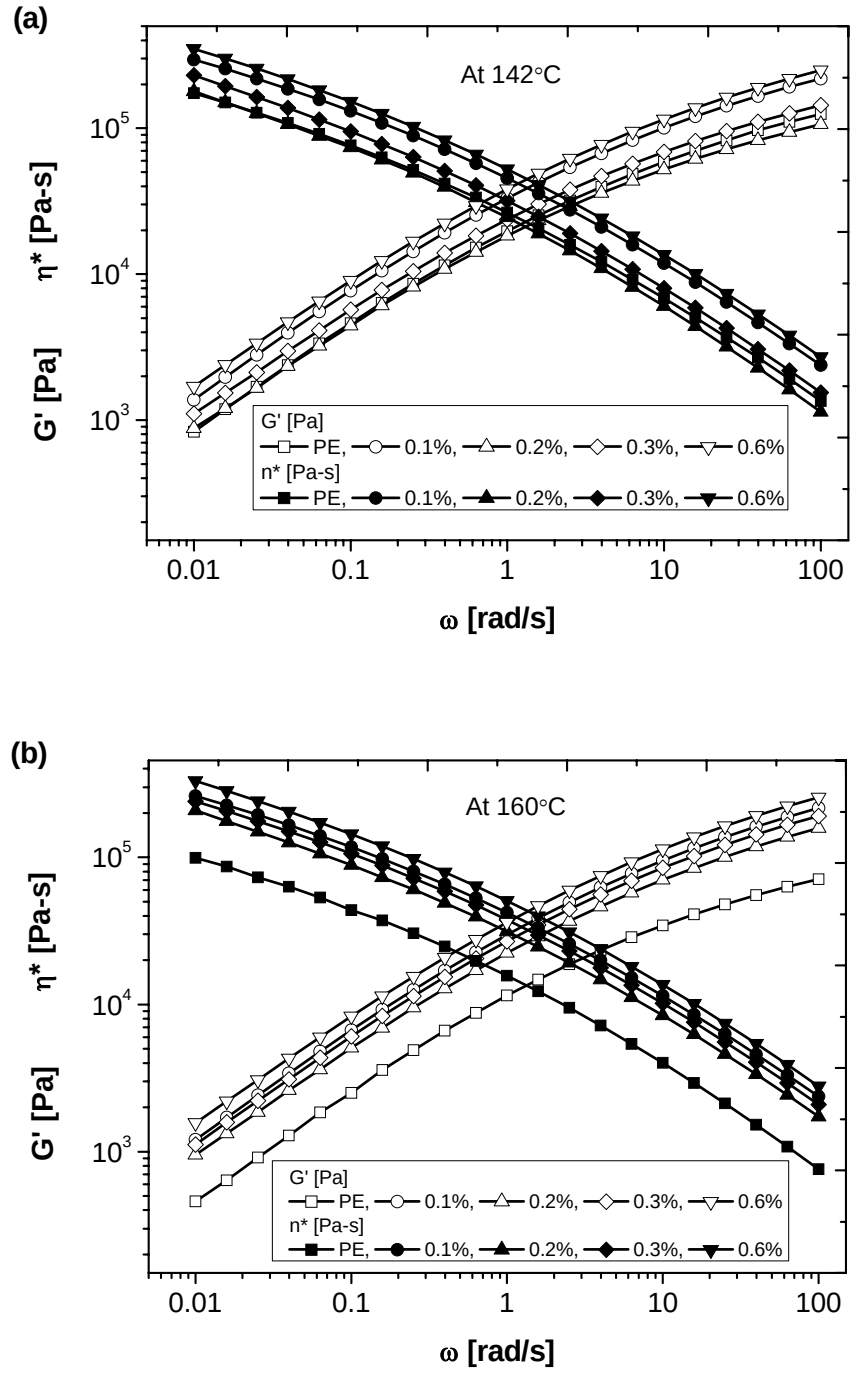

Figure 4.16: Storage modulus G' of SWCNT/PE as the function of frequency for two different temperatures (a) represents the SWCNT/PE composites at 142 °C (b) represents the SWCNT/PE composites at 160 °C.

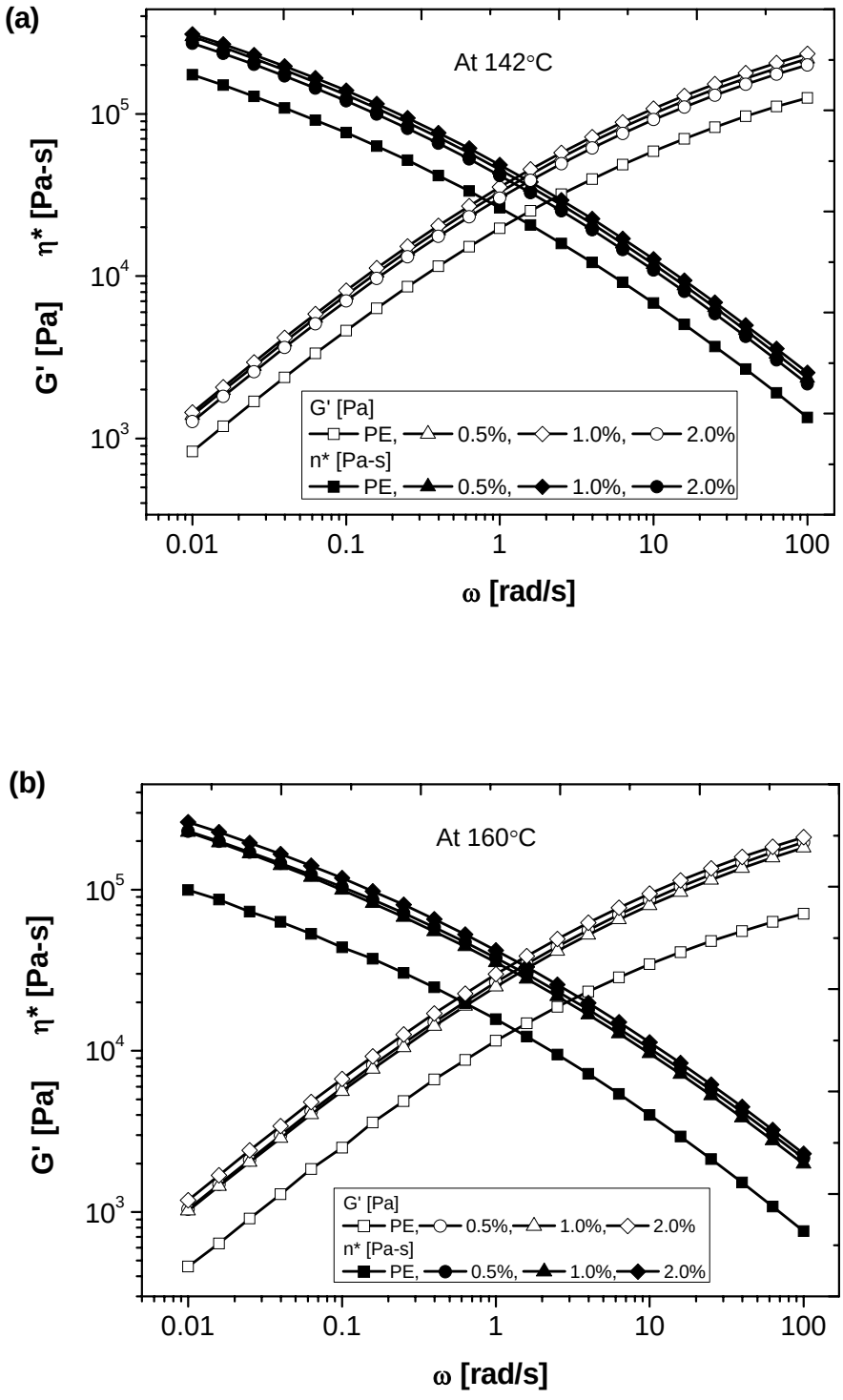

Figure 4.17: Storage modulus G′ of PE in presence of zirconia nanoparticles as the function of frequency for two different temperatures (a) at 142 °C (b) at 160 °C.

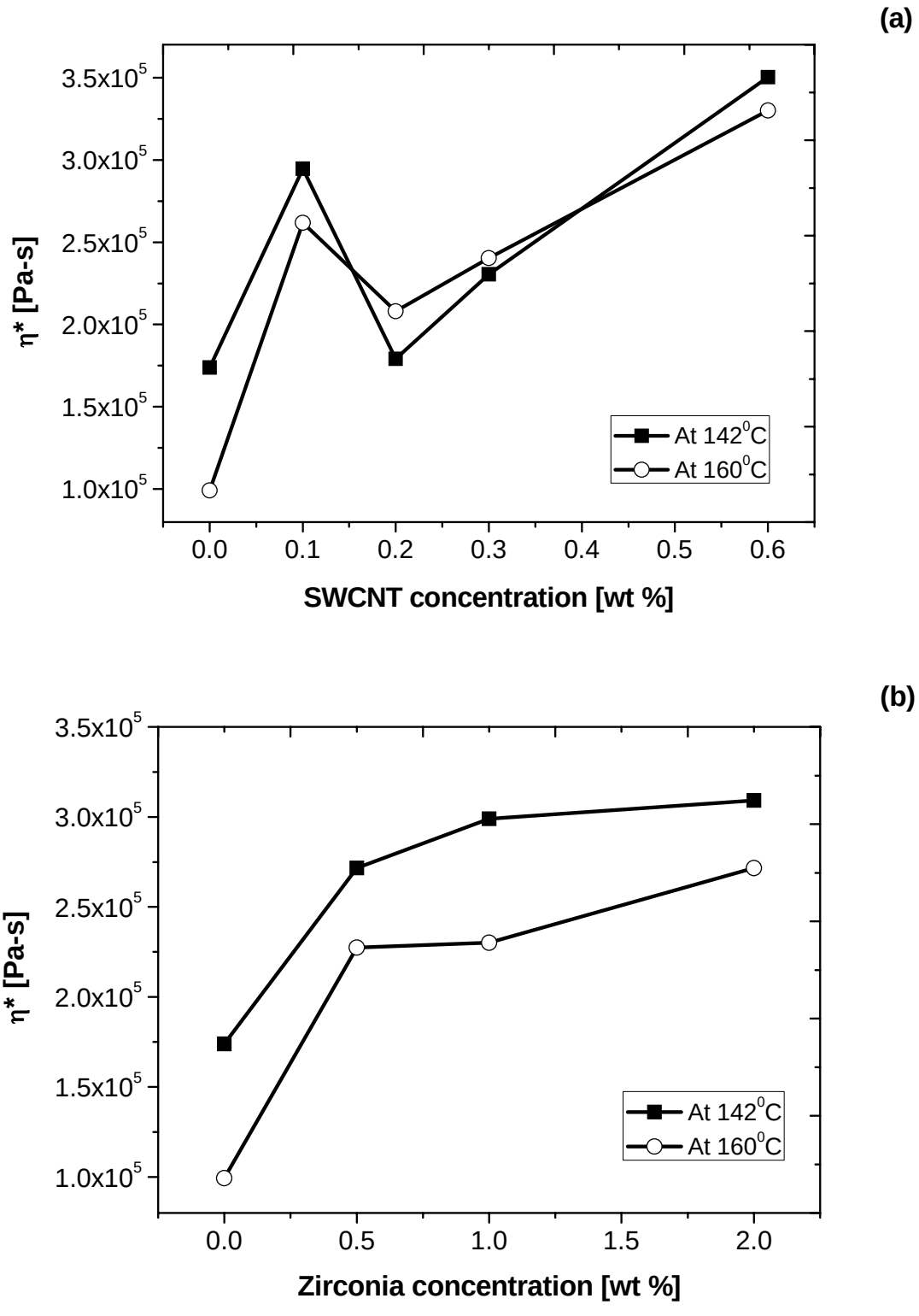

Figure 4.18: Complex viscosity as a function of nanoparticles at two different temperatures. (a) For SWCNT/PE composites (b) For zirconia/PE composites.

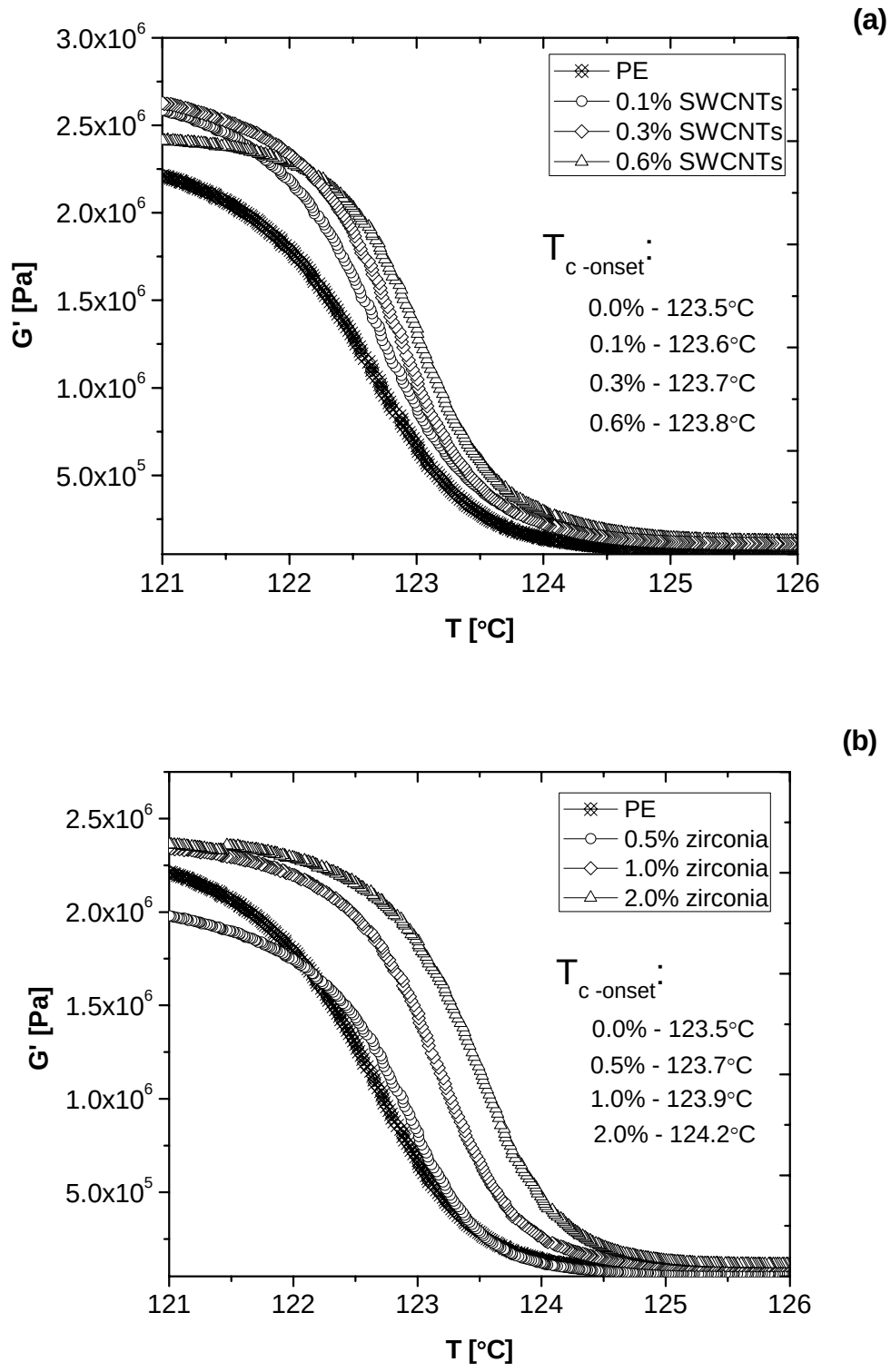

Figure 4.19: Evolution of the storage modulus, G', during cooling (slow cooling rate of 0.1 °C/min.) from 142 °C at constant strain ($\gamma = 2.0\ \%$) and frequency (10 rad/s), (a) PE in presence of SWCNTs (b) PE in presence of zirconia nanoparticles.

4.4 Conclusions

The X-ray synchrotron facility was utilised to investigate the origin of shish-kebab structures in the presence of nanoparticles. The results suggest an increase in the amount of shish-kebab structures in the presence of nanoparticles in the polymer matrix. The intense scattering of intensity at the equator in the early stages of crystallisation in the form of streaks indicated the presence of shish while steady increase in intensity in the meridian suggested the growth of kebabs. The estimation of Herman's orientation function indicates a higher degree of chain orientation in the presence of nanoparticles in the early stages of crystallisation. Chain orientation in the presence of SWCNTs was found to be more than with zirconia nanoparticles in the polymer matrix. The orientation fraction was found to increase in the presence of nanoparticles. Ruland's streak analysis showed the increase in shish length due to the presence of nanoparticles in the polymer. The higher shish length in the presence of a small concentration of SWCNTs (between 0.1 wt% to 0.6 wt%) as compared to zirconia nanoparticles in the polymer indicates the possible alignment of SWCNTs in the flow direction. The shish length increases with the amount of nanoparticles. The higher shish length favors the growth of kebabs in the later stages (>100 s) of crystallisation. The rheological study provided insight into the selective adsorption of polymer chains on to the nanoparticles. A non linear increase in viscosity was observed with the increase in SWCNTs in the polymer. The drop in viscosity in the presence of SWCNTs was suppressed at a higher melt temperature, whereas, a regular increase in viscosity was observed with increased zirconia loading in the polymer. The shift in the onset of crystallisation is more pronounced in the presence of SWCNTs (between 0.1 wt% to 0.6 wt%) as compared to zirconia in the polymer matrix, where it is obsereved above 0.5 wt%. The results conclusively demonstrate the role of nanoparticles in crystallisation.

Chapter 5

A study on the chain-particle interaction and aspect ratio of nanoparticles on structure development of a linear polymer

The objective of this chapter was to study the effect of surface area and aspect ratio of two nanoparticles viz. single walled carbon nanotube (SWCNT) and zirconia, on chain-particle interaction in polymer melt. The stability of metastable flow induced precursor (FIPs) in polyethylene melts in the presence of nanoparticles, was studied above (T = 142 °C) but close to the equilibrium melting point of unconstrained extended chain crystals. The results conclusively demonstrate the influence of chain-particle interaction between PE and the nanoparticles on the stretch of the long chains. With applied flow SWCNTs together with PE chains are observed to align along the flow direction, giving rise to a strong streak like pattern along the equator. At the initial stages, intensity of the observed streak is stronger than that for the neat polyethylene. The streak intensity stabilises with time, where the time required for the stabilisation depends on the amount of dispersed nanotubes in the polymer matrix. On the contrary, in the presence of zirconia nanoparticles, where the chain-particle interactions between PE and the nanoparticles are weak the initially observed streak tends to disappear with time, where the time required is strongly dependent on the concentration of the nanoparticles in the polymer matrix. The chain orientation along the flow direction was determined using Herman's orientation function and the length of the oriented chains by Ruland's streak analysis. On cooling with the crystallisation of the polymer scattering develops along the meridian, indicating the development of folded chain crystals, where the oriented chains present along the flow direction provide epitaxial matching thus suppressing the nucleation barrier. The meridional intensity (arising with the formation of crystals, called kebabs) at room temperature show strong dependence on the stable streak intensity (chain orientation along the flow direction, called shish) along the equator prior to cooling.

5.1 Introduction

The study of flow induced precursors (FIPs) in initial stages of crystallisation of polymers in the melts under the influence of flow field is important for achieving final properties in polymers. The applied flow field at a suitable temperature and deformation shear and strain rates promote the crystallisation process and subsequently the resultant morphology associated with the final product. Many studies have shown the role of flow conditions in the formation of primary nuclei during the early stages of crystallisation. Under flow, the polymer chains get aligned in the flow direction giving rise to maximum density fluctuation in the perpendicular direction as can be detected by time resolved small angle X-ray scattering (SAXS) techniques. Depending on the temperature and heterogeneities present the applied flow influences the molecular conformation in the polymer melt and may form stable primary nuclei. Time resolved small angle X-ray scattering techniques are applied in detecting the spatial arrangements and morphology developments due to rapid formation of primary nuclei in nanoseconds during the early stages. [231]

The anisotropic precursor leads to the formation of shish-kebab morphology during the crystallisation process under shear. The anisotropic structure influences the mechanical properties of polymeric materials. The initial structures obtained after immediate shear can be metastable in nature and can undergo either crystallisation or dissolution at high crystallisation temperatures. The basis of formation of FIPs is a subject of interest in recent years [90, 110, 217, 232-233, 240, 243] and is studied in this chapter at high temperature. The concept of coil-stretch transition by De Gennes [109, 234-235] shows the transition of polymer chains from random coil to fully extended chain conformation without intermediate stable chain conformation above a critical strain rate under flow. Keller et al. [68] proposed the existence of a critical orientation molecular weight (M^*) in the formation of oriented structures under shear flow. The study proved that polymer chains longer than M^* can remain in an extended state after deformation while short chains quickly relax back to form a random coil state due to short relaxation times. Further, the crystallisation of these extended chains leads to the shishes and epitaxial crystallisation of the coiled state leading to the formation of kebabs in later stages.

Hsiao et al. [64] studied sheared polyethylene (PE) blends containing a very low concentration of ultrahigh molecular weight polyethylene (UHMWPE). The study revealed the presence of shish-kebab structures with multiple shish. According to them, the multiple shish originate from stretched chain sections and kebabs originate from coiled chain sections following a diffusion controlled crystallisation process. Wu et al. [236] investigated poly(vinylidene fluoride) (PVDF) fibers spun under stretch-hold deformation at room temperature. They obtained streak-like scattering in the equator of SAXS patterns and attributed this to the formation of microfibrils and microvoids respectively.

In contrast to the Cahn-Hilliard (CH) theory [237] for spinodal decomposition, which basically suggests the spontaneous growth of fluctuations indicative of thermodynamic instability, some studies [238] have provided a possible explanation for the concept of spinodal decomposition as the extension of rigid segments having crystalline conformation caused by the conformational change of molecules from amorphous to crystalline state with the lowering of temperature below the melting temperature. [239-241] The presence of metastable liquid-liquid (LL) phase coexistence curve buried inside the equilibrium liquid-crystal co-existence region forms a basis of spinodal dynamics in polymer melts. It is understood that a polymer chain having the correct conformation will crystallise. But chain conformation alone cannot drive phase transition in melt condition; hence, it is usually coupled with density. Chains having helix conformations will pack more densely than chains with random conformations. Thus, part of the chain in the dense region will be crystalline while it will be amorphous in dilute region. The metastable (LL) phase is a result of conformation-density coupling and has been previously proved. This conformation-density coupling is vaguely believed to act as a precursor to polymer crystallisation. Hence, it is often considered that spinodal decomposition is not necessary to induce the shish-kebab structure formation. [154] The simulation studies by Frenkel [242] and Dukovski and Muthukumar [152] proved the mechanism that governs the formation of shish-kebab structures. The study revealed the role of shishes as nucleating substrates in promoting epitaxial crystallisation of low molecular weight (M_w) chains to form kebabs. The simulation study clearly showed that the kebab growth was significantly influenced by the rate of addition or diffusion of

chains. Kumaraswamy et al. [83, 197] demonstrated the formation of oriented crystals on the basis of critical shear rate and shearing time. They showed stronger dependence of the shear rate than the shearing time on the orientation of crystals. Seki et al. [66] proved the influence of high molecular weight chains exceeding the overlap concentration in the formation of oriented nuclei.

According to Ogino et al. [199], the critical concentration is two to three times larger than the overlap concentration of chains (C^*_{Rg}), indicating the role of entanglements of *UHMW* PE chains in the formation of oriented structures. Further, it has been reported that the crystallisation rate and the relaxation rate of the ultrahigh molecular weight component have significant effects on the shish-kebab formation process. [220]

Under flow conditions, [102] Deborah numbers (*De*) associated with reptation and stretch can be defined as

$$De_{\mathrm{rep}}, De_{\mathrm{s}} > 1,\ \lambda > \lambda^*(T) \tag{5.1}$$

where λ is stretch ratio and λ^* is the transition between two stretching regimes (i.e. the global configuration of the chain and the rotational isomerisation (RI)) at temperatures well above the melting temperature, T_m. The chain segments are strongly oriented and the chain conformation becomes similar to that of the crystalline state. Due to this, the critical fluctuations in the orientation and conformation of the chain segments are no longer required during flow. The application of the flow field therefore shifts the nucleation dynamics, ultimately resulting in an increase of the observed nucleation rate. Van Meerveld et al. [102] applied four different approaches for determining reptation time (τ_{rep}) and stretching time (τ_{s}) to classify flow induced crystallisation. First, they used an approach based on zero shear rate viscosity, $\tau^{\eta}_{\mathrm{rep}}$ and τ^{η}_{s}. Since the magnitude of zero shear viscosity is primarily related to M_{w}, the magnitude of $\tau^{\eta}_{\mathrm{rep}}$ is an average reptation time and not that of the high molecular weight (HMW) tail. Ultimately, the $De^{\mathrm{HMW}}_{\mathrm{s}} < 1$ for all shear rates was in disagreement with the fact that chain stretching

governs flow induced crystallisation and hence was found inappropriate. Second, they used average reptation time from the spectrum of Maxwell modes, τ_{rep}^{*} and τ_{s}^{*}. Moreover, the resulting magnitudes of τ_{rep}^{*} and τ_{s}^{*} are greater than τ_{rep}^{η} and τ_{s}^{η} but the equal rheological considerations apply for τ_{rep}^{η} and τ_{s}^{η}, hence the approach was not acceptable. The third approach was related to the longest relaxation time from a spectrum of Maxwell models τ_{rep}^{HMW} and τ_{s}^{HMW}. The difficulties associated with this approach were: (a) The τ_{rep}^{HMW} was related to HMW chains only when the storage modulus G' and loss modulus G'' were measured in terminal regimes. (b) The contribution of the *HMW* tail may be screened by remaining part of the melt. Thus, the magnitude of τ_{rep}^{HMW} is expected to be a good estimate if the effect of tube dilation and fast Rouse relaxation modes on τ_{rep}^{HMW} for determining intrinsic reptation time of *HMW* is corrected. The fourth approach was based on MWD, τ_{rep}^{MWD} and τ_{s}^{MWD}. It had the major advantage over other assumptions required for determining τ_{s} and τ_{rep}. The benefit of this approach is the procedure to estimate τ_{s}^{MWD} avoids the problems in determination of τ_{s} and τ_{rep} in other approaches. Further, τ_{s} is not affected by MWD if Z_{HMW} and τ_{e} are known. The limitation is that the magnitude of τ_{rep}^{MWD} is larger as it does not account for tube dilation and fast Rouse relaxation modes. [107] The τ_{s}^{MWD} is supported by the formation of shish-kebab structure with a magnitude of $De_{s} \approx$ 1-10. Thus, it was found in agreement that strong chain stretching governs the formation of shish-kebab structures.

It was also resolved that the precursor formation occurs at temperatures close to the equilibrium melting point, and the time scale for the growth of a nucleus decreases with increasing temperature. One of the studies from Balzano et al. [89, 175] proved the formation of FIPs at temperatures close to the equilibrium melting point. The investigations were carried out using specially synthesised linear high density polyethylene (HDPE) having a bimodal molecular weight distribution. The possibility of obtaining a suspension of extended chain shish crystals only at high temperatures above but close to the equilibrium melting point of unconstrained extended chains crystals

requiring the stretch of longest chains of MWD was demonstrated. Keum et al. [243] studied the formation and stability of shear induced shish-kebab structures in highly entangled melts using blends of UHMWPE and HDPE at a temperature of 142^0C. They confirmed the formation of shish without kebabs and absence of HDPE chains in shish formation. The thermal stability of oriented structures suggested the entanglement restraints of the stretched chain network as a governing factor for the melting behavior of shishes. Recently, [157] small angle neutron scattering (SANS) has been utilised to show that long chains are not overrepresented in the shish relative to their concentration in the material as a whole. The molecular deformation of short and medium chains in the shish being greater than that of long chains, enhanced fluctuations in the local molar mass distribution due to shear, or a difference in concentration of short and medium chains in the shish relative to the bulk.

Recently, [244] SAXS/WAXD studies confirmed the nature and thermal stability of flow induced crystallisation precursor structures in blown LLDPE and HDPE/LLDPE films during constrained melting, proving the significance of the high molar mass tail in the enhancement of highly oriented structures. Even though the last several decades have seen considerable efforts to understand the nucleation and growth behavior of polymers under shear flow, with conventional theories and kinetics process associated with flow induced crystallisation, the basic mechanism responsible for nucleation and growth processes in the very early stages of crystallisation is still a matter of uncertainty. The aim of this chapter is to understand the governing factors in the formation of flow induced oriented precursor formation by using the linear PE with broad molecular weight distribution (MWD) using a time-resolved SAXS technique. To elucidate the molecular nature of such oriented structures in the initial stages as a result of shish only, a temperature (T_c = 142 °C) above but close to equilibrium melting point of linear PE was chosen. At this temperature, efforts have been made to resolve the issues related to chain alignment and high anisotropy as a result of chain extension. Further, nanoparticles such as single walled carbon nanotubes (SWCNTs) and silica nanoparticles have been widely used for improving mechanical and electrical properties. [105, 130-131, 138-139, 245-248] Under flow, molecules of nucleating agents act as point nuclei to form oriented crystals. [93-94, 113-114] The presence of nanoparticles often suppresses the nucleation

barrier and favours the physical properties. For instance, nanoclay modifies the local stress levels and orientation of iPP [160], SWCNTs counterbalance nuclei relaxation by providing surfaces favouring polymer crystallisation in PE [130, 146, 149-150] and poly (butylene terephthalate). [161] However, flow induced crystallisation in the presence of nanoparticles using time-resolved X-ray scattering techniques has never been studied in detail and is addressed in this chapter. The role of two types of nanoparticles, having considerably different interfacial free energies for the polyethylene chains (SWCNTs and Zirconia) in chain orientation at high temperatures under strong shearing conditions were investigated.

5.2 Experimental section

5.2.1 Materials and sample preparation

Based on the earlier work [89] on polyethylene (PE), the topic has been exploited for critical investigations to advance steps using the PE of broad molecular distribution (MWD). The sample was polymerised using Zeigler- Natta catalyst in a slurry process and obtained in powder form. Detailed information regarding the molar mass and molar mass distribution of PE determined using gel permeation chromatography (GPC) and thermal characterization using differential scanning calorimetry (DSC) is shown in chapter 2 (Table-2.1). The nanoparticles used in the study consist of single walled carbon nanotube (SWCNT) and nanozirconia. The dimension of nanoparticles and method of their dispersion [130, 222] in the polymer matrix is given in chapters 2 and 3. The supplier's information of materials (PE, SWCNTs and Zirconia) used in the present study is also provided in chapters 2 and 3. The samples in the form of flat disks of 400 μm thickness were obtained from compression molding of powder of neat PE and PE having different concentrations of uniformly dispersed nanoparticles at molding temperature of 160 °C for 5 min for time-resolved X-ray scattering (SAXS) measurements. All the samples were mixed with Irganox 1010 to avoid possible degradation while processing.

5.2.2 Time resolved small angle X-ray scattering (SAXS)

The two dimensional (2D) time-resolved SAXS measurements were perfomed in the DUBBLE/BM26B beamline at the European Synchrotron Radiation Facility (ESRF), Grenoble, France. The detailed schematic of beamline is represented in figure 4.1 of chapter 4. A 2D gas filled detector having resolution of 512×512 pixels and $260\ \mu m \times 260\ \mu m$ pixel size was employed to detect time-resolved small angle X-ray scattering (SAXS) patterns for shear experiments. The sample to detector distance for SAXS was 6.057 m respectively. The beamline consists of a vacuum chamber in between the sample and detector to reduce the scattering and absorption from air. The wavelength of synchrotron radiation used in our SAXS experiments was 1.24 Å. An acquisition time of 10 s was used to acquire images with the dead time of 0.5 s for data transferring following the correction of intensity of the primary beam, sample thickness and absorption needed between the adjacent images. The images were integrated to determine the scattered intensity (I) as a function of scattering vector (q). The integrated intensity as function of time is defined as, $I_{SAXS}(t) = \int_{q_{min}}^{q_{max}} I(q,t)dq$, where q_{max} and q_{min} being the maximum and minimum of q values. The obtained intensity data is subtracted with intensity prior to the application of shear. The range of length of scattering vector q in the SAXS measurements was 0.001 – 0.5 nm^{-1}, where q is given by $q = 4\pi \cdot \sin\theta / \lambda$, ($2\theta$ being scattering angle). A Linkam shear cell CSS-450 modified by replacing the quartz windows of the shear cell with kapton windows to avoid x-ray absorption was adopted to apply steady shearing conditions. The shear cell was calibrated with a tolerance limit of $\pm 30\ \mu m$ to have maximum contact of plates while shearing under preferred flow conditions. The flat disk-like samples were placed between the two plates of a shear cell CSS-450 and were completely enclosed in the cell. The 400 μm thick sample was compressed in the shear cell upto 200 μm in the melt to ensure the correct application of shear on the sample during measurements. The chosen flow conditions were; shear rate $\gamma^{\bullet}$ = 100 s^{-1} for time duration t_s = 1 s, with constant strain ($\in$) = 100 units. The temperature and shear plan is illustrated in figure 5.1 for this study, and summarized:

1. The sample was heated from room temperature to 160 °C at a heating rate of 30 °C/min

2. The sample was held at 160 °C in the melt above the melting temperature (T_m) for 5 min to remove complete melt history
3. The samples were cooled to isothermal temperature ($T > T_m^o$ = 142 °C) at a cooling rate of 10 °C/min
4. A shear rate $\gamma^{\bullet}$ = 100 s^{-1} for time duration t_s = 1 s was applied at $T > T_m^{\circ}$ = 142 °C to study the early stage - FIP development for 5 min under isothermal conditions.
5. The samples were cooled to T = 60 °C at cooling rate of 10 °C/min to study the crystallisation process in the later stages.

The steady 2D SAXS patterns were captured after each 10.5 s during complete temperature and shear plan.

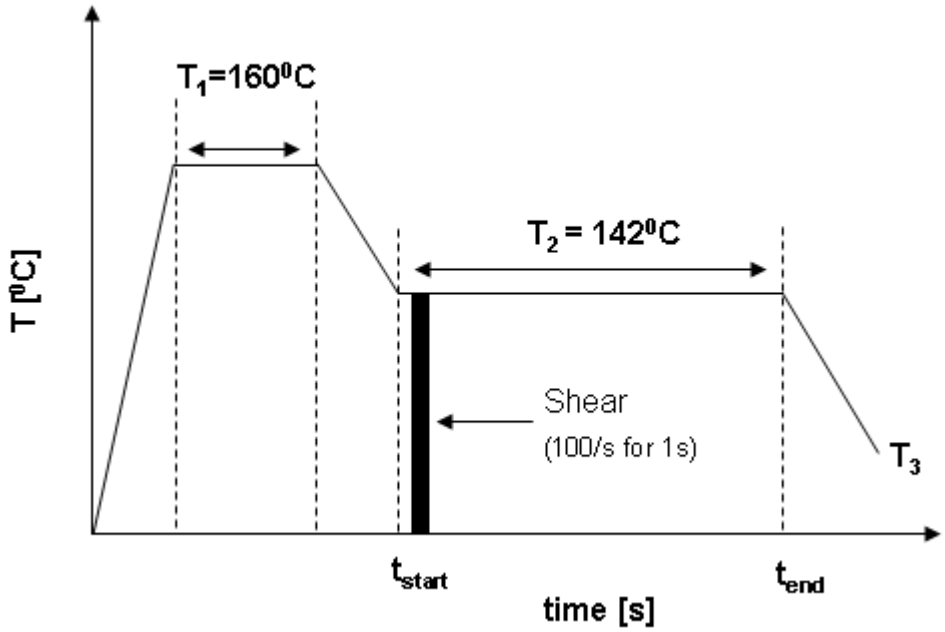

Figure 5.1: The schematic of the temperature and shear plan utilised in the present study. The fast flow condition with shear rate of 100 s^{-1} for 1 s is applied in isothermal temperature of 142 °C to study the FIPs in the early stages of crystallisation process. Here, T_1 represents the temperature in the melt, i.e. $T > T_m$ = 160 °C for 5 min, where, T_m^o = 141.2 °C to remove the complete melt history. T_2 represents the isothermal temperature, i.e., $T_2 > T_m^o$ = 142 °C and T_3 is 60 °C.

5.3 Results and discussions

5.3.1 Flow induced precursor (FIP) formation (shishes) in broad molecular weight distribution (MWD) polyethylene (PE) at $T > T_m^o$ = 142 °C under fast flow conditions

The 2D SAXS patterns collected after selected times at the isothermal crystallisation temperature ($T > T_m^o$ = 142 °C) above but just close to the equilibrium melting point of linear polyethylene is shown in the figure 5.2. A shear rate of $\gamma^{\bullet}$ = 100 s^{-1} for time duration t_s = 1 s was applied and the X-ray diffraction patterns were collected before and after the application of shear. The pattern collected just before shear at t = 0 s at 142 °C shows the diffuse scattering in the vicinity of the beamstop, suggesting the absence of any structure in the melt. The first pattern collected after the application of shear, t = 10 s shows scattering along the equator in the form of a streak. The streak-like scattering is associated with metastable precursor formation that under suitable conditions tends to grow to form stable shish. The pattern captured after t = 50 s shows strong streak-like scattering in the equator and further the steady growth of intensity with time corresponding to streaks at this temperature are noticed. The increase in intensity with time suggests the growth of shish in the vicinity of the equilibrium melting temperature. Considering these high temperatures the stable growth of shish structure is associated with the formation of extended chain crystals, which tend to be stable in the constrained condition.

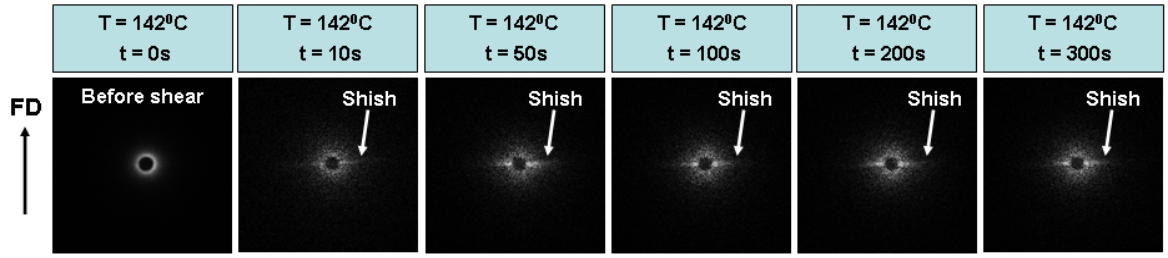

Figure 5.2: Selected 2D-SAXS patterns after the application of shear at isothermal temperature prior to crystallisation above equilibrium melting point of linear PE. The intense streak-like scattering in the equator can be noticed at t = 50 s becomes sharp as a function of time.

The streak-like scattering is the result of strong electron density variation occurring between the shish and polymer melt as polymer chains get aligned in the flow direction with fast flow conditions. The streak-like scattering relates to the presence of shishes in the polymer melt at a temperature above the equilibrium melting point of linear polyethylene in our studies. The anisotropic structures in the polymer melt consist of metastable bundle of stretched polymer chains aligned due to strong flow conditions. Thermodynamically, the anisotropy produces a decrease in the total free energy ($\Delta G_{\text{total}} < 0$) resulting in change in dimensions of shishes promoting the growth of precursors. The energy associated with the formation of metastable flow induced precursors can be related by equation 5.2.

$$\Delta G_{\text{total}}\left(L,D\right) = -\left\{\frac{\pi LD^2}{4}\right\}\left|\Delta g\right| + \left\{\frac{\pi D^2}{2}\right\}\sigma_{\text{end}} + \pi LD\sigma_{\text{lateral}} \tag{5.2}$$

Where, L and D are the length and diameter of FIPs. σ_{end} and σ_{lateral} are the free energies at the end and lateral surfaces. Δg is the difference in the specific free energy of the crystalline state and sheared polymer melt. The stability of a precursor, [80] is retained only if the order of magnitude for L/D ratio exceeds the value of 10,

$$\left[\frac{\sigma_{\text{end}}}{\sigma_{\text{lateral}}}\right] \sim 10 \tag{5.3}$$

From the rheological point of view, the flow reduces the chain conformations at high temperatures promoting the chain orientation in the direction of stretch. The governing criteria for chain orientation and stretch under suitable flow depend on the Deborah numbers. Considering the high molecular weight chains (HMW ~ 1.184×10^6 g/mol) of polyethylene, it is expected that the chain orientation and stretch of high molar mass chains above the equilibrium melting point (T_{m}^{o}) under strong shearing conditions ($\dot{\gamma}$ = 100 s^{-1} for time duration t_{s} = 1 s) for unconstrained extended chain crystals with no chain folding possibility is achieved. This result is supported by Deborah number approach.

The detailed information of Deborah number calculation is provided in chapter 2. The Arrhenius type of temperature dependence with activation energy E_a = 29.659 kJ/mol is found for the horizontal shift factor (a_T) at T = 142 °C. The calculated relaxation times and Deborah numbers at 142 °C for the applied shear rate are reported in Table-5.1

Table 5.1: The relaxation times and the Deborah numbers of reptation and stretch of HMW chains at 142°C

Shear rate (s^{-1})	Shear time (s)	$a_T(T)$	E_a (kJ/mol)	τ_{rep}^{HMW} (s)	τ_s^{HMW} (s)	De_{rep}^{HMW}	De_s^{HMW}
100	1	2.439	29.659	56.651	0.0143	13812	3.48

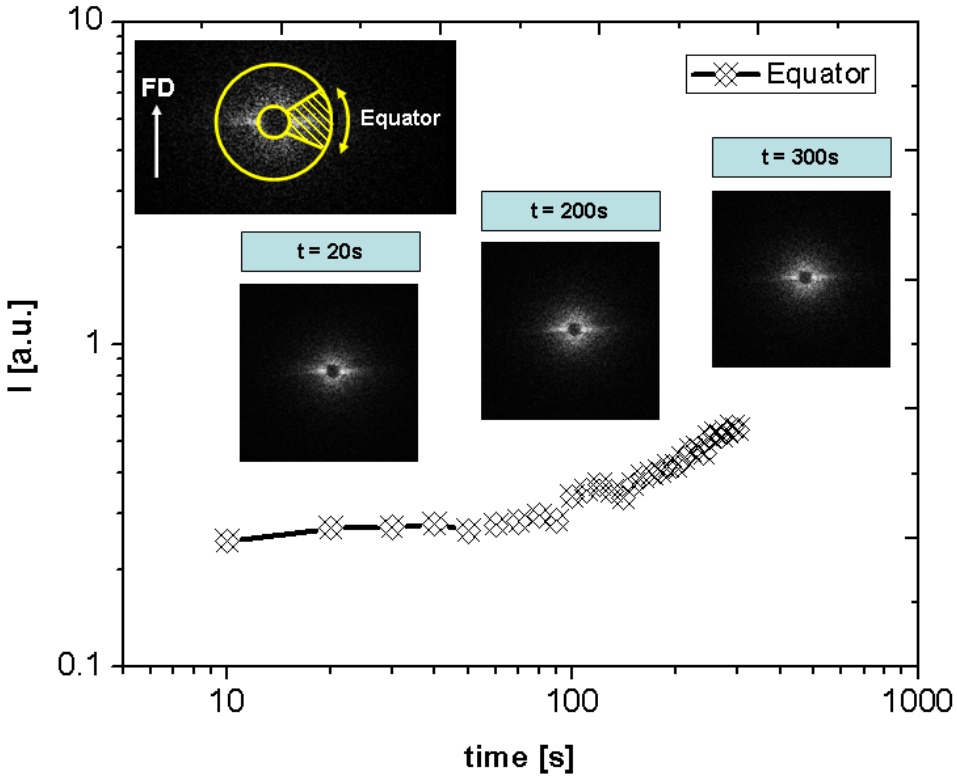

Figure 5.3: The integrated intensity obtained as a result of streak-like scattering in the equator from the SAXS analysis. The intensity has been integrated along the cake as shown in the shaded region. The plot consists of patterns acquired after selected time in the isothermal temperature condition. The result shows the presence of clear streak-like structures in the polymer melt. The intensity increases as the function of time suggesting the growth of FIPs.

Figure 5.3 shows the intensity build up at the equator after application of high and fast shear. The steady growth of SAXS intensity and the flow induced crystals are observed as a function of time. The evolution of integrated scattered intensity along the equator is shown in figure 5.4 as a function of *q* and time. The intensity tends to grow as a function of time after the application of shear suggesting the growth of shishes as apparent from figure 5.3. Figure 5.5 shows the evolution of the azimuthal peak at the equator after application of shear. Immediately after the application of shear the azimuthal peak tends to become sharp. The scattering obtained in the equator as a function of azimuthal angle is used in determination of shish length as demonstrated.

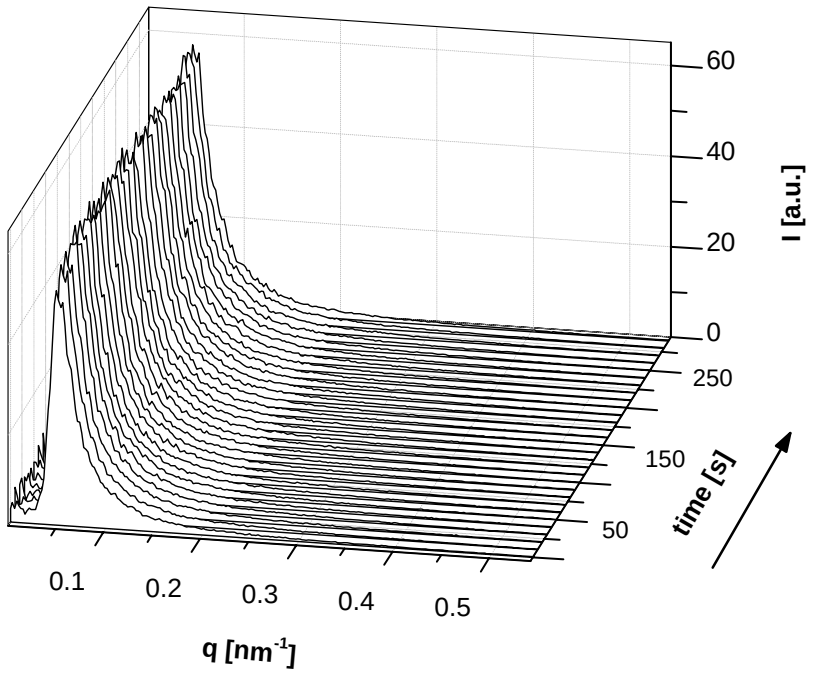

Figure 5.4: The time resolved evolution of equatorial integrated scattered intensity as a function of scattering vector (q) in polymer melt, at isothermal temperature (142 °C) prior to crystallisation. The increase in the scattered intensity at low q-values is associated with streaks in the equator.

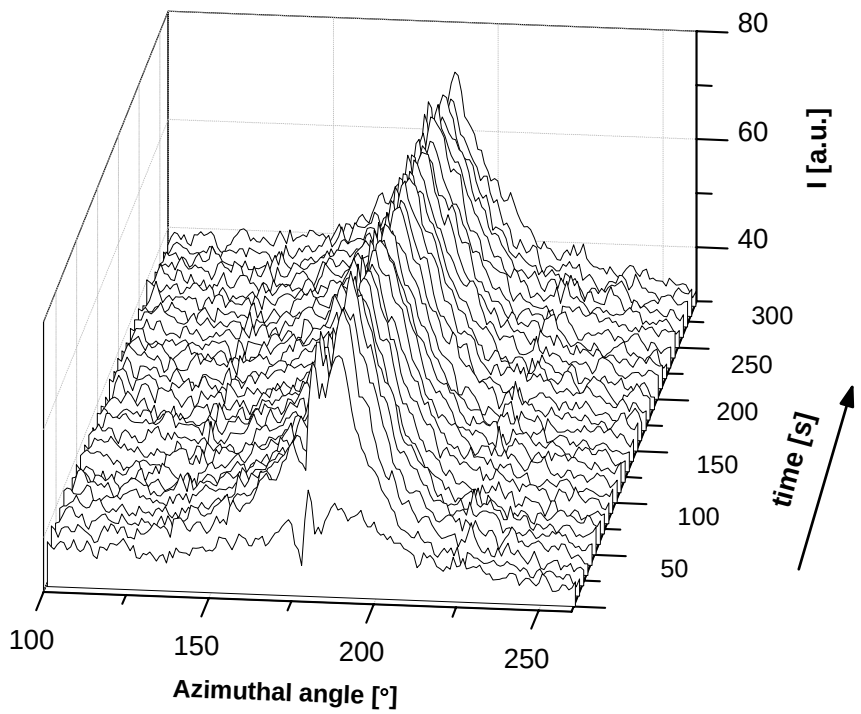

Figure 5.5: The time resolved evolution of azimuthally integrated intensity at the equator in neat polymer. The peak in the equator (θ = 180°) is the result of scattering in the equator associated with the metastable flow induced precursors (FIPs) obtained at high isothermal temperature (T = 142 °C) after the application of strong short-term shear.

5.3.2 Probing the stability of FIPs obtained in broad molecular weight distribution (*MWD*) polyethylene (PE) in the presence of nanoparticles at $T > T_m^o$ = 142 °C

The stability of flow induced precursors was studied in the presence of two different nanoparticles, having different chain-particle interaction for polyethylene chains. For example, due to the similar chain-particle architecture of carbon nanotubes and polyethylene chains a strong interaction between SWCNTs and PE is anticipated. Moreover, the higher aspect ratio of the SWCNTs compared to the zirconia nanoparticles will also favour the molecular interaction between SWCNTs and polyethylene chains. Strong interaction would provide easy stretchability of polyethylene chains with the SWCNTs. On the contrary, due to poor chain-particle interaction between the zirconia and polyethylene, the polyethylene chains adhered to the nanoparticles will tend to slip

under shear. Further, the entropy driven relaxation process will tend to transform the stretched chains into random coils. To investigate such a possibility the following experiments were performed.

The samples of physically dispersed nanoparticles on the polymer powder are subjected to shear as defined in figure 5.1. 2D-SAXS patterns for selected times before and after the application of shear were acquired. Figure 5.6a shows the composite of 2D-SAXS patterns recorded at different times after shear in the presence of different wt% of SWCNTs in the polymer matrix. Compared to the neat polyethylene (Figure 5.2 and 5.3) the scattered intensity just after the shear is found to be much higher in the presence of SWCNTs. This suggests that the presence of SWCNTs enhances the formation of flow induced precursor immediately after the application of shear. However, with time the intensity along the equator tends to decrease suggesting dissolution of the precursors with time. Such a phenomenon is apparent in the polyethylene matrix having 0.1 wt% of SWCNT. With increase in the concentration of SWCNTs, from 0.1 wt% to 0.3 wt%, transformation of the streak-like scattered intensity in to broad maxima along the equator is observed. The broadening suggests an increase in the number of shishes in the polymer melt. With time, after the applied shear, the intensity of the broad equatorial maxima decreases before the scattered intensity stabilises and remains constant, even at this high temperature. The decrease in scattered intensity after applying shear suggests dissolution of some metastable flow induced precursors, while on increasing the concentration of SWCNTs from 0.3 wt% to 0.6 wt%, the broad intensity along the equator after shear tends to increase. It is to be realised that for homogeneously dispersed SWCNTs in the HMW polymer matrix, 0.6 wt% of SWCNTs correspond to a percolation threshold resulting into the formation of a stable overlapping network of SWCNTs. [130] The presence of such a network will provide the maximum surface of favorable heterogeneous nuclei for the crystallisation of polyethylene. Considering the anisotropic distribution of intensity, mainly perpendicular to the flow direction, the SWCNTs are likely to align along the flow direction, thus promoting the alignment of anchored chains on SWCNTs. Efficient chain stretching requires sharing of a chain between two or more SWCNTs. Such a probability would be highest for the long molecules in the polymer. Further the high relaxation times of the high molar mass component under stress will also

favor chain orientation and the formation of extended chain crystals required for the stabilisation at this high temperatures.

Figure 5.6b shows the 2D-SAXS patterns of polymer melt in the presence of zirconia nanoparticles. The nanoparticle size of zirconia (20 nm) provides a very high surface to volume ratio, thus a good probability for a chain to anchor with different nanoparticles. At the lowest concentration of zirconia (0.5 wt%) after application of shear strong equatorial scattering is observed. However, the scattering tends to decrease with time suggesting dissolution of the shish. It is interesting to note that with increasing concentration of zirconia nanoparticle though the surface area of heterogeneous nuclei increases dramatically (as shown in Table 5.2) the arising equatorial intensity due to shish formation decreases considerably. Unlike PE having 0.6 wt% of SWCNTs, where the streak intensity increases with time, with a higher concentration of zirconia the intensity along the equator vanishes with time suggesting complete loss of a detectable oriented structure arising due to applied flow.

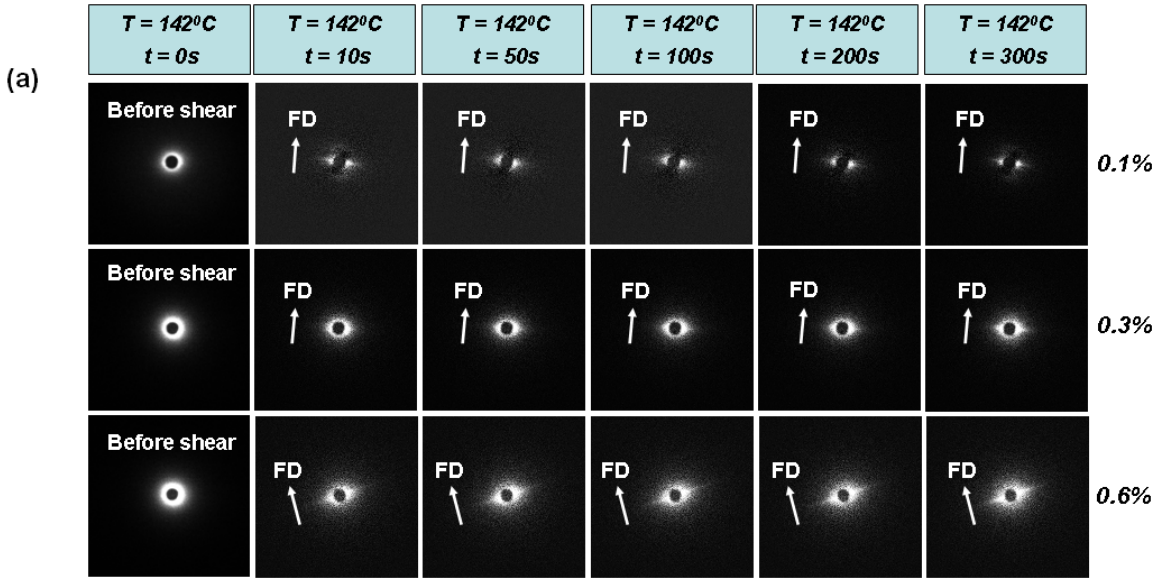

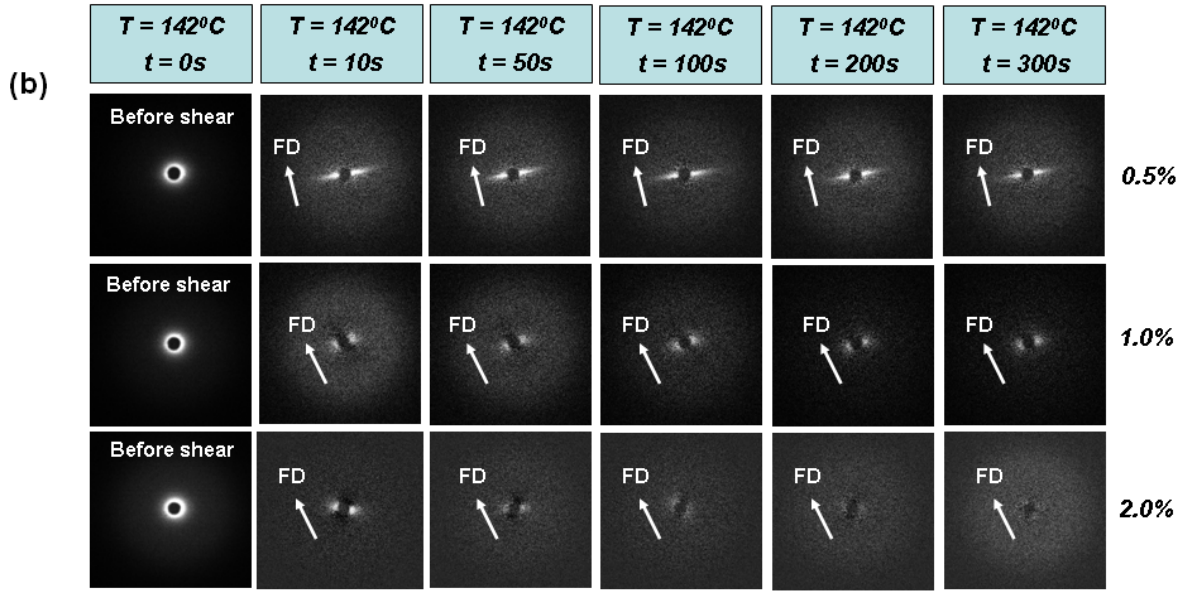

Figure 5.6: The 2D-SAXS patterns acquired at selected times at high isothermal temperature condition. The images was acquired before application of shear to confirm the preferred scattering after the application of shear, (a) shows the patterns of polymer melt in presence of increasing SWCNTs concentrations (b) shows the patterns of polymer melt in presence of different concentration of zirconia nanoparticles

Table 5.2: Estimated surface area of different concentration of nanoparticles dispersed in 1 g of polyethylene (PE).

SWCNT conc. (wt %)	Surface area (m^2/g)	Zirconia conc. (wt %)	Surface area (m^2/g)
0.1	40.04	0.5	0.99
0.3	119.40	1.0	1.99
0.6	240.24	2.0	3.97

Figure 5.7, shows the integrated SAXS profiles from the equator at different concentrations of nanoparticles obtained after t = 300 s of the application of shear at 142 °C. Changes in the intensity with q, ($q = 4\pi \cdot \sin\theta / \lambda$) are observed with the increasing concentration of nanoparticles. With the increasing concentration of SWCNTs, the overall scattered intensity increases. The scattered intensity for 0.5 wt% of zirconia concentration in PE is more compared with neat PE. However, the intensity at higher q-values is significantly lowered in polyethylene containing a higher concentration of zirconia nanoparticles suggesting a decreased streak length.

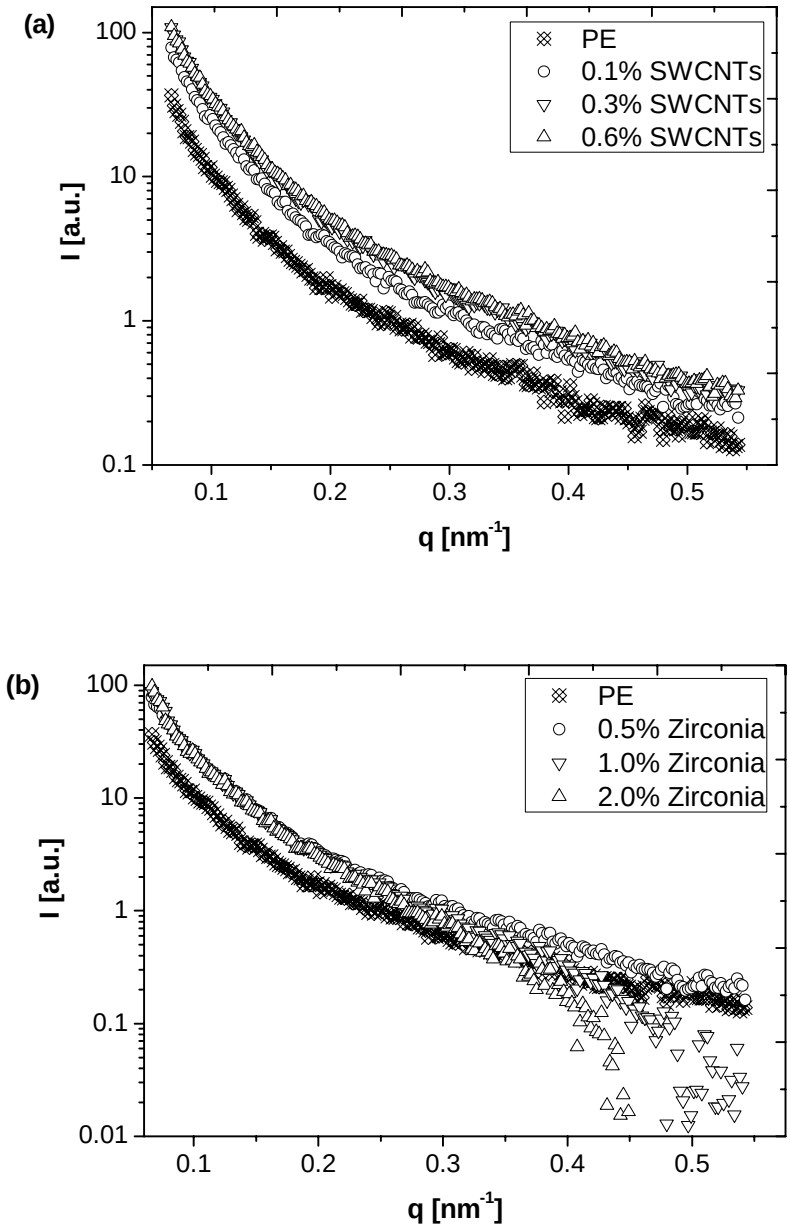

Figure 5.7: The scattered intensity in the equator obtained after application of shear for the 2D-SAXS patterns of polymer melt in the presence of different concentration of nanoparticles collected after t = 300 s of high temperature isothermal condition prior to crystallisation. (a) in presence of SWCNTs and (b) in presence of Zirconia nanoparticles. The intensity at the y-axis is the integrated intensity in logarithmic scale along the q, (where, $q = 4\pi \cdot \sin\theta / \lambda$, 2θ being scattering angle).

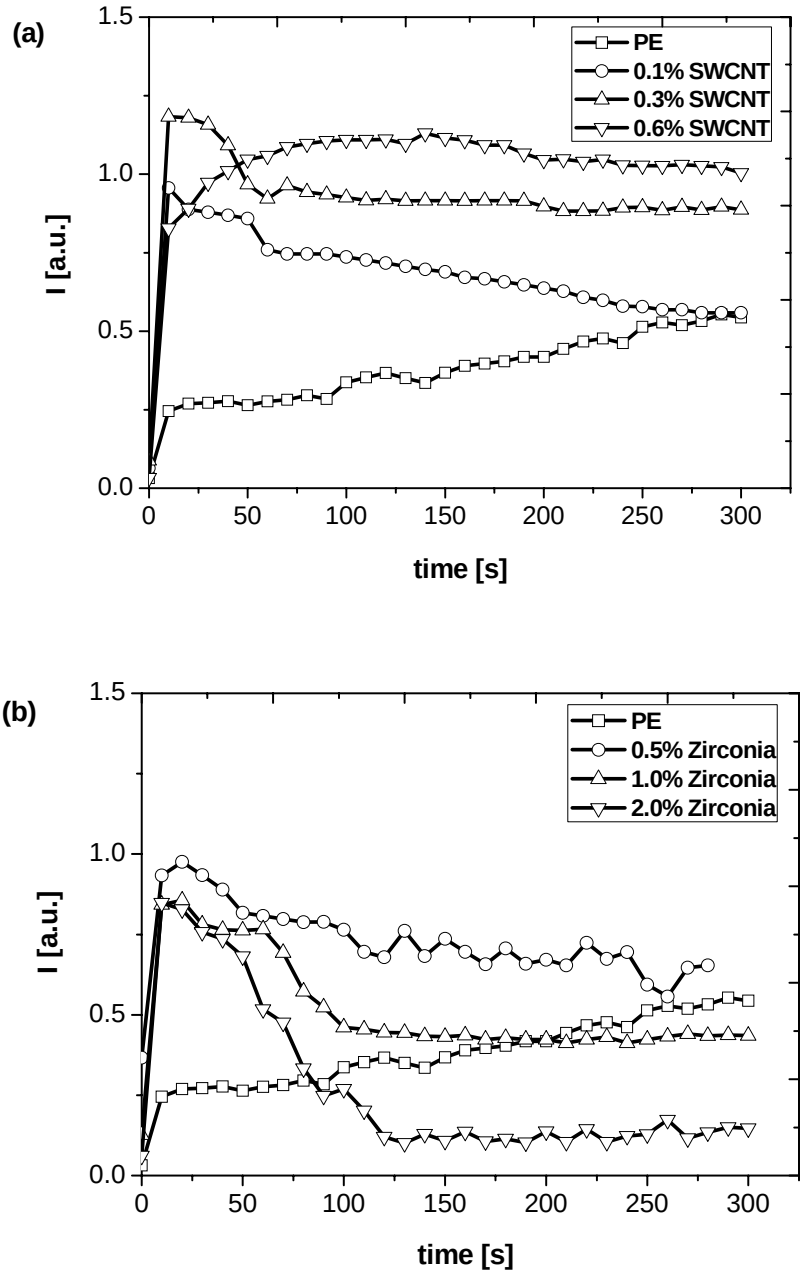

Figure 5.8: The equatorial integrated intensity obtained from SAXS data analysis as a function of time. (a) in presence of SWCNTs; (b) in presence of Zirconia nanoparticles. The rapid rise in the intensity immediately after the application of shear is noticed in the presence of nanoparticles in polymer melts at isothermal temperature (T = 142 °C). The intensities are subtracted with the intensity prior to the application of shear. The subtraction is performed to follow the development of resultant intensity due to structure formation after the application of flow.

Figure 5.8, shows changes in the integrated 2D-SAXS intensity in the equatorial region as a function of time at an isothermal temperature of 142 °C after the application of shear. It is evident that in all samples with the application of shear intensity along the equator increases, favoring the formation of flow induced precursors. After cessation of the shear while in the neat polyethylene the intensity continues to increase gradually with time, in the presence of the nanoparticles the intensity (though higher initially) tends to decrease with the exception of the polymer composite with 0.6 wt% SWCNTs. Compared to the SWCNTs, strong decrease in the scattered intensity is observed in the presence of zirconia, highlighting the influence of interfacial free energy in the stabilisation of oriented extended chain crystals at this high temperature. A cause for the stabilisation of the oriented structures close to the equilibrium melting point can be associated with the presence of local constraints on the extended chain crystals, even after cessation of the shear. Growth of the shish in the neat polyethylene may also arise due to change in pressure in the vicinity of the growth front of shish during crystallisation. The shish growth is likely to be favored because of the presence of the high molar mass in the polyethylene. However, the possibility of the involvement of low molar mass component in the shish during the shish growth process after cessation of the flow cannot be elucidated nor ignored. A schematic presentation arising from the information obtained on the shish formation in neat PE and PE with the nanofillers is shown in figure 5.9. Considering the requisite of chain overlap on the fillers to transfer the stresses on shear, shish formation at the initial stages should involve high molar mass chains. Since the concentration of SWCNTs (upto 0.6 wt%) considered in study is below the electrical percolation threshold, the formation interconnected structures or entangled SWCNTs network can be neglected. It is believed that at electrical percolation threshold SWCNTs form interconnected structures resulting in the increase in conductivity. Hence, we attribute the chain-particle interaction as a result of dilute SWCNTs system.

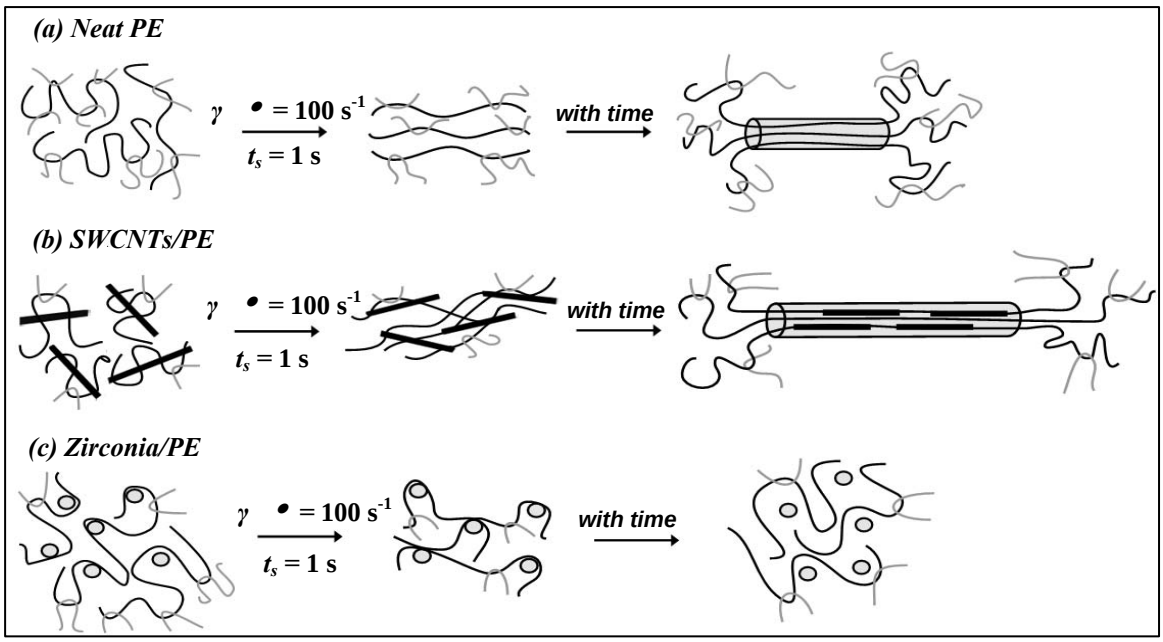

Figure 5.9: Shish formation in the neat polyethylene and PE in the presence of nanofillers. (a) the growth of shish formation in neat polyethylene depicting the stretch of long chain in broad molar mass distribution (b) in presence of SWCNTs, the shish formation is promoted due to anchoring of polymer chains on SWCNTs (c) in presence of zirconia, the shish formation is perturbed due to weak chain-particle interactions.

The polymer melt in the presence of zirconia nanoparticles at high 142 °C shows a different scenario, see figure 5.8. We observe high electron density contrast in the equator in the early stages at low concentration, which tends to decrease with increase in zirconia nanoparticle concentration in the polymer. The presence of zirconia nanoparticles is found to perturb the chain extension in the polymer melt. The rise of intensity in the early stages is followed by a decrease in intensity indicating the dissolution of precursors (shishes) in the polymer melt. It is generally assumed that local anisotropic crystalline structures are formed due to high molecular orientation especially near particles. In the case of zirconia nanoparticles, it may be anticipated that poor chain-particle interaction between zirconia nanoparticles and the polymer chain affects the chain orientation and with time, the chains slip over the surface of zirconia nanoparticles further prohibiting stable shish formation.

5.3.3 Orientation function of shish based on scattered 2D-SAXS intensities

Information about orientation in a preferred direction was obtained using the Herman's orientation function for the polymer melt sheared above the equilibrium melting point of unconstrained extended chain crystals, requiring the stretch of the longest chains of MWD. Extensive analysis of obtained plots of intensity as a function of azimuthal angle from the SAXS data was performed to obtain orientation parameters. For a given 2D-SAXS pattern, the orientation parameters are determined using equations for the Herman's function [81, 181-182] as explained in chapter 2 of the thesis. The regions corresponding to one quadrant (θ = 90° to 180°) of azimuthally integrated 2D-SAXS patterns in anticlockwise direction is considered for the estimation of orientation functions in all the samples. The data analysis gives values of the Herman's function (f_h), i.e. f_h = 1, when scattered intensity is concentrated in the equator (i.e. perpendicular to flow direction in 2D-SAXS patterns, in otherwords, considered to be the signature of chain orientation in our case), f_h = -0.5, when scattered intensity is concentrated in the meridian (i.e. parallel to flow direction in 2D-SAXS patterns), and f_h = 0, when scattered intensity is diffused (isotropic in nature) and spread across the pattern.

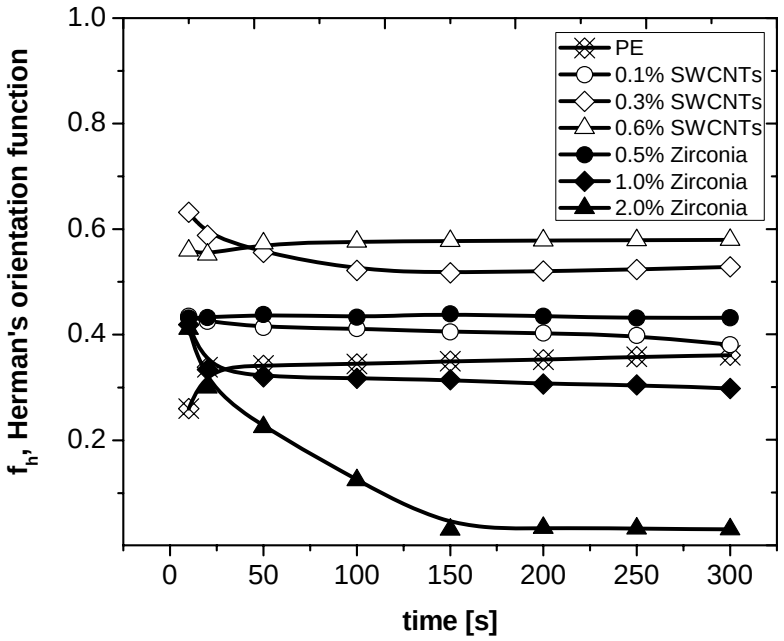

Figure 5.10: The calculated Herman's orientation functions for the different concentration of nanoparticles in polymer melt at isothermal temperature (T = 142 °C) prior to crystallisation.

Figure 5.10, shows the Herman's orientation functions estimated. The data shows good agreement with the 2D-SAXS images obtained (refer to figures 5.6a and 5.6b). An increased concentration of SWCNTs favors the chain orientation process in the polymer melt, whereas an increased concentration of zirconia nanoparticles perturbs the chain orientation. The decrease of chain orientation in the presence of zirconia nanoparticles is due to dissolution of metastable precursors. The entropy driven process of chain relaxation having constraints due to presence of physical entanglements in polymer melt is affected strongly in the presence of SWCNTs. This results in a higher orientation function towards the chain axis. The decrease in chain orientation in the presence of zirconia nanoparticles is caused by the poor chain-particle interaction between zirconia and polyethylene chains.

5.3.4 Ruland's streak method for estimation of shish length

The time evolution of flow induced precursors (shish) formation was further investigated to determine changes in the length of shish (L) using Ruland's streak analysis. [183, 223-226] The method was originally used to determine the size and orientation distributions of longitudinal voids in polymer and carbon fibers in real space. The method can be used to estimate the shish length based on the equatorial scattering in the reciprocal space.

The integral width of angular distribution of the scattered intensity B_{obs} was used to estimate the true width of the orientation distribution B_ϕ (misorientation) and the average length (L) of the shishes aligned in the direction of the c-axis. The parameters obtained from the Ruland streak method were used to analyse the scattered equatorial streak. The azimuthally distributed scans of intensities at different q values were analysed using the Lorentz function to yield the average width of angular distribution. The width of the equatorial streaks in reciprocal space can be used to obtain the length of shish (L). The relationships obtained from equation 4.5 of chapter 4, gives a linear plot between $q^2B^2_{obs}$ and q^2 as shown in figure 5.11.

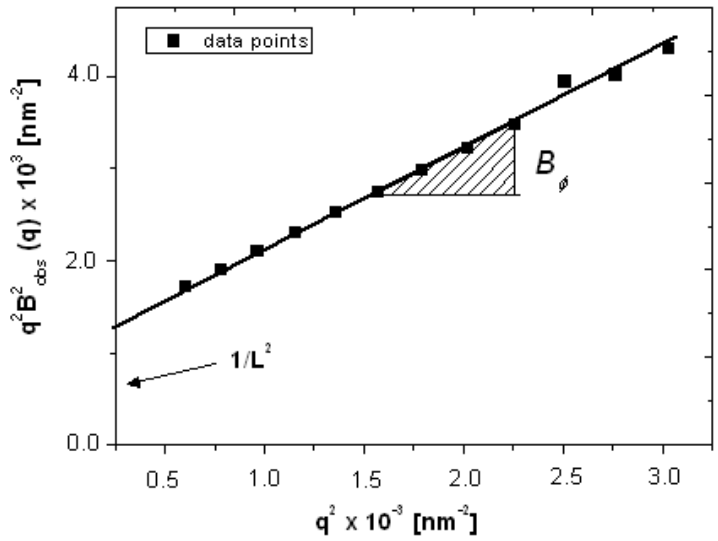

Figure 5.11: The plot of $q^2B^2_{obs}$ vs. q^2 used for the calculation of shish length (L) and misorientation (B_ϕ). The orientation distribution is approximated using Lorentzian fit with perfect linearisation of observed azimuthal integral breadth as function of scattering vector (q)

The shish length (L) and degree of misorientation (B_ϕ) were determined by linear least square fitting. In the relation, $q = 4\pi \cdot \sin\theta / \lambda$ (2θ is the scattering angle; q is the scattering vector, λ is wavelength). The length of shish (L) is determined from the intercept of the linear plot while B_ϕ represents the misorientation parameter. The interpretation of 'L' for shish is considered to be aligned in the direction of the c-axis.

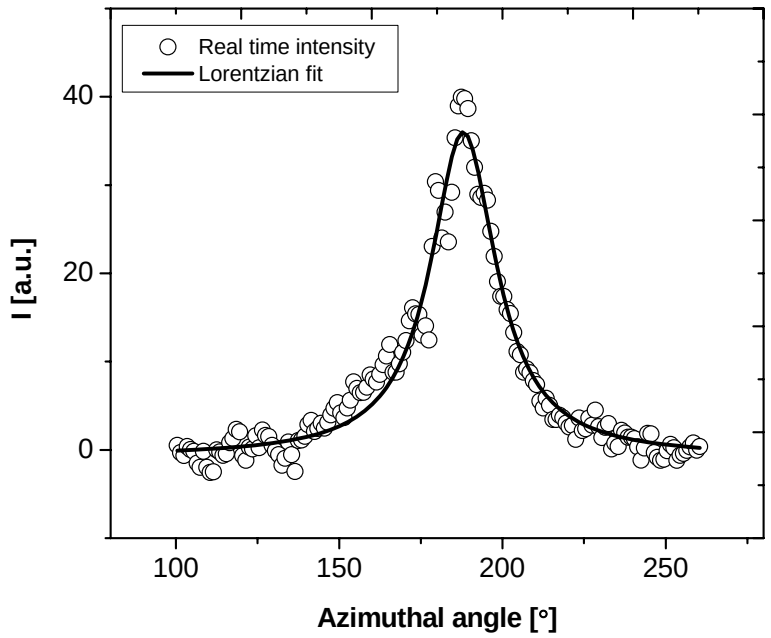

Figure 5.12: The example of typical Lorentz corrected distribution of scattered intensity in the equator as function of azimuthal angle for specific value of scattering vector (q) obtained for sample containing 0.6 wt% SWCNTs in PE.

The typical intensity distribution obtained at the equator as a function of azimuthal angle is shown in figure 5.12. The azimuthal peak at the equator was fitted by the Lorentz correction method due to fluctuations to get a precise integral width of angular distribution required for the calculation. The shish lengths as a function of time at the isothermal crystallisation temperature above the equilibrium melting point for unconstrained extended chain crystals were obtained in PE in presence of nanoparticles to study the effect. Figure 5.13a shows variation in the shish length obtained over the period of isothermal condition at 142 °C after the application of shear. A steady rise of shish

length (upto 20 nm) is observed in the neat polymer. In the presence of nanoparticles, the shish length was found to decrease from t = 0 s to 150 s and become stable after 150 s. The increase of SWCNTs in the polymer melt was found to increase shish length by ~120 nm (can be noticed in the presence of 0.6 wt% SWCNTs) after 300 s. The rapid decrease in the shish length as a result of variation in chain relaxation is observed in the early stages after the application of shear. In the presence of zirconia nanoparticles, compared to neat polymer, the shish length decreases indicating the dissolution of metastable precursors in the polymer melt.

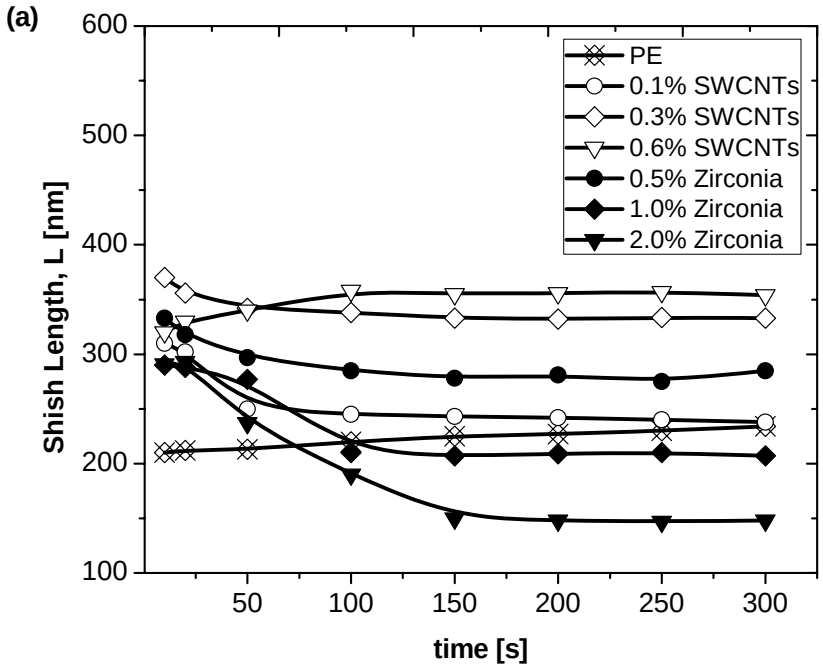

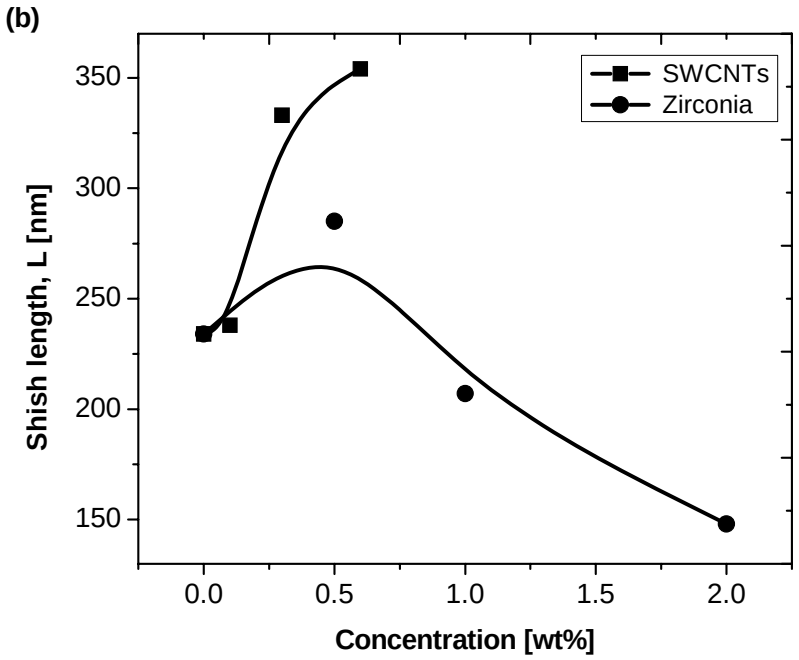

Figure 5.13: Estimated shish length of polymer melts in presence of nanoparticles. (a) refers to the deviation in the shish lengths as a function of time during high isothermal temperature (b) shows the variation in the shish length with the increasing nanoparticle concentration in polymer at T =142 °C , t = 300 s.

Figure 5.13b shows the comparison of average shish length as a function of different concentrations of nanoparticles at 142 °C. A small amount of SWCNTs leads to higher chain extension, eventually increasing the shish length by several tens of nm. The spherical rigid zirconia nanoparticles were found to decrease the average shish length with increase in concentration. The 2.0 wt% zirconia in polymer melt showed a large extent of disorientation after 300 s. Zhang et al. [130, 222] reported that addition of SDS surfactant below 2 wt% in polymer matrix do not have any effect on complex viscosites using rheology. Hence the effect of SDS on rheological and crystallisation behaviour of polymer can be neglected. Therefore SDS itself can neither enhance chain orientation nor chain stretching in polymer matrix.

5.3.5 Crystallisation studies in later stages of experiment

Figure 5.14 shows patterns collected at 60 °C after cooling the sample from 142 °C as shown in Figure 5.1, where T_3 = 60 °C. The crystallised oriented chains (shish) provide epitaxial matching for the crystal growth by the formation of lamellae (kebabs).The patterns in figure 5.14a showed the steady growth of kebab formation with increase in SWCNTs in polymer. The higher amount of oriented lamella in later stages is the outcome of stable shishes present in the polymer melt after the application of shear. The increase in kebab formation with the increase of SWCNTs in the polymer confirms our studies carried out in the earlier stages at high isothermal temperature where the increase in precursor formation was noticed. On the contrary kebab formation was found to decrease with increase in zirconia nanoparticle concentration during later stages (refer figure 5.14b). The results prove the reduction in flow induced precursor formation and/or chain orientation in the polymer in the presence of zirconia nanoparticles at higher concentrations ultimately influencing the radial growth of lamellae (kebabs) perpendicular to the central core (shish).

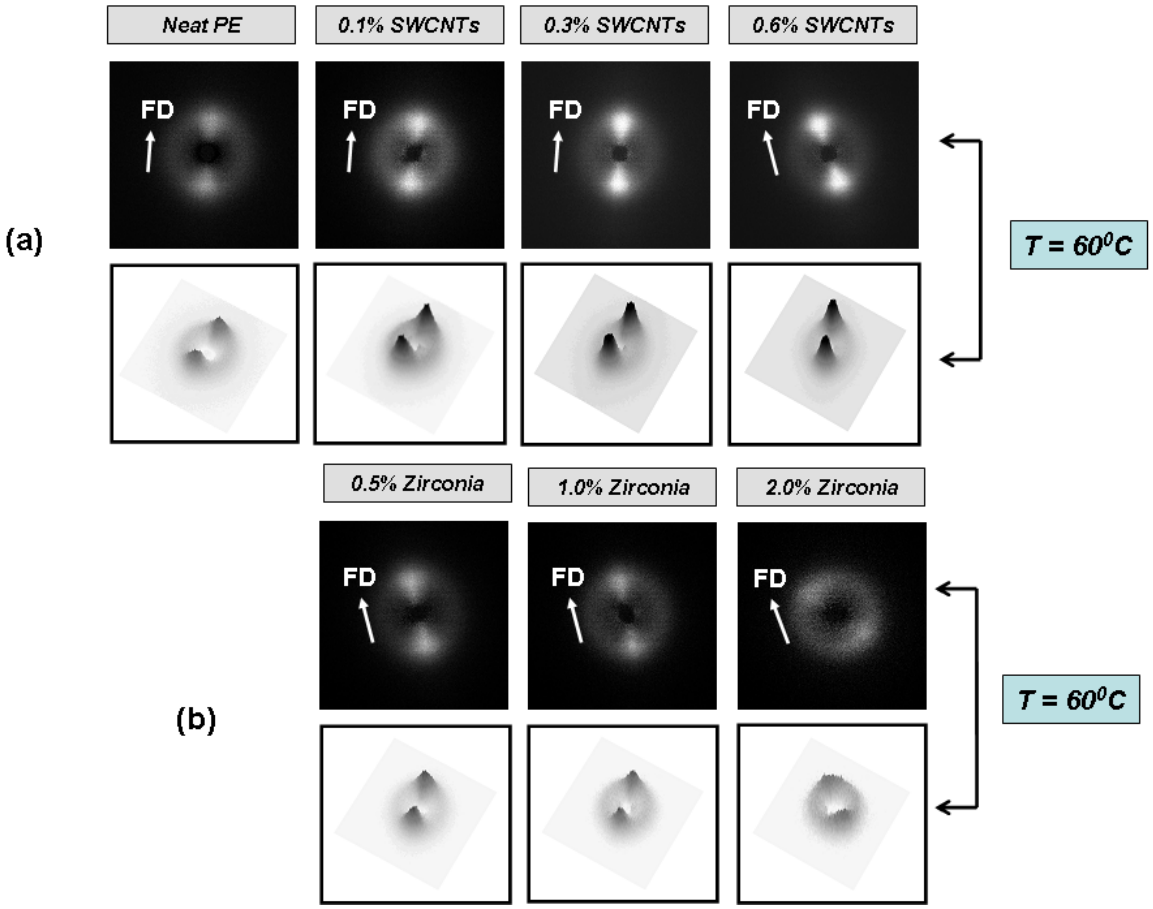

Figure 5.14: 2D-SAXS patterns obtained after cooling at T = 60 °C for the polymer and in presence of different concentration of nanoparticles. (a) indicates the increase in the oriented structure formation with the increase of SWCNTs concentration. (b) indicates the decrease in the oriented structure formation with the increase in zirconia particles in polymer.

Figure 5.15 shows change in the integrated intensity as a function of temperature while cooling from 142 °C to 60 °C As expected, the nanoparticles, in general, are found to accelerate crystallisation kinetics, apparent from the slope of integrated intensity. The intensity rises at higher temperature while cooling, due to the earlier onset of crystallisation in the presence of nanoparticles. The accelerated crystallisation kinetics depends on shear rate, temperature, melt memory and influence of additives etc. In our case, we expect the accelerated crystallisation kinetics is a result of the combined effect of shear rate ($\gamma^{\bullet}$ = 100 s^{-1} for time duration t_s = 1 s), high shearing temperature ($T > T_m^o$ = 142 °C) and influence of nanoparticles (SWCNT and zirconia).

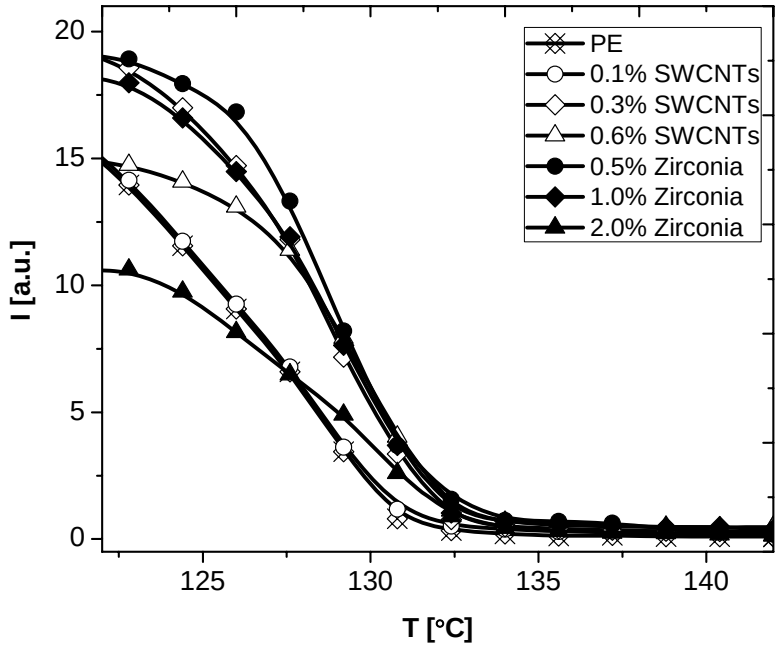

Figure 5.15: The integrated intensity as a function of temperature while cooling for different samples to room temperature. The early rise of intensity can be noticed in presence of nanoparticles.

5.4 Conclusions

The chapter demonstrated the role of HMW component of broad MWD in the formation of flow induced precursors (FIPs) in the polymer melt above the equilibrium melting point of unconstrained extended crystals of linear PE. A time resolved X-ray scattering (SAXS) technique was utilised to study the stability of precursors at the isothermal temperature prior to crystallisation. The precursor formation in PE, in the presence of SWCNTs and zirconia nanoparticles, is compared with neat PE. The result confirms the influence of SWCNTs in promoting precursor formation due to change in the chain relaxation process favoring the stability of oriented metastable structure. In contrast, the presence of zirconia nanoparticles perturbs the precursor formation as compared to the neat polymer. The calculated orientation functions reveal the influence of nanoparticles on chain orientation. SWCNTs promoted chain alignment in the flow direction leading to flow induced precursors (FIPs), eventually orienting the crystals towards the chain axis, as compared to neat PE prior to crystallisation. The zirconia nanoparticles showed random orientation of crystals at higher concentration. The Ruland's streak method was utilised to estimate the length of shishes. A small amount of SWCNTs (~0.6 wt%) leads to increase in the average shish length by ~120 nm. The spherical zirconia nanoparticles were found to decrease the average shish length by ~90 nm with increase in concentration.

Chapter 6

Conclusions

In this thesis a study on a broad molecular weight distribution polyethylene in the presence of nanoparticles is reported. The influence of high molecular weight component in the development of oriented structures is in agreement with the previous studies performed on the neat polymer having broad or bimodal molar mass distribution. [89, 68, 64] The novelty of this study is that by making use of specific nanoparticles, the shish-kebab formation can be enhanced under flow. Since shish-kebab structures have structural origin to ultra-high strength and ultra-high modulus fiber, the study in this thesis has direct implication in obtaining high-modulus fibers. For this purpose, the FIC experiments are performed above and below the equilibrium melting point of the linear PE.

6.1 FIC of broad MWD PE

From the FIC experiments reported in chapters 4 and 5 the following conclusions can be drawn. Using time resolved X-ray scattering (SAXS), both above and below the equilibrium melting point of linear PE i.e. 142 °C and 136°C, the results conclusively demonstrated the role of HMW component of broad MWD in chain extension. For instance: Just after the application of shear below the equilibrium melting point (136 °C) there is scattering on the equator in the form of streaks (shish) which facilitate the occurrence of scattering in the meridian (kebab) as the polymer crystallises during the residual time. Even the application of shear just above equilibrium melting point (142 °C) leads to streak-like (shish) scattering in equator confirming the presence of oriented structures in the polymer. The experiments reported in chapter 2 also revealed that strong shearing conditions are requisite to form shish-kebab structures in the neat polymer.

6.2 FIC of broad MWD PE in presence of nanoparticles

FIC experiments on broad MWD PE in the presence of nanoparticles are reported in chapters 2 and 3. The SAXS patterns show the evolution of scattering along the equator immediately after the cessation of shear and subsequent increase in intensity along the meridian on cooling. Emergence of the intensity along and perpendicular to the flow direction during or after cessation of shear is indicative of the shish-kebab morphology. The shish-kebab structure formation is enhanced by addition of nanoparticles in PE. For an example, the formation of shish-kebab structure is realised in the presence of SWCNTs at relatively low shear rates, thus suggesting that the presence of SWCNTs have a significant role in the formation of shish-kebabs. Shish formation in the presence of SWCNTs at the low shear rates is indicative of strong molecular interaction between the polymer and the dispersed nanoparticles. The molecular interaction will influence chain relaxation of PE, thus stabilising the formation of oriented structures at low shear rates.

The influence of aspect ratio and change in surface to volume ratio, have been investigated by substituting the cylindrical nanotubes by spherical zirconia particles. Scattering data analysis on the polymer with zirconia, as depicted in chapter 3, provides information on crystal orientation in PE after the cessation of shear. With increasing amount of zirconia in PE, the overall crystallinity and the degree of orientation increases. Shift in the onset of crystallisation to higher temperatures with increasing amount of zirconia is observed.

From the SAXS studies in chapters 4 and 5, after the application of shear, the role of nanoparticles of different aspect ratio in increasing the stability of flow induced precursors (FIPs) is demonstrated both above and below the equilibrium melting point of linear PE i.e. 142 °C and 136 °C. A higher degree of chain orientation is observed in the presence of SWCNTs in PE as compared to zirconia nanoparticles. The stability of FIPs is maintained in presence of SWCNTs in PE more than with zirconia nanoparticles. At 142 °C, SWCNTs with a high aspect ratio, having strong interactions with polyethylene molecules favour the molecular extension. On the contrary, zirconia nanoparticles having low aspect ratio and poor molecular interaction hinder the molecular extension. The results provided insight into the influence of chain-particle interaction between PE and

the nanoparticles on the stretch of the long chains above but close to the equilibrium melting point of unconstrained extended chain crystals.

6.3 Rheological studies of PE melt in presence of nanoparticles

The rheological studies reported in Chapter 4 provide insight into the selective adsorption of polymer chains on to the nanoparticles. The presence of nanotubes in the polymer matrix shows a non-linear increase in the viscosity with increasing amount of nanotubes whereas a steady increase in viscosity is observed with increased zirconia loading in PE. With the increase in SWCNT content in PE, the effect of drop in the viscosity is suppressed at higher temperature. The drop in the viscosity is attributed to the selective adsorption of high molecular weight chains on to the dispersed particles. PE chains tend to be adsorbed on the SWCNTs due to the van der Waals interaction. Hence, the probability of the high molar mass to remain adsorbed on the SWCNTs is higher than the low molar mass chains. The adsorbed high molar mass polymer is assumed as an immobilised part of the SWCNT for larger times. Thus, the polymer forming the remaining matrix effectively has a lower average molecular weight than the pure polymer. This causes faster relaxation of chains thus a decrease in the viscosity. The isothermal crystallisation experiments performed using rheometry matches with DSC (reported in Chapters 2 and 4) to conclusively assert the role of nanoparticles to accelerate crystallisation kinetics of PE. However, the onset temperature of crystallisation is increased and overall crystal growth is improved due to the presence of SWCNTs in PE and is more pronounced compared with zirconia in polymer matrix.

6.4 Recommendations

The thesis covers the important topics of flow induced crystallisation and provides a significant background for future research. The flow induced crystallisation experiments although suitable for studying the physics behind polymers have been performed over a limited range of shear rates which are far from the range experienced during processing operations like extrusion or injection moulding. Hence, as the flow

effects on polymer crystallisation are nonlinear, it is necessary to understand the structure development at high shear and/or strain rates using other advanced techniques with real-time processing conditions.

The results obtained during this research are mainly experimental and more detailed correlation with a theoretical model is required. For instance, the studies explained in chapter 5 using two nanoparticles (*viz.* SWCNT and zirconia), having different aspect ratio investigates the effect of molecular interaction of nanoparticles on stretched long chains of PE. However, it is important to compare the FIC results of PE obtained using zirconia with other fillers like carbon black having the same diameter and high surface area to volume. The obtained data could be further related to the studies performed in this thesis on SWCNTs to provide the conclusions about the surface chemistry and structure and/or geometry of nanofillers. It is also observed in figure 5.6a (reported in chapter 5) that broadness of intensity in the equator is attributed to flow aligned SWCNTs. Based on this thesis, it is not possible to show whether the streak-like broadening obtained on the equator is due to bundled or entangled SWCNTs and needs more experimental data with some studies on the effects of molecular parameters on applied shear flow.

Bibliography

1. Fawcett, E. W.; Gibson, R. O; Perrin, M. W.; Patton, J. G; Williams, E. G. 'Improvements in or relating to the polymerisation of ethylene', GB 471590, **1937.**
2. Ziegler, K. 'Alumino-organic syntheses in the field of olefinic hydrocarbons', *Angew. Chem.* **1952,** 64, 323.
3. Ziegler, K. 'Verfahren zur polymerisation und mischpolymerisation von olefinen', *DE* 878560, **1953.**
4. Natta, G.; Corradini, P. 'The crystalline structure of a new type of polypropylene', *Atti. Accad. Nazl. Lincei, Mem.* **1955,** 8, 73.
5. Natta, G. 'Une nouvelle classe de polymeres d'-olefines ayant une régularité de structure exceptionnelle', *J. Polym. Sci.* **1955,** 16, 143.
6. Keller, A. 'Morphology of crystallising polymers', *Nature* **1952**, 169, 913.
7. Keller, A. 'Single crystals in polymers: evidence of a folded-chain configuration', *Phil. Mag.* **1957,** 2, 1171.
8. Pennings, J.; Kiel, A. M. 'Fractionation of polymers by crystallisation from solution, 3. On the morphology of fibrillar polyethylene crystals grown in solution', *Kolloid-Z. Z. Polym.* **1965,** 205, 160.
9. Binsbergen, F. L. 'Orientation-induced Nucleation in Polymer Crystallisation', *Nature* **1966,** 211, 516.
10. Capaccio, G.; Ward, I. M. 'Properties of Ultrahigh Modulus Linear Polyethylenes', *Nature Phys. Sci.* **1973,** 243, 143.
11. Flory, P. J.; Yoon, D. Y. 'Molecular morphology in semicrystalline polymers', *Nature* **1978**, 272, 226.
12. Smith, P.; Lemstra, P. J. 'Ultrahigh-strength polyethylene filaments by solution spinning/drawing, 2. Influence of solvent on the drawability', *Makromol. Chem.* **1979**, 180, 2983.
13. Smith, P.; Lemstra, P. J. 'Ultra-high-strength polyethylene filaments by solution spinning/drawing', *J. Mater. Sci.* **1980,** 15, 505.
14. Smith, P.; Lemstra, P. J. 'Ultradrawing of high molecular weight polyethylene cast from solution', *Colloid Polym. Sci.* **1980**, 258, 891.
15. Sinn, H.; Kaminsky, W. 'Ziegler-Natta catalysis', *Adv. Organomet. Chem.* **1980**, 18, 99.
16. Bunn, C. W. 'The crystal structure of long-chain normal paraffin hydrocarbons. The "shape" of the <CH2 group', *Trans. Faraday Soc.* **1939**, 35, 482.
17. Peacock, A. J. *Handbook of Polyethylene*, Marcel Dekker, New York, **2000**.
18. Busing, W. R. 'X-ray diffraction study of disorder in Allied Spectra-1000 polyethylene fibers', *Macromolecules* **1990**, 23, 4608.

19. Bassett, D. C.; Block, S.; Piermarini, G. J. 'High pressure phase of polyethylene and chain extended growth', *J. Appl. Phys.* **1974**, 45, 4146.
20. Hikosaka, M.; Okada, H.; Rastogi, S.; Keller, A. 'Lamellar Thickness Determination of Polymer Single Crystal from Melt', *J. Chem. Soc. Faraday Trans.* **1995**, 91, 2573.
21. Rastogi, S.; Kurelec, L. 'Polymorphism in polymers; its implications for polymer crystallisation', *J. Mater. Sci*. **2000**, 35, 5121.
22. Bassett, D. C.; Hodge, A. M.; Olley, R. H. 'On the morphology of melt crystallised polyethylene 2. Lamellae and their crystallisation conditions', Proc. *Roy. Soc. Lond. – A.* **1981**, A377, 39.
23. Keller, A. 'Reminiscences on the discovery of chain folded single crystals', *Polymer* **2000**, 41, 8751.
24. Fischer, E. W. 'Stufenformiges und spiralformiges kristallwachstum bei hochpolmeren', *Z Naturforsch* **1957**, 12, 753.
25. Till, P. H. Jr. 'The growth of single crystals of linear polyethylene', *J. Polym. Sci.* **1957**, 24, 301.
26. Kobayashi, K. 'Properties and structure of polymers', *Kagaku Chem.* **1962**, 8, 203.
27. Bassett, D. C.; Frank, F. C.; Keller, A. 'Lamellae and their Organisation in Melt-Crystallised Polymers', *Phil. Trans. Roy. Soc. Lond. – A.* **1994**, 348, 29.
28. DiCorleto, J.A.; Bassett, D.C. 'On circular crystals of polyethylene', *Polymer* **1990**, 31, 1971.
29. Patel, D.; Bassett, D. C. 'On the formation of S-profiled lamellae in polyethylene and the genesis of banded spherulites', *Polymer* **2002**, 43, 3795.
30. Wunderlich, B. *Macromolecular Physics*, Vol. 2. Academic Press, New York, **1976**.
31. Sadler, D. M.; Gilmer, G. H. 'Model for chain folding in polymer crystals: rough growth faces are consistent with the observed growth rates', *Polymer* **1984**, 25, 1446.
32. Weeks, J. J. 'Melting temperature and change of lamellar thickness with time for bulk polyethylene', *J. Res. Nat. Bur. Std-A Phys. Chem.* **1963**, 67A, 441.
33. Hoffman, J. D. 'Role of reptation in the rate of crystallisation of polyethylene fractions from the melt', *Polymer* **1982**, 23, 656.
34. Organ, S. J.; Ungar, G.; Keller, A. 'Isothermal refolding in crystals of long alkanes in solution. 11. Morphological changes accompanying thickening', *J. Polym. Sci. Polym. Phys.* **1990**, 28, 2365.
35. Hobbs, J. K.; Hill, M. J.; Barham, P. J. 'Isothermal thickening of single crystals of C294H590 in dilute solution', *Polymer* **2000**, 41, 8761.
36. Voigt-Martin, I. G.; Mandelkern, L. 'A quantitative electron-microscopic study of a linear polyethylene fraction crystallised at different temperatures', *J. Polym. Sci. Polym. Phys. Ed* **1981**, 19, 1769.
37. Basset, D. C.; Hodge, A. M. 'On Lamellar Organisation in Certain Polyethylene Spherulites', *Proc. Roy. Soc. Lond. - A.* **1978**, A359, 121.

38. Voigt-Martin, I.G.; Fischer, E. W.; Mandelkern, L. 'Morphology of melt-crystallised linear polyethylene fractions and its dependence on molecular weight and crystallisation temperature', *J. Polym. Sci. Polym. Phys. Ed* **1980**, 18, 2347.
39. Basset, D. C.; Hodge, A. M. 'On lamellar organisation in banded spherulites of polyethylene', *Polymer* **1978**, 19, 469.
40. Reneker, D. H.; Geil, P. H. 'Morphology of polymer single crystals', *J. Appl. Phys.* **1960**, 31, 1916.
41. Bassett, D. C. *Principles of Polymer Morphology*, Cambridge University Press, Cambridge, **1981**.
42. Conde Braña, M. T.; Gedde, U. W. 'Morphology of binary blends of linear and branched polyethylene: composition and crystallisation-temperature dependence', *Polymer* **1992**, 33, 3123.
43. Defoor, F.; Groeninckx, G.; Schouterden, P.; Van der Heijden, B. 'Molecular, thermal and morphological characterisation of narrowly branched fractions of 1-octene LLDPE: 2. Study of the lamellar morphology by transmission electron microscopy', *Polymer* **1992**, 33, 5186.
44. Zhou, H.; Wikes, G. L. 'Comparison of lamellar thickness and its distribution determined from DSC, SAXS, TEM and AFM for high-density polyethylene films having a stacked lamellar morphology', *Polymer* **1997**, 38, 5735.
45. Ungar, G.; Zeng, X. B.; Spells, S. J. 'Non-integer and mixed integer forms in long n-alkanes observed by real-time LAM spectroscopy and SAXS', *Polymer* **2000**, 41, 8775.
46. Winkel, A. K.; Hobbs, J. K.; Miles, M. J. 'Annealing and melting of long-chain alkane single crystals observed by atomic force microscopy', *Polymer* **2000**, 41, 8791.
47. Loos, J.; Tian, M.; Rastogi, S.; Lemstra, P.J. 'An investigation on chain mobility in solid state polymer systems', *J. Mater. Sci.* **2000**, *35*, 5147.
48. Rastogi, S.; Spoelstra, A. B.; Goossens, J. G. P.; Lemstra, P. J. 'Chain mobility in polymer systems: on the borderline between solid and melt. 1. Lamellar doubling during annealing of polyethylene', *Macromolecules* **1997**, 30, 7880.
49. Keller, A. 'The spherulitic structure of crystalline polymers. 2. The problem of molecular orientation in polymer spherulites', *J. Polym. Sci.* **1955**, 17, 351.
50. Hoffman, J. D.; Frolen, L. J.; Ross, G. S.; Lauritzen, J. I. 'On the growth rate of spherulites and axialites from the melt in polyethylene fractions: Regime 1 and Regime 2 crystallisation', *J. Res. Nat. Bur. Std-A Phys. Chem.* **1975**, 79A, 671.
51. Rego-Lopez, J. M.; Gedde, U. W. 'Morphology of binary linear polyethylene blends', *Polymer* **1988**, 29, 1037.
52. Maxfield, J.; Mandelkern, L. 'Crystallinity, supermolecular structure, and thermodynamic properties of linear polyethylene fractions', *Macromolecules* **1977**, 10, 1141.
53. Nwabunma, D.; Kyu, T. *Polyolefin Composites*, Wiley-VCH, New Jersey, **2008**.
54. Bower, D. I. *An Introduction to Polymer Physics*, Cambridge University Press, Cambridge, **2002**.

55. Kitamaru, R.; Horii, F.; Murayama, K. 'Phase structure of lamellar crystalline polyethylene by solid-state high-resolution carbon-13 NMR detection of the crystalline-amorphous interphase', *Macromolecules* **1986**, 19, 636.
56. Strobl, G. R.; Hagedorn, W. 'Raman spectroscopic method for determining the crystallinity of polyethylene', *J. Polym Sci, Polym. Phys. Ed* **1978**, 16, 1181.
57. Mandelkern, L.; McLaughlin, K. W.; Alamo, R. G. 'Phase and supermolecular structure of binary mixtures of linear polyethylene fractions', *Macromolecules* **1992**, 25, 1440.
58. Mutter, R.; Stille, W.; Strobl, G. 'Transition regions and surface melting in partially crystalline polyethylene: A raman spectroscopic study', *J. Polym. Sci. Polym. Phys. Ed* **1993**, 31, 99.
59. Flory, P.J. 'Thermodynamics of Crystallisation in High Polymers. 1. Crystallisation Induced by Stretching', *J. Chem. Phys.* **1947**, *15*, 397.
60. Bashir, Z.; Odell, J.A.; Keller, A. 'High modulus filaments of polyethylene with lamellar structure by melt processing; the role of the high molecular weight component', *J. Mater. Sci* **1984**, 19, 3713.
61. Mackley, M. R.; Frank, F. C.; Keller, A. 'Flow-induced crystallisation of polyethylene melts', *J. Mater. Sci* **1975**, 10, 1501.
62. Hill, M. J.; Barham, P. J.; Keller, A. 'On the hairdressing of shish-kebabs', *Colloid Polym. Sci.* **1980**, 258, 1023.
63. White, H. M.; Bassett, D. C. 'On variable nucleation geometry and segregation in isotactic polypropylene', *Polymer* **1997**, 38, 5515.
64. Hsiao, B. S.; Yang, L.; Somani, R, H.; Avila-Orta, C. A.; Zhu, L. 'Unexpected Shish-Kebab Structure in a Sheared Polyethylene Melt', *Phys. Rev. Lett.* **2005**, 94, 117802.
65. Pennings, A. J. 'Bundle-like nucleation and longitudinal growth of fibrillar polymer crystals from flowing solutions', *J. Polym. Sci. Polym. Symp.* **1977**, 59, 55.
66. Seki, M.; Thurman, D. W.; Oberhauser, J. P.; Kornfield, J. A. 'Shear-mediated crystallisation of isotactic polypropylene: the role of long chain-long chain overlap', *Macromolecules* **2002**, 35, 2583.
67. Jerschow, P.; Janeschitz-Kriegl, H. 'The role of long molecules and nucleating agents in shear induced crystallisation of isotactic polypropylenes', *Intern. Polym. Proc.***1997**, 12, 72.
68. Keller, A.; Kolnaar, J. H. W. 'Flow-induced orientation and structure formation', In: H. E. H. Meijer, Editor, Mater. Sci. Tech. *VCH: New York*, **1997***,* 18, 189.
69. Ziabicki, A. *Fundamentals of Fiber Formation*, Wiley-VCH, New York, **1976**.
70. Eder, G.; Janeschitz-Kriegl, H. 'Crystallisation', In: H.E. H. Meijer, Editor, Mater. Sci. Tech. *VCH: New York*, **1997**, 18, 268.
71. Lee, O.; Kamal, M. R. 'Experimental study of post-shear crystallisation of polypropylene melts', *Polym. Eng. Sci.* **1999**, 39, 236.
72. Ward, I. M. *Structure and Properties of Oriented Polymers*, Chapman and Hall, London, **1997**.

73. Bassett, D.C. *Proceedings International Conference on Flow Induced Crystallisation of Polymers* (Salerno, Italy), 59, **2001**.
74. García Gutiérrez, M. C.; Alfonso, G. C.; Riekel, C.; Azzuri, F. 'Spatially resolved flow-induced crystallisation precursors in isotactic polystyrene by simultaneous small- and wide- angle X-ray microdiffraction', *Macromolecules* **2004***,* 37, 478.
75. Li, L.; de Jeu, W. H. 'Shear-induced crystallisation of Poly(butylene terephthalate): A real-time small-angle X-ray scattering study', *Macromolecules* **2004**, 37, 5646.
76. Strobl, G. 'From the melt via mesomorphic and granular crystalline layers to lamellar crystallites: A major route followed in polymer crystallisation?', *Eur. Polym. J.* **2000**, *E3*, 165.
77. Yang, L., Somani, R. H.; Sics, I.; Hsiao, B. S.; Kolb, R.; Fruitwala, H.; Ong, C. 'Shear-induced crystallisation precursor studies in model polyethylene blends by in-Situ rheo-SAXS and rheo-WAXD', *Macromolecules* **2004**, 37, 4845.
78. Nogales, A.; Hsiao, B.S.; Somani, R.H.; Srinivas, S.; Tsou, A.H.; Balta-Calleja, F.J.; Ezquerra, T. A. 'Shear-induced crystallisation of isotactic polypropylene with different molecular weight distributions: in situ small- and wide-angle X-ray scattering studies', *Polymer* **2001**, 42, 5247.
79. Eder, G.; Janeschitz-Kriegl, H.; Liedauer, S. 'Crystallisation processes in quiescent and moving polymer melts under heat transfer conditions', *Prog. Polym. Sci.* **1990**, 15, 629.
80. Wunderlich, B. *Thermal Analysis of Polymeric Materials*, Springer-Verlag: Berlin, **2005**.
81. Samuels, R. J. *Structured Polymer Properties: The Identification, Interpretation, and Application of Crystalline Polymer Structure*, John Wiley & Sons: New York, **1974**.
82. Elmoumni, A.; Winter, H. H.; Waddon, A. J.; Fruitwala, H. 'Correlation of material and processing time scales with structure development in isotactic polypropylene crystallisation', Macromolecules 2003, 36, 6453.
83. Kumaraswamy, G.; Kornfield, J. A.; Yeh, F.; Hsiao, B. S. 'Shear-enhanced crystallisation in isotactic polypropylene. 3. Evidence for a kinetic pathway to nucleation', *Macromolecules* **2002**, 35, 1762.
84. Langouche, F. 'Orientation development during shear flow-induced crystallisation of i-PP', *Macromolecules* **2006**, 39, 2568.
85. Kumaraswamy, G.; Issaian, A.; Kornfield, J. K. 'Shear-enhanced crystallisation in isotactic polypropylene. 1. correspondence between in situ rheo-optics and ex situ structure determination', *Macromolecules* **1999***,* 32, 7537.
86. Bove, L.; Nobile, M. R. 'Shear flow effects on polymer melts crystallisation: kinetics features', *Macromol. Symp*. **2002**, 180, 169.
87. Somani, R. H.; Hsiao, B. S.; Nogales, A.; Fruitwala, H.; Srinivas, S.; Tsou, A. H. 'Structure development during shear flow-induced crystallisation of i-PP: In-situ wide angle X-ray di raction study', *Macromolecules* **2001**, 34, 5902.

88. Koscher, E.; Fulchiron, R. 'Infuence of shear on polypropylene crystallisation: morphology development and kinetics', *Polymer* **2002**, 43, 6931.
89. Balzano, L.; Rastogi, S.; Peters, G.W.M.; Chadwick, J.C. 'Crystallisation and dissolution of flow induced precursors', *Phys. Rev. Lett.* **2008**, 100, 048302.
90. Azzurri, F.; Alfonso, G. C. 'Lifetime of Shear-Induced Crystal Nucleation Precursors', *Macromolecules* **2005**, 38, 1723.
91. Braun, J.; Wippel, H.; Eder, G.; Janeschitz-Kriegl, H. 'Industrial solidification processes in polybutene-1. Part 2. Influence of shear flow',*Poly. Eng. Sci.* **2003**, 43, 188.
92. Chai, C. K.; Auzoux, Q.; Randrianatoandro, H.; Navard, P.; Haudin, J. M. 'Influence of pre-shearing on the crystallisation of conventional and metallocene polyethylenes', *Polymer* **2003**, 44, 773.
93. Isayev, A. I.; Chan, T. W.; Shimojo, K.; Gmerek, M. 'Injection molding of semicrystalline polymers. 1. material characterisation', *J. Appl. Polym. Sci.* **1995**, 55, 807.
94. Govaert, L. E.; Bastiaansen, C. W. M.; Leblans, P. J. R. 'Stress-strain analysis of oriented polyethylene', *Polymer* **1993**, 34, 534.
95. Mackley, M. R.; Keller, A. 'Flow-induced crystallisation of polyethylene melts', *Polymer* **1973**, 14, 16.
96. Lagasse, R. R.; Maxwell, B. 'An experimental study of the kinetics of polymer crystallisation during shear flow', *Polym. Eng. Sci.* **1976**, 16, 189.
97. Kornfield, J. A.; Kumaraswamy, G.; Issaian, A. M. 'Recent advances in understanding flow effects on polymer crystallisation', *Ind. Eng. Chem. Res.* **2002**, 41, 6383.
98. Vleeshouwers, S.; Meijer, H. E. H. 'A rheological study of shear induced crystallisation', *Rheol. Acta* **1996**, 35, 391.
99. Somani, R. H.; Hsiao, B. S.; Nogales, A.; Srinivas, S.; Tsou, A.H.; Sics, I.; Balta-Calleja, F. J.; Ezquerra, T. A. 'Structure development during shear flow-induced crystallisation of i-PP: in-situ small-angle X-ray scattering study', *Macromolecules* **2000***,* 33, 9385.
100. Wang, M.; Hu, W.; Ma, Y. 'Orientational Relaxation Together with Polydispersity Decides Precursor Formation in Polymer Melt Crystallisation', *Macromolecules* **2005**, 38, 2806.
101. Agarwal, P. K.; Somani, R. H.; Weng, W. Q.; Mehta, A.; Yang, L.; Ran, S. F.; Liu, L.; Hsiao, B. S. 'Shear-Induced Crystallisation in Novel Long Chain Branched Polypropylenes by in Situ Rheo-SAXS and WAXD', *Macromolecules* **2003**, 36, 5226.
102. Van Meerveld, J.; Peters, G.W. M.; Hütter, M. 'Towards a rheological classification of flow induced crystallisation experiments of polymer melts', *Rheol. Acta* **2004**, 44, 119.
103. Acierno, S.; Palomba, B.; Winter, H. H.; Grizzuti, N. 'Effect of molecular weight on the flow-induced crystallisation of isotactic poly(1-butene)', *Rheol. Acta* **2003**, 42, 243.
104. Nakajima, N.; Yamaguchi, Y. 'Strain-induced crystallisation of cis-1,4-Polybutadiene containing dispersed 1,2-Polybutadiene crystalline particles', *J. Appl. Polym. Sci.***1996**, 62, 2329.

105. Jain, S. 'Nano-scale events with macroscopic effects in PP/silica nanocomposites', *Ph.D. Thesis*, TU/e (Eindhoven), **2005**.
106. Spruiell, J. E.; Lu, F. M.; Ding, Z.; Richeson, G. 'The influence of isotacticity, ethylene comonomer content, and nucleating agent additions on the structure and properties of melt-spun isotactic polypropylene filaments', *J. Appl. Polym. Sci.* **1996**, 62, 1965.
107. Huo, H.; Jiang, S. C.; An, L. J.; Feng, J. 'Influence of Shear on Crystallisation Behavior of the β Phase in Isotactic Polypropylene with β-Nucleating Agent', *Macromolecules* **2004**, 37, 2478.
108. Baird, D. G. *Polymer Processing, Encyclopedia of Physical Science and Technology*, Academic Press, California, **2001**.
109. De Gennes, P. G. *Scaling Concepts in Polymer Physics*, Cornell University Press, Ithaca, NY, **1979**.
110. Doi, M.; Edwards, S. F. *The Theory of Polymer Dynamics*, Clarendon Press, Oxford, **1986**.
111. Doi, M. 'Explanation for the 3.4 Power Law of Viscosity of Polymeric Liquids on the Basis of the Tube Model', *J. Polym. Sci.***1983**, 21, 667.
112. Bower, C.; Rosen, R.; Jin, L.; Han, J.; Zhou, O. 'Deformation of carbon nanotubes in nanotube–polymer composites', *Appl. Phys. Lett.* **1999**, 74, 3317.
113. Balzano, L.; Rastogi, S.; Peters, G. W. M. 'Flow induced crystallisation in iPP-DMDBS blends: implications on morphology of shear and phase separation', *Macromolecules* **2008**, 41, 399.
114. Balzano, L.; Portale, G.; Peters, G. W. M.; Rastogi, S. 'Thermo-reversible DMDBS phase separation in iPP: effect of flow induced crystallisation', *Macromolecules* **2008**, 41, 5350.
115. Tseng, W. J.; Teng, K. H. 'Effect of surfactant adsorption on aggregate structure and yield strength of zirconia-wax suspensions', *J. Mater. Sci.* **2001**, 36, 173.
116. Lewis, J. A. 'Colloidal processing of ceramics', *J. Am. Ceram. Soc.* **2000**, 83, 2341.
117. Lenz, L. K.; Heuer, A. H. 'Stress-induced transformation during subcritical crack growth in partially stabilized zirconia', *J. Am. Ceram. Soc.* **1982**, 65, 192.
118. Gravie, R. C.; Hannink, R. H.; Pascoe, R. T. 'Ceramic steel?', *Nature* **1975**, 258, 703.
119. O'Connell, M. J. *Carbon nanotubes: properties and applications*, CRC Press, Boca Raton, Florida, **2006**.
120. Ajayan, P. M.; Schadler, L. S.; Braun, P. V. *Nanocomposite science and technology*, Wiley-VCH, Weinheim, **2003**.
121. Harris, P. J. F. *Carbon nanotube science: synthesis, properties and applications*, Cambridge University Press, Cambridge, **2009**.
122. Avrami, M. 'Kinetics of Phase Change. I. General Theory', *J. Chem. Phys.* **1939**, 7, 1103.
123. Avrami, M. 'Kinetics of Phase Change. II. Transformation-Time Relations for Random Distribution of Nuclei', *J. Chem. Phys.* **1940**, 8, 212.
124. Avrami, M. 'Kinetics of Phase Change. III. Granulation, Phase Change, and Microstructure', *J. Chem. Phys.* **1941**, 9, 177.

125. Hoffman, J. D.; Miller, R. L. 'Kinetic of crystallisation from the melt and chain folding in polyethylene fractions revisited: theory and experiment', *Polymer* **1997**, 38, 3151.
126. Zuidema, H.; Peters, G. W. M.; Meijer, H. E. H. 'Development and validation of a recoverable strain-based model for flow-induced crystallisation of polymers', *Macromol. Theory Simul*. **2001**, 10, 447.
127. Janeschitz-Kriegl, H.; Ratajski, E.; Wippel, H. 'The physics of athermal nuclei in polymer crystallisation', *Colloid Polym. Sci*. **1999**, 277, 217.
128. Lieberwirth, I.; Loos, J.; Petermann, J.; Keller, A. 'Observation of shish crystal growth into non-deformed melts', *J. Polym. Sci. Polym. Phys.* **2000**, 38, 1183.
129. Kumaraswamy, G.; Verma, R. K.; Kornfield, J. A.; Yeh. F.; Benjamin, B. S. 'Shear-enhanced crystallisation in isotactic polypropylene. In-situ synchrotron SAXS and WAXD', *Macromolecules* **2004**, 37, 9005.
130. Zhang, Q.; Lippits, D.; Rastogi, S. 'Dispersion and rheological aspects of SWCNTs in ultrahigh molecular weight polyethylene', *Macromolecules* **2006**, 39, 658.
131. Jain, S.; Goossens, J. G. P.; Peters, G. W. M.; Van Duin, M.; Lemstra, P. J. 'Strong decrease in viscosity of nanoparticle-filled polymer melts through selective adsorption', *Soft Matter* **2008**, 4, 1848.
132. Iijima, S. 'Helical microtubules of graphitic carbon', *Nature* **1991**, 354, 56.
133. Treacy, M. M. J.; Ebbesen, T. W.; Gibson, J. M. 'Exceptionally high Young's modulus observed for individual carbon nanotubes', *Nature* **1996**, 381, 678.
134. Odom, T. W.; Huang, J. L.; Kim, P.; Quyang, M.; Lieber, C. M. 'Atomic structure and electronic properties of single-walled carbon nanotubes', *Nature* **1998**, 391, 62.
135. Baughman, R. H.; Zakhidov, A. A.; De Heer, W. A. 'Carbon nanotubes - the route toward applications', *Science* **2002**, 297, 787.
136. Berber, S.; Kwon, Y. K.; Tomanek, D. 'Unusually high thermal conductivity of carbon nanotubes', *Phys. Rev. Lett.* **2000**, 84, 4616.
137. Ajayan, P. M.; Stephan, O.; Colliex, C.; Trauth, D. 'Aligned carbon nanotube arrays formed by cutting a polymer resin—nanotube composite', *Science* **1994**, 265, 1212.
138. Moniruzzaman, M.; Winey, K. I. 'Polymer nanocomposites containing carbon nanotubes', *Macromolecules* **2006**, 39, 5194.
139. Haggenmueller, R.; Guthy, C.; Lukes, J. R.; Fischer, J. E.; Winey, K. I. 'Single wall carbon nanotube/polyethylene nanocomposites: thermal and electrical conductivity', *Macromolecules* **2007**, 40, 2417.
140. Uehara, H.; Kato, K.; Kakiage, M.; Yamanobe, T.; Komoto, T. 'Single-walled carbon nanotube nucleated solution-crystallisation of polyethylene', *J. Phys. Chem. C* **2007**, 111, 18950.
141. Grady, B. P.; Pompeo, F.; Shambaugh, R. L.; Resasco, D. E. 'Nucleation of polypropylene crystallisation by single-walled carbon nanotubes', *J. Phys. Chem. B* **2002**, 106, 5852.

142. Bhattacharyya, A. R.; Sreekumar, T. V.; Liu, T.; Kumar, S.; Ericson, L. M.; Hauge, R. H.; Smalley, R. E. 'Crystallisation and orientation studies in polypropylene/single wall carbon nanotube composite', *Polymer* **2003**, 44, 2373.

143. Assouline, E.; Lustiger, A.; Barber, A. H.; Cooper, C. A.; Klein, E.; Wachtel, E.; Wagner, H. D. 'Nucleation ability of multiwall carbon nanotubes in polypropylene composites', *J. Polym. Sci., Part B: Polym. Phys*. **2003**, 41, 520.

144. Probst, O.; Moore, E. M.; Resasco, D. E.; Grady, B. P. 'Nucleation of polyvinyl alcohol crystallisation by single-walled carbon nanotubes', *Polymer* **2004**, 45, 4437.

145. Minus, M. L.; Chae, H. G.; Kumar, S. 'Single wall carbon nanotube templated oriented crystallisation of poly(vinyl alcohol)', *Polymer* **2006**, 47, 3705.

146. Vega, J. F.; Martinez-Salazar, J.; Trujillo, M.; Arnal, M. L.; Muller, A. J.; Bredeau, S.; Dubois, Ph. 'Rheology, processing, tensile properties, and crystallisation of polyethylene/carbon nanotube nanocomposites', *Macromolecules* **2009**, 42, 4719.

147. Trujillo, M.; Arnal, M. L.; Muller, A. J.; Laredo, E.; Bredeau, St.; Bonduel, D.; Dubois, Ph. 'Thermal and morphological characterisation of nanocomposites prepared by in-situ polymerisation of high-density polyethylene on carbon nanotubes', *Macromolecules* **2007**, 40, 6268.

148. Trujillo, M.; Arnal, M. L.; Muller, A. J.; Laredo, E.; Bredeau, St.; Bonduel, D.; Dubois, Ph.; Hamley, I. W.; Castelletto, V. 'Thermal fractionation and isothermal crystallisation of polyethylene nanocomposites prepared by in situ polymerisation', *Macromolecules* **2008**, 41, 2087.

149. Haggenmueller, R.; Fischer, J. E.; Winey, K. I. 'Single wall carbon nanotubes / polyethylene nanocomposites: Nucleating and templating polyethylene crystallites', *Macromolecules* **2006**, 39, 2964.

150. Li, C. Y.; Li, L.; Cai, W.; Kodjie, S. L.; Tenneti, K. K. 'Nano-hybrid shish-kebab: Polymer decorated carbon nanotubes', *Adv. Mater.* **2005**, 17, 1198.

151. Strobl, G. *The physics of polymers*, Springer-Verlag, Berlin, **1997**.

152. Dukovski, I.; Muthukumar, M. 'Langevin dynamics simulations of early stage shish-kebab crystallisation of polymers in extensional flow', *J. Chem. Phys.* **2003**, 118, 6648.

153. Yang, L.; Somani, R.H.; Sics, I.; Hsiao, B. S.; Kolb, R.; Lohse, D. 'The role of high molecular weight chains in flow-induced crystallisation precursor structures', *J. Phys.: Condens. Matter* **2006**, 18, S2421.

154. Keum, J. K.; Zuo, F.; Hsiao, B. S. 'Formation and stability of shear-induced shish-kebab structure in highly entangled melts of UHMWPE/HDPE blends', *Macromolecules* **2008**, 41, 4766.

155. Schultz, J. M.; Hsiao, B. S.; Samon, J. M. 'Structural development during the early stages of polymer melt spinning by in-situ synchrotron X-ray techniques', *Polymer* **2000**, 41, 8887.

156. Somani, R. H.; Yang, L.; Hsiao, B. S.; Agarwal, P. K.; Fruitwala, H. A.; Tsou, A. H. 'Shear-induced precursor structures in isotactic polypropylene melt by in-situ rheo-SAXS and rheo-WAXD studies', *Macromolecules* **2002**, 35, 9096.
157. Kimata, S.; Sakurai, T.; Nozue, Y.; Kasahara, T.; Yamaguchi, N.; Karino, T; Shibayama, M.; Kornfield, J. A. 'Molecular basis of the shish-kebab morphology in polymer crystallisation', *Science* **2007**, 316, 1014.
158. Sherwood, C. H.; Price, F. P.; Stein, R. S. 'Effect of shear on the crystallisation kinetics of poly(ethylene oxide) and poly(e-caprolactone) melts', *J. Polym. Sci. Polym. Symp.* **1978**, 63, 77.
159. Kharchenko, S. B.; Douglas, J. F.; Obrzut, J.; Grulke, E. A.; Migler, K. B. 'Flow-induced properties of nanotube-filled polymer materials', *Nature Mater.* **2004**, 3, 564.
160. Somwangthanaroj, A.; Lee, E. C.; Solomon, M. J. 'Early stage quiescent and flow-induced crystallisation of intercalated polypropylene nanocomposites by depolarised light scattering', *Macromolecules* **2003**, 36, 2333.
161. Garcia-Gutirrez, M. C.; Hernandez, J. J.; Nogales, A.; Panine, P.; Rueda, D. R.; Ezquerra, T. A. 'Influence of shear on the templated crystallisation of poly(butylene terephthalate)/single wall carbon nanotube nanocomposites', *Macromolecules* **2008**, 41, 844.
162. Thostenson, E. T.; Ren, Z.; Chou, T. W. Advances in the science and technology of carbon nanotubes and their composites: a review. *Compos. Sci. Technol.* **2001**, 61, 1899.
163. Liu, C.; He, J.; Van Ruymbeke, E.; Keunings, R.; Bailly, C. 'Evaluation of different methods for the determination of the plateau modulus and the entanglement molecular weight', *Polymer* **2006**, 47, 4461.
164. Wu, S. 'Chain structure and entanglement', *J. Polym. Sci., Part B: Polym. Phys.* **1989**, 27, 723.
165. Nobile, M. R.; Cocchini, F. 'Evaluation of molecular weight distribution from dynamic moduli', *Rheo. Acta* **2001**, 40, 111.
166. Regev, O.; Elkati, P. N. B.; Loos, J.; Koning, C. E. 'Preparation of conductive nanotube-polymer composites using latex technology', *Adv. Mater.* **2004**, 16, 248.
167. Wunderlich, B. *Macromolecular physics*, Vol. 3. Academic Press, New York, **1973**.
168. Lorenzo, A. T.; Arnal, M. L.; Albuerne, J.; Muller, A. J. 'DSC isothermal polymer crystallisation kinetics measurements and the use of the Avrami equation to fit the data: Guidelines to avoid common problems', *Polym. Test.* **2007**, 26, 222.
169. Mandelkern, L. 'Crystallization of polymers – kinetics and mechanisms', Vol. 2. *Cambridge University Press, Cambridge,* **2004**.
170. Reiner, M. 'The Deborah number', *Phys. Today* **1964**, 17, 62.
171. Astarita, G. 'Two dimensionless groups relevant in analysis of steady flows of viscoelastic materials', *Ind. Eng. Chem. Fundamentals* **1967**, 6, 257.
172. Malkin, A. Y. *Rheology fundamentals*, ChemTech Publishing: Ontario, **1994**.
173. Noll, W. 'Motions with constant stretch history', *Arch. Rational Mech. Anal.* **1962**, 11, 97.

174. Oldroyd, J. G. 'Some steady flows of the general elastico-viscous liquid', *Proc. Roy. Soc. – A* **1965**, 283, 115.
175. Balzano, L. 'Flow induced crystallisation of polyolefins', Ph.D. thesis, *TU/e (Eindhoven)*, **2008**.
176. Macosko, C. W. *Rheology: principles, measurements and applications*, Wiley-VCH, New York, **1994**.
177. Larson, R. G. *The structure and rheology of complex fluids*, Oxford University Press, New York, **1999**.
178. Wunderlich, B. *Thermal analysis of polymeric materials*, Springer-Verlag, Berlin, **2005**.
179. Fetters, L. J.; Lohse, D. J.; Richter, D.; Witten, T. A.; Zirkel, A. 'Connection between Polymer Molecular Weight, Density, Chain Dimensions, and Melt Viscoelastic Properties', *Macromolecules* **1994**, 27, 4639.
180. Ramos, J.; Vega, J. F.; Theodorou, D. N.; Martinez-Salazar, J. 'Entanglement relaxation time in polyethylene: simulation versus experimental data', *Macromolecules* **2008**, 41, 2959.
181. Hermans, P. H.; Platzek, P. 'Beiträge zur kenntnis des deformations mechanismus und der feinstruktur der hydratzellulose', *Kolloid-Z.* **1939**, 88, 68.
182. Alexander, L. E. *X-Ray diffraction methods in polymer science*, John Wiley & Sons: New York, **1969**.
183. Stribeck, N. *X-Ray scattering of soft matter*, Springer - Heidelberg, New York, **2007**.
184. Patil, N.; Balzano, L.; Portale, G.; Rastogi, S. 'Influence of nanoparticles on the rheological behaviour and initial stages of crystal growth in linear polyethylene', *Macromol. Chem. Phys.* **2009**, 210, 2174.
185. Keller, A.; Odell, J. A. 'Fluid flow: turbulence splits polymers', *Nature* **1984**, 312, 98.
186. Somani, R. H.; Yang, L.; Zhu, L.; Hsiao, B. S. 'Flow-induced shish-kebab precursor structures in entangled polymer melts', *Polymer* **2005**, 46, 8587.
187. Odell, J. A.; Grubb, D. T.; Keller, A. 'A new route to high modulus polyethylene by lamellar structures nucleated onto fibrous substrates with general implications for crystallisation behaviour', *Polymer* **1978**, 19, 617.
188. Bashir, Z.; Odell, J. A.; Keller, A. 'Stiff and strong polyethylene with shish-kebab morphology by continuous melt extrusion', *J. Mater. Sci.* **1986**, 21, 3993.
189. Van Hutten, P. F.; Pennings, A. J. 'Characterisation of polyethylene shish-kebabs by small-angle X-ray scattering', *J. Polym. Sci.: Polym. Phys.* **1980**, 18, 927-942.
190. Zuo, F.; Keum, J. K.; Yang, L.; Somani, R. H.; Hsiao, B. S. 'Thermal stability of shear-induced shish-kebab precursor structure from high molecular weight polyethylene chains', *Macromolecules* **2006**, 39, 2209.
191. Hill, M. J.; Keller, A. 'Direct evidence for distinctive, stress-induced nucleus crystals in the crystallisation of oriented polymer melts', *J. Macromol. Sci., Phys.* **1969**, B3, 153.

192. Hill, M. J.; Keller, A. 'Further studies on polyethylene crystallised under stress: morphology, calorimetry, and stress relaxation', *J. Macromol. Sci., Phys.* **1971**, B5, 591.

193. Bayer, R. K.; Eliah, A. E.; Seferis, J. C. 'Structural characterisation of polyethylene injection molded by elongational flow', *Polym. Eng. Rev.* **1984**, 4, 201.

194. Ulrich, R. D.; Price, F. P. 'Morphology development during shearing of poly(ethylene oxide) melts', *J. Appl. Polym. Sci.* **1976**, *20*, 1077.

195. Wereta, A. Jr.; Gogos, C. 'Crystallisation studies on deformed polybutene - 1. Melts', *Polym. Eng. Sci.* **1971**, 11, 19.

196. Liedauer, S.; Eder, G.; Janeschitz-Kriegl, H. 'On the limitations of shear induced crystallisation in polypropylene melts', *Int. Polym. Process.* **1995**, *10*, 243.

197. Kumaraswamy, G.; Verma, R. K.; Kornfield, J. A. 'Novel flow apparatus for investigating shear-enhanced crystallisation and structure development in semicrystalline polymers', *Rev. Sci. Instrum.* **1999**, *70*, 2097.

198. Coppola, S.; Balzano, L.; Gioffredi, E.; Maffetone, P.L.; Grizzuti, N. 'Effects of the degree of undercooling on flow induced crystallisation in polymer melts', *Polymer* **2004**, *45*, 3249.

199. Ogino, Y.; Fukushima, H.; Matsuba, G.; Takahashi, N.; Nishida, K.; Kanaya, T. 'Effects of high molecular weight component on crystallisation of polyethylene under shear flow', *Polymer* **2006**, 47, 5669.

200. Hoffman, J.D.; Lauritzen, Jr. J. I. 'Crystallisation of bulk polymers with chain folding: theory of growth of lamellar spherulites', *J Res Natl Bur Stand (US)* **1961**, *65A*, 297.

201. Bassett, D. C.; Hodge, A. M. 'On lamellar organisation in banded spherulites of polyethylene', *Polymer* **1978**, 19, 469.

202. Keith, H. D.; Padden, F. J. 'Twisting orientation and the role of transient states in polymer crystallisation', *Polymer* **1984**, 25, 28.

203. Lotz, B.; Cheng, S.Z.D. 'A critical assessment of unbalanced surface stresses as the mechanical origin of twisting and scrolling of polymer crystals', *Polymer* **2005**, 46, 577.

204. Schultz, J. M. 'Self-induced field model for crystal twisting in spherulites', *Polymer* **2003**, 44, 433.

205. Schrauwen, B. A. G.; Breemen, L. C. A.; Spoelstra, A. B.; Govaert, L. E.; Peters, G. W. M.; Meijer, H. E. H. 'Structure, deformation and failure of flow oriented semicrystalline polymers', *Macromolecules* 2004, 37, 8618.

206. Keller, A.; Machin, M. J. 'Oriented crystallisation in polymers', *J. Macromol. Sci. Part B: Phys.* **1967**, 1, 41.

207. Byelov, D.; Panine, P.; Remerie, K.; Biemond, E.; Alfonso, G. C.; De Jeu, W. H. 'Crystallisation under shear in isotactic polypropylene containing nucleators', *Polymer* **2008**, 49, 3076.

208. Wilchinsky, Z. W. *Advances in X-ray analysis*, Vol 6. **1962**.

209. Cullity, B. D.; Stock, S. R. *Elements of X-ray diffraction*, Prentice-Hall, New Jersey, **2001**.

210. Patterson, A. L. 'The Scherrer formula for X-ray particle size determination', *Phys. Rev.* **1939**, 56, 978.
211. Glatter, O.; Kratky, O. *Small angle X-ray scattering*, Academic Press, London, **1982**.
212. Pennings, A. J.; van der Mark, J. M. A. A.; Kiel, A. M. 'Hydrodynamically induced crystallisation of polymers from solution 3. morphology', *Kolloid Z. Z. Polym.* **1970**, 237, 336.
213. Pennings, A. J. 'Polymer crystallisation', *J. Cryst. Growth* **1980**, 48, 574.
214. Heeley, E. L.; Fernyhough, C. M.; Graham, R. S.; Olmsted, P. D.;Inkson, N. J.; Embery, J.; Groves, D. J.; McLeish, T. C. B.; Morgovan, A. C.; Meneau, F.; Bras, W.; Ryan, A. J. 'Shear-induced crystallisation in blends of model linear and long-chain branched hydrogenated polybutadienes', *Macromolecules* **2006**, 39, 5058.
215. Turnbull, D.; Fisher, J. C. 'Rate of nucleation in condensed systems', *J. Chem. Phys.* **1949**, 17, 71.
216. Eder, G.; Janeschitz-Kriegl, H.; Krobath, G. 'Shear induced crystallisation, a relaxation phenomenon in polymer melts', *Prog. Colloid Polym. Sci.* **1989**, 80, 1.
217. Janeschitz-Kriegl, H.; Eder, G. 'Shear induced crystallisation, a relaxation phenomenon in polymer melts: A re-collection', *J. Macro. Sci., Part B: Phys.* **2007**, 46, 591.
218. Samon, J. M.; Schultz, J. M.; Hsiao, B. S. 'Structure development in the early stages of crystallisation during melt spinning', *Polymer* **2002**, 43, 1873.
219. Keum, J. K.; Burger, C.; Zuo, F.; Hsiao, B. S. 'Probing nucleation and growth behavior of twisted kebabs from shish scaffold in sheared polyethylene melts by in situ X-ray studies', *Polymer* **2007**, 48, 4511.
220. Matsuba, G.; Sakamoto, S.; Ogino, Y.; Nishida, K.; Kanaya, T. 'Crystallisation of polyethylene blends under shear flow. Effects of crystallisation temperature and ultrahigh molecular weight component', *Macromolecules* **2007**, 40, 7270.
221. Balzano, L.; Rastogi, S.; Peters, G.W.M. 'Crystallisation and precursors during fast short-term shear', *Macromolecules* **2009**, 42, 2088.
222. Zhang, Q. H.; Lippits, D. R.; Rastogi, S.; Lemstra, P. J. 'Low percolation threshold in single-walled carbon nanotube/high density polyethylene composites prepared by melt processing technique', *Carbon* **2006**, 44, 778.
223. Ruland, W. 'X-ray small-angle scattering studies of carbonised rayon fibers', *J. Polym. Sci., Part C* **1969**, 28, 143.
224. Perret, R.; Ruland, W. 'Single and multiple X-ray small-angle scattering of carbon fibres', *J. Appl. Cyst.* **1969**, 2, 209.
225. Perret, R.; Ruland, W. 'The microstructure of PAN-base carbon fibres', *J. Appl. Cyst.* **1970**, 3, 525.
226. Ruland, W. 'Small-angle scattering of two-phase systems: determination and significance of systematic deviations from Porod's law', *J. Appl. Cyst.* **1971**, 4, 70.

227. Somani, R. H.; Yang, L.; Hsiao, B.S.; Sun, T.; Pogodina, N.V.; Lustiger, A. 'Shear-induced molecular orientation and crystallisation in isotactic polypropylene: Effects of the deformation rate and strain', *Macromolecules* **2005**, 38, 1244.

228. Potschke, P.; Abdel-Goad, M.; Alig, I.; Dudkin, S.; Lellinger, D. 'Rheological and dielectrical characterization of melt mixed polycarbonate-multiwalled carbon nanotube composites', *Polymer* **2004**, 45, 8863.

229. Du, F.; Scogna, R. C.; Zhou, W.; Brand, S.; Fischer, J. E.; Winey, K. I. 'Nanotube networks in polymer nanocomposites: rheology and electrical conductivity', *Macromolecules* **2004**, 37, 9048.

230. Mackay, M. E.; Dao, T. T.; Tuteja, A.; Ho, D. L.; Brooke van, H.; Kim, H. C.; Hawker, C. J. 'Nanoscale effects leading to non-Einstein-like decrease in viscosity', *Nature Mater.* **2003**, 2, 762.

231. Gee, R. H.; Fried, L. E. 'Ultrafast crystallisation of polar polymer melts', *J. Chem. Phys.* **2003**, 118, 3827.

232. Somani, R. H.; Yang, L.; Hsiao, B. S. 'Precursors of primary nucleation induced by flow in isotactic polypropylene', *Physica A* **2002**, 304, 145.

233. Kanaya, T.; Takayama, Y.; Ogino, Y.; Matsuba, G.; Nishida, K. 'Precursor of primary nucleation in isotactic polystyrene induced by shear flow', *Lect. Notes Phys.* **2007**, 714, 87.

234. De Gennes, P. G. 'Coil-stretch-transition of dilute flexible polymer under ultra-high velocity gradients', *J. Phys. Chem.* **1974**, 60, 5030.

235. De Gennes, P. G. 'Reptation of polymer chain in the presence of fixed obstacles', *J. Chem. Phys.* **1971**, 55, 572.

236. Wu, J.; Schultz, J. M.; Yeh, F.; Hsiao, B. S.; Chu, B. 'In-situ simultaneous synchrotron small- and wide-angle X-ray scattering measurement of poly(vinylidene fluoride) fibers under deformation', *Macromolecules* **2000**, 33, 1765.

237. Cahn, J.W.; Hilliard, J. E. 'Free energy of a nonuniform system. 1. Interfacial free energy', *J. Chem. Phys.* **1958**, 28, 258.

238. Matsuba, G.; Kanaya, T.; Saito, M.; Kaji, K.; Nishida, K. 'Further evidence of spinodal decomposition during the induction period of polymer crystallisation: Time-resolved small-angle x-ray scattering prior to crystallisation of poly(ethylene naphthalate)', *Phys. Rev. E.* **2000**, 62, R1497.

239. Olmsted, P.D.; Poon, W.C.K.; McLeish, T.C.B.; Terrill, N.J.; Ryan, A.J. 'Spinodal-assisted crystallisation in polymer melts', *Phys. Rev. Lett.* **1998**, 81, 373.

240. Ryan, A.J.; Fairclough, P.A.; Terrill, N.J.; Olmsted, P.D.; Poon, W.C.K. 'A scattering study of nucleation phenomena in polymer crystallisation', *Faraday Discuss.* **1999**, 112, 13.

241. Wang, Z.G.; Hsiao, B.S.; Sirota, E.B.; Srinivas, S. 'A simultaneous small- and wide-angle X-ray scattering study of the early stages of melt crystallisation in polyethylene', *Polymer* **2000**, 41, 8825.

242. Hu, W.; Frenkel, D.; Mathot, V. B. F. 'Shish-kebab crystallites induced by a single pre-aligned macromolecule', *Macromolecules* **2002**, 35, 7172.
243. Keum, J. K.; Zuo, F.; Hsiao, B. S. 'Probing the flow-induced shish-kebab structure in entangled polyethylene melts by synchrotron X-ray scattering', *J. Appl. Cryst.* **2007**, 40, 48.
244. Keum, J. K.; Somani, R. H.; Zuo, F.; Burger, C.; Sics, I.; Hsiao, B. S.; Chen, H.; Kolb, R.; Lue, C-T. 'Probing flow-induced precursor structures in blown polyethylene films by synchrotron X-rays during constrained melting', *Macromolecules* **2005**, 38, 5128.
245. Terrones, M. 'Science and technology of the twenty-first century: synthesis, properties, and applications of carbon nanotubes', *Annu. Rev. Mater. Res.* **2003**, 33, 419.
246. Dresselhaus, M. S.; Eklund, P. C. 'Phonons in carbon nanotubes', *Adv. Phys.* **2000**, 49, 705.
247. Jain, S.H.; Goossens, J.G.P.; van Duin, M.; Lemstra, P.J. 'Effect of in situ prepared silica nano-particles on non-isothermal crystallisation of polypropylene', *Polymer* **2005**, 46, 8805.
248. Jain, S.H.; Goossens, J.G.P.; van Duin, M. 'Synthesis, characterisation and properties of (vinyl triethoxy silane-grafted PP)/silica nanocomposites', *Macromol. Symp.* **2006**, 233, 225.